Cylindrical Thin Concrete Shells

Structural Analysis of the Frontón Recoletos roof

JOSE ANTONIO LOZANO GALANT

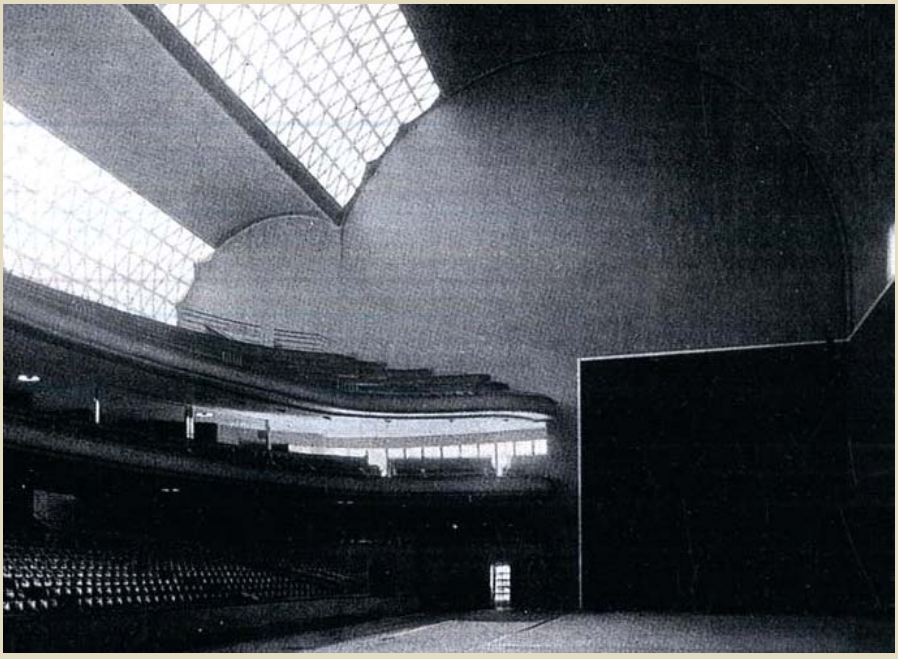

Master of Science Thesis
Stockholm, Sweden 2009

KTH Architecture and
the Built Environment

KTH Architecture and
the Built Environment

Cylindrical Thin Concrete Shells

Structural Analysis of the Frontón Recoletos roof

Jose Antonio Lozano Galant

May 2009
TRITA-BKN. Master Thesis 277, 2009
ISSN 1103-4297
ISRN KTH/BKN/EX-277-SE

Royal Institute of Technology (KTH)
Department of Civil and Architectural Engineering
Division of Structural Design and Bridges
Stockholm, Sweden, 2009

Preface

There are many persons who have been invaluable for the undertaking of this thesis. Some of them who have played a special role I will take the opportunity to acknowledge here.

First, I would like to acknowledge the "Instituto Torroja" for providing me the information necessary to know the Torroja's structure. Then, I would like to extend my deepest gratitude to my main supervisors Hakan Sundquinst and Ignacio Payá Zaforteza, who with never ending patience, have shared with me their great scientific knowledge and experience. Assistant supervisors Costin Lacoste, Jose Luís Ádam and Cárlos Lázaro deserve special acknowledgment. Special thanks to José Antonio Torroja and Javier Antuña for the interest showed and the help provided in the discussion of the results.

I am indebted to my mother Isabel, my father Jose Antonio, my brother Fidel, my grandparents, my girlfriend Monte and the rest of my family and friends, who have never failed to support me and are a constant source of encouragement.

Stockholm, May 2009

José Antonio Lozano Galant

Abstract

Geometry, truth, simplicity and art are the four cardinal points that guided the work of Eduardo Torroja and Frontón Recoletos is a clear example of its application as discussed throughout this thesis.

El Fronton Recoletos from conception was considered as a structural challenge because it incorporated many features that had not hitherto been studied in cylindrical concrete roofs: bigger size, absence of beam at the connection between the two cylindrical sections, skylights as well as asymmetrical directrix[1]. None of these conditions permitted the application of existing methods in 1930 when the design of the shell was raised. These methods were based on solving a system of equations that model the structural behaviour of the cylindrical thin concrete shells. However, far from surrendering Torroja adapted these methods to a number of simplifications in order to solve the problem by hand. Furthermore, this adaptation was conceived as a way to improve understanding of such structures so that at different stages of the design, the deflections and stresses were measured. Subsequently, analysis of these results was awarded by the Royal Spanish Academy of Sciences and published in order to promote the advancement of science. This thesis is proposed as a way to continue the legacy of Torroja checking the arguments and assumptions that were considered throughout the design process of this roof.

During the Spanish Civil War in the spring of 1937, the roof received several hits, which caused severe deformations in the structure. Soon after, a design to repair the structure was made. This design was based on reinforcement ribs in the bigger cylinder as it aims to recover the initial geometry through braces as well as increasing the rigidity of the structure. However, the night of the 15th August of 1939, the roof collapsed.

Given the impossibility of studying the structure at present, a structural analysis was based on the development of successive models with the finite element program Lusas. These models were based on the basic model used in the theoretical calculations carried out by Torroja and different assumptions were incorporated: consideration of variation in thickness, consideration of the wind suction effects, skylights as well as real concentrated supports, in order to bring the model closer to the real structure by steps. Finally, the reinforcement ribs proposed by Torroja were studied with the purpose of checking their influence on the roof.

Keywords: Thin, Concrete, Shell, Models, Torroja.

[1] Directrix: Orthogonal shape to the generators, which is based on two intersected circles.

Resumen

Geometría, verdad, simplicidad y arte son los cuatro puntos cardinales que guiaron la obra de Eduardo Torroja y el Frontón Recoletos es un claro ejemplo de su aplicación como se analiza a lo largo de la tesis.

El Frontón Recoletos fue considerado desde su concepción como un reto estructural debido a que incorporaba numerosas características que no habían sido estudiadas hasta entonces en las cubiertas cilíndricas de hormigón: mayor tamaño, ausencia de viga en la conexión entre las dos secciones cilíndricas, lucernarios así como la directriz asimétrica. Todas estas condiciones no permitían la aplicación de los métodos existentes en 1930 cuando se planteó el proyecto de la cubierta. Estos métodos estaban basados en la resolución de un sistema de ecuaciones que modelaba el comportamiento estructural de las cubiertas cilíndricas con espesor reducido de hormigón armado. Sin embargo, Torroja lejos de rendirse, adaptó estos métodos con una serie de simplificaciones para poder resolver el problema manualmente. Además, esta adaptación fue pensada como una forma de mejorar el conocimiento de este tipo de estructuras por lo que en las diferentes etapas del proyecto, las deformaciones y esfuerzos fueron medidos. Posteriormente, el análisis de estos resultados fue premiado por la Real Academia de Ciencias Española y publicado con el objetivo de favorecer el avance de la ciencia. Esta tesis se planteó como una forma de continuar el legado de Torroja comprobando los razonamientos e hipótesis que fueron considerados en todo el proceso de diseño de esta cubierta.

Durante la guerra Civil Española, en la primavera de 1937, la cubierta del Frontón recibió varios impactos, cuya onda expansiva causó severas deformaciones en la estructura. Poco después, fue realizado un proyecto con el fin de reparar la cubierta. Este proyecto estaba basado en unas costillas de refuerzo situadas en el cilindro mayor que tenían como objetivos recuperar la geometría inicial por medio de tirantes así como aumentar la rigidez transversal de la estructura. Sin embargo, la noche del 15 de Agosto de 1939 el techo colapsó.

Dada la imposibilidad de estudiar la estructura en la actualidad, se planteó un análisis estructural basado en el desarrollo de sucesivos modelos con el programa de elementos finitos Lusas. Estos modelos partían del modelo básico usado por Torroja en los cálculos teóricos e iban incorporando diferentes hipótesis: consideración de variación de espesor, consideración de las succiones del viento, consideración de lucernarios y consideración de apoyos reales, con el objetivo de acercar el modelo a la estructura construida. Finalmente, se estudiaron las costillas de refuerzo propuestas por Torroja para comprobar su influencia en la cubierta.

Palabras Clave: Hormigón, Espesor, Modelos, Torroja.

Contents

Chapter 1

Introduction

1.1 Purpose and Scope of the Thesis

My interest in the Frontón Recoletos was inspired by the enthusiasm and affection shown by Professor Ignacio Payá Zaforteza to this structure during my civil engineering degree in Valencia. After that, the great illusion and interest in the Torroja's work shown by Professor Hakan Sundquist and the proposal of the title by Professor Payá made me decide the Frontón Recoletos as a topic of my master thesis.

The Frontón Recoletos was conceived by Torroja as a way to improve the knowledge about the cylindrical thin concrete shells and therefore, the main purpose of this thesis is to continue the hard work shown by the designer through the study of the roof using existing computing resources: the finite element program Lusas.

The additional objectives of the thesis are as follow:

- Review the characteristics of the Frontón Recoletos shell.
- Study the state of the art of the cylindrical thin concrete shells.
- Analyze the Torroja's beliefs considered in the design of the structure.
- Analyze the theoretical methods used in the shell's calculations.
- Check the Torroja's simplifications.
- Study of the different innovative elements: skylights, supports and reinforcement ribs, incorporated in the Frontón Recoletos.

This thesis has been supported by three basic pillars: Firstly, the study of the state of the art of the similar cylindrical thin concrete shells. Secondly, the research and analysis of the characteristics of the Frontón Recoletos: constructions drawings, hypotheses, calculation procedure, analysis' results and structural Torroja's beliefs. Finally, the structural analysis based on the development of successive models, which consisted of incorporating different hypotheses to the basic Torroja's model used in the theoretical calculations, with the purpose of checking all the hypotheses carried out by Torroja.

1.2 Background

Shell roofs with single and double curvature have been commonly used by the nature for different purposes. The tree leaf (figure 1), for example, carries out the photosynthesis to obtain energy from the sun. Furthermore, these sheets are used by insects, like ants, to protect themselves from the rain. This knowledge was imitated and improved by different civilizations along the history. At the beginning, the humans only looked for these shapes in the nature to refuge it from the elements, using caves and other natural constructions. Afterwards, they were able to build new shell structures, like igloos (figure 1), to protect from the changes in temperatures. Finally, these shells were adapted to cover large spans in buildings, usually creating more appreciated structures than other kind of roofs without curvature.

Figure 1: *Tree leaf*: Double curvature structure in the nature and *Igloo*: Snow house originally constructed by indigenous people inhabiting the arctic regions, the Inuit.[2]

1.2.1 Material

The material has always conditioned the engineer's imagination, maybe more in this kind of constructions where the importance of the shape is indisputable. Frank Lloyd argued, "Each material has its own message to the creative artist" (Torroja 1962, p.24). Therefore, before designing any structure, it is necessary to understand the properties of the material to use. The first material used to build modern shell structures was stone which constructions were monolithic mass (figure 2). Afterwards, the stone masonry, technique where the stone was cut in equal pieces and assembled in layers, appeared. Soon after, some mechanical properties of the masonry structures were improved with mortar joints (Torroja 1962, p.25). The problem of the stone is the difficulty to materialize the shapes dreamed by the architect because this material needs great mass and cannot resist tension stresses.

[2] All the figures are described from left to right and the references are listed in the Figures' Chapter.

Figure 2: *Lion Gate* in Greece: Stone gate constructed in 1350 B.C. and the *Agrippa's pantheon* in Rome: Temple of all the gods made of unreinforced concrete with pozzuolana.

The vast majority of the current shell structures have been constructed of concrete or reinforced concrete. This material was similar to the stone masonry and was used since centuries ago by different old villages, like Romans (Torroja 1962, p.31). The first concrete was easily mouldable but it was relatively week in tensions. As a result the span to thickness ratios obtained, were less than 50:1 (Chilton 2000, p.12). A well-known example is the Agrippa's pantheon (figure 2), the oldest standing domed structure in Rome made of unreinforced concrete with pozzuolana joints. In this cupola, the ratio varies between 6.4:1 and 44.8:1. Afterwards, the reinforced concrete incorporated another advantage: tensions were resisted by steel bars. This material was described by Eduardo Torroja, as "technically the most nearly perfect material" (Torroja 1962, p.56) With the reinforced concrete the increase of the span to thickness ratios was possible; for instance the reinforced concrete roof structure of the Eduardo Torroja's sporting hall Frontón Recoletos had a ratio of 680:1.

Other materials such as prestressed concrete, material applied in the Sidney Opera (figure 3), or steel fibre reinforced concrete (SFRC), used in L'Oceanográfico (figure 3), can also be used in order to increase this ratio. However, when the ratio is increased some problems like buckling can easily appear in the structure. Furthermore, the structural behaviour is more difficult to understand due to the growing complexity of the stress distribution.

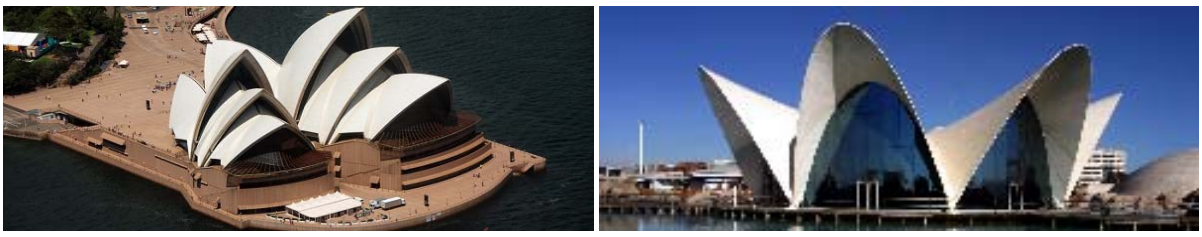

Figure 3: *Sidney Opera* designed by Jørn Utzon in 1973 and made of prestressed concrete and *L'Oceanogràfic* in Valencia: Structure inspired by Felix Candela's designs and constructed of steel fiber reinforced concrete.

1.3 Why shells are used in Engineering

"In order to successfully conceive and to plan a structure or building of any kind it is necessary to investigate and to know well its reasons for existence, its major and minor capacities to resist and to bear" Eduardo Torroja (Torroja 1962, p.1).

Natural shells have been studied by numerous architects and engineers in order to design organic shapes in their structures. These shapes are generally more attractive than the designs based on the straight line. For example, the relaxation park designed by Toyo Ito in Alicante (figure 4) shows different buildings inspired by the natural shell shape. Nevertheless, not only the aesthetic characteristics are improved with these designs because the structural behaviour is also usually better. Heinz Insler explained this characteristic by the next experiment (Chilton 2000, p.12): He made two surfaces of thin plastic with the same volume of material. The difference between these sheets was the curvature. The first surface was flat and the second one had curvature in two perpendicular directions, like a cupola. Then he put the same weight over the both structures. As a result, Insler stated that the single-double curved structures are much more efficient than the flat plate because the applied forces can be resisted with fewer deformations and stresses.

Figure 4: *Relaxation Park* in Alicante designed by Toyo Ito: Building made of wood.

The efficiency of load-carrying behaviour explained by Insler is only one more of the numerous advantages of the shell structures. For example, shells structures are much superior to other structural system having the same span and overall dimensions because these shapes have a high strength to weight ratio, this criterion is commonly used to estimate the structural component efficiency. Furthermore, more slenderness and lighter structures can be constructed adapting better the shape to the requirements of the building (Torroja 1962, p.96).

The most structural efficient shell's form is different for each design, according to the building local conditions, and has to be found by the designer. There are different methods to determine the shape of the shells' structures. For example, the technique used by Gaudí to design the Sagrada Familia (figure 5) in Barcelona was founded on the principle that a loaded structure in pure tension, like centenarian (figure 5), when inverted will be the perfect form for a similarly loaded pure compression structure. This technique was used by Heinz Insler to design more than 1000 shells.

Figure 5: *Sagrada Familia* in Barcelona and *Antonio Gaudí's reversed model* used to determine the forces in pure compression.

The essential geometrical property of all the shell structures that distinguishes then from other structural forms is the possession of both "surface" and "curvature" providing strength and stiffness (Calledine 1983, p.3). Therefore, many shell structures have been constructed with the purpose of providing roofing for temples, cathedrals, monuments or other buildings. Nevertheless, besides of roofing, shells find application in many other fields. For example, the shell's shape is used to cover the Fedala water tank (figure 6) designed by Torroja.

Figure 6: *Fedala water tank*: hyperbolical-concrete silo for the storage of water in Morocco.

1.4 Classification of shells

There are many different ways to classify shell structures. In order to better understanding the cylindrical thin concrete shells, they were catalogued by three different criterions. The first criterion was the material, which the shell is made of: like reinforced concrete, plywood or steel, because each one has different properties that can determine the shape of the building and therefore, these characteristics have to be considered in the design. The second consideration is the shell thickness: the shells can be thick or thin. A shell is called "thin" if the maximum value of the Ratio A (formula 1) can be neglected in comparison with unity, in other cases, are called thick. Finally, the last criterion, which is explained in this section, consists of using the shell Gaussian Curvature to classify the shape.

$$Ratio\ A = \frac{Thickness}{Radio\ in\ the\ middle\ surface} \qquad [1]$$

1.4.1 Gaussian Curvature

The geometry of the shell is completely described by the curved shape of the middle surface and the thickness of the shell at all points. The Gaussian curvature K_g is the product of the two principal curvatures (formula 2), the maximum and the minimum, and it is used in order to classify the shells in three different groups, according to the K_g sign (Calladine 1983, p.124): synclastic shells, anticlastic shells, both with double curvature, and developable shells with simple curvature. There is other one additional group, free-forms structures, which cannot be classified by the curvature.

$$K_g = K_1 \cdot K_2 = \frac{1}{r_1 \cdot r_2} \qquad [2]$$

where, r_i =*Principal ratio of curvature in each direction* (Calladine 1983, p.156).

The synclastic shells are those with positive Gaussian Curvature at a given point of a curved surface, such curvatures occurring in the two principal planes, which are perpendicular to each other. For these surfaces, the centres of maximum and minimum curvature at a given point lie on the same side of the surface. A dome is an example of synclastic shell; it is a space structure covering a more or less square or circular area. The domes of revolution are formed by a surface generated by a curve of any form revolving about a vertical line. This surface has double curvature. The simplest dome of revolution is a portion of a sphere. However, other curves are also satisfactory, such as the ellipse, the parabola, other conic sections, or random curves. A well-known dome is the Palazzetto dello Sport (figure 7), designed by Pier Luigi Nervi in 1958, which was made of ribbed reinforced concrete. The most remarkable factor of this structure is the lower half of the dome, which consists of continuous windows around the circular stadium.

Figure 7: *Palazetto dello Sport* (Roma) designed by Nervi.

Other important example is the Kupolen Exhibition Hall and Sports Arena (figure 8) constructed in 1989 in Sweden by Hakan Sundquist and T. Granaht. This design consisted of a dome structure with a free span of 123 meters made up with beam elements. The erection of the dome was done using an innovative system based on no false work, similar to the procedure used in the construction of the snow igloos.

Figure 8: *Kupolen Exhibition Hall and Sports Arena* (Sweden) designed by Sundquist.

The second group classify by the Gaussian curvature is the developable[3] shells. These surfaces as the name implies, are those that can be flattered into a plane superficies, either directly or after making a simple straight-line cut in the surface. These shells are characterized by zero Gaussian curvature and are singly curved. The most common shape of this kind of surfaces is the barrel, semicircular or parabolic. These shapes are less resistant than the doubled curved surfaces and usually need additional flexural strength to resist the effects of wind. An innovative solution to solve this problem was used in the Hangar d'Orly (figure 9) by Eugene Freyssinet in 1923. In this structure, the flexural strength was increased using a surface, which shape was similar to the accordion membrane. This procedure to increase the lateral stiffness can also be applied by means of the combination of folded plates as for example in the church designed by Willian Gooden in Las Vegas (figure 9).

[3] The possibility to be developed or not is a geometrical property of the surface. Shells that cannot be developed, like surfaces with double curvature, require more energy in order to be deformed. Therefore, these surfaces are stronger and more resistant than shells that can be developed however, the frameworks are more complex and expensive (Billington 1979, p.20).

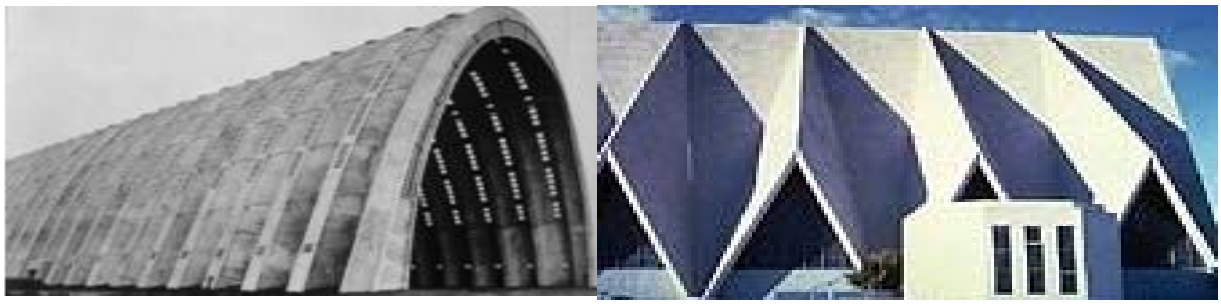

Figure 9: *Hangar d'Orly* designed by Freyssinet, and *church building* in Las Vegas designed by Gooden.

The next group is the anticlastic shells. These surfaces are characterized by negative Gaussian curvature and therefore, the centres of maximum and minimum curvature are located on opposite sides of the surface. Well-known examples of this kind of shells are the conoids, hyperbolic paraboloids and hyperboloids. The structural behaviour is different for each shape. One of the most appreciated examples of this kind of surfaces is the restaurant designed by Félix Candela in 1955 called Los Manantiales (figure 10). This roof consists of four hyperboloid paraboloids intersecting to form an octagonal and very innovative shape, which has inspired the design of current structures like the L'Oceanográfico in Valencia (figura 3).

Figure 10: *Los Manantiales* restaurant designed by Candela.

An additional group that cannot be classified by the Gaussian curvature is the free-form structures, because these shapes do not have principal directions of curvature. These surfaces allow much greater versatility and freedom of form than the preceding described surfaces. The free-form shells can be analysed by different methods like combinations of simple regular shell forms or experimenting with small shell models. An innovative irregular shell structure is The Trans World Airline Terminal (figure 11) designed by Eero Saarinen in 1962. This structure is located at Kennedy International Airport in New York. The design was based on the Saarinen's words "I want to catch the excitement of the trip" (Saarinen 1962, p.115). This shape can be considered as a giant bird with it wings spread out ready for flight. This shell is an example of how the freedom of form can be used to carry out the designer's aesthetic thoughts.

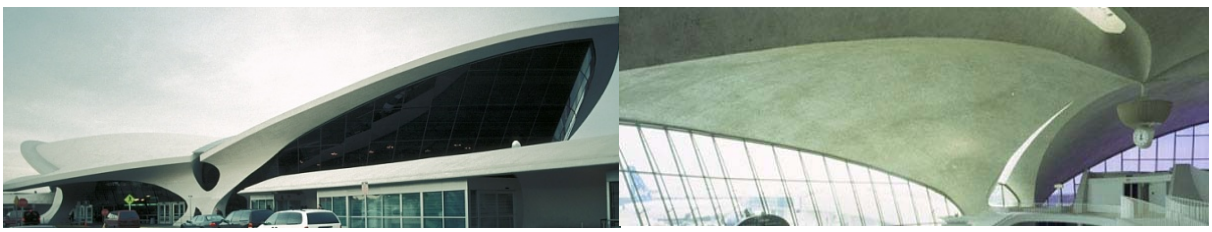

Figure 11: *Trans World Airline Terminal* in New York designed by Saarinen.

1.5 Thin Concrete Shells

The thin concrete shell structures are a lightweight construction composed of a relatively thin shell made of reinforced concrete, usually without the use of internal supports giving an open unobstructed interior. The shells[4] are most commonly domes and flat plates, but may also take the form of ellipsoids or cylindrical sections, or some combination thereof. Most concrete shell structures are commercial and sports buildings or storage facilities.

1.5.1 History

There are two important factors, the shape and the thickness, to be account to better understanding the evolution of the thin concrete shell structures (figure 12). The first factor was developed along the history of these constructions: The pioneer structures, as the dome in Jena, can be classified as synclastic shells. As it was explained before, these shapes are more resistant and can be erected easier than other surfaces with single curvature. Afterwards, different developable shapes, principally consisted of barrel structures, like the elliptical barrel build in Frankfurt in 1927 or the shallow circular barrel constructed in Budapest in 1930, were constructed. However, the designer's incessant desire for more ambitious structures did not stop and new shapes, consisting of intersected barrels, were designed. The most famous examples of these shapes are the Frontón Recoletos and the Iglesia de Villaverde, which span to thickness ratios were 690:1 and 500:1 respectively. The second factor to be considered in the thin concrete shell structures is the thickness, which is usually less than 10 centimetres. For example, the thickness of the Hayden planetarium was 7.6 centimetres (Appendix B.2).

[4] A primary difference between a shell structure and a plate structure is that, in the unstressed state, the shell has curvature as opposed to plate surface, which is flat. In this chapter, only the thin concrete shells structures with curvature, which have the same structural behaviour of the Frontón Recoletos were studied.

Name of construction	Year	Location	Type	w(m)	L(m)	d(m)	h(cm)	Ratio
Dome at church of St. Blasten	1912	St. Blasten,Germany	Shallow dome	34	34	5,3	12	250:1
Century Hall	1913	Breslau, Germany	Hemisphere	65	65	32	Ribs	
Test Planetatium	1922	Jena, Germany	Hemisphere	16	16	8	3	535:1
Zeiss Works Factory 23 Roof	1924	Jena, Germany	Barrel	19	7	9	6	315:1
Schott Dome	1925	Jena, Germany	Shallow dome	40	40	7.9	6	665:1
Werft Hall	1925	Neuss, Germany	Barrel	12	16	3.8	4	400:1
Test Barrel Shell	1925	Biebrich, Germany	Elliptical barrel	4	6	1.8	1.5	400:1
Dywidag Exhibition Hall	1926	Duesseldorf, Germany	Elliptical barrel	12	23	3.5	5.5	460:1
Test barrel shell, 1/3 scale	1927	Frankfurt, Germany	Elliptical barrel	4.7	12	1.3	2.3	520:1
Wholesale market hall	1927	Frankfurt, Germany	Circular barrel	14	37	4	7	530:1
Hangar	1927	Kowno, Lithuania	Shallow circular barrel	8.2	20	1.4	6	335:1
Market Halls	1929	Leipzig, Germany	Octagonal domes	76	76	30	9	845:1
Wholesale market hall	1930	Budapest, Hungary	Shallow circular barrel	12	40	1.9	6	665:1
Katschuppen	1930	Hamburg, Germany	Shallow circular barrel	9.2	24	2.5	5.5	435:1
Salt storage hall	1930	Tertre, Belgium	Short barrel	44	11	14,4	6	735:1
Dischinger shell	1932	Biebrich, Germany	Dome on square plan	7.1	7.1	1.7	1.5	475:1
Flight school hangar	1933	Kottbus, Germany	Short barrel	35	40	12.3	9	445:1
Hayden Planetarium	1934	New York, U. S.	Hemisphere	25	25	25	7.6	335:1
Fronton de Recoletos	1935	Madrid, Spain	Intersected circular barrels	32.5	55	24.4	8	690:1
Iglesia de Villaverde	1935	Villaverde, Spain	Intersected elliptical barrels	17.5	25		5	500:1
Hershey Arena	1936	Pennsylvania. U.S.	Short barrel	68	12	8	9	755:1
U.S. Army Warehouses	1941	Ohio. U. S.	Circular barrel	14	12	2.2	9	155:1
Signal Corps Hangar	1942	Ohio. U. S.	Short barrel	49	12	11	9.5	515:1
Budd Manufacturing Plant	1943	Pennsylvania U.S.	Short barrel	37	6.1	8.5	9.5	390:1
Garage Shop Hangar	1943	Virginia U.S.	Short barrel	49	12	11	9.5	515:1
North Hangar	1944	Maryland U.S.	Short barrel	53	10	12	9.5	560:1
U.S. Air force Hangar	1948	South Dakota U.S.	Short barrel	104	7.6	23	13	800:1
Western Electric Warehouses	1948	Denver U.S.	Shallow circular barrel	15	15	2.3	9.5	160:1
U.S. Air force Warehouses	1958	Pennsylvania. U.S.	Shallow ribless barrel	12	20	2.3	7.6	265:1

Figure 12: *Thin concrete shell structures*. The characteristics are width in metres, w (m), length in metres, L (m), diameter in metres, d (m), thickness in centimetres, h (m), and the span to thickness Ratio[5].

The modern era of thin concrete shells began in 1922 with the construction of the dome in Jena, Germany (figure 13) by Frank Dischinger of the German engineering firm Dyckerhoff and Widmann (Hines 2004, p.1641). This modern structure was 16 metres in diameter, 30 millimetres thick and the span to thickness ratio was near to 550:1. In 1934 Anton Tedesko, another Dyckerhoff and Widmann engineer, introduced the thin concrete shells in U.S. with a hemisphere structure called Hayden[6] planetarium in New York (figure 13), which ratio was approximately 330:1 (Hines 2004, p.1642).

[5] The span to thickness Ratio was calculated dividing the maximum value of span, defined as the maximum value between the diameter and the width, by the shell's thickness.

[6] Several important thin concrete shell structures have recently been demolished, including the Hayden planetarium in New York in 1997 due to the functional obsolescence and maintenance problems.

Figure 13: *Dome in Jena* designed by Dischinger and the *Hayden planetarium* in New York designed by Tadesko.

Between the 1920s and 1960s, considered the "golden age of thin shell structures" (Meyer 2005, p.44), these constructions were developed as an engineering solution in order to achieve large spans for industrial, commercial or public structures and it were embraced by the architectural profession as a potent means of architectural expression. Some of the most important shell designers in this period, whose "advanced the state of the art" (Meyer 2005, p.43), were Pier Luigi Nervi, Eduardo Torroja, Heinz Insler and Felix Candela.

Subsequently, after these three decades, the number of new concrete shell structures constructed declined noticeably (Meyer 2005, p.44) due mainly to the high cost of construction and removal of temporary formwork and associated falsework for concrete casting in the construction of a thin concrete shell. This labour intensive and costly process of construction, coupled with the increasing ease in analyzing complex skeletal spatial structures offered by advances in computer technology, has made concrete shells much less competitive than they were few decades ago.

Over the years, there have been several methods for eliminating the need for temporary formwork in the construction of thin concrete shell roofs. Until now, the most successfully techniques have been on one hand, the use of inflated membranes as forms. On the other hand, the use of precast concrete panels with in-situ cast joints. Both methods are explained a in this section.

The inflated membrane method was appreciated by many engineers. For example, the President of Monolithic Constructors and Chair of Joint ACI-ASCE Committee 334, David South, argued that "The construction of thin shells nearly came to a standstill until inflated membrane forms were introduced" (Meyer 2005, p. 44).

The origin of the inflated membrane forms, also known as air-inflated forms, was in 1942 when Wallace Neff received a patent on a system where the form was inflated to the shape of the structure, and after that, the reinforcing bar and shotconcrete were placed on the exterior of the structure. Particularly noteworthy was the system invented by Dante Bini. In this method, in approximately 120 minutes, the formwork is constructed. Final forms are spherical sectors with radius less than 40 metres. The Bini's system is divided into two successive phases. Firstly, the reinforcing steel and concrete are placed over a layer of fabric while it lies flat on the ground. Finally, the fabric is inflated by air pressure in order to create the shell form (figures 14 and 15).

Figure 14: *First phase of the Bini's System.*

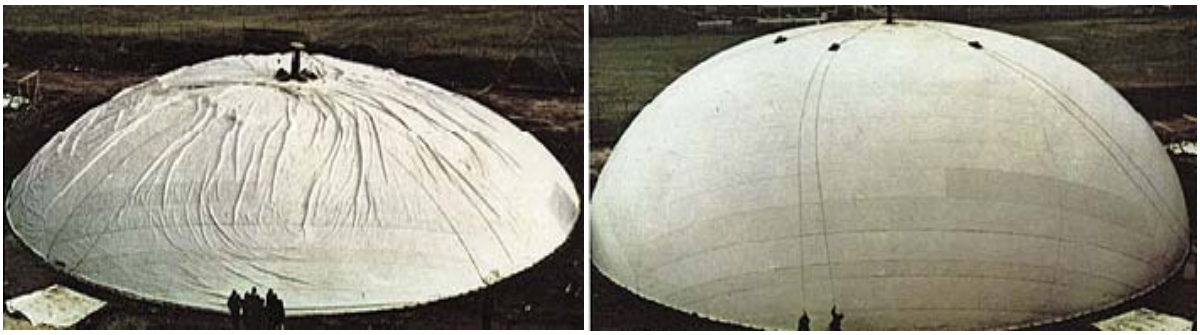

Figure 15: *Second phase of the Bini's System.*

In the late 1970s, David and Barry South developed other system, which consisted of a shotconcrete applied to the inside of an inflated fabric form (figure 16). This technique had some differences compared with the Bini's System: First, shell is inflated using polyurethane foam. This material gives the form the stiffness required to support the weight of reinforcing steel placed on the inside. The second difference is that the shotconcrete is applied to the interior of the form when this shape has been inflated. According to David South, spans of up to 300 meters can be obtained using this technique (Meyer 2005, p.45).

Figure 16: *Inflating process* using polyurethane foam and *Application of the shotconcrete.*

The shells constructed by inflated membrane techniques have some disadvantages. Firstly, the shape and thickness of the shell as well as the position of reinforcement is difficult to control during the construction process. The second problem is that these techniques require the use of special construction equipment increasing the cost of the roof. Lastly, these methods are limited to the construction of circular-based domes with a spherical or nearly spherical meridian and therefore, the architect has less freedom in their designs because the shape of the formwork cannot be practically changed.

One innovative method designed to reduce the cost of the formwork is the Precast concrete panels with in-situ cast joints. In these structures, the formwork consists of small-prefabricated panels, which are transported to the site for assembly into a shell (figure 17). Joints between these panels are sealed by in-situ casting of concrete. The latest development in the forming of thin concrete shell roofs is the steel-concrete composite shell system, also called Comshell system, which "is believed to be a solution to the difficult problem of forming" (Wong 2004, p.180-189).

Teng was the first who defined this system: "The Comshell roof is a steel-concrete composite shell roof formed by pouring concrete on a thin steel base shell which serves as permanent formwork as well as tensile steel reinforcement. The steel base shell is constructed by bolting together modular steel units (figure 17) in the form of an open-topped box consisting of a flat or slightly curved base plate surrounded by edge plates" (Teng 2001, p.102).

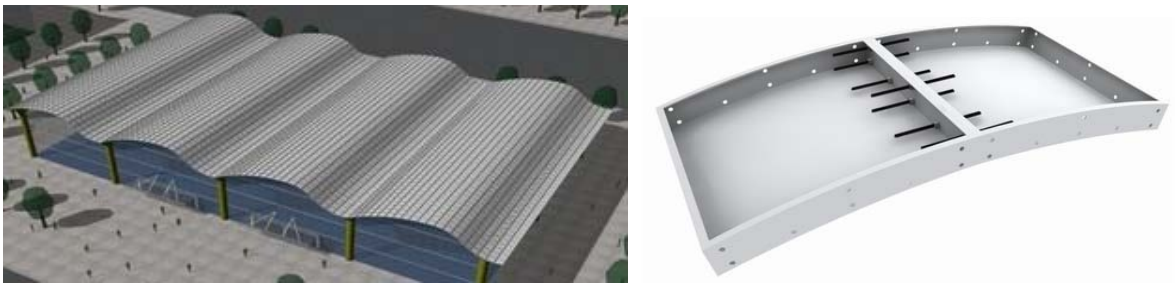

Figure 17: *Modular steel units* and *real structure* formed by the Comshell system.

The main disadvantages of the method are the following: Firstly, extra work in transportation and assembly of the elements is required. Secondly, the Comshell system is being studied and the structural behaviour of the structures made of this technique is not well known yet.

The future of thin concrete shells is based on the forming-problem solution. Medwadosky argued, "Forming remains the great, unsolved problem of construction of concrete thin shell roofs. Any and all ideas should be explored, without prejudice." (Medwadosky 1998, p. 21) Therefore, science has to find new systems to obtain the shape of the structure using the imagination as well as new construction techniques.

1.5.2 Characteristics

Since the beginning of the architecture, the designers have dreamt about one light surface, like the skin used in the ancient tents or in the African villages (figure 18), to cover large spans in buildings (Torroja 1976, p.69). This dream, considered before as unachievable, was come truth when appeared the thin concrete shells. The material of these structures was able to be casted forming any imaginable shape. For example, the tent's shape was imitated by Candela in the Lomas de Cuernavaca's shell (figure 18).

Figure[7] 18: *African tent* in the Sahara desert: the surface is made of sheepskin, *Sami tent* and *Lomas de Cuernavaca* designed by Candela.

The thin concrete shells are designed with the purpose to resist loads through membrane forces. These forces consist of compression stresses, resisted by the concrete, and tension stresses, resisted by the reinforcement bars made of steel, in the direction of the tangent plane. Consequently, shells made of reinforced concrete can resist moderate bending stresses and be constructed thinner and lighter. Nevertheless, when the bending moments are needed in order to achieve the equilibrium of the shell, the thickness and the reinforcements bars have to be increased and therefore, the advantages of the thin concrete shells are reduced (Torroja 1976, p.79).

These structures are constructed by casting onto a mould called formwork, which is kept in place until the concrete has hardened. When the formwork is removed, the shell is obliged to carry its own weight. The shell exists originally under condition of effectively zero gravity in a perfect shape, and with zero stress throughout. Afterwards, at a certain time, gravity is switched on, and the shell thereafter carries its own weight. To improve the structural behaviour, the formwork tends to provide single or double curved surfaces. Furthermore, the curved surfaces made of reinforced concrete, above all the synclastic shells, are naturally

[7] The elements are described from up to down and from left to right.

strong structures, allowing wide areas to be spanned without the use of internal supports, achieving an open and unobstructed interior usually pursued by the designer.

In addition to the possibility of covering areas without internal supports, the thin concrete shells have the following benefits. Firstly, the efficient use of the material because the structural lightness is the common starting point in designing. Secondly, the method of construction has been used since the concrete was discovered and is therefore well known. Thirdly, the concrete is relatively inexpensive and easily cast into desired curves. Finally, the thin concrete shells offer the possibility of more visually interesting geometries to improve the aesthetic value of the building.

Thin concrete shells have historically had the following problems: Firstly, functional obsolescence because the small thickness makes worse the bars isolation and corrosion can occur easily. Secondly, the structure has to be intensely maintained in order to avoid the functional obsolescence and this factor increase the future cost of the building. Thirdly, rainwater can seep through the roof and leak into the interior of the building because the concrete is a porous material and therefore, this material is usually complemented with waterproof isolation. Fourthly, the thin thickness produces that these structures usually need thermal and acoustic insulation. For example, the air chamber layer and the cork are used to improve the thermal conditions. Nevertheless, today the main problem of the thin concrete shell structures is that the cost to erect the formwork is considered prohibitive in Europe. This cost depends of the type of formwork. For example, structures with double curvatures as domes are difficult to erect and makes it necessary to cut the panels individually into non-regular shapes and therefore, the cost of the formwork is higher. Edward DePaola mentioned that the best way to reduce the cost of temporary formworks is to develop alternate construction techniques like innovative forming systems: "Flexible and easily adjustable forms would make complicated shapes easier and much less expensive to build" (Meyer 2005, p. 46).

The problem of the forming cost could be the main explanation for the decrease of popularity of the thin concrete shells all around the world. An interesting proposal suggested by John Abel of Cornell University with the purpose of reducing this cost, was based on the collaboration between the designer and the builder "the designer can work with the builder to devise construction processes that are efficient, for example, by together designing reusable form modules that are appropriate for the shell" (Meyer 2005, p. 48). This proposal was used by successful shell designers, such as Torroja in the Frontón Recoletos, who maintained close relationships with the builder of this shell, Secundino Zuazo, to both train them in proper shell construction techniques as well as to sharpen their own insight into effective design and construction procedure. Nevertheless, the work of Heinz Isler is an example that spectacular shells are still constructed. Therefore, the cost cannot be the only explanation of the current loss of popularity, according to Meyer “such cost reductions alone will not be sufficient, as thin concrete shells need to be repopularized and reintroduced into the minds of builders if they are to be considered as a viable structural solution at all” (Meyer 2005, p.48).

1.5.3 Designers

Some of the most important designers of cylindrical thin concrete shells were Eduardo Torroja, Félix Candela and Heinz Insler. In this chapter, some of the most important factors of these designers are analyzed.

The first designer analyzed is Eduardo Torroja (1899–1961), which was one of the most innovative engineers of the early twentieth century, notable for the exceptional use of the reinforced concrete and its application to the thin shell structures in Spain. His work was based on three basic pillars. Firstly, the philosophy of the structures: Many different architects and engineers have been influenced by the Torroja's structural thought among, which stand out the next three: the integration of the functional and structural requirements in the structure, the perfect correlation between the real nature and the apparent form of the work, as well as the formal and structural simplicity. Secondly, the geometric: Influenced by his father, Eduarto Torroja y Caballé, Torroja looked for new innovative shapes in his designs. Well-known examples are the hyperboloids applied in the Hipódromo de la Zarzuela and Fedala water storage (figure 6). Thirdly but not least important, the art: Torroja's aesthetic interest began to shine already in his first works, for example in the Tempul aqueduct (figure 19), constructed in 1925, the designer included arches between supports of the tension members where the faster solution would have been putting a simple straight line (Torroja 2007, p.98).

The main characteristics of one of the most emblematic Torroja's structures, the Market Hall in Algeciras, were studied in order to better understanding the conception of the design and the application of Torroja's thoughts.

The Market Hall (figure 19), constructed by Torroja in Algeciras (Spain) in 1933, is a splendid octagonal space enclose with a bold lamella roof with 47.8 metres diameter and only 9 centimetres thickness, which is supported by eight pillars. This structure shows the three Torroja's thoughts, explained before, which hold the design up. The first belief is that the architectonic requirements were integrated in the structure. On one hand in the shell that carries out different complementary functions: encloses the space, acts as enclosure without the need of additional elements and allows that the sun light shines by the nine skylights[8]. On the other hand, in the connection between the wall and the shell: the structure does not use any kind of raking shores in order to resist the forces transmitted. The shores usually allow improving the shell aesthetic. For example, these additional elements were used in the Palazzetto dello Sport, constructed by Nervi, to bring the beauty of the shell's interior view out (figure 7). Nevertheless, Torroja did not use the shores in the Market Hall because in his aesthetical beliefs was enough with the bare geometrical shape (Torroja 2007, p.100). The second thought observable in the structure is that geometric is used to join the sphere with the radial cylindrical vaults defining a shape apparently simple for the observers. Finally, the last belief is the importance of the structural truth. This thought is appreciable, for example in the structural behaviour, which is easily understood and not hidden.

More examples of the Torroja's thoughts are presented in the Appendix D.

[8] The skylights are located at the top of the roof as well as at the connection between the walls and the octagonal shell.

Figure 19: *Aqueduct Tempul* and *Market Hall* in Algeciras both structures designed by Torroja.

The second analyzed designer is Félix Candela (1910-1997), which is acknowledged as a master builder and structural artist who designed and constructed great thin shell concrete roof structures. However, he never took a formal course on this kind of constructions and all Candela's knowledge was acquired on his own reading articles and experimenting with the forms. This way of understanding the thin concrete structures, based on full-scale models, provided a new method of designing and building innovative structures, as for example the Restaurante Los Manantiales (figure 9), which is based on the hyperbolic paraboloid form.

Finally, the third analyzed designer is Heinz Insler, which is a Swiss engineer and a pioneer for shell-form designs whose works transcends the definition of mere structural engineering to the extent of becoming structural art.

The environment observed by Insler, for example pillows or flowers, has inspired his thin concrete shells. These forms are calculated by experiment using catenary models, instead of by sophisticated mathematical method, (Chilton 1979, p.32) in much the way that Antonio Gaudí had used (figure 20). A well-known example is the Deitingen service station on A12 motorway in Switzerland constructed in 1968 (figure 20).

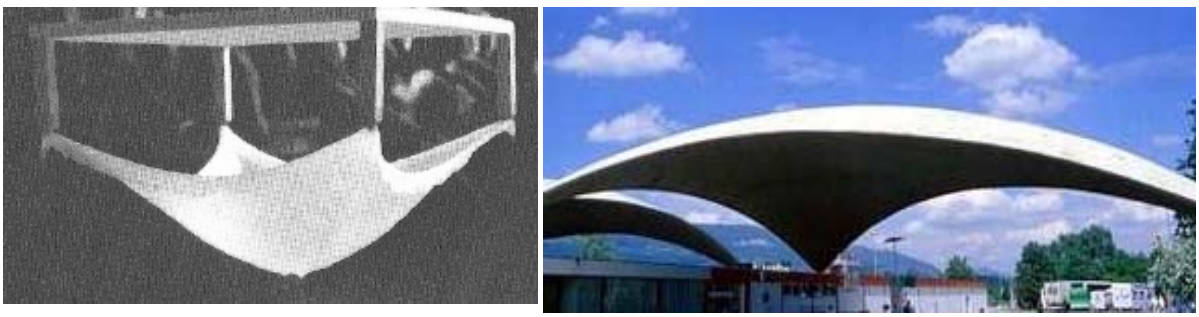

Figure 20: *Hanging membrane model* generated by self-setting polyester resin and *Station-service* in Deitingen designed by Isler.

1.6 Cylindrical Thin Concrete Shells

The cylindrical thin concrete shells should not be confused with the vaults, despite the huge similarity in the shape of both structures, because each of these structures has a different structural behaviour as well as different requirements in the minimum thickness and the trace of the directrix. On one hand, the structural behaviour of the vault is based on connected parallel arches, which transmit the same effort to the supports (figure 21). Therefore, the materials used in these structures have to be able to resists compressions and the thickness is usually higher. For example, stone has been commonly used as material for the vaults and the spans to thickness Ratios for this material are usually less than 50:1. Furthermore, the directrix shape of the vaults must be as similar as possible to the arch in order to achieve the optimum structural behaviour. On the other hand, the structural behaviour of the cylindrical thin concrete shell is similar to a longitudinal beam along the generator directions (figure 21) and therefore, the materials have to resist both compression and tension stresses. This factor takes advantage of the bars of the reinforced concrete, because these elements can be placed where tension forces are needed and therefore, the span to thickness Ratios can be increased. Furthermore, the directrix shape has fewer requirements than the vaults and therefore, new curves like the ellipse or the parabola can be used improving the aesthetic quality of the structure (Torroja 1976, p.69-71).

The cylindrical thin shells, also called barrels, can be classified in three different groups: long barrels, short barrels and intermediate barrels. The differences between these groups are the relation between the span and the width as well as the structural behaviour.

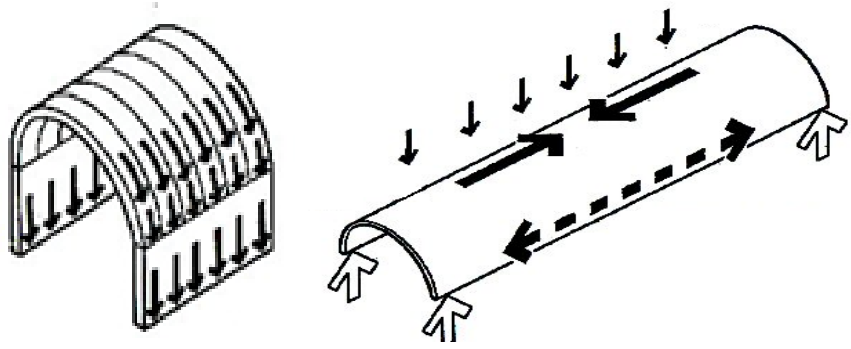

Figure 21: *Structural behaviour of the vault* and *structural behaviour of the long barrel*

The most efficient structural behaviour of thin shells is obtained when these structures are working as membranes. The membrane is able to resist the applied loads acting only compression and tension in the tangent plane. Nevertheless, sometimes these stresses are not enough to resist the applied loads and other forces, like the transversal bending moments regarding the middle surface, have to provide additional resistance. When the bending moments are needed, the thickness and the framework of the shell have to be prepared to resist these stresses. Furthermore, considering the bending moments in the shell structures means more difficult and less intuitive calculations as well as an increase of the thickness. When the thickness is increased the main load, the dead weight, is higher and the benefits of the thin concrete shells decreased.

The structural behaviour of the cylindrical thin concrete shell is more similar to the membrane when the wall, where the directrix is supported, is more rigid. For example, this increase of the stiffness was used the Frontón Recoletos by means of vertical and transversal stiffener

beams (figure 22), which connected the shell with the wall. The holes between the shell and the wall were filled with bricks to achieve the continuous surface for playing pelota game (figure 23 and 24). However, even with these rigid walls, the structure is not able to work as a pure membrane and additional bending moment resistance is needed. This bending resistance depends on the shape of the directrix and usually means to increase the cost of the structure (Torroja 1976, p.79).

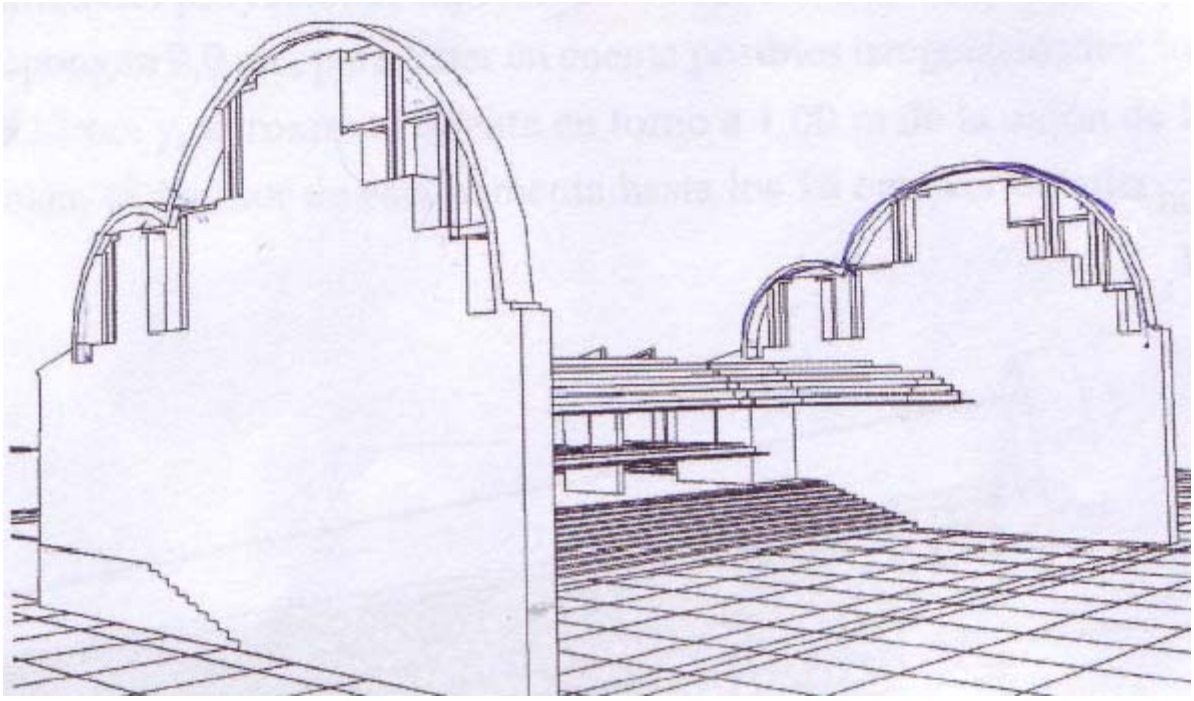

Figure 22: *3-D model of the front walls.*

Chapter 2

Frontón Recoletos

The Frontón Recoletos (figure 23 and 24) was constructed in 1935 in the Villanueva Street in Madrid. This structure consisted of a sport facility building designed to play pelota game, also called jai alai. The roof is based on a thin concrete shell formed by the intersection of two cylindrical sectors and was considered one of the most emblematic structures in the 30s.

The Frontón recoletos was designed by the collaboration of two complementary specialists: one architect, Secundido Zuazo, and one engineer, Eduardo Torroja.

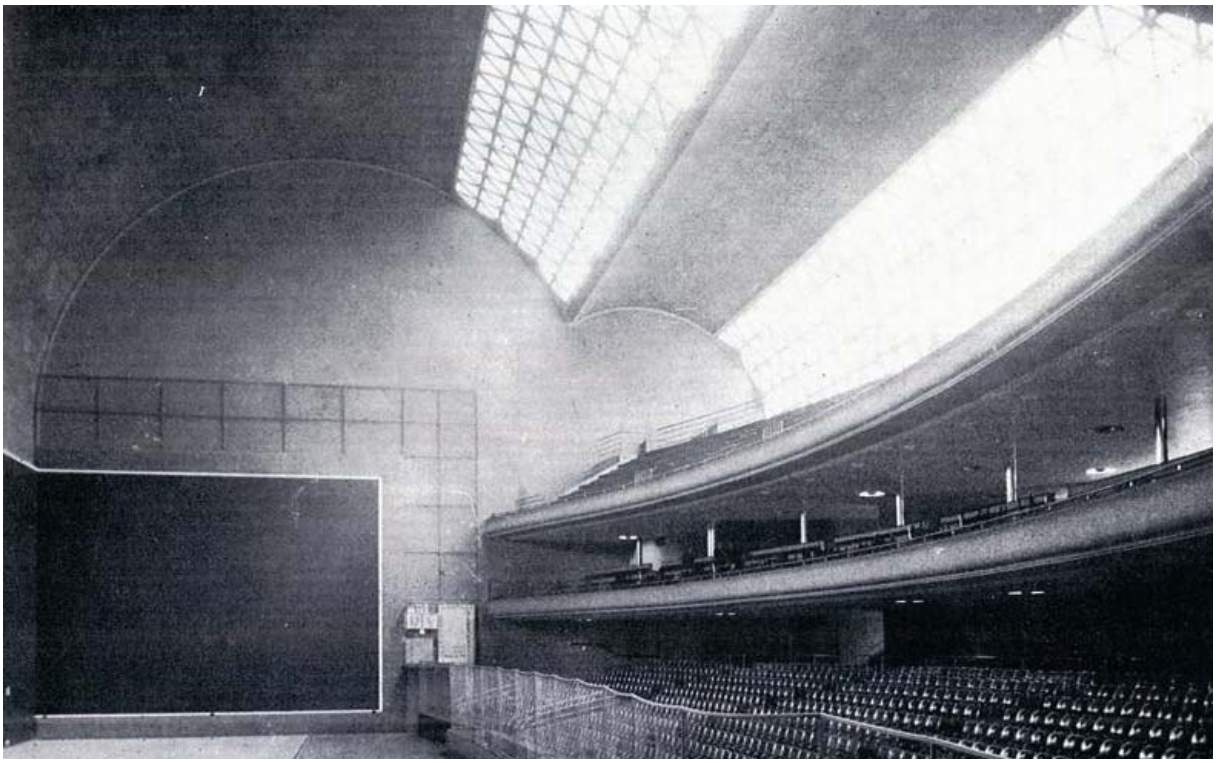

Figure 23: *Picture of the inside of the structure of the Frontón Recoletos.*

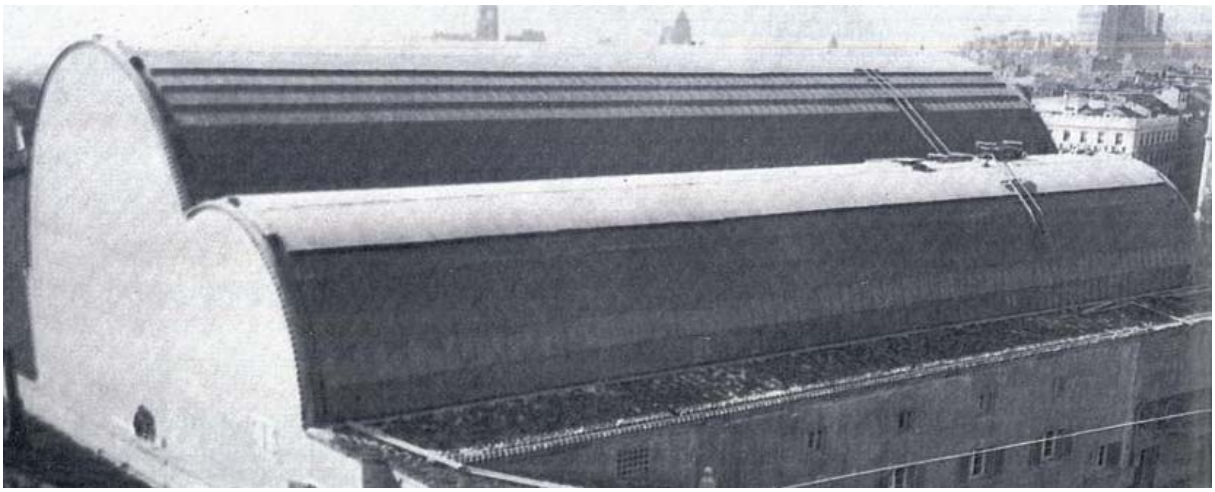

Figure 24: *Real picture of the outside of the structure of the Frontón Recoletos.*

The roof of the Frontón Recoletos was considered a structural challenge since the conception of the structure for different reasons: Firstly, the overall dimensions, 55 per 32.5 metres, were higher than the similar roofs constructed before (figure 25), as for example the Budapest shell, which dimensions were 40 per 11.6 metres (Appendix B.1). Secondly, the shape of the roof incorporated two innovations that it had never been constructed before in this kind of structures: On one hand, the asymmetric directrix without beam at the connection between both cylindrical sectors. On the other hand, the roof included two longitudinal skylights consisted of a lattice frame of equilateral triangles. Lastly, the roof had a variation of thickness, from 8 centimetres, at the big lobe, to 30 centimetres, at the connection of both cylinders. Consequently, the span to thickness Ratio (Appendix B.1) was 690:1. This value was higher than two times the radio obtained in the first cylindrical thin concrete shell, constructed in Jena, which value was 290:1 (Appendix B.1).

The contemporary designers were not sure if the theoretical models and the simplifications carried out by Torroja in order to calculate the shell showed correctly the structural behaviour of this roof because all the considered innovations had not been studied before and therefore, a scale model was constructed.

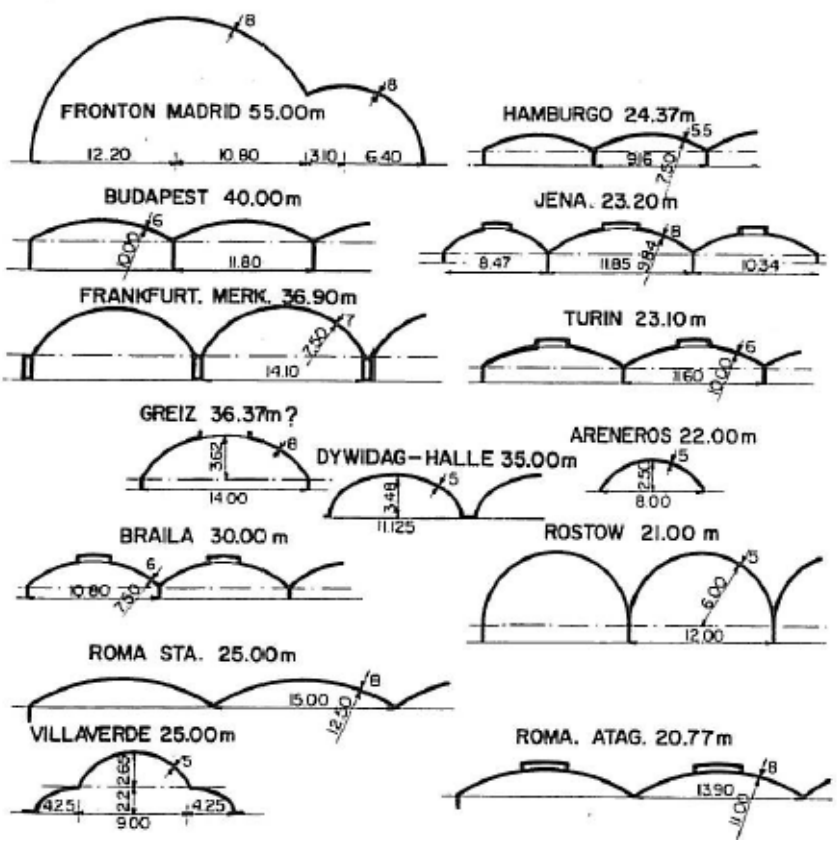

Figure 25: *Cylindrical thin concrete shells constructed in the 30s*. The overall characteristics are showed in the Appendix B.1.

2.1 Basque Pelota Sport

This structure was designed to play Basque Pelota, also called Jai Alai (figure 26). This Sport was invented in the 19th century in the Basque region in Spain, where it remains highly popular today. The game is played against three walls: the font wall, the back wall and the side wall. The three walls and the court together, are known as the "frontón".

The object of the sport is to throw the ball at the wall in such a way that it is hard for the opponent to catch and return. The opponent needs to be able to catch it before it hits the ground or after its first bounce and return it back to the wall. This sport is played as either singles or doubles on a fronton with a hard rubber ball, called pelota, which is hurled with a wicker basket[9] attached to the player arm. The speed of the fastest ball recorded is 300 km/h (Fortin 2000, p.47) and for this reason, Jai-Alai is known as the fastest game in the world. (Guiness 1990, p.122) This factor has to be considered in the design of the structure in order to avoid future problems caused by the ball impact.

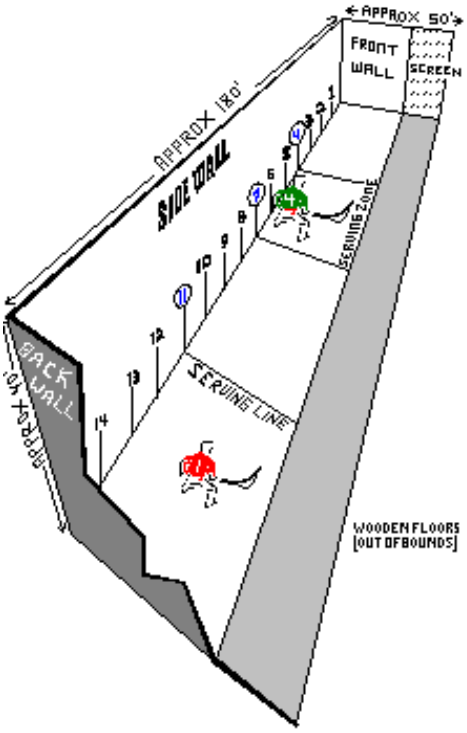

Figure 26: *Jai Alai court* and *Jai Alai player*.

[9] The cesta is basically made up of a glove, for a player to insert his/her hand, and a basket, where the ball would go when it is caught.

2.2 Roof design

The design of the basque pelota facility demands very functional conditions. Firstly, the roof has to cover a well light rectangular pitch, enclosed by three walls for the rebound of the ball (figure 26). These walls should be at least 25 metres in height. Furthermore, the place needs sunlight in order to play Jai Alai without any artificial light during the day (Fernández 2000, p.130).

Torroja searched different ways to cover the building based on all the preceding factors as well as the aesthetic design of the structure. The first solution thought was to arrange a number of transverse trussed girders connected by longitudinal joists (figure 27) however, the shape of these trusses were both structurally and aesthetically unsatisfactory. The next alternative was to place two longitudinal girders across the skylights, thereby making them support the roof (figure 27). This design had also some disadvantages: very large skylights are needed and the left side was too much illuminated. Finally, all the conditions were solved with the design of the constructed structure, which consisted of a very thin shell, whose thickness varies from eight to 16 centimetres, with a tubular section of reinforced concrete (figure 27). The directrix consisted of two sections of cylindrical sectors, which radius were 6.4 metres and 12.2 metres, intersected orthogonally along a joint forming the outline of a seagull (Torroja 1962a, p.1).

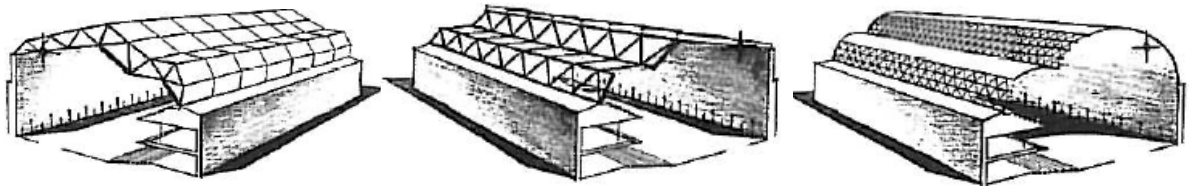

Figure 27: *Transverse trussed girders, longitudinal girders* as well as *two intersected lobes.*

Sunlight was obtained by the construction of two skylights (figure 23), on each of the two cylindrical sections, consisting of a lattice frame of equilateral triangles whose sides measured 1.4 metres. In the original Torroja's design, these structures were located only along the centre of the shell but, after the report carried out by Mr. Ribera and Aguirre with the purpose of checking the work viability, the extension of the skylights along all the generators length was recommended. These longer skylights improved the resistant and functional behaviour of the shell as well as the roof aesthetic value (Torroja 1942, p.109).

The designer based the roof design on the following idea "The primarily essence of beauty is the perfect correlation between the real nature and the apparent form" (Torroja 1962b, p.269). In this structure, Torroja showed his deep philosophical thought using the next explanation. "On the other hand, we thought it necessary to dismiss the idea held by traditionalists that the project involved two barrel vaults resting on a longitudinal beam. This prevalence of this idea would have meant an ignorance of the resistant phenomenon of the shell structure which, in the part closest to the intersection or seagull outline has its own specific characteristics" (Torroja 1942, p.15). Furthermore, the aesthetic value was always considered in the Torroja's works. In this structure, the designer tried to "suppressing superfluous elements" (Torroja 1942, p.16), which means not using anything more than what is strictly necessary because the spaciousness inside the facility as well as the roof aesthetic value are decreased when unnecessary elements are considered.

During the Spanish Civil War, the shell roof received several hits, some of them passing through it. The shock wave from the explosions caused severe deformation in the structure. After the war, a design to repair the structure was made. It involved reinforced concrete ribs[10] in order to improve the roof structural behaviour. However, the roof collapsed when the repair work was beginning. Torroja argued after the incident "No doubt the collapse of the shell could also have been avoided if these reinforcement rings had been supplied at the time of its erection" (Torroja 1962a, p.7). Furthermore, the aesthetic and economic factors of the roof, after this reinforcement, would have not been so much worth. This is one of the thesis objectives: determining if the ribs would have improved the structural behaviour of the shell.

"Had I to build it again, I should provide such reinforcement ribs" (Torroja 1962a, p.7). This declaration shows how the designer was able to develop his ideas even after that, the structures were built; at the beginning, he said that these ribs decrease the roof aesthetic value. However, then he changed his consideration because the ribs were finally considered by Torroja structural elements instead of "superfluous elements". This is one example of how the designer is always growing up with his/her designs and how he/she is always learning from them.

[10] The study of the ribs thought by Torroja is showed in the section 3.6.

2.3 Theoretical calculations

Nowadays, computers can easily be used to model the behaviour of shell structures. However, in 1952 when the Frontón Recoletos was calculated, this technology was not available and all the calculations were done by hand. If the calculations are done by hand the structure cannot be completely analyzed because the problem is too complex and it is indispensable considering some hypotheses in order to simplify the problem. All the previous theories of cylindrical shells have assumed different simplifying hypotheses. For example, the material is considered homogeneous and follows the Hooke's and Kirchoff's laws as well as all the deflections at the surface of the shell are reduced.

The Frontón Recoletos incorporate new characteristics that had never been studied in the preceding structures and therefore, in addition to all the classics assumptions, new simplifying hypotheses were considered: Firstly, the designer assumed that the shell had uniform thickness, density and Elasticity Modulus. These hypotheses are not obviously justifiable in general for the construction made of reinforced concrete: after all, one of the most important advantages of this material is the possibility of disposing the steel reinforcing bars non-uniformly over the surface of the shell in order to give local strengthening: and this gives non-uniform Elasticity Modulus and surface density. Secondly, the skylights were modelled like a normal shell section with the same loads, thickness, materials and stiffness because a similar structural behaviour was assumed. Thirdly, the transverse contractions can be considered null because the shell's thickness was thin and therefore, the Poisson number was supposed negligible by Torroja. This hypothesis was also considered by other designers in preceding shell structures, like Dischinger in Budapest (Torroja 1942, p.19). Fourthly, the designer supposed in the theoretical calculations that the edged generators and directrixes were connected with the walls by continuous supports. However, the construction drawing showed that the connection between the edges of the shell and the wall consisted on concentrated connection acting as springs. Finally, the wind and snow load laws were supposed as simplified model based on the preceding obtained results in similar structures.

The shell analysis could not be done directly because the problem presented some mathematical difficulties. Therefore, in order to achieve the solution, the method applied by Finsterwalder and Dischinger in the roofs of Frankfurt and Budapest was followed. This method was based on physical and mathematical exact theories and the shell analysis was divided into two partial problems, where different hypotheses were considered. On one hand, the shell had different ways to working in each of these problems: as a membrane in the first analysis, which means without considering the flexural actions and as a plate in the second one, taking into account the flexural actions. On the other hand, different elements in each problem were analyzed: in the first analysis the external load, while in the second one the edge effects (Torroja 1942, p.31-32).

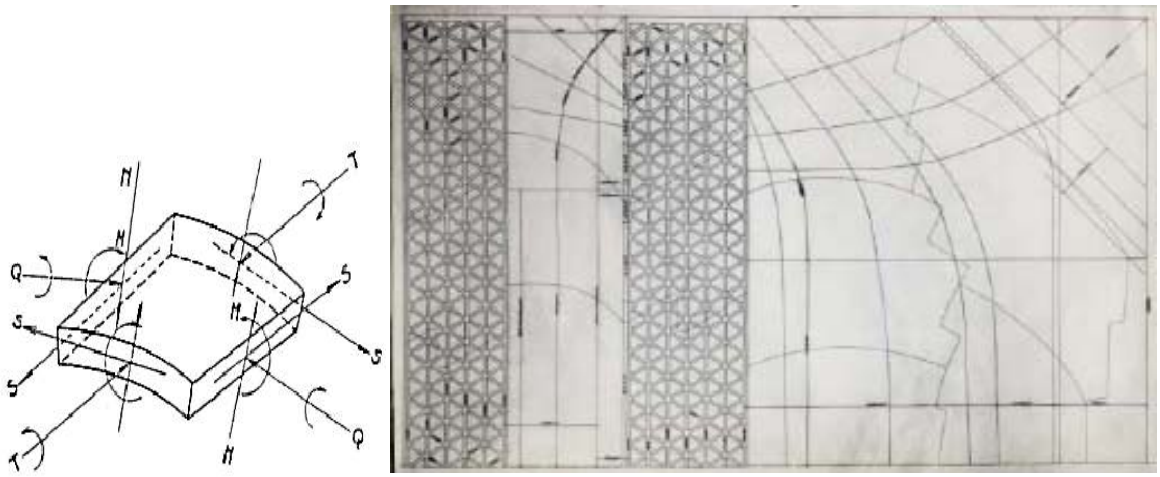

Figure 28: *Differential element of the shell* including the stresses considered in the calculations and *reinforced plan of middle developed section of the Fronton Recoletos.*

The calculations were based on a nine differential equations system obtained from the equilibrium and compatibility conditions of the shell's structure. Afterward, the stresses[11] and the deflections were calculated using these equations. Once the stresses and the deflections had been obtained for all the points of the shell, Mohr's circles corresponding to the stresses in the tangent plane were drawn on a plan. These circles served as a basis for drawing the isostatic system and the isobars (figure 35) along the shell middle surface. Finally, these diagrams were used in order to obtain the steel-reinforcing bars (figure 28) (Torroja, 1942, p.19-56).

Since the conception of the building, the Frontón Recoletos was considered a structural challenge because new structural conditions, which had never been constructed before, were introduced in this work. The innovative Fronton's characteristics, compared with the roof constructed in Budapest by Dischinger, which was calculated, using the same method (Antuña 2003, p.144), were:

- Greater size: The Budapest shell was 40 metres long and 11.8 metres wide while, Frontón Recoletos structure, only in the biggest lobe, was 55 meters long and 23 metres wide (figure 29).
- Asymmetric directrix: The Budapest roof was composed by two symmetric cylindrical sectors. Nevertheless, in the Frontón structure the directrix consisted of two asymmetric cylindrical sectors in size and position (figure 29).
- Absence of large beams at the intersection points between the two cylindrical sectors: In the Budapest shell, both sectors were joined by a beam, however in the Frontón roof both lobes were joined forming the outline of a seagull. This innovation improved the aesthetic perception of all the structure because the connection was visually less heavy (figure 29).

[11] The stresses (figure 28) considered in the shell analysis were: the flexions along the directrix, the stresses along the generator and directrix directions as well as the shear stresses. Nevertheless, the longitudinal bending moments and the torsion moments were considered negligible.

- The Joins between the roof and the walls: In the Budapest shell, the cylindrical sectors and the walls were connected by large beams, however in the Frontón roof, the well-known Freyssinet's hinges made of reinforced concrete were used. In this joins, the rotations and longitudinal movements are allowed however, the transversal movements, vertically and horizontally, are not allowed (figure 30).
- Skylights: The Frontón Recoletos was the first thin concrete shell roof which included this kind of longitudinal skylights with 55 metres length. Therefore, exact theoretical model in order to analyze the structural behaviour was not available.
- Finally, the bigger size of the large slope curve of the Torroja's structure produced more complex load laws, like wind and snow, than the Budapest shell.

Figure 29: *Size comparison in plan between the Frontón and Budapest shells* and *Directrix comparison* between the same both structures.

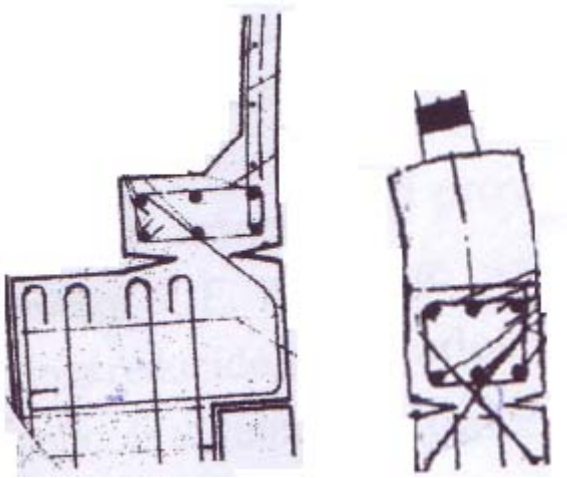

Figure 30: *Joins between the wall and the shell along the generators of the Frontón Recoletos.*

All these introduced structural innovations did not allow the exact mathematical solution applying the Finsterwalder and Dischinger's method. Nevertheless, Torroja instead of refrain from building the structure adapted the existing methods in order to obtain an approximate solution of the behaviour of the shells. Furthermore, the designer considered this work as a way of developing the cylindrical shells theory. For that reason, Torroja carried out real deflections measure during and after the construction of the structure, all the results and calculations were published. The capacity of changing the available methods, without fear of cannot know the exact solution, is considered a common practice in the structural artist. Other designers who created their own structural models in order to understand, design, analyze and calculate their new and innovative structures were for example Gaudí or Insler.

The adaptations carried out by Torroja were produced in different parts of the Finsterwalder and Dischinger's method. The first important modification was the absence of beam at the connection of the cylinder sectors, which forced the designer to include a strong tie beam in

that location, which represents an important part of the reinforcements bars needed in the shell (Torroja 1942, p.16). The second change consisted of including the skylights creating a lighter and more flexible structure because the continuity of the shell was broken. However, these structures were not considered in the differential equations because the exact calculations would have been too much complex. The third modification consisted of the consideration of more complex loads laws: Firstly, the wind load could not be considered negligible because the structure was bigger than the similar preceding roofs. Secondly, the snow load cannot be assimilated to the dead weight because more snow was accumulated over the roof because the large slope curve of the Frontón Recoletos shell was higher. Thirdly, the effects of the loads were studied separately and therefore, three load cases: dead weight, the snow and the wind, were considered. The analysis of these three loads is presented in this chapter. Lastly, the symmetric condition could not be applied because the directrix was asymmetric and therefore, the problem was more complex.

The exact wind forces in the Frontón Recoletos shell could not easily been determined because it shapes had not been studied before. Torroja explained that the structure should be analyzed by wind tunnel test in order to obtain the accurate wind load laws along the shell directrix. Nevertheless, to study the wind effect using this technique was not possible because this test greatly increases the cost of studying the structure. Hence, a wind law was proposed by Torroja. This law consisted of constant values at generators and sinoidal variation along the directrix (formula 3). This variation depended on the angle between the vertical and the directrix perpendicular line "φ" as well as on the maximum value of wind stress measured in Madrid "*A*". According to the Spanish regulation, "Instrucción para estructuras urbanas" proposed by Mendizabal, the maximum value of wind stress was 40 kg/m^2 (Torroja 1942, p.21). The maximum values of this law were located at the edges of the slopes as well as the minimums on the top of the shell.

$$Wind = A \cdot \sin \varphi \qquad [3]$$

Torroja based the wind load on two assumptions. On one hand, the both sides of the shell were supposed simultaneously in compression due to the existence of buildings near from the location of the structure (figure 31). On the other hand, the wind suction was not considered because Torroja supposed that the structural behaviour was improved when the suction effects were considered. This Torroja's hypothesis is checked in the section 3.3 of this thesis. However, when the shell had been calculated, the report carried out by Mr Ribera and Aguirre to check the work viability recommended the study of the wind suction effects in a scale-model of 1/10. Consequently, Torroja used the experimental results of the cylinder case to approximate the wind suction law along the directrix (figure 66 and formula 4). This hypothesis depends on the maximum pressure over the cylinder "v", which value was approximated to 40 kg/m^2 by the formulas of Stenton, Dines and Nipher (formulas 5, 6, 7). All these formulas depend on the maximum wind speed measured in Madrid "*V*", which value, 30 m/s, was proportioned by the Spanish Meteorological Department (Torroja 1942, p.21- 24).

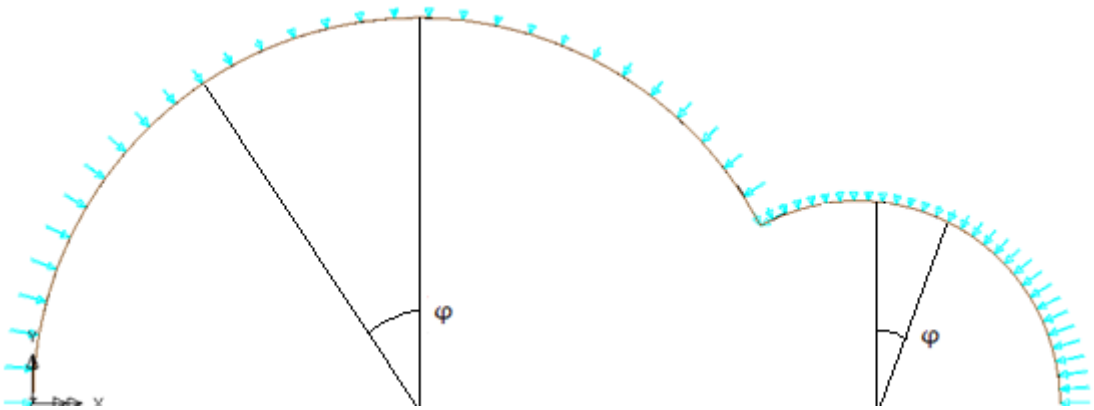

Figure 31: Wind load law at the directrix without considering the suction

$$Wind\ Suction = -3 \cdot v \cdot cos\,\varphi + v \cdot \sin\varphi = -120 \cdot \cos\varphi + 40 \cdot \sin\varphi \quad [4]$$

$$Stenton\ v = 0{,}7 \cdot 0{,}064 \cdot V^2 = 0{,}7 \cdot 0{,}064 \cdot 30^2 = 40\ \mathrm{kg/m^2} \quad [5]$$

$$Dines\ v = 0{,}7 \cdot 0{,}06 \cdot V^2 = 0{,}7 \cdot 0{,}06 \cdot 30^2 = 37\ \mathrm{kg/m^2} \quad [6]$$

$$Nipher\ v = 0{,}05 \cdot V^2 = 0{,}05 \cdot 30^2 = 45\ \mathrm{kg/m^2} \quad [7]$$

With the purpose of checking easily the suctions effects in the theoretical model, without the necessity of repeating the calculations, the wind load law, considering the suctions effects, was modified by Torroja in order to obtain a linear combination law of the other calculated laws, snow and wind without considering the wind suction effects (formula 8). Accordingly, the wind load law considering the suction effects were obtained (figure 28) by combination of the wind and snow load laws. This way of defining the wind suction effects is another example of the capacity showed by Torroja of adapting the available method to obtain useful approximate results.

$$Wind\ Suction = -130 \cdot cos\,\varphi + 40 \cdot \sin\varphi = 0{,}4 \cdot Wind - 2 \cdot Snow \quad [8]$$

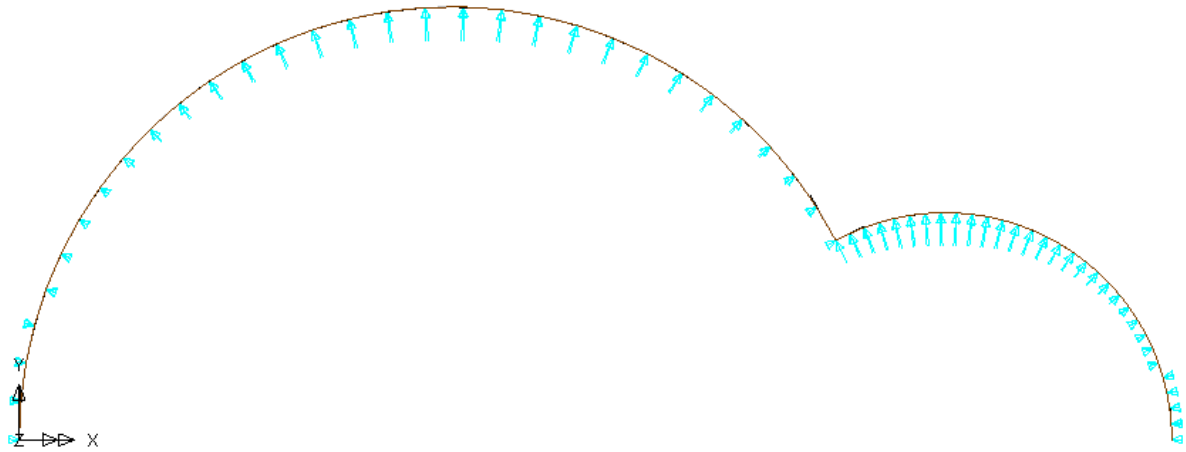

Figure 32: *Wind load law considering the suction effects along the directrix.*

The snow load law was proposed constant at generators and cosenoidal variation at directrix (formula 9), with maximum values on the top of the cylinder and minimum at the edges of the slope (figure 33). This hypothesis depends on the parameter "φ" explained before and on the parameter "*B*", which value, according to the same regulation proposed by Torroja, was 65 kg/m^2 (Torroja 1942, p.20).

$$Snow = B \cdot \cos\varphi \qquad [9]$$

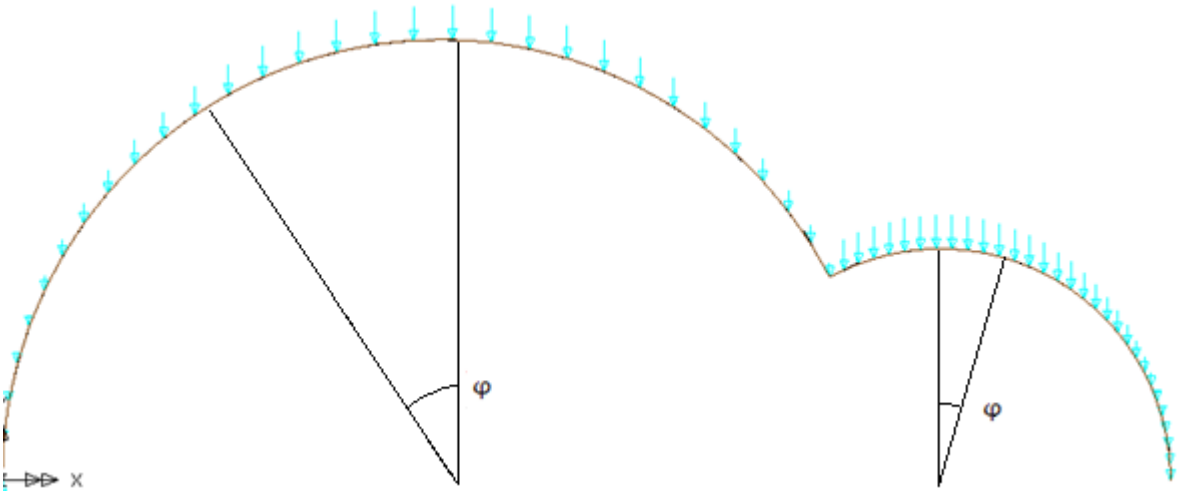

Figure 33: *Snow load law along the directrix.*

The last load, the dead weight (figure 34), was considered 250 kg/m^2 constant in all the shell and therefore, the difference with skylight weight was considered negligible. This constant load was calculated considering a constant thickness of 9 centimetres along the shell (Torroja 1942, p.20).

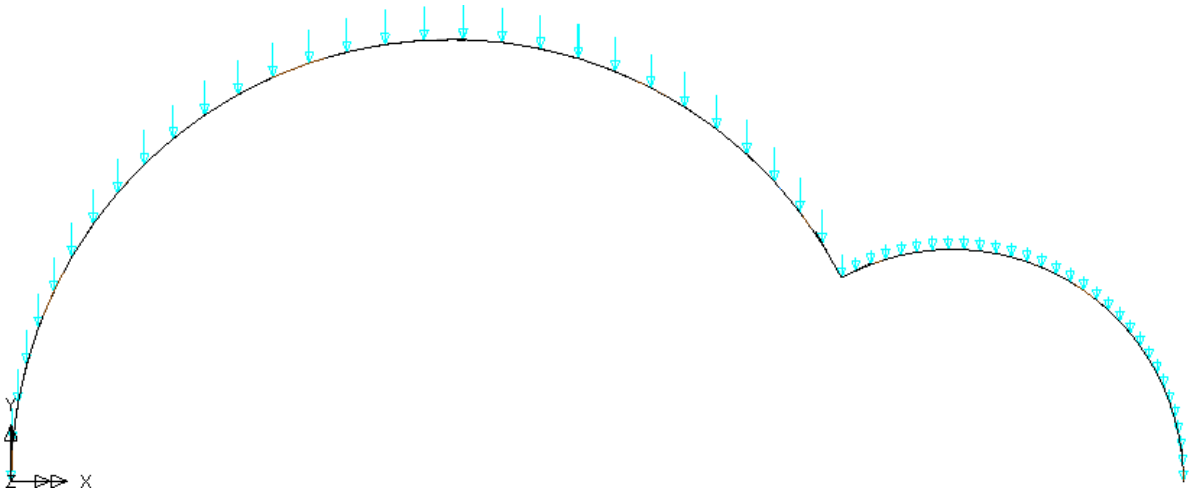

Figure 34: *Dead weight load law along the directrix.*

Chapter 3

Structural Analysis

The structural analysis presented in this report was based on the development of successive models, which consisted of incorporating different hypotheses to the basic model. This initial model tried to be as similar as possible to the structure calculated by hand, considering the same simplifications and hypotheses, with the purpose of checking the theoretical calculations, carried out by Torroja, using current ways to calculate shell structures. Afterwards, this basic model was brought closer to the reality by successive steps: Firstly, it was studied the variation of shell's thickness, which had not been considered in the Torroja's model. Secondly, the wind suction effects were considered. Thirdly, the skylights were modelled as lattice frames of equilateral triangles instead of a constant-thick shell as was supposed in the calculations done by hand. Fourthly, the effect of the real supports, modelled by springs in the structure, was studied. Lastly, a study about the reinforcement ribs proposed by Torroja in order to improve the structural behaviour of the shell was carried out. The purposes of all these successive models were checking the hypotheses considered during the simplifications assumed by the designer during the calculation of the shell as well as comparing the behaviour of the different Lusas' models with the values measured in the actual structure and in the small-scale model.

The analysis was principally based on the isobars calculated by Torroja (figure 35). This assumption can be logically assumed because these diagrams were used to calculate the reinforcement bars in the shell. However, along the structural analysis two more factors were supposed. The first additional study was the absence of transversal bending moments along the shell in order to check the efficient structural behaviour of the shell working as a membrane. This effect was studied comparing the shape and the maximum values measured by Torroja along the central directrix (figure 36) with the results obtained by Lusas. The other factor considered was the deformations, which were measured in the theoretical, actual structure and small-scale model (figure 37) as well as in the small-scale tests carried out by Torroja (Torroja 1942, p.123-126), with the purpose of comparing the maximum values and the overall shape of the deformations in the different models.

The problems found during the analysis of the structure were the following: Firstly, the load combination used to obtain all the diagrams was not explained in all the bibliography consulted. Therefore, in order to solve this problem, a brief study of the possible load cases considered by Torroja in his diagrams was done. Secondly, the units of the isobar lines and the thickness of the shell used to calculate isobar diagrams were not described. The first of these factors, the units of the isobars obtained by Torroja, were supposed as kg/cm^2 because

all the rest of parameters in the Torroja's report were expressed with these units, as for example the maximum value of concrete working load, 50 kg/cm^2 (Torroja 1942, p.20). The second factor, the shell thickness considered in the isobars' diagrams, was assumed to be constant 8 centimetres to the safe side because the values of the isobars are lower when the thickness is increased. Lastly, the location of the section where the deflections and the transversal bending moments were measured was supposed at the central directrix because this section is the most unfavourable section when symmetrical loads are applied.

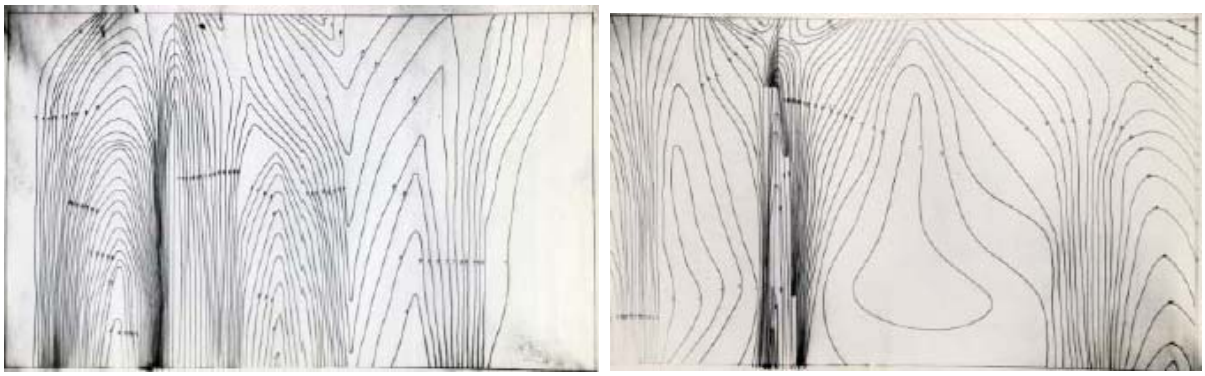

Figure 35: *Isobars of maximum compression stress and maximum tension stress obtained by Torroja*. These diagrams consist on half section[12] of the developed plan. In horizontal is located the directrix: on the left is located the smallest cylindrical sector and on the right the biggest one.

In each successive model, the overall shape and the maximum values obtained by Torroja in the isobars, the transversal bending moments and the deflections, were compared with the results presented by Lusas. In order to make these comparisons easier: Firstly, the maximum values of the isobars obtained by Torroja[13] were considered in the Lusas models by means of the representation in different colour, red in tensions and blue in compressions, of all the points where these maximum values of isobars were exceeded. Secondly, the Lusas transversal bending moments were coloured in the same colours in the points where the maximum values obtained by Torroja[14] were exceeded (Appendix B.2). Lastly, the deflections obtained by Torroja were drawn using splines in order to join the points in a new figure where the Lusas deflections were included.

[12] Half section considering all the directrix and only half generator because the structural behaviour when symmetric loads are applied, is symmetric.

[13] The maximum values measured in the isobars presented by Torroja (figure 35) were $8 \cdot 10^6$ kg/cm^2 for maximum tension stress located at the connection between both cylindrical sectors and $-5.8 \cdot 10^6$ kg/cm^2 for maximum compression stresses measured close form the central generator of the bigger cylindrical sector. These values were approximated along the analysis as 8 MPa and -5.8 MPa.

[14] The maximum value of the transversal bending moments was 1030 kg·m/m (Torroja 1942, p.98).

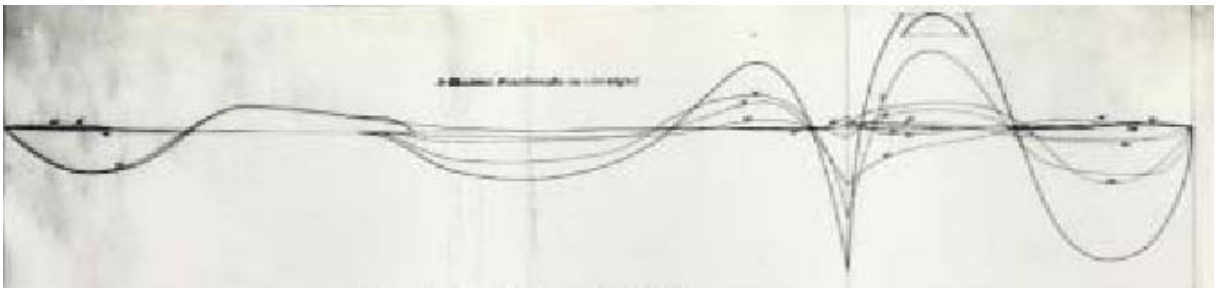

Figure 36: *Torroja's transversal bending moments*. The maximum value, around -300 kg·m/m, is located at the connection between both cylindrical sectors and in the middle surface of the smallest lobe. This diagram consists of a directrix viewed in plan: On the left is located the biggest cylinder and on the right the smallest cylinder. The vertical line represents the seagull profile.

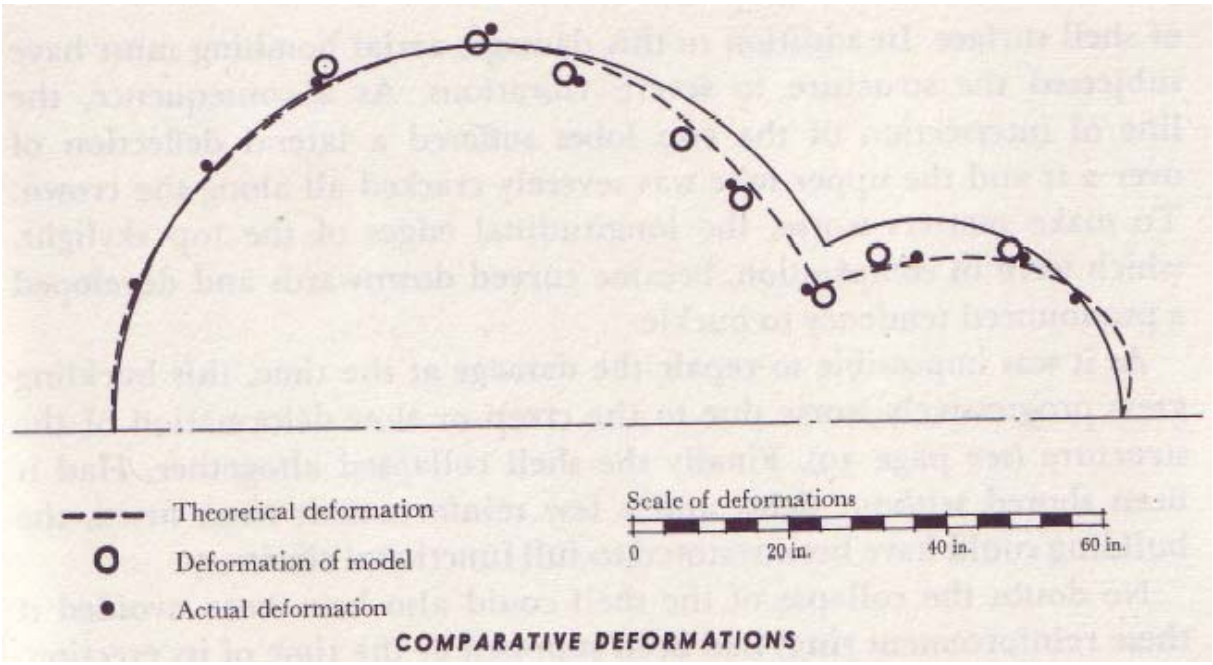

Figure 37: *Deformations obtained by Torroja in different models*. The discontinue lines represent the theoretical deformations, the biggest points represent the deformations in the small-scale model and the smallest points represent the deformations in the actual structure.

Different simplifications along the structural analysis were carried out. Firstly, the isobars obtained by Torroja (figure 35), maximum compressions and tensions along the middle surface of the shell, were developed in a flat surface. However, the stress and deflection diagrams cannot be developed easily with the programme used to analyze the structure. Therefore, in order to simplify the model, the plan of the diagrams obtained by Lusas was compared with the developed diagrams presented by Torroja. This simplification can be assumed with an acceptable margin of error. On one hand, the comparison between both methods is based on the maximum values of the isobars, which do not depend on the development of the diagrams. On the other hand, the overall shape of the Isobars' lines is very similar for the both diagrams because of the high value of the large slope curve in the cylindrical sector shape. Secondly, the deformations obtained by Torroja in the reality and in the small-scale models consisted of non-continuous deflections along the directrix. Nevertheless, with the purpose of comparing easily these points with the programme outputs, these deformations were connected by splines in order to make a deformation line for each case, which overall shape can be easily compared. These lines were drawn trying to imitate

the shape presented by Torroja in the theoretical calculations (figure 36) as well as considering that the stiffness of the seagull profile produces an orthogonal joint between both lobes when the loads are applied (Torroja 1942, p.48). In order to model the deformation lines, the next considerations were followed: each cylindrical sector had different spline line, both lobes joined orthogonally at the seagull's profile, both spline lines joined with the wall considering vertical tangent. Thirdly, some factors, which value was not clearly stated in the available plans, were measured directly in the diagrams presented by Torroja. For example, the location and overall dimensions of the real supports at the generators (figure 87) and the directrix (figure 86) or the deflections obtained by Torroja for the different models[15]. This assumption can logically be assumed because the plans, after being printed, keep the dimensions of the structure. Fourthly, the values of the bending moment diagram were measured directly using the scale proposed by Torroja in figure 30. However, these values were based on mistakes during the calculation process (Torroja 1942, figure 9). For that reason, the maximum values measured in that diagram were considered only like approximate numbers. Lastly, the real supports located at the connection between the shell and the walls were approximated as beams working as springs as explained in Appendix A.5 instead of modelling all the beams proposed by Torroja. This simplification can be considered as an approximation of the real supports with enough accuracy considering the scope of this thesis.

At the end of this chapter, some factors that could be studied in the future in order to improve the knowledge of the structural behaviour of the Frontón Recoletos thin concrete shell were studied.

[15] The deformation obtained by Torroja can be easily measured using the scale rule in the figure 37.

3.1 First Model: Similar to Calculus.

The structural analysis was based on the development of successive models, which consisted of incorporating different hypotheses to the basic model. This initial model tried to be as similar as possible to the structure calculated by hand, considering the same simplifications and hypotheses, with the purpose of checking the theoretical calculations, carried out by Torroja, using current ways to design shell structures. Afterwards, this basic model was brought closer to the reality by successive steps, which were studied in the following models.

3.1.1 Hypotheses and Objectives.

The first model (figure 38) was considered similar to the model used by Torroja in his calculations because it was based on the same hypotheses: Firstly, the thickness variation was not considered and 8 centimetres constant thickness were supposed. However, in the dead weight 9 centimetres thickness were assumed (Torroja 1942, p.20). Secondly, the skylights were modelled as a normal closed shell section with constant thickness instead of the lattice frames of equilateral triangles constructed in the real structure. Thirdly, the supports used by Torroja in the theoretical calculations[16] were considered (figure 38) instead of the supports presented in the plans. Lastly, the concrete was considered an elastic, homogeneous and linear material that obeying Hooke's law with the Elasticity Modulus equal to $30 \cdot 10^9$ N/m^2 and the Poisson number negligible as was explained at the section 2.3 of this thesis.

The Lusas model was based on the following characteristics: Firstly, the geometry consisted of four surface elements QSI4[17] (figure 38) in order to model the support conditions. These surfaces were meshed with 30 divisions along the both local-surface directions producing a balanced model considering the accuracy and the speed of calculation. Secondly, the supports in the Lusas model (figure 38) were based on two different defined elements: the “Support 1”, which fixed all the translations and allowed the rotations, and the “Support 2”, which fixed the translations along the Y and X-axis and allowed the rotations. The first element was associated to the central point of the end of the generators and the other to the rest of edged lines. Finally, the procedure used to define the dead weight as well as the wind and snow loads is explained in Appendix A.3.

[16] The theoretical support consisted on a continuous supports permitting the longitudinal expansion of the shell at the directrix and starting points at the edges joined to the wall at their centre, and along the rest of their length, which rest on continuous supports similar to the directrix (Torroja 1942 page 11).

[17] The elements QSI4 are usually used in the analysis of three-dimensional thin shells and takes into account both membrane and flexural deformations (Appendix A.1).

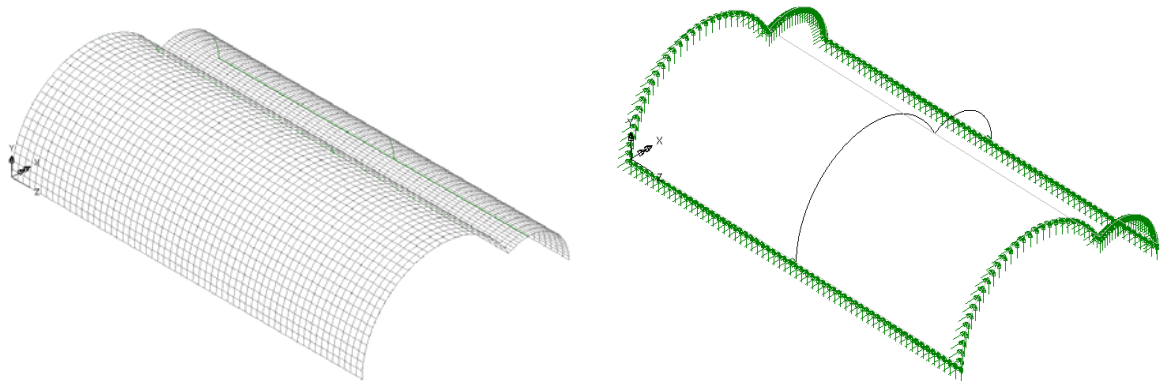

Figure 38: *Mesh of the first Lusas model*, *the surfaces* and *the supports*: all the translations are fixed at the central points of the generators, at the rest of the edges only the vertical and horizontal translations are fixed (X and Y[18]-axis) and the rotations are free for all the edge points.

The principle objective of the first Lusas model was checking the accuracy of the theoretical method used to calculate the structure by hand using current ways to design shell structures.

The structural analysis is divided into three parts: First, a brief analysis about the load case used in the deflections and isobar diagrams was done because this factor was not clearly explained in all the consulted bibliography. Secondly, the overall shape and the maximum values of the measured deflections are studied. Thirdly, the transversal bending moments are analyzed. Finally, the isobar diagrams are studied because the reinforcement bars were obtained from these stresses. After that analysis, the obtained conclusions are showed.

3.1.2 Study of the Load cases.

As was explained before, in all the bibliography consulted, the load combination considered by Torroja in the calculation of the isobars and deflections could not be found. Knowing this load case is a crucial step in the comparison of the different models. Therefore, the starting point of the analysis is a brief study of the load cases, which objective is obtaining the most probable load case considered by Torroja in the isobar and deflection diagrams. In this study, the next assumptions were supposed: Firstly, the load combination should be the same for the calculation of the deflections and the isobars. Secondly, the Lusas results had to be as similar, in shape and maximum values, as possible to the results obtained by Torroja. Thirdly, the wind suction effects were considered as a combination of the wind and snow load laws when the calculations had been done. Therefore, the wind suction effects could not be considered in the load combination. Lastly, the most logical load combinations should be the most unfavourable because the calculations of the reinforcement bars were based on the isobars.

The analysis was based on the comparison[19] of the isobars diagrams presented by Torroja with the Lusas results considering four different load cases[20]:

---

[18] The axis used in Lusas (figure 38) were X along the directrix, Z along the generators and Y along the vertical.

[19] In order to make this comparison easier the Lusas diagrams were coloured, in red in tension and blue in compression, at the points where the maximum values presented by Torroja were exceeded.

- Load case one: Dead weight.
- Load case two: Dead weight with wind load.
- Load case three: Dead weight with snow load.
- Load case four: Dead weight with snow load and wind load.

The study was initially based on the isobar diagrams calculated by Lusas considering the four load cases (Appendix A.6). However, in order to compare easily the shape of these diagrams, the isobar values along the undeveloped central directrix between the both different models[21] were compared (figures 39 and 40). The analysis of these diagrams showed some conclusions: Firstly, the Lusas values are more similar to the results obtained by Torroja in the isobar diagram of maximum compression stress. Secondly, the effects of the wind, without suctions, are highly similar to the effects of the snow as is showed by the comparison between the maximum values of both isobar diagrams in the load cases two and three. Thirdly, the most similar results to the isobars obtained by Torroja are obtained when the first load case is considered. For this load case, the Lusas isobars are around 2.5 times higher in tension stresses than the values presented by Torroja (Appendix A.6). However, this load case cannot be considered the load case used by Torroja because the reinforcement bars, which were based on the isobar diagram, were calculated supposing the most unfavourable load combination to be on the safe side. Lastly, the load case four is the most unfavourable load case. For example, the maximum values of the tension stress isobars are around 3.5 times higher than the values presented by Torroja (Appendix A.6). Therefore, analyzed all these assumptions, the load case four: dead weight with snow and wind loads can be logically assumed as the load case used by Torroja in the calculation of the isobar diagrams.

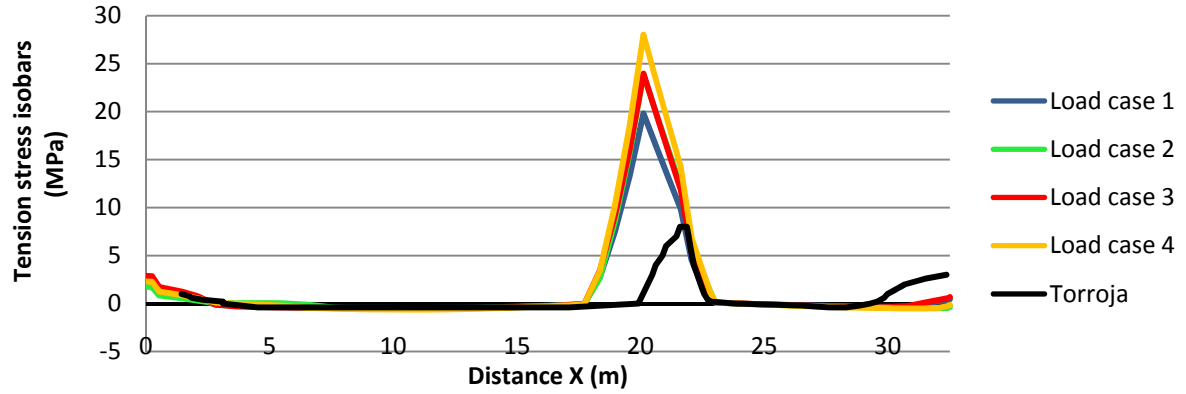

Figure 39: *Maximum values of the tension stress isobars along the central undeveloped directrix*. The diagram is based on five lines: four load cases calculated by the first Lusas model, which are coloured in blue, green, red and orange as well as the values presented by Torroja measured in figure 35, which are coloured in black.

---

[20] These four load cases were obtained considering the load cases tested by Torroja in the small-scale model without the wind suction effects. Furthermore, in the Appendix C the same load cases were presented in the Torroja's deflections. Therefore, the hypothesis supposed at the beginning of the analysis that the same load case was used in both isobars and vertical deflections diagrams can be logically assumed.

[21] The values of the isobars along the central directrix supposed in the theoretical model were directly measured from the isobars diagrams. However, these values could not be compared directly with the Lusas results because both models were based on different hypotheses. Therefore, the central directrix of the Torroja's model was undeveloped in order to homogenize both methods.

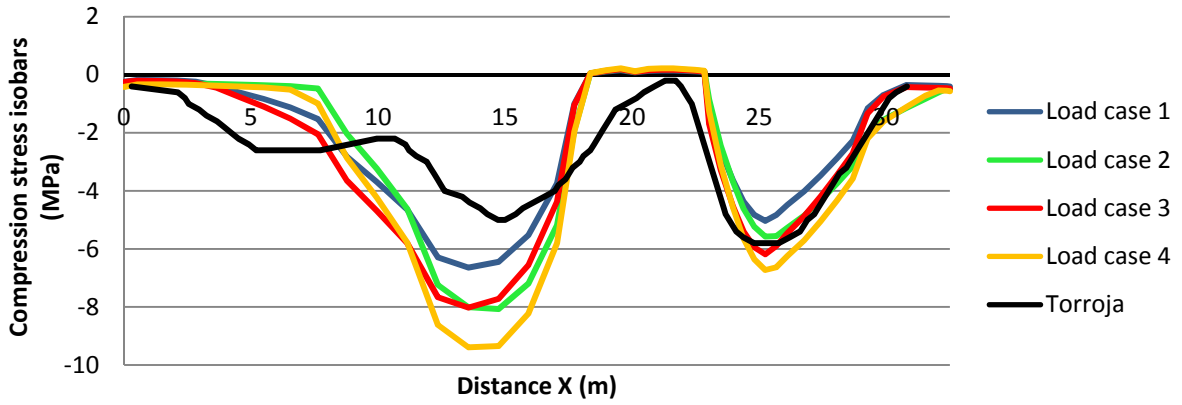

Figure 40: *Maximum values of the compression stress isobars along the central undeveloped directrix*. The diagram is based on five lines: four load cases calculated by the first Lusas model, which are coloured in blue, green, red and orange as well as the values obtained by Torroja measured in figure 35, which are coloured in black.

3.1.3 Analysis.

Three different elements are analyzed in the first model: the deflections, the bending moments and the isobars. For all these results, the load case obtained in the preceding study: dead weight with snow and wind loads, was considered.

The analysis of the deflections is divided into two parts. First, the structural behaviour and the overall deformations of the three-dimensional Lusas model are analyzed. After that, the deformations obtained by Torroja are compared with the Lusas results.

The analysis of the shape of the deflections in the three-dimensional Lusas model (3-D model) (figure 41 and 42) showed two different conclusions: Firstly, the most unfavourable sections are located parallel to the Z-axis because these sections act like a simply supported beam, with 55 metres length. Therefore, as an example to better understanding these sections, the deflections in the Y-axis at the connection between both cylindrical sectors (figure 43) were analyzed. These vertical deformations are symmetric: starting with null value at edges, due to the support conditions, and following a parabolic law, which maximum value, 15.3 centimetres, is located at the centre of the diagram. Furthermore, this section at the connection between both vertical walls had a symmetric movement along the Z-axis (figure 44), which maximum value 8 millimetres allows reducing the bending moments in the structure imitating the membrane behaviour pursued by the designer.

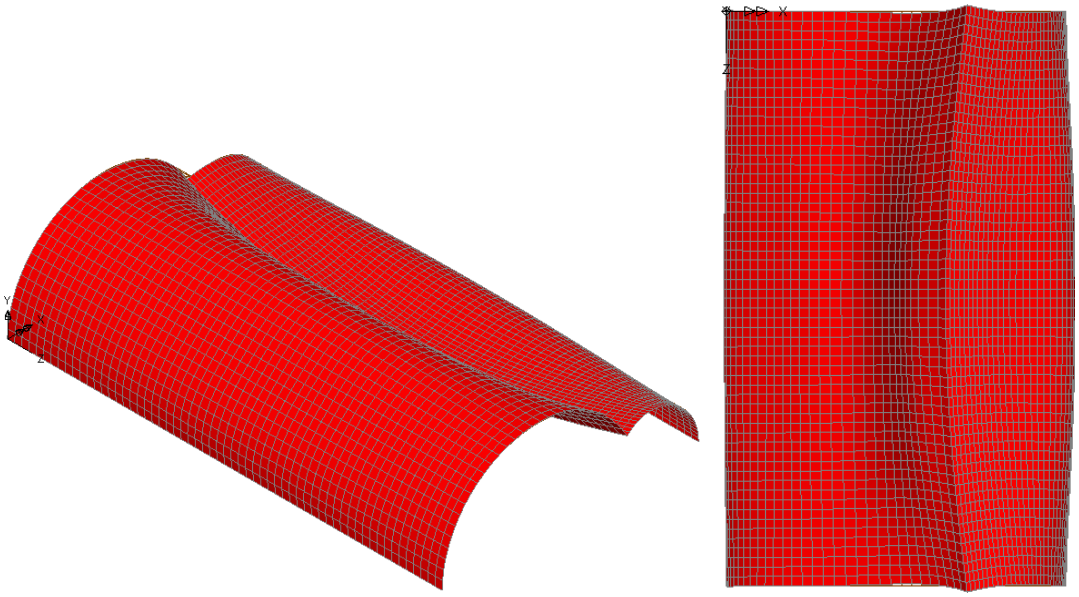

Figure 41: *Deflections in the 3-D model calculated by the first Lusas model*: Isometric view and the plan view.

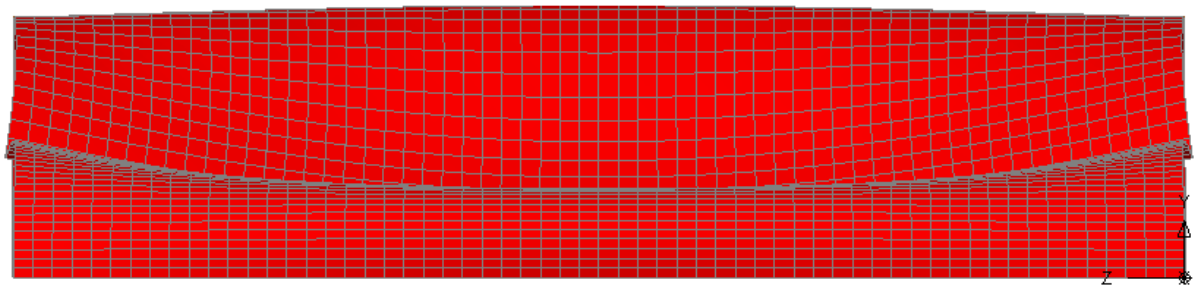

Figure 42: *Deflections in the in the 3-D model calculated by the first Lusas model*: View parallel to X-axis at the section X = 32.5 metres.

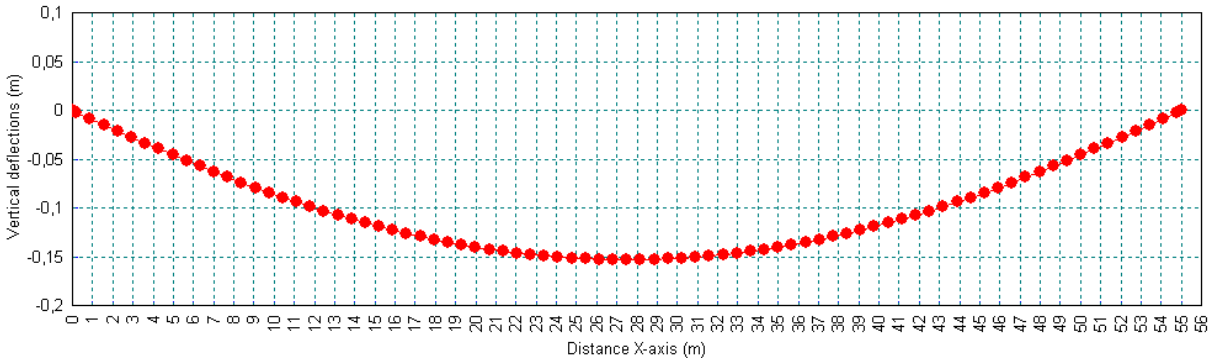

Figure 43: *Absolute vertical-deflections in the connection between both cylinders* (seagull profile) *along the Z-axis*[22] *calculated by the first Lusas model*. The maximum value 15.3 centimetres is located at the central section, Z = 27.5 metres.

[22] All the axes were measured in metres and are drawn in figure 32. The Z-axis corresponds to the generators. The Y-axis is associated with the vertical and the X-axis with the horizontal. The common origin is the generator joined with the wall at the biggest cylinder.

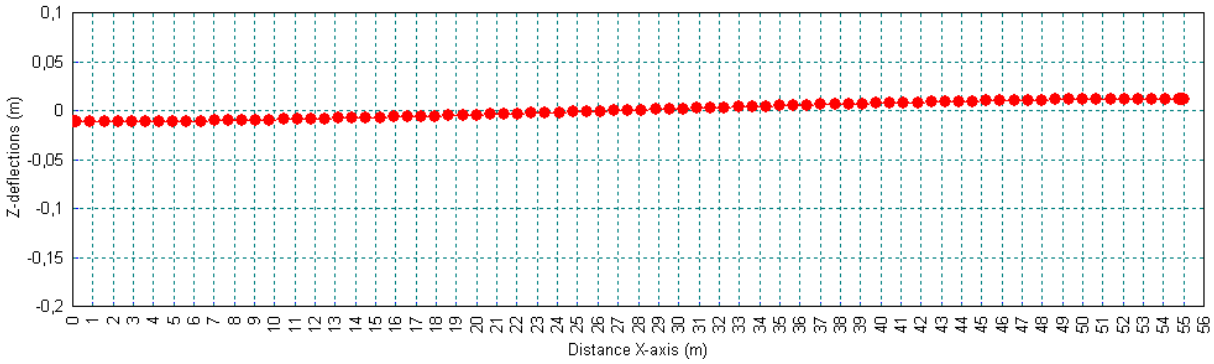

Figure 44: *Absolute Z-deflections along the seagull profile calculated the first Lusas model.* The maximum values 8 millimetres are located at the edges, Z = 0 metres and Z = 55 metres.

The overall shape and the values obtained by Lusas were compared with the different deflections presented by Torroja. These deflections were measured in the theoretical model, in the actual structure as well as in the small-scale model. However, during the comparison procedure, one problem appeared; the location of the section where the deflections had been measured was not clearly explained (figure 37). Therefore, this directrix was supposed, to be on the safe side, as the most unfavourable section, which corresponds to the central directrix when symmetric loads[23] are applied, as was explained before.

The overall shape of the deformations obtained by Lusas (figure 45) was practically equal to the theoretical Torroja's deformations (figure 37): At the connection with the generators, null deflections were measured as well as the deformed seagull profile kept orthogonal to the connection between the two cylindrical sectors[24]. Therefore, both models could be compared.

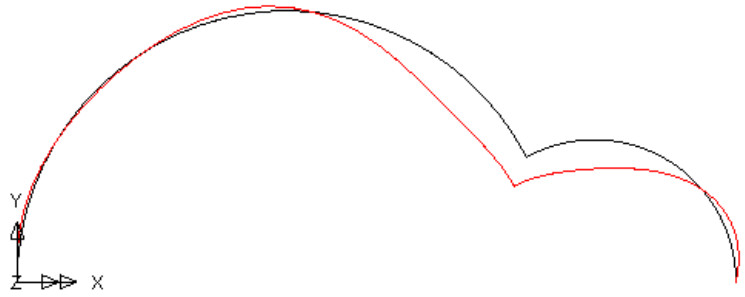

Figure 45: *Vertical Lusas deformations at the central directrix*. The red line represents the deformations calculated by the programme and the the black one the geometry without applied loads.

After the study of the overall shape, the absolute deflection diagrams were studied. Firstly, the highest vertical deflections are located at the smallest cylindrical sector (figure 46). This localization is explained by the different stiffness along the structure, which is highest at the smallest lobe because the span was lowest. Furthermore, the points where the directrix is

[23] During the research carried out by the Professor Ignacio Payá Zaforteza in the "Archivo Torroja". A original diagram of deflections was found. In this diagram, the hypothesis of the location of the measured deflections at the central directrix was checked. All the taken pictures of the original diagrams calculated by Torroja are presented in the Appendix C.

[24] The orthogonality of the deformed seagull profile is checked in the diagram obtained by Torroja (Appendix C).

connected with the wall had null vertical deflection due to the hypotheses considered at the supports. Finally, some points at the biggest cylinder, where positive deflections are measured, were identified. At these points, the position of the reinforcement bars must be changed because the bending moments had different directions.

The comparison of the vertical deflections and deformations along the directrix (figure 47 and 48) showed: Firstly, the differences of the three models, in most of the points measured by Torroja, are lower than 2 centimetres. However, in other points the difference is higher as for example at the point located around the skylight of the biggest cylindrical sector, which X-coordinate was 15.3 metres. At this point, the Lusas vertical deflection is 4.2 centimetres lower than the values presented by the other models. This value represents only 48 % of the deflections measured by Torroja. Secondly, the maximum value obtained by Lusas, 16.4 centimetres, is around 9 % higher than the maximum value measured in the other models, 15 centimetres (Tables 2 and 3, Appendix B.2). Both discrepancies can be explained by the higher weight and stiffness of the skylights that was not considered in the first model as well as by the fact that all the deflections presented by Torroja were measured directly from figure 37 and this procedure has an important measurement error. However, taking the variation of the thickness into consideration a stiffer structure is produced. Therefore, in the second model the vertical deflections will probably be reduced regarding first Lusas model.

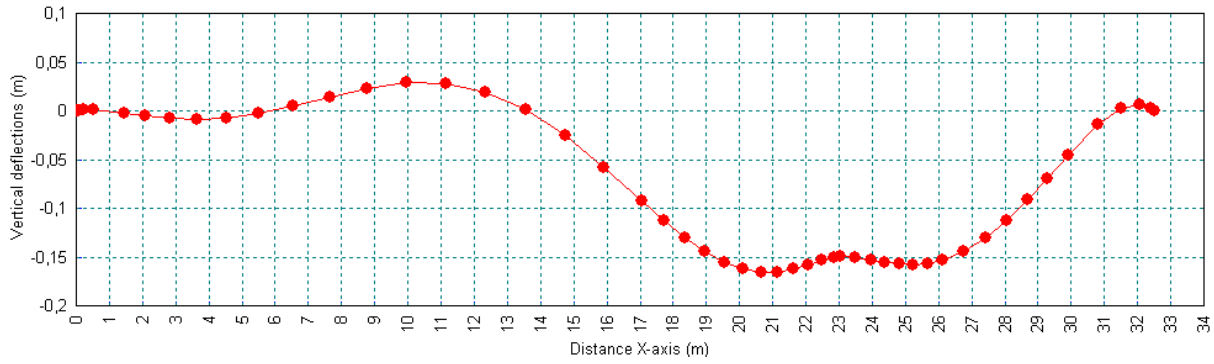

Figure 46: *Absolute Lusas vertical deflections presented by the first Lusas model along the central undeveloped directrix*[25]. The maximum vertical deflection is 16.4 centimetres and it is located at the point with coordinate X = 20.4 metres.

[25] From the coordinate X = 0 metres to X = 23 metres defines the biggest cylindrical sector, and from coordinate X = 23 metres to X = 32.51 metres the smallest lobe is defined. This diagram is the same for all the Lusas vertical deflections presented in the succesive models.

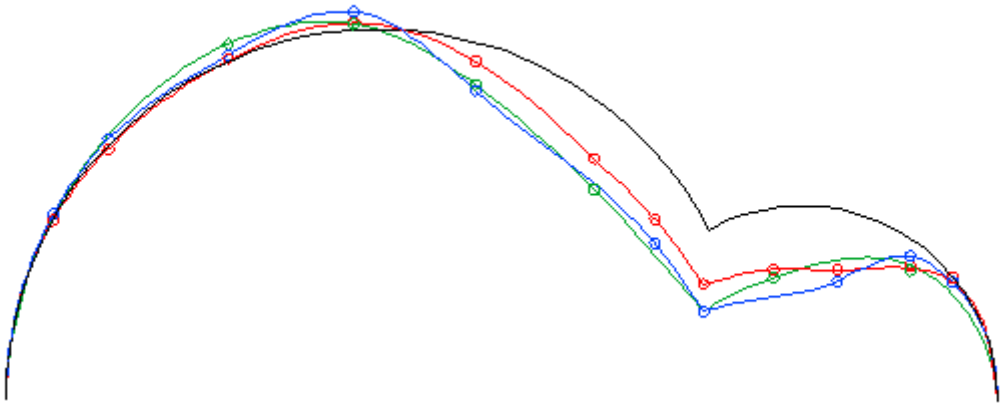

Figure 47: *Comparison of the deformations measured by different models*. The Lusas deflections are coloured in red, the shape without applied loads is coloured in black, the deflections measured in the actual structure in blue and in the small-scale model deflections in green. These deformations are presented along the central directrix with a scale deformation 1/200.[26]

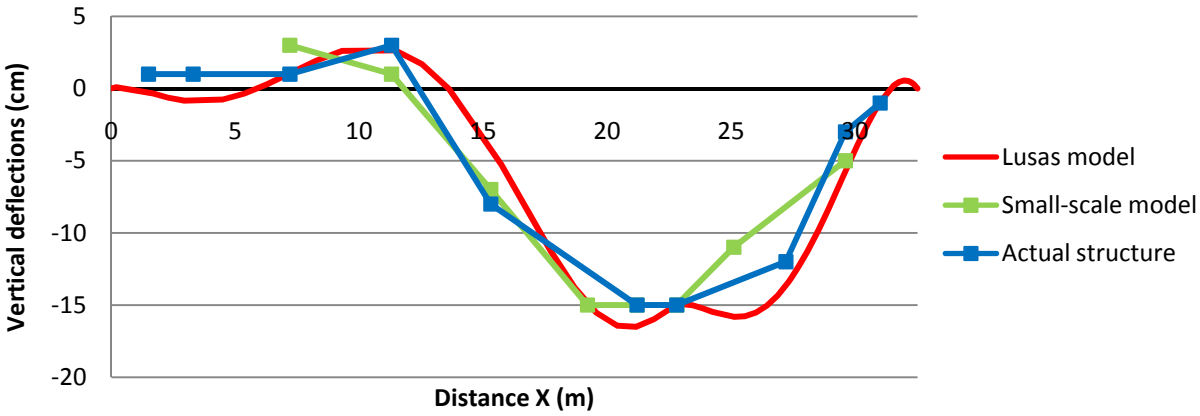

Figure 48: *Absolute vertical deflections along the central undeveloped directrix considering different models*. The Lusas deflections are coloured in red, the results measured in the actual structure in blue and in the small-scale model in green.

Additionally, the behaviour of the shell under symmetrical loads was checked. The procedure used was based on the analysis of the deformation in the Z-axis along the central directrix (figure 49). These deflections are practically negligible showing the symmetrical behaviour of the section.

[26] To make this figure, the simplifications explained in the section 3.1 of this thesis about the way of joined the different points in each model were used. All the distortions and the X-coordinates are presented in Tables 2 and 3 in Appendix B.2.

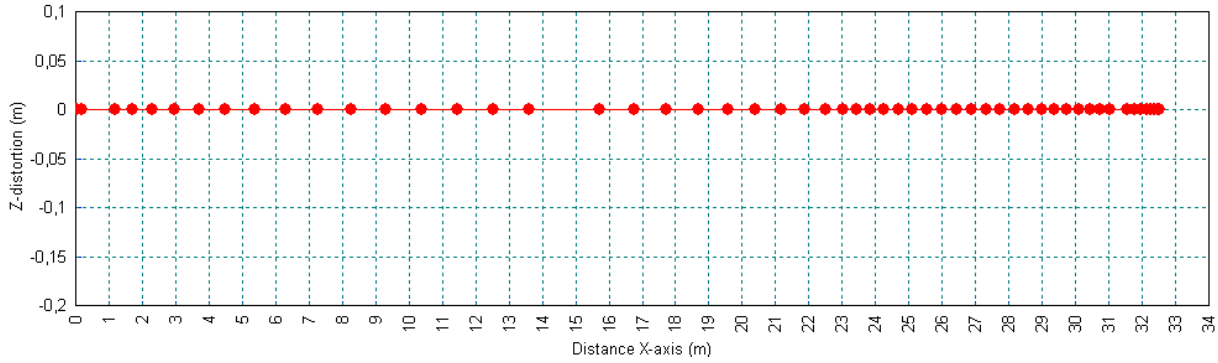

Figure 49: *Absolute Lusas Z-deflections presented by the first Lusas model along the central undeveloped directrix.*

After the study of the deflections, the bending moments were studied in order to check the efficient structural behaviour of the shell working as a membrane. These moments appear in the structures in order to provide additional resistance when the membrane stresses are not enough to resist the applied loads. However, if the bending moments are needed, the calculations are more difficult and less intuitive as well as the thickness of the shell has to be greater, as was explained before.

The analysis of the bending moments was divided into three parts: Firstly, the shape and the maximum transversal bending moments presented in the diagrams presented by Torroja (figure 36) were compared with the Lusas results. After that, the maximum values supposed in the calculation of the reinforcement bars were studied. Finally, the absence of longitudinal bending moments was checked.

The initial analysis of the transversal bending moments was based on the comparison between the Lusas results (figure 50) and the diagrams obtained by Torroja (figure 36), where the transversal bending moments along one transversal section were presented. The location of this diagram was assumed to be at the central directrix as was explained before. The analysis showed that the shape of both diagrams is highly similar[27] at the connection between both cylindrical sectors as well as at the smallest lobe. However, at the connection of the biggest lobe with the wall, the shape presents higher slope in the Lusas results. The maximum of the values measured by Torroja in this diagram around 300 kg·m/m are approximately 33 % of the maximum Lusas bending moments, which value was around 2000 kg·m/m. This difference could be explained by the assumption of different hypotheses in both models, as for example the thickness variation along the shell. However, after the analysis of the assumptions carried out by Torroja the most logical explanation was that his calculations were not accurate enough because the diagram was based on some previous mistakes (Torroja 1942, p.97). For that reason, the values measured in the isobar diagrams presented by Torroja are not considered in the next successive models and only the overall shape is compared.

[27] The Lusas diagram has the opposite bending moment sign. Therefore, in order to compare the results obtained by Lusas with the diagram presented by Torroja (figure 37) one of these diagrams was turned.

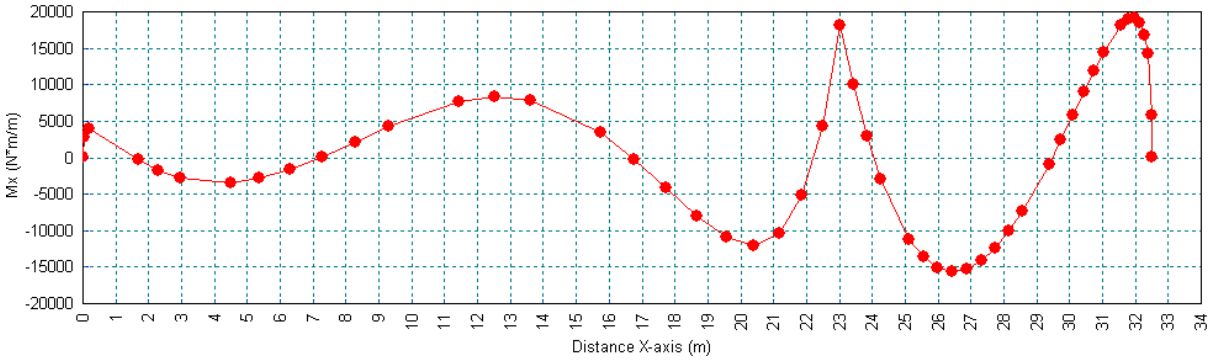

Figure 50: *Transversal bending moments presented by the first Lusas model along the central undeveloped directrix.* The maximum value, around 20000 N·m/m or 2000 kg·m/m, is located at the connection between both cylindrical sectors and in the middle surface of the smallest lobe.

The transversal bending moments considered by Torroja in order to calculate the reinforcement bars along the directrix (Torroja 1942 page 98) were around three times higher than the results presented in the bending moment diagram (figure 36). This assumption had two opposed consequences: On one hand, the price of the structure was higher because more steel was needed. On the other hand, the safety level of the building was also higher in order to avoid the made mistakes in the calculation process.

In order to check if the bending moments used to define the reinforcement bars were similar to the results presented by Lusas, both were compared drawing a common diagram[28] (figure 51). This figure showed that the bending moments calculated by Lusas are higher, above all regarding the positive bending moments. For example, the value obtained by Torroja located at the seagull profile is around five times lower than the Lusas bending moment (Table 16, Appendix B.3). These differences could be explained by different hypotheses considered in both models. Therefore, one of the objectives proposed in the next model was studying if the variation of thickness along the shell reduced the bending moments.

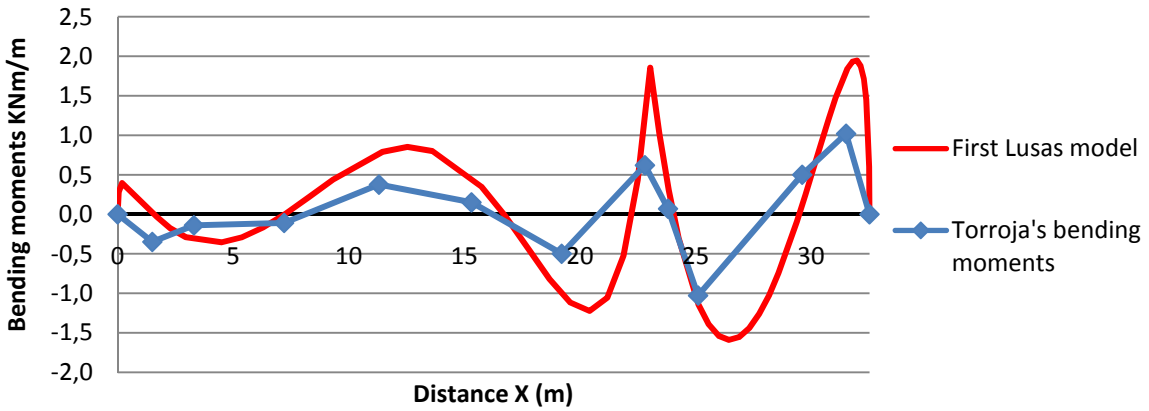

Figure 51: *Transversal bending moments along the central undeveloped directrix considering different models*. The Lusas bending moments are coloured in red, and the results obtained by Torroja in blue. All the coordinates and differences are presented in Table 16 in Appendix B.3.

[28] The bending moment sign was based on figure 36, which was based on the theoretical calculations.

After the study of the transversal bending moments, the longitudinal bending moments "*My*" were studied in Appendix A.7. These stresses were supposed negligible in the theoretical calculations carried out by Torroja. The maximum Lusas longitudinal bending moment, 456 kg·m/m, is located at the connection between the seagull and the edge. However, this value can be considered practically negligible in comparison with the maximum value of the transversal bending moments[29]. Therefore, the hypothesis assumed by Torroja was confirmed.

The last studied element was the isobars because the reinforcement bars were based on these diagrams. The analysis was divided into different parts: Firstly, the overall shape and the maximum values along the central directrix were studied. After that, the overall shape of the along the plan of half-undeveloped section diagrams was analyzed.

The first study of the isobars, based on the values along the central directrix, consisted of the comparison between the Lusas results, considering the load case four, and the Torroja's diagrams (figures 39 and 40). This analysis shows the following conclusions: Firstly, the shapes have different peaks localization in both models. For example, in the maximum tension stress diagram, the maximum value obtained by Torroja is reached closer from the connection between both lobes, at the coordinate X = 20.11 metres, than in the Lusas results, located at X = 21.59 metres (Table 19, Appendix B.4). Other example is presented in the maximum compression stress diagram; the maximum value obtained by Torroja was located at the smallest cylindrical sector, at X = 24.8 metres, instead of at the biggest lobe, X = 13.55 metres, as is obtained by Lusas (Table 20, Appendix B.4). Secondly, in the Torroja's diagram of maximum tension stress, the highest values are located around the connection between the smallest cylinder and the wall. For example, at the point X = 32 metres, the Lusas value is 5 % of the results obtained by Torroja (Table 21, Appendix B.4). Thirdly, in the Torroja's diagram of maximum tension stress, more points with null value around the maximum peak were measured. Fourthly, in the Torroja's diagram of maximum compression stress, there was less number of points with null value than in the Lusas results.

The second study of the isobars, based on the plan of half section of the shell, consists of the comparison between the results calculated by Lusas (figures 52 and 53) and the Torroja's diagrams (figure 35). In order to make easier this comparison, the points where the maximum values measured by Torroja were exceeded, were coloured in red for tension stress and in blue for compression stress. After this analysis, some conclusions were obtained: Firstly, the overall shape of both plans is highly similar. Therefore, as the reinforced bars are located following the isobars, the localization of the reinforcement was right. Secondly, the maximum values calculated by Lusas[30] are higher[31] than the results obtained by Torroja. These differences observed between both models are too much notable to be explained only for errors in the procedure of calculation. Consequently, this problem has two logical explanations: Torroja's calculations were wrong or some assumption introduced in the Lusas model is not true. The possible solution of this problem was found in the last page of the Torroja's report where Torroja wrote a note for Dischinger, who was considered that the

[29] The maximum value of the transversal bending moments was around four times higher than the maximum value of longitudinal bending moment (Appendix A.7).

[30] 28 MPa for maximum tension stress.

[31] 3.5 times higher for the maximum tension stress.

thickness of 8 centimetres at the smallest cylindrical sector was too small[32]. In that note, Torroja explained that the theoretical thickness considered at the smallest lobe was 11 centimetres, instead of the 8 centimetres supposed by Dischinger (Torroja 1942, p.166). This thickness corresponded to the real thickness for that section. Therefore, the hypothesis of real thickness in the theoretical calculations carried out by Torroja is more probable. For that reason, in the second model the variation of the thickness along the shell was studied with the purpose of identifying the observed discrepancies in the first model.

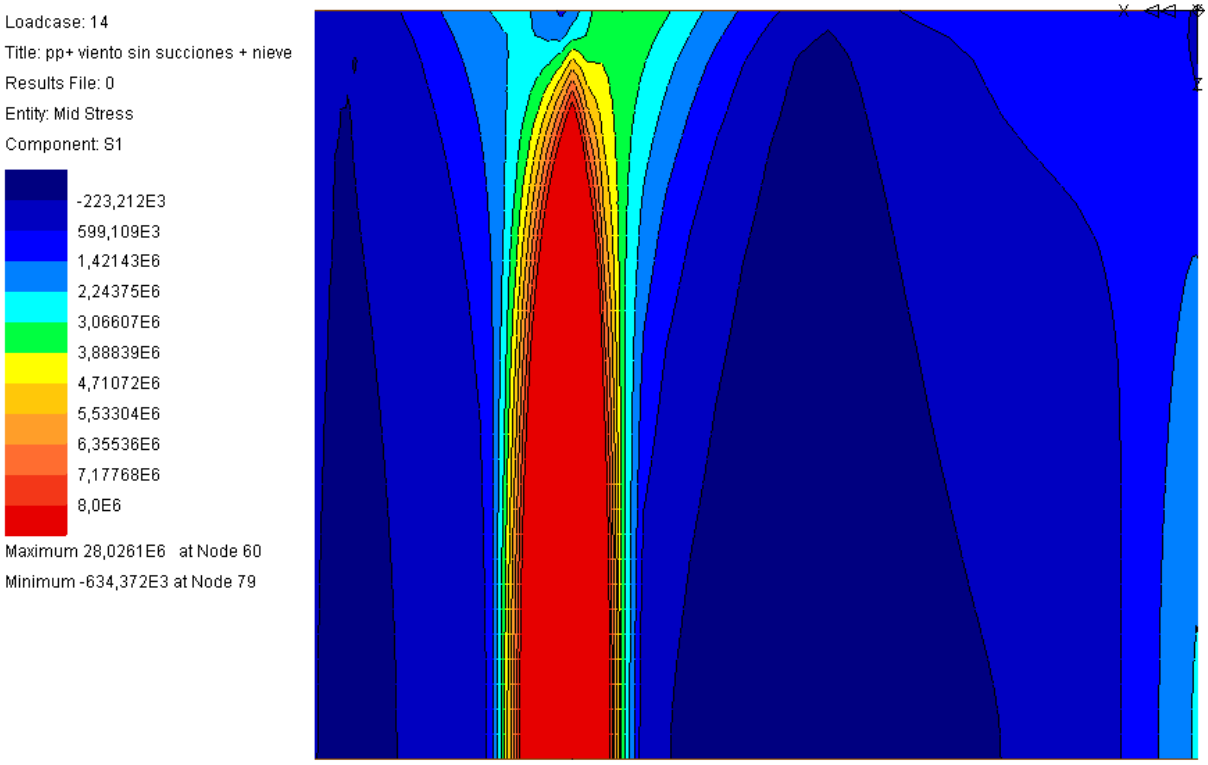

Figure 52: *Maximum tension stress isobars along the plan of the half-undeveloped section in the first Lusas model*: The smallest cylindrical sector is located on the left. The maximum value, 28 MPa, is located at the connection between both lobes.

[32] Dischinger wrote this observation in his work "Entwicklung und Fortschritte im Eisenbeton".

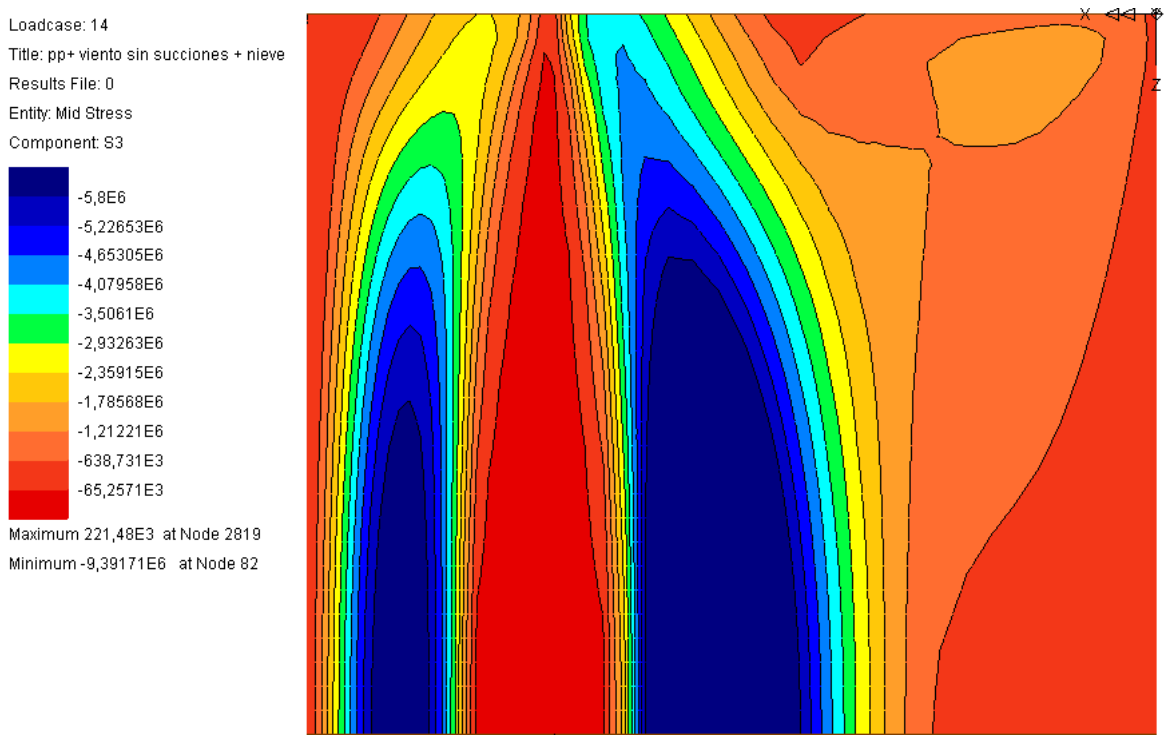

Figure 53: *Maximum compression stress isobars along the plan of the half-undeveloped section in the first Lusas model*: The smallest cylindrical sector is located on the left .The maximum value, 9.39 MPa, is located at the biggest lobe.

3.1.4 Conclusions.

Along the analysis of the first model, the following conclusions were obtained. Firstly, the model shows correctly the structural behaviour of the theoretical model considered by Torroja. For example, symmetrical vertical deflections is obtained when symmetrical loads are applied. Secondly, the most probable load case used by Torroja in the calculation of the isobars and deflections is the load case four consisting of dead weight, snow and wind load. Thirdly, the diagram of vertical deflections presented in figure 37, was measured in the central directrix. Fourthly, the maximum values of vertical deflections are located at the small cylindrical sector. Fifthly, the Lusas vertical deflections are generally lower than the results obtained by Torroja. These discrepancies can be explained by the higher weight and stiffness of the skylights because this hypothesis are not considered in the first model. Other factor that can explain these discrepancies is the error made in the measurement of the Torroja's deflections, which were measured directly in figure 37. However, the assumption of the thickness variation, carried out in the second model, produces a stiffer structure reducing the vertical deflections. Therefore, the results obtained in the second Lusas model will probably be more different to the Torroja's deflections. Sixthly, the bending moments presented in figure 36 by Torroja were based on calculation mistakes. Therefore, these values were not considered in the following models. Seventhly, the Lusas bending moments are higher than values supposed in the calculation of the reinforcement bars. This factor can be explained by different hypotheses considered in both models. For example, the assumption of the thickness variation along the shell might reduce the transversal bending moments. Eighthly, the longitudinal bending moments can be considered negligible, as was supposed by Torroja in the theoretical calculations. Ninthly, the peak of the isobars of maximum tension stress

obtained by Torroja along the central directrix is located closer from the connection between both cylindrical sectors than in the Lusas results. Tenthly, the peak of the isobars of compression stress obtained by Torroja was located at the biggest lobe. However, in the Lusas model this point is located at the smallest cylindrical sector. Eleventh, the overall shape of the Lusas isobars is highly similar to the Torroja's diagrams. Therefore, as these diagrams were used in order to calculate the reinforcement bars, the localization of these reinforcements were right. Twelfth, the differences of the maximum values calculated by Lusas in the isobar diagrams are too much pronounced to be explained only for errors in the procedure of calculation. The possible explanation of this problem can be the assumption of the hypothesis of real thickness in the theoretical calculations. For that reason, the second model was studied with the purpose of identifying if the variation of thickness can explain the observed differences in the maximum values of the isobars.

3.2 Second Model: Variable Thickness.

The shell was designed with thickness variation along the directrix (figure 54) in order to optimize the structural behaviour of the roof. The thickness began with 8 centimetres at the connection between the biggest cylindrical sector and the wall. The thickness is increased 8 centimetres in order to connect with the skylights. At the skylight edges, the thickness was not measured in the consulted construction drawing and it was assumed 16 centimetres (Antuña 2003, p.142). The maximum thickness, 30 centimetres, was located at the seagull profile in order to cover the tie bars proposed by Torroja (Torroja 1942, p.16). Finally, at the top of the smallest lobe the thickness was 11 centimetres.

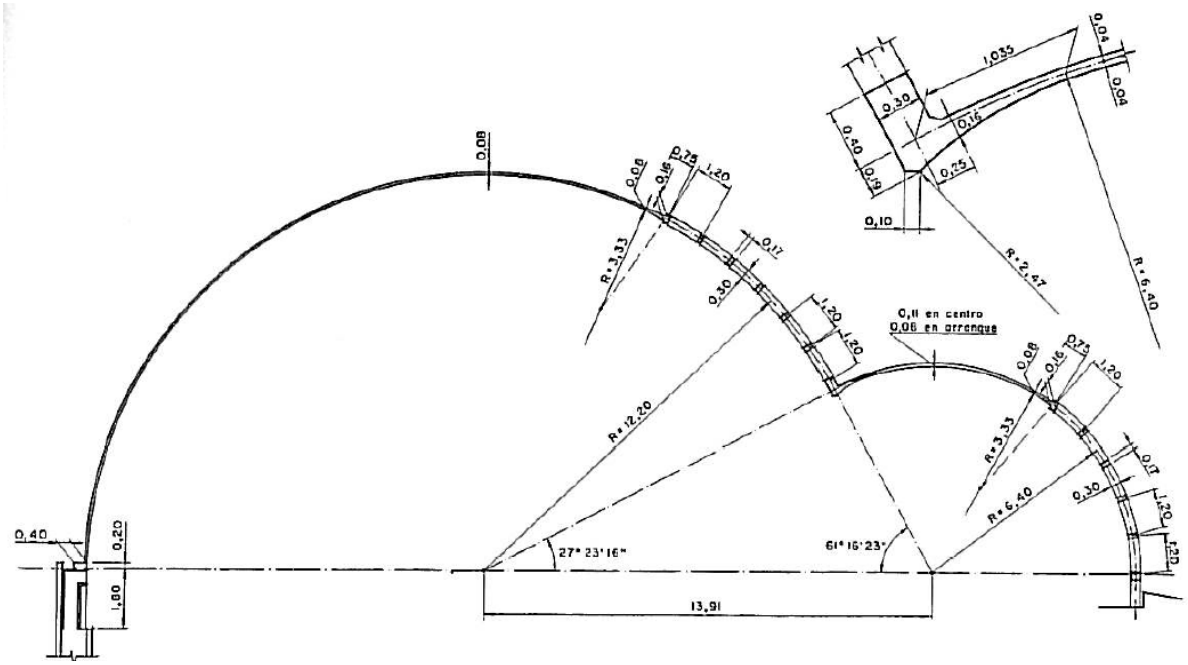

Figure 54: *Variation of thickness along the central directrix*. All the distances are measured in metres.

3.2.1 Hypotheses and Objectives.

The second model (figure 55) was studied in order to find the explanation for the values obtained in the Lusas isobars, which were too much higher than the results presented by Torroja. The additional objectives were checking if the hypothesis of constant thickness was used in the calculation of the bending moments obtained by Torroja as well as if the increase of the thickness improved the structural behaviour of the shell.

The element incorporated to the first model is only the assumption of variable thickness along the surface of the shell. However, the dead weight of the shell was supposed to be constant with the same value, 250 kg/m^2, considered in the first model. Therefore, the difference between both first models is that the second model is stiffer than the first one. The assumption that the variation of thickness could reduce the maximum values of the isobar diagrams is a logical because if, as approximation, the thickness used to calculate the first Lusas isobars is

increased by hand[33], the value is more similar to the results presented by Torroja. For example, the maximum tension stress obtained in the first model changes from 28 MPa to 7.5 MPa (formula 10). This stress is more similar to the maximum value calculated by Torroja, 8 MPa. However, the accurate results have to be obtained changing the thickness in all the elements in order to consider the effects of the shell as a whole.

$$\frac{28 \cdot 0{,}08}{0{,}30} = 7{,}5 \text{ MPa} \qquad [10]$$

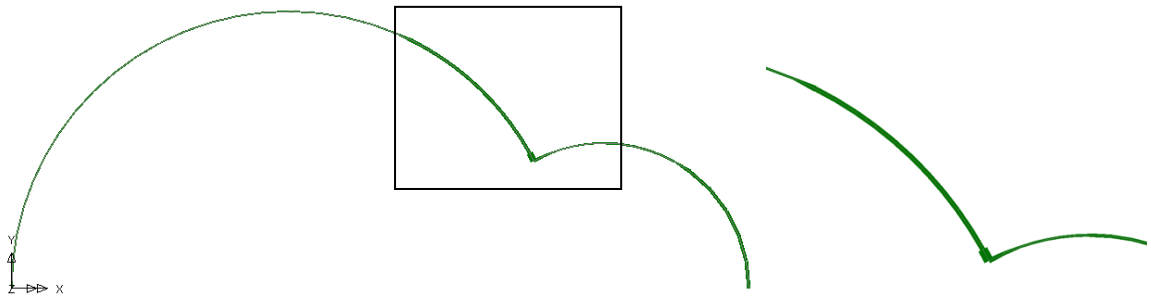

Figure 55: *Variation of thickness along the directrix in the second Lusas model* and *zoom of the seagull profile.*

The Lusas model was based on the following characteristics: Firstly, the geometry was defined by 36 surface elements QSI4 (figure 56) in order to model the thickness variation along the shell as well as the support conditions (Appendix A.4). These surfaces were meshed considering a number of finite elements that balanced the accuracy and the calculation speed in the Lusas model. Secondly, the supports and the procedure used to define the loads consisted of the same elements as defined in the first model.

[33] Multiplying the stress for the real thickness in each point and dividing for the constant thickness considered in the first model.

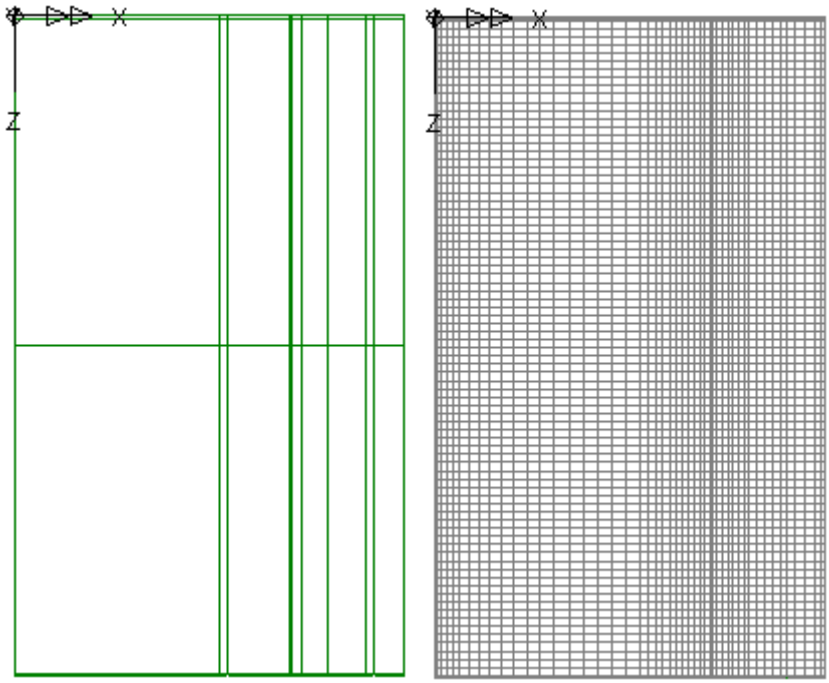

Figure 56: *Plan of the surface elements used in the second Lusas model* and *plan of the mesh used in the second Lusas model.*

3.2.2 Analysis.

The analysis is divided in the same parts studied in the first model: Firstly, the overall deformation shape and the maximum values of the deflections are studied. Secondly, the bending moments are analyzed. Finally, the diagrams of isobars are studied.

In the second model, the load combination considered is the load case four: dead weight, snow and wind loads.

In addition of the hypothesis explained in the section 3.1.2, the analysis started from other additional premises: Firstly, the vertical deflections and the bending moments might be reduced because the structure is stiffer and has to resist the same applied loads. Secondly, the deflections should be more similar to the deformations obtained by Torroja in the actual structure as well as in the small-scale model because both shells were constructed considering the variation of thickness. Thirdly, the structural behaviour under symmetrical loads should be symmetric. All these assumptions are studied along this chapter.

The first analysis was based on the vertical deflections along the central directrix as well as along the seagull profile. In both diagrams, the shapes are similar to the results obtained in the first Lusas model. For example, the deflection shape at the seagull profile under symmetrical loads continues following a parabolic law (figure 57). However, the obtained deflections are lower because the stiffness of the structure is increased by the assumption of real thickness along the shell. For example, the maximum value of the vertical deflection, around 7 centimetres, is located at the smallest cylindrical sector. This value is approximately 10 centimetres lower than the deformation obtained in the first model, which means 50 % of the deformations measured by Torroja in the actual structure and in the small-scale model at the same location (Tables 4 and 5, Appendix B.2). Another example is the maximum value at the

seagull profile (figure 58), which is around 9 centimetres lower than the value obtained by Torroja.

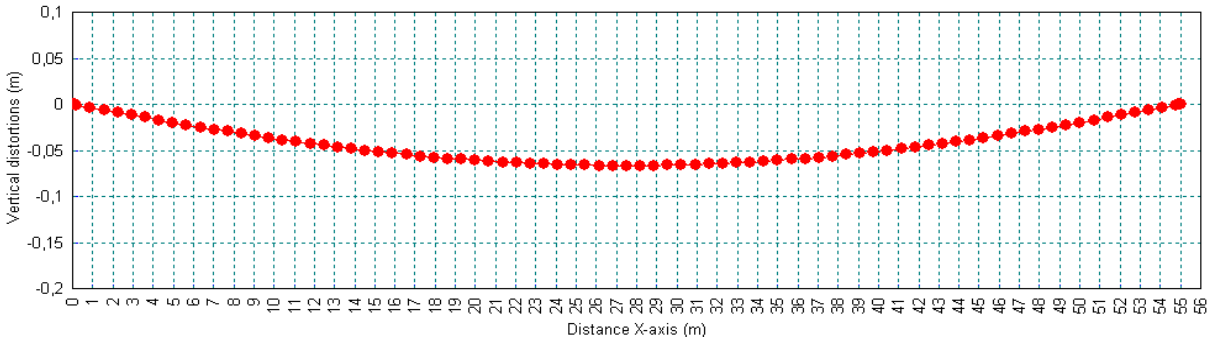

Figure 57: *Absolute vertical deflections presented by the second Lusas model along the seagull profile*. The maximum vertical deflection, around 6 centimetres, is located at Z = 27.5 metres.

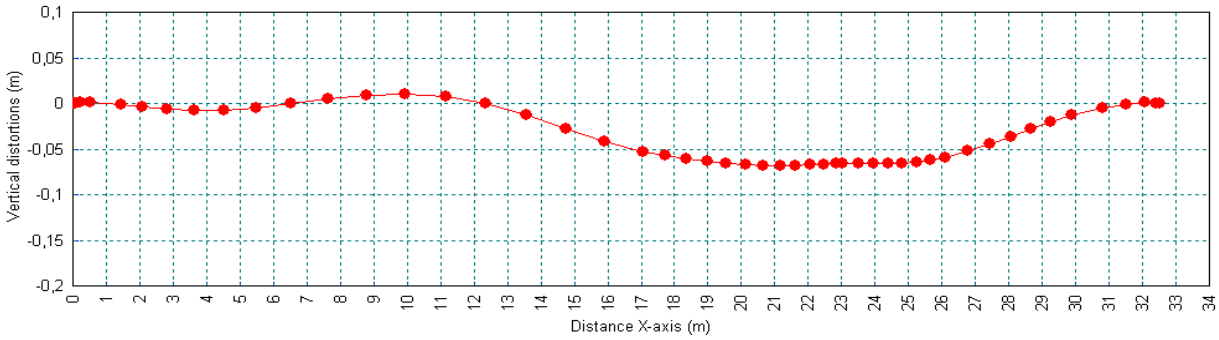

Figure 58: *Absolute vertical deflections presented by the second Lusas model along the central undeveloped directrix*. The maximum vertical deformation 6.84 centimetres is located at X = 21.4 metres.

The analysis of the deflections lead to different conclusions: Firstly, as was supposed in the starting premises, the vertical deflections are improved with the assumption of variable thickness because the structure is less flexible. Secondly, Torroja probably used 8 centimetres constant thickness in the calculation of the theoretical deflection shapes (figure 37) because the values of the first model are more similar to the deformations obtained by Torroja than the results calculated by Lusas in the second model. Thirdly, the results of the actual structure and the small-scale model should be more similar to the deflections presented in the second Lusas model than the deflections calculated in the first one because both models are based on the hypothesis of variation of thickness (figure 59).

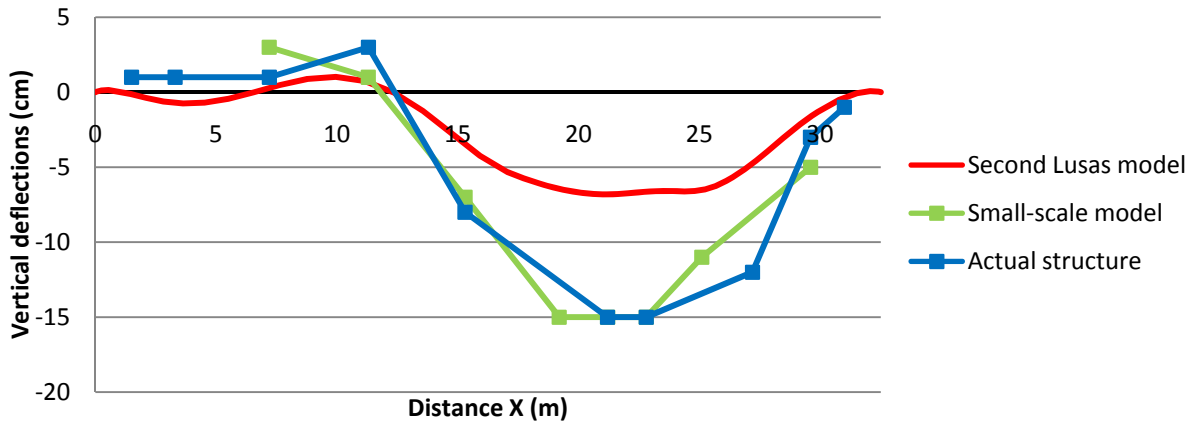

Figure 59: *Vertical deflections along the central undeveloped directrix considering different models*: Lusas deflections (red line), the results measured in the actual structure (blue line) and in the small-scale model (green line).

The second study was based on the bending moments, which analysis is divided into two parts: Firstly, the transversal bending moments are studied. In this section, the both first models as well as the theoretical results are compared. After that, the absence of longitudinal bending moments is checked comparing the results also with the first model.

The first analysis of the bending moments was based on the shape of the transversal bending moment diagrams. The shape obtained by Lusas (figure 60) is similar to the diagram presented by Torroja. Nevertheless, the values are generally higher in the Lusas model (figure 61). For example, 937 kg·m/m higher at the point 43, located at the biggest cylinder, this value is around three times higher than the values obtained by Torroja (Table 17, Appendix B.3).

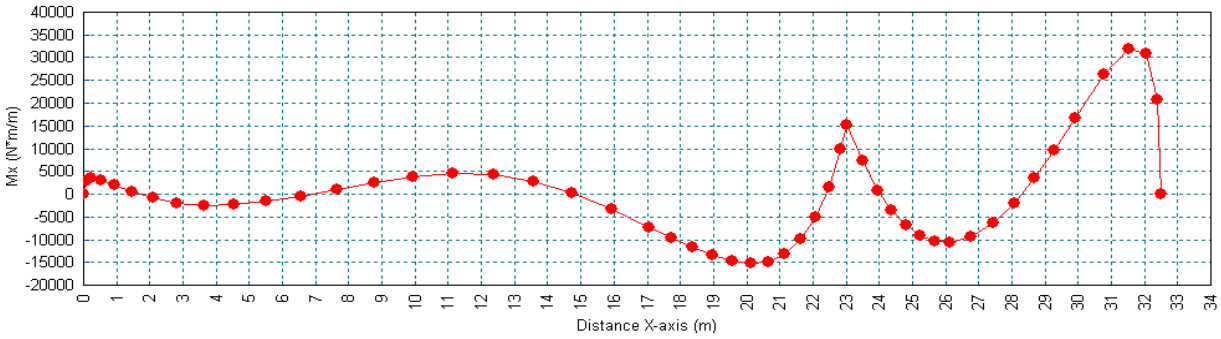

Figure 60: *Transversal bending moments presented by the second Lusas model along the central undeveloped directrix*. The maximum value, around 30000 N·m/m, is located at the smallest lobe.

The comparison between the first and the second Lusas models (figure 61) showed the following conclusions: First of all, the variation of thickness along the shell increases the transversal bending moments at the places where the thickness is increased, for example at the skylights. For that reason, the maximum value, located at the point 47, is 1458 kg·m/m higher than the results obtained in the first model. This value is aproximately three times higher than the maximum value calculated by Torroja (Table 17, Appendix B.3).

Analyzing all the previous results, the following conclusions, regarding the transversal bending moments, were obtained: Firstly, the assumption of constant thickness can be logically applied in the points located at the bigger cylinder and at the connection between both lobes because the bending moments calculated in the first model were higher. Secondly,

the assumption of variation of thickess increases the bending moments at the points where the thickness is increased. Therefore, in the calculation of the reinforcement bars located in those places, to be on the safe side, the hypothesis of constant thickness cannot be supposed because the values obtained by Torroja were lower above all at the smallest cylinder. For example at the point 47, the value obtained by Torroja was 2222 kg·m/m lower than the results obtained by the second Lusas model (Table 17, Appendix B.3).

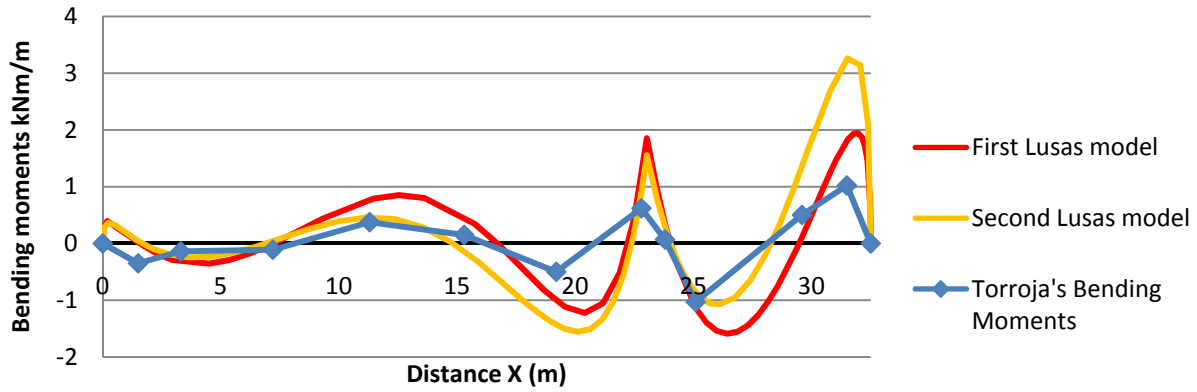

Figure 61: *Transversal bending moments along the central undeveloped directrix considering different models*. The values obtained by Torroja are coloured in blue, the first Lusas model is coloured in red, and the second Lusas model is coloured in orange.

After the study of the transversal bending moments, the longitudinal bending moments were studied. This analysis can be found in Appendix A.7. The maximum value is approximately 600 kN·m/m and is located at the connection between the seagull and the edge. However, this value is practically negligible in comparison with the maximum value of the transversal bending moments[34] confirming the hypothesis considered by Torroja.

The third element studied was isobars, which analysis is divided into different parts: Firstly, the overall shape of the isobar diagrams and the maximum values measured along the central undeveloped directrix are analyzed. After that, the overall shapes of the plan diagrams of isobars are studied.

The first study of the isobars consisted of the analysis of the values along the central directrix by means of the comparison between the Lusas results, considering the load case four in the first and the second model, and the values of the diagrams obtained by Torroja along the central directrix[35] (figures 62 and 63).

[34] The maximum value of the transversal bending moments was around five times higher than the maximum value of longitudinal bending moment (Appendix A.7).

[35] As was explained before, the values of the isobars presented by Torroja along the central directrix were measured directly from figure 35.

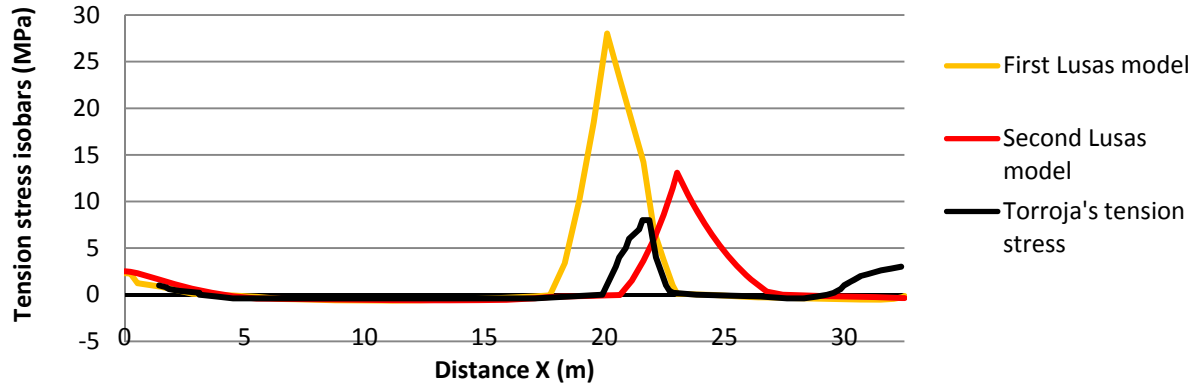

Figure 62: *Maximum tension stress isobars along the central undeveloped directrix considering different models*. The diagram is based on three lines: the first and the second Lusas model, which are coloured in orange and red, and the values obtained by Torroja, which are coloured in black.

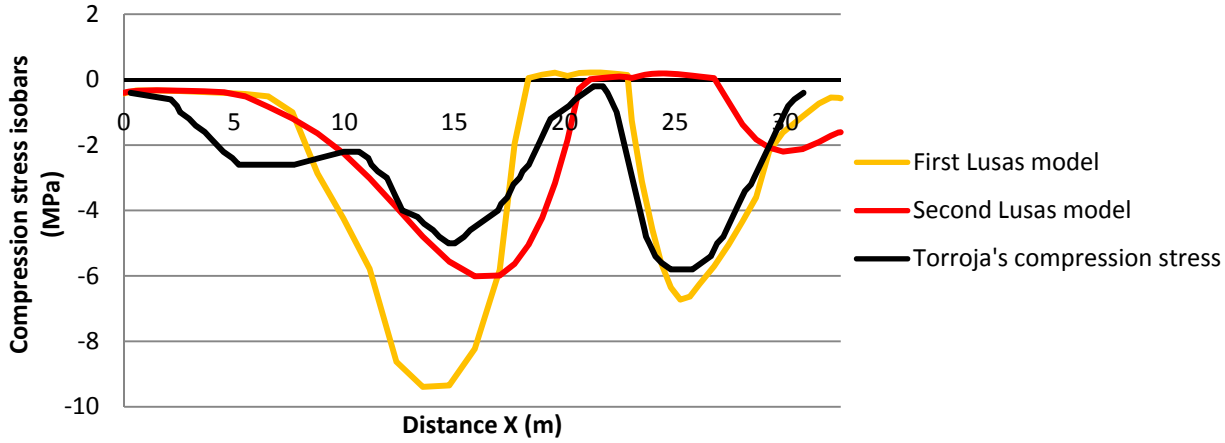

Figure 63: *Maximum compressions stress isobars along the central undeveloped directrix considering the load case four*. The diagram is based on three lines: the first and the second Lusas model, which are coloured in orange and red, and the values obtained by Torroja, which are coloured in black.

The analysis of the isobars of tension and compression stress showed the following conclusions: Firstly, the assumption of the thickness variation reduces all the maximum values observed in the first model. For example, considering the maximum tension stress the highest value changes from 28 MPa/m to 13.1 MPa/m. This variation means than in this peak the compression stresses are around 50 % lower in the second model. Secondly, the maximum value of the tension stress in the second model is located at the connection between both cylindrical sectors, coordinate X = 23 metres. However, this peak is located in the others models at the biggest lobe. For example, in the Torroja's model at the coordinate X = 21.59 metres (Table 22, Appendix B.4). Thirdly, in the diagram of tension stress presented by Torroja, highest values around the connection between the smallest cylindrical sector and the wall were calculated as well as there were more points with null value around the maximum peak. Fourthly, in the diagram of compression stress presented by Torroja, there was less number of points with null value than at the Lusas results. Fifthly, the shape of the isobars of compression stress in the Lusas models have the maximum values located at the biggest cylindrical sector. For example, the maximum value of the isobars of compression stress in the second model is located at the coordinate X = 15.91 metres. However, the maximum values in the Torroja's model were measured at coordinate X = 24.8 metres, located in the

smallest cylindrical sector (Table 23, Appendix B.4). Sixthly, the value of the isobars of compressions stress in the second Lusas model located at the smallest lobe, are highly similar to the values presented by Torroja. For example, at the point X = 24.8 metres, it was reached the peak in the diagrams presented by Torroja, which value was -5.8 MPa/m, as well as the value measured for the first model was -6.36 MPa/m. However, the value obtained in the second model at the same point is only 11 % of the maximum value obtained by Torroja (Table 24, Appendix B.4).

The second study of the isobars was based on the comparison of the plan diagrams of isobars calculated by Lusas with the diagrams presented by Torroja in figure 35. In order to make easier this comparison, the points where the maximum values measured by Torroja were exceeded, were coloured in red for tension stress and in blue for compression stress.

The analysis showed that the hypothesis of variable thickness was used in the diagrams of isobars presented by Torroja for different reasons: Firstly, the overall shapes (figures 64 and 65) are more similar to the isobars obtained by Torroja than the shapes calculated by the first model. Secondly, the maximum Lusas values[36] are more similar to the maximum values calculated by Torroja, for example the maximum compression stress the value is approximately only 4 % higher in the Lusas model. However, the maximum value of the isobars of tension stress is 63 % higher than the results presented by Torroja (Table 25, Appendix B.4). This value showed that probably it could be errors in the calculation of the maximum values of the tension stress calculated by Torroja. This question was raised[37] to Jose Antonio Torroja Canavillas, Eduardo Torroja's son, who is a very prestigious and well-known civil engineering. He argued that the observed differences can be logically assumed because the calculations were done by hand. This procedure made usually some mistakes as a consequence of the complexity of the calculations. For that reason, Soler explained in the article "Eduardo Torroja profesor" published in the book "Eduardo Torroja: La vigencia de un legado" how Torroja entrusted two calculation teams with the check of the solution of the equation system. However, both groups presented two different solutions. After that, Torroja tried that the solution proposed by each team would be obtained by the other team and finally four different solutions were presented. (Soler 2002, p.221). As a consequence of this high variation of the calculations made by hand, Torroja decided to build the small-scale model in order to be sure of the results.

[36] 13.07 MPa for maximum tension stress and -6.01MPa for maximum compression stress (figures 64 and 65).

[37] Consultation realized by Ignacio Payá Zaforteza. The 6th of April 2009 in Madrid.

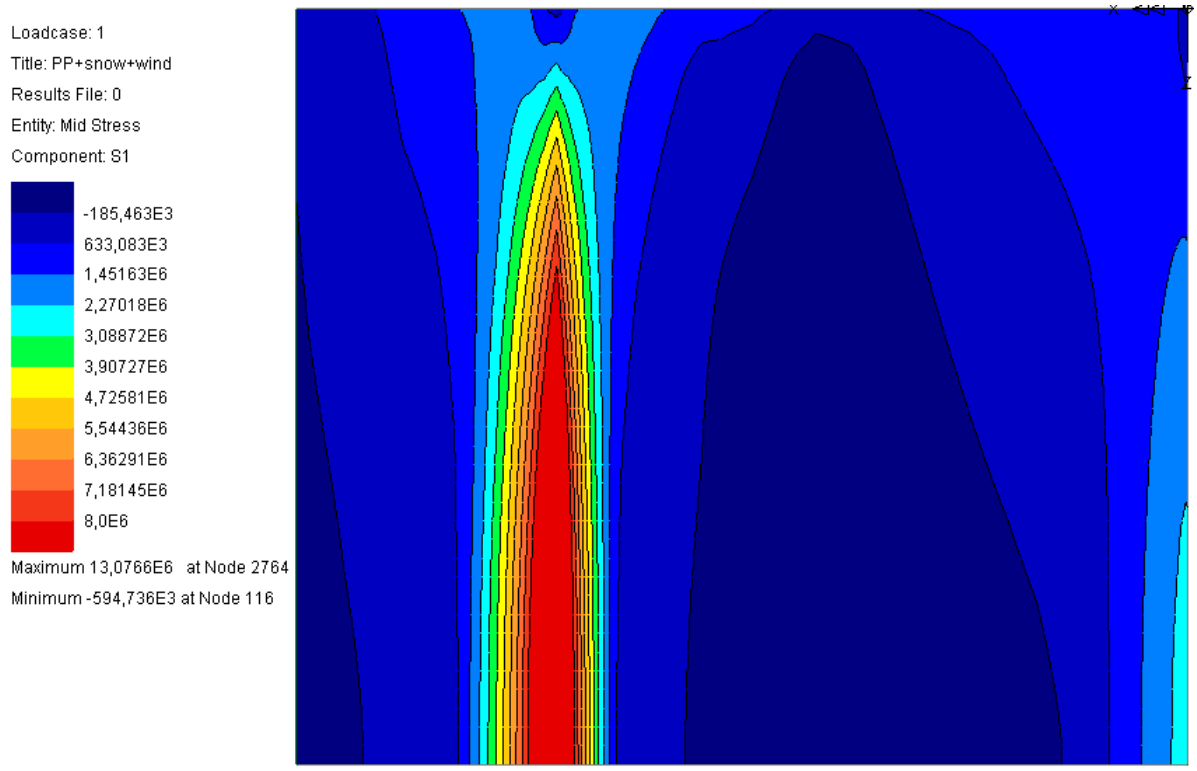

Figure 64: *Maximum tensions stress isobars in half-undeveloped plan obtained by the second Lusas model.* The maximum value, 13.08 MPa, is located at the connection between both cylinders.

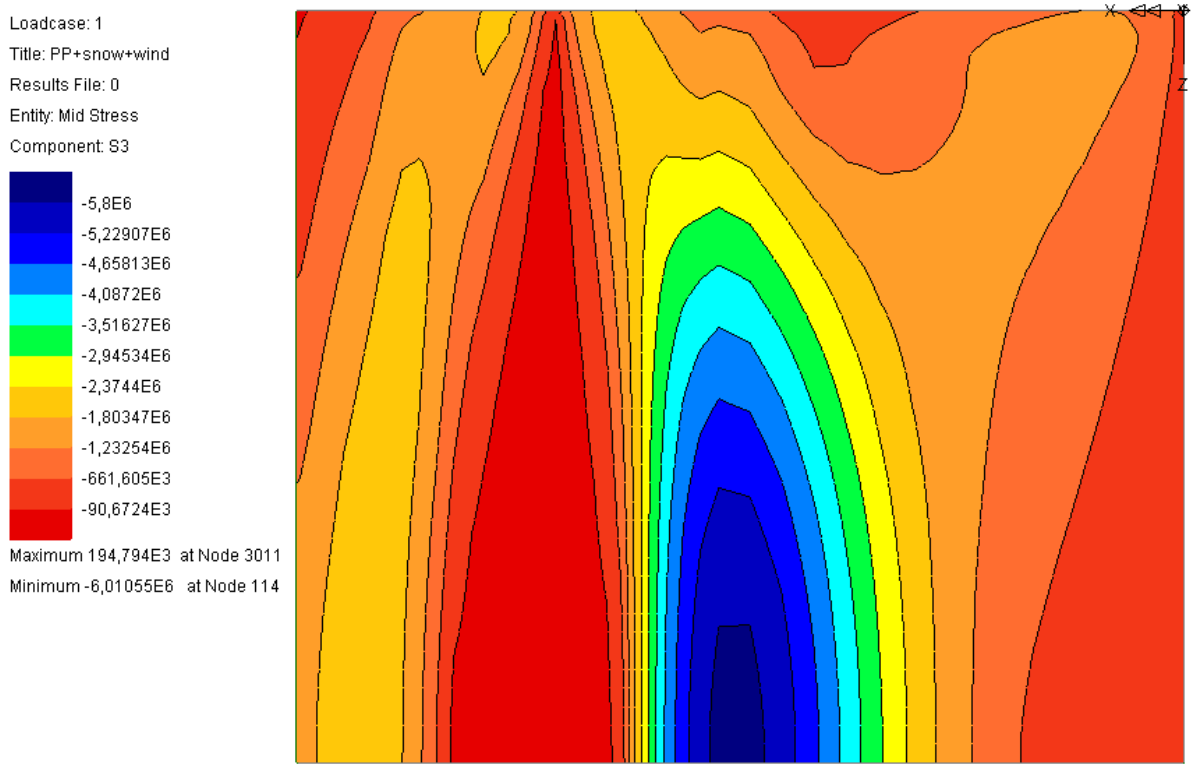

Figure 65: *Maximum compression stress isobars presented in half-undeveloped plan obtained by the second Lusas model*. The maximum value is -6.01MPa and is located at the biggest cylindrical sector.

3.2.3 Conclusions.

Along the analysis of the second model, the following conclusions were obtained: Firstly, the shape of the deflections calculated by the second Lusas model is similar to the results obtained by the first model. However, the vertical deflections measured in the second model are lower because the assumption of thickness variation increases the stiffness of the model. Secondly, Torroja probably used 8 centimetres constant thickness in the calculation of the theoretical deflection shape (figure 37), because the values of the first model are more similar to the deformations obtained by Torroja than the deflections measured in the second model. Thirdly, the assumption of constant thickness can be applied in the points located at the bigger cylinder and at the connection between both lobes because the bending moments calculated in the first model were higher than results obtained in the second Lusas model. Fourthly, the assumption of variation of thickess increases the bending moments at the smallest cylinder. Therefore, in the calculations of that area, to be on the safety side, the hypothesis of constant thickness cannot be supposed. Fourthly, the transversal bending moments supposed by Torroja in the calculation of the reinforcement bars were on the side of the insecurity above all at the smallest cylinder because the values were lower than the results obtained by the second Lusas model. Fifthly, the longitudinal bending moments can be negliged, as was supposed by Torroja. Sixthly, the maximum values of the isobars of compression stress are located, as in the first Lusas model, at the biggest cylindrical sector instead of at the possition supposed by Torroja at the smallest lobe. Seventhly, the maximum values of the isobars of tension stress are located at the connection between both lobes instead of at the biggest cylinder as was obtained by Torroja. Eightly, the consideration of thickness variation reduced highly the isobars of compression stress at the smallest cylindrical sector. Ninetly, as was supposed at the beginning of the study, the maximum values of the isobars are reduced regarding the first model because the structure is less flexible. For example, the maximum value of the compression stress is only 4 % higher than the results presented by Torroja. However, the maximum value of the tension stress continues being too much higher and the possible explanation is the errors produced during the calculation procedure as was explained by José Antonio Torroja Canavillas.

3.3 Third Model: Wind Suction Effects.

The effect of the wind suction was originally not considered in the theoretical calculations because the importance of this phenomenon would be reduced regarding to the cylindrical shape by the height and proximity of the nearby buildings as well as by the shape of the lobes. Furthermore, Torroja supposed that the suction effects improved the structural behaviour of the shell because its effect would be similar to reducing the dead weight and increasing the lateral compression stress. However, when the shell had been calculated, in the report carried out by Mr Ribera and Aguirre to check the work viability of the structure, the study of the wind suction effects in a small-scale model of 1/10 was recommended. Consequently, Torroja used the experimental results of the cylindrical shape to approximate the wind suction law along the directrix (figure 66). This law consisted of a linear combination of the snow and wind loads, which were explained before, in order to obtain the wind suction without repeating the theoretical calculations (Torroja 1942, p. 21).

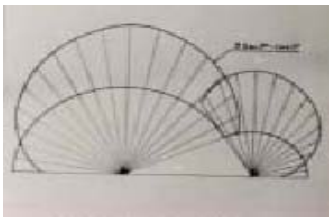

Figure 66: *Suction along the directrix proposed by Torroja.*

The study of the third model is divided into different parts: Firstly, the hypotheses and the objectives are presented. Secondly, the analysis of the model is showed. Finally, the conclusions are showed.

3.3.1 Hypotheses and Objectives.

The third model consisted of the same Lusas model used in the second model because both models were based on the same general hypotheses. However, the incorporated difference to the second model was the consideration of the wind load law including suction effects (figure 66) instead of the wind hypotheses supposed in the initial calculations carried out by Torroja.

The main objective of the third model is modelling the behaviour of the shell considering the suction effects and comparing the obtained results with the Lusas model results. After that, the different hypotheses considered by Torroja regarding the wind suction effects are analyzed.

3.3.2 Analysis.

The analysis is divided in three different sets of results[38]: the vertical deflections, the bending moments and the isobars. For each of these sets four load cases were studied:

[38] All the diagrams of the isobars considering the different load cases are presented in Appendix A.8.

- Load case A: Dead weight.
- Load case B: Dead weight and wind including suction load.
- Load case C: Dead weight, snow load and wind without suction load.
- Load case D: Dead weight, snow load and wind with suction load.

The defined load cases followed two different objectives: On one hand, the purpose of the load cases A and B was checking the hypothesis proposed by Torroja "the suction effects reduce the dead weight" (Torroja 1942, p.21). This assumption was studied considering the wind suction effects without other overloads. On the other hand, the objective of the load cases C and D was analyzing the effect of the suction when all the overloads were applied.

The analysis of the deflections was divided into the two parts explained before: the assumption of the wind suction effects without other overloads and the assumption with the rest of overloads.

The first element studied was the deflections considering the wind suction effects without other overloads and the analysis was based on the comparison of the vertical deflection diagrams along the central undeveloped directrix considering the load cases A and B (figure 67). This analysis showed that the vertical deflections are highly similar for both load cases from the connection between the biggest cylindrical and the wall, X = 0 metres, to the biggest lobe axes, located at the coordinate X = 12.2 metres. For example, at the coordinate X = 10 metres, the vertical deflection difference is only 0.11 centimetres (Table 8, Appendix B.2). However, in the rest of the directrix the deflection differences are higher. For example, at the seagull profile, X = 23 metres, the vertical deflection variation between both load cases is 1.5 centimetres. Furthermore, the vertical deflections measured at the same point considering the load case B are 67 % of the deformations measured in the load case A (Table 9, Appendix B.2).

After the study of all the previous considerations, the next conclusion was obtained: the assumption of the wind suction effects, when there other overloads are not applied, reduces the vertical deflections in all the points with X coordinate higher than 12.2 metres, because the shell is raised by the suction phenomenon. Therefore, in these points the Torroja's hypothesis, "the wind suction effects reduce the deflections produced by the dead weight", was confirmed.

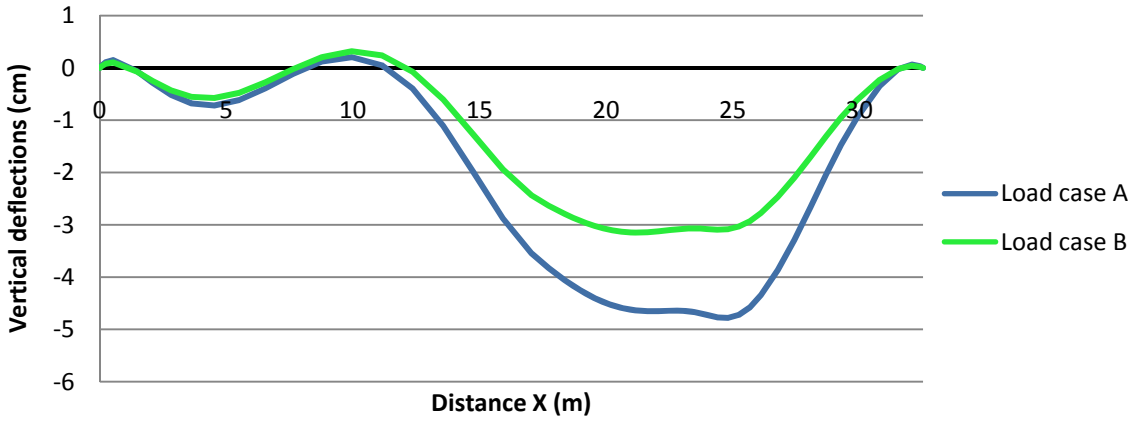

Figure 67: *Vertical deflections along the central undeveloped directrix considering different load cases in the third Lusas model.* The load case A is coloured in blue, and the load case B is coloured in green.

The second part of the study of the deflections consisted of the analysis of the deflection shape along the central undeveloped directrix, considering the load cases C and D (figure 68). This analysis showed favourable differences in both cylindrical sectors. On one hand, the assumption of the wind suction effects reduces the negative vertical deflections in the points with X coordinate higher than 12.2 metres. For example at the seagull profile, X = 23 metres, the vertical deflections are 2.56 centimetres higher in the load case C (Table 10, Appendix B.2). On the other hand, the assumption of the wind suction effects reduces also the positive deflections at the biggest cylindrical sector. For example, at the point X = 10 metres the values measured in the load case D are practically 16 % of the results obtained in the load case C (Table 10, Appendix B.2).

The analysis of the deflections showed as a conclusion that the assumption of the wind suction effects reduces the vertical deflections in all points of the shell when the overloads are or not considered. Therefore, the hypothesis supposed by Torroja in the theoretical calculations, the wind suction effects improves the structural behaviour, was confirmed in the vertical deflections.

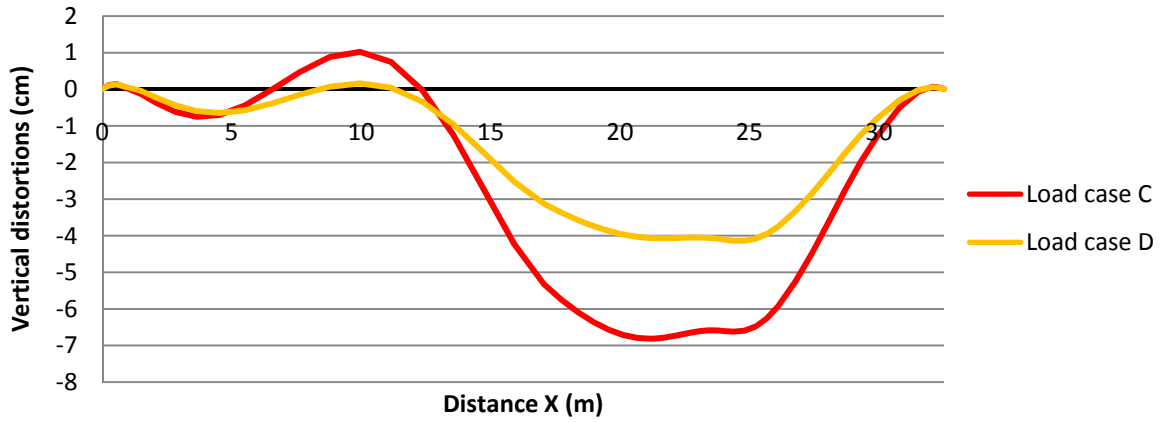

Figure 68: *Vertical deflections along the central undeveloped directrix considering different load cases in the third Lusas model*. The load case C is coloured in red and the load case D in orange.

After the analysis of the deflection, the bending moments as well as the isobar diagrams were studied. The initial consideration in the study of these stresses was that if the wind suction effects improved the vertical deflections, the stresses would be reduced in the structure. In order to check this hypothesis, an analysis of the bending moments and isobars along the central undeveloped directrix, considering the four load cases, was carried out (Appendix A.8). Analyzed the obtained diagrams, the initial supposition for both stresses were confirmed.

3.3.3 Conclusions.

After the study of the third model, the following conclusions were obtained: Firstly, the wind suction effects reduce the deflections, the bending moments and isobars of the dead weight. Secondly, when the wind suction loads and the rest of overloads are considered, the Lusas results along the central directrix are reduced. Lastly, the hypothesis that the suction phenomenon improves the structural behaviour was confirmed. Therefore, the hypothesis supposed in the theoretical calculations regarding not considering the wind suction effects, can be logically assumed.

3.4 Fourth Model: Skylights.

The sunlight was one of the initial objectives pursued in the design of the Frontón Recoletos by Torroja. Finally, this factor was obtained by the construction of two large longitudinal skylights, which consisted of a frame[39] of equilateral triangles (figure 69) whose sides measured 1.4 metres. These skylights were placed close to the connection between both lobes in the biggest cylindrical sector and close to the connection with the wall in the smallest sector.

The Frontón Recoletos was the first thin concrete shell structure where these skylights were used. Furthermore, the existing theoretical methods, in the period when the structure was constructed, were based exact theoretical models resolved by hand. However, these methods had never been used before in any discontinuous shell and therefore the structure was considered a structural challenge and one way to improve the knowledge about the behaviour of this kind of shells. These theoretical methods were simplified by Torroja supposing the skylight behaviour as a normal closed shell in order to calculate the structure by hand.

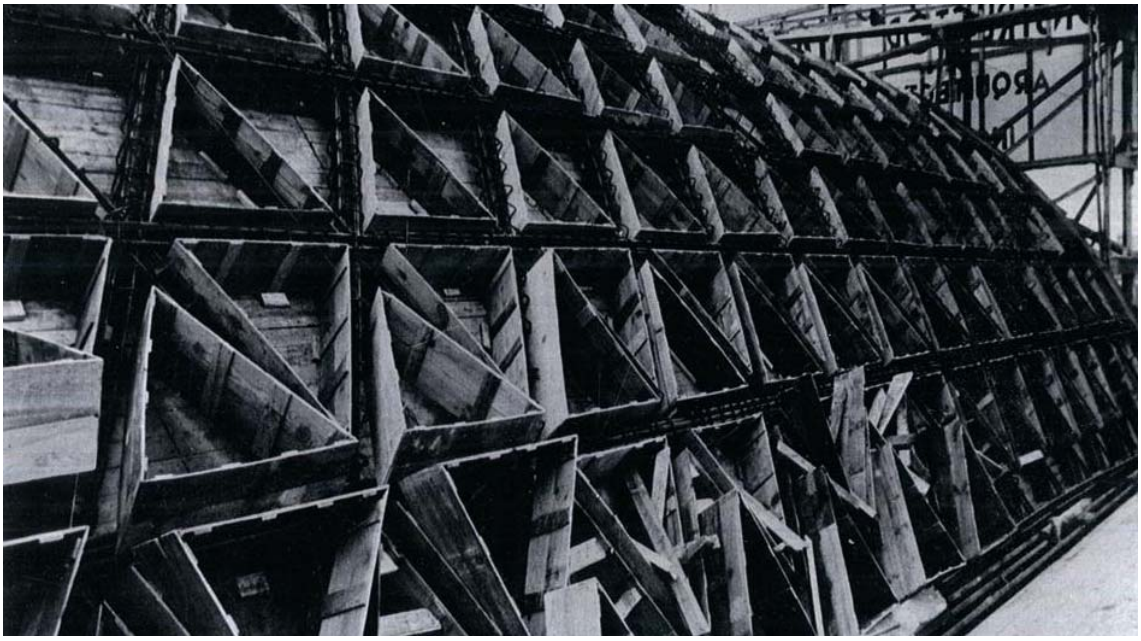

Figure 69: *Construction of the skylight beams using wooden frameworks.*

The study of the fourth Lusas model is divided into three parts: First, the hypotheses and objectives are explained. Secondly, the principal characteristics of the results obtained by Lusas are analyzed. Finally, the obtained conclusions are showed.

[39] The frame was based on rectangular beams 30 per 17 centimetres (Antuña 2003, p.142).

3.4.1 Hypotheses and Objectives.

The fourth model (figure 70 and 71) was based on the same hypotheses[40] considered in the preceding model, incorporating the real skylights instead of the closed shell section.

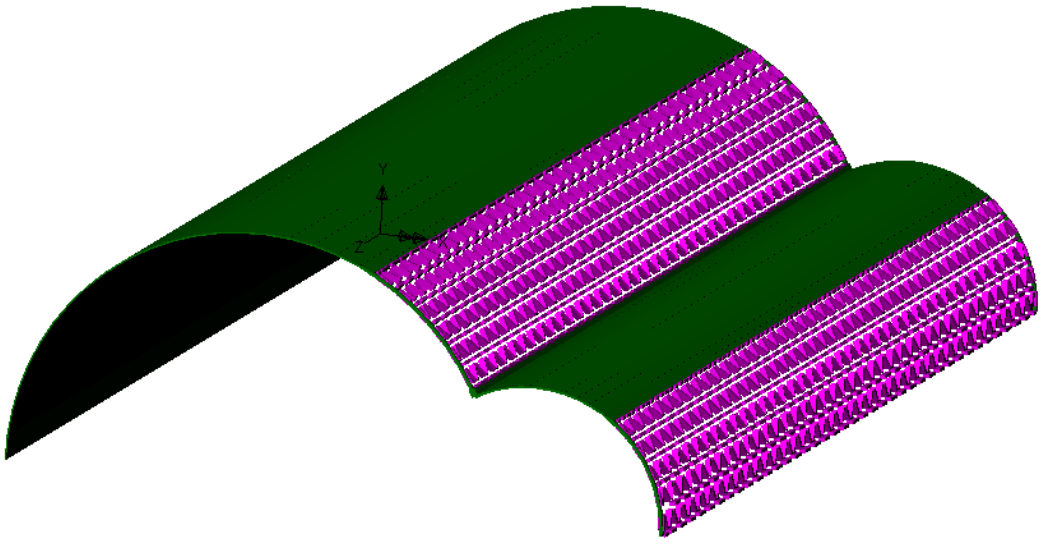

Figure 70: *3-D view of the fourth Lusas model*. The skylights are coloured in purple as well as the normal shell surface in green.

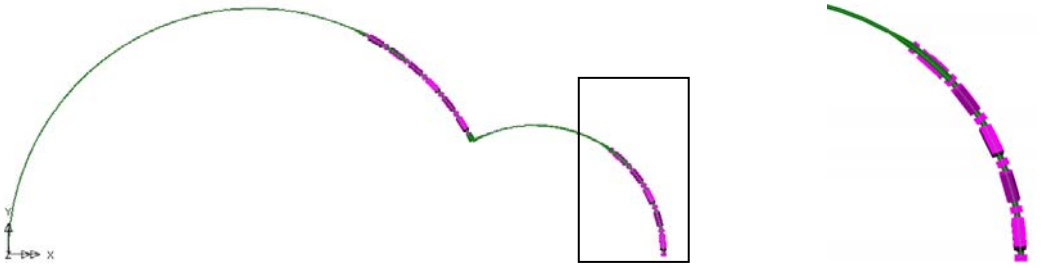

Figure 71: *Directrix of the fourth Lusas model* and *zoom of the skylight in the smallest cylindrical sector.*

The Lusas model was based on the following characteristics: Firstly, the geometry (figure 72) was divided into two different parts: On one hand, the shell consisted of 468 surface elements QSI4 in order to model the variation of thickness and the connection with the skylights[41]. These surfaces were meshed considering a balanced model between the accuracy and the calculation speed. On the other hand, the skylights were modelled with 1435 beam elements called BMS3 (Appendix A.1). These beams were divided in five finite elements. Secondly, the supports were modelled as in the first Lusas model. Finally, the procedure used to define the dead weight as well as the wind and snow loads, in the surfaces and skylights, is explained in Appendix A.3.

---

[40] Variation of thickness along the shell, homogenous material with null Poisson number, load case four: dead weight with snow and wind loads, supports continuous along the edges.

[41] At the connection between both elements were supposed beams elements in order to model correctly the real structural behaviour.

The main objective of the fourth model was checking the hypothesis considered in the theoretical calculations of replacing the skylights frames with closed surfaces in order to simplify the mathematical analysis. The other objective is checking the comparison with the results obtained by Torroja and the preceding models.

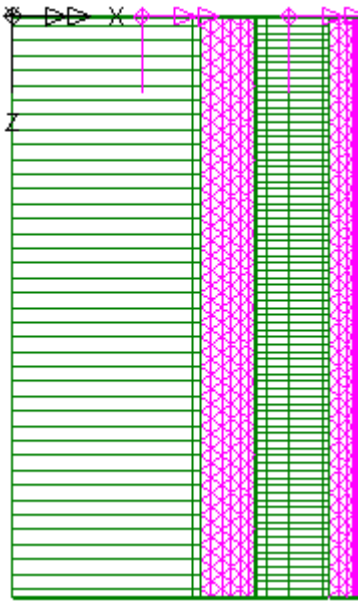

Figure 72: *Fourth Lusas model consisted of surfaces*, which are coloured in green, *and beam elements*, which are coloured in purple.

3.4.2 Analysis.

The initial hypotheses considered, analyzed all the results of the preceding models, were that the structural behaviour of the shell under symmetrical loads would probably be symmetric as well as the vertical deflections in the fourth model might be higher than the second model deflections because the assumption of the real skylights decreased the stiffness of the structure.

The first element studied was the deflections. This analysis was divided into three parts. First, the three-dimension Lusas model was studied analyzing the structural behaviour of the shell. After that, the Lusas deflections of the fourth model were compared with the results obtained in the second model in order to study the effect of the real skylights. Finally, the Lusas deflections obtained in the fourth model were compared with the vertical Torroja's deflections.

The first study of the deflections consisted of the analysis of the shape in the 3-D Lusas model (figure 73 and 74). The conclusions obtained from this analysis were the following: Firstly, the most unfavourable sections, referring to vertical deflections, are located parallel to the Z-axis. For example, the maximum deflection, 9.2 centimetres, is located at the central directrix (Table 6, Appendix B.2). Secondly, as was supposed at the beginning, the deflections are symmetrical when symmetrical loads are applied. Thirdly, the longitudinal movements along the Z-axis in the edged directrix allow reducing the bending moments in the structure

imitating the membrane behaviour. All these characteristics are highly similar to the previous models, where the skylights were modelled as a closed shell. Therefore, the hypothesis considered in the theoretical calculations of replacing the skylights frames with closed shell surface, can be logically assumed because the general behaviour of the both models is highly similar.

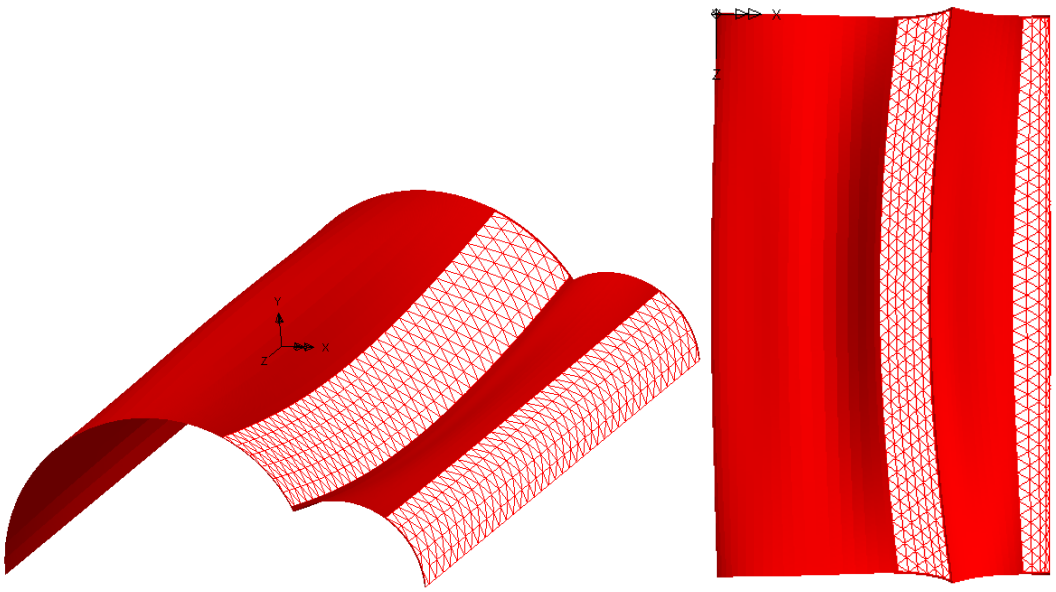

Figure 73: *Deflections in the 3-D view of the fourth Lusas model:* Isometric view and the plan view.

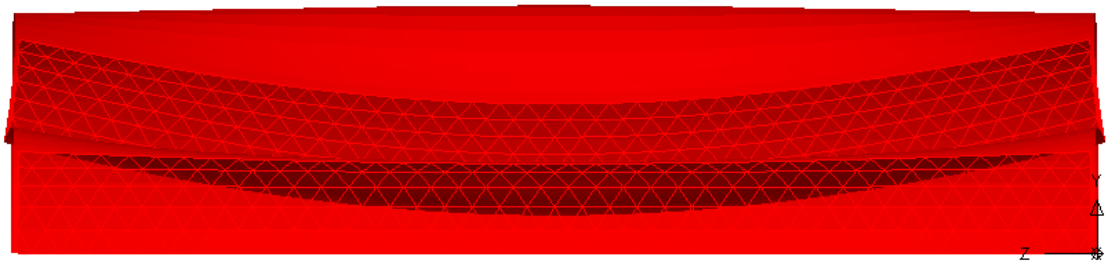

Figure 74: *Deflections in the 3-D view of the fourth Lusas model*. View parallel to X-axis at the section X = 32.5 meters.

The second study of the deflections was based on the comparison between the second and the fourth Lusas model. This comparison was studied in order to know how varied the deflections when the real skylights are introduced in the model. This study was based on the vertical deflection diagrams along the two most unfavourable sections: the seagull profile (figure 75) and the central directrix (figure 763). This study showed as a conclusion that the vertical deflections along the central directrix and the seagull profile are higher when the skylights are modelled as frames. For example, in the central directrix, at the coordinate X = 23 metres, the deflections are 35 % higher than the results calculated by the second model (Table 13, Appendix B.2). This conclusion can be explained by the fact that the hypothesis of real skylights produces a more flexible structure because the shell continuity is broken. Furthermore, the real loads in the skylights, which were heavier than the supposed in the preceding models loads, produced higher deflections.

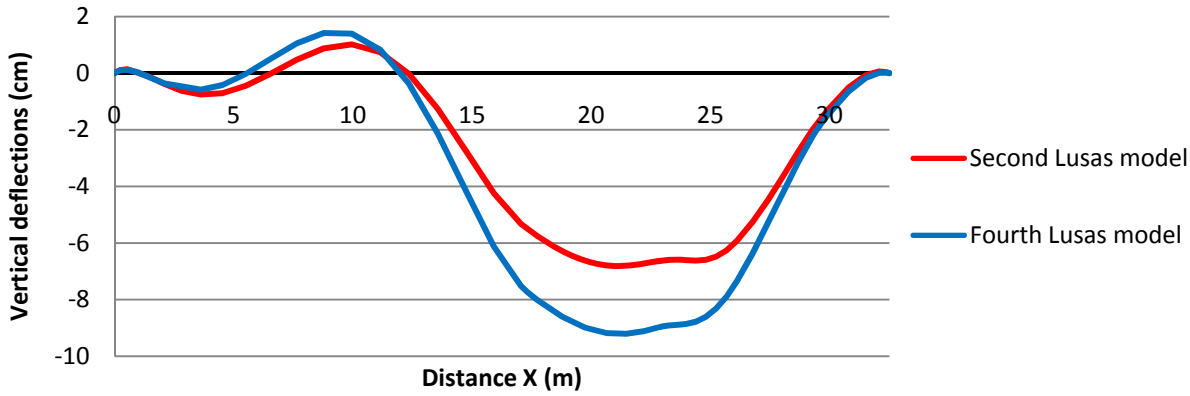

Figure 75: *Vertical deflections along the central undeveloped directrix considering different models*. The results of the second Lusas model are coloured in red and results of the fourth Lusas model in blue.

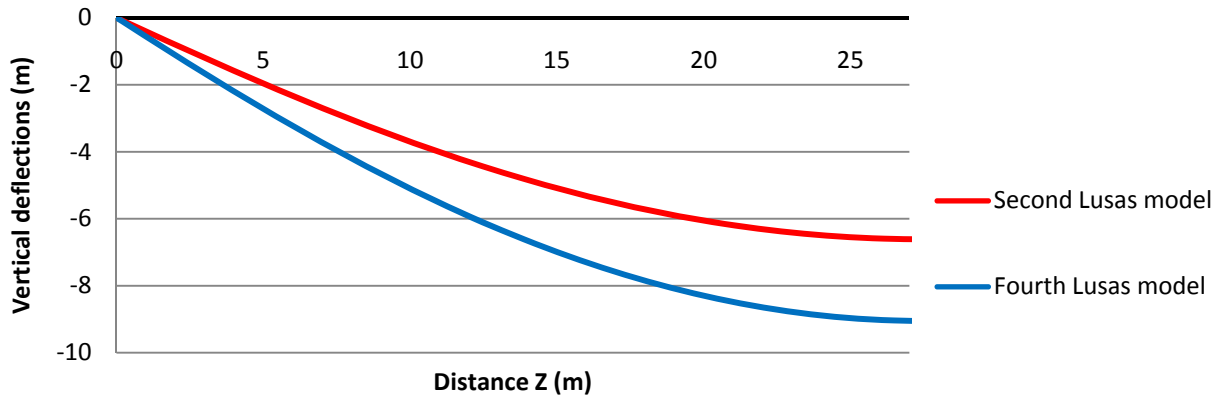

Figure 76: *Vertical deflections along half seagull profile, from the coordinate Z = 0 metres to Z = 27.5 metres considering different models*. The results of the second Lusas model are coloured in red and the results of the fourth Lusas model in blue.

The next study of the deflections was based on the comparison with the results obtained by Torroja in the actual structure and in the small-scale model. Both Torroja's models were based on the following hypothesis: Variation of thickness, consideration of skylights, and consideration of real supports. This last assumption was the only difference with the fourth Lusas model. Therefore, the last Lusas model was more similar to the Torroja's hypotheses than the preceding models. This conclusion implied than the vertical deflections calculated by the fourth Lusas model might be also more similar to the results presented by Torroja. The initial analysis was based on the comparison between the deflections measured by the fourth Lusas model and the Torroja' deflections considering the load case four (figure 37). This study showed two different conclusions: Firstly, the Torroja's deflections are higher than the results calculated by the fourth Lusas model, above all at the connection between both cylindrical sectors. For example, at the coordinate X = 22.5 metres, the Lusas vertical deflections are 60 % of the deflections measured in the actual structure and the small-scale model (Table 6 and 7, Appendix B.2). This factor is explained because the Torroja's models were based on discontinuous supports and therefore the structure was more flexible and higher deflections were measured. Secondly, as was supposed before, the vertical deflections calculated by the fourth Lusas model are more similar to the results presented by Torroja than the second model. For example, at the same coordinate considered before, the vertical deflections calculated by the second model were 45 % of the actual structure and the small-

scale model deflections. This conclusion is explained because the second model was too much rigid due to the assumption of the continuous supports and closed skylights. Therefore, when the real skylights are considered the structure is more flexible and the results are more similar to the deflections obtained by Torroja.

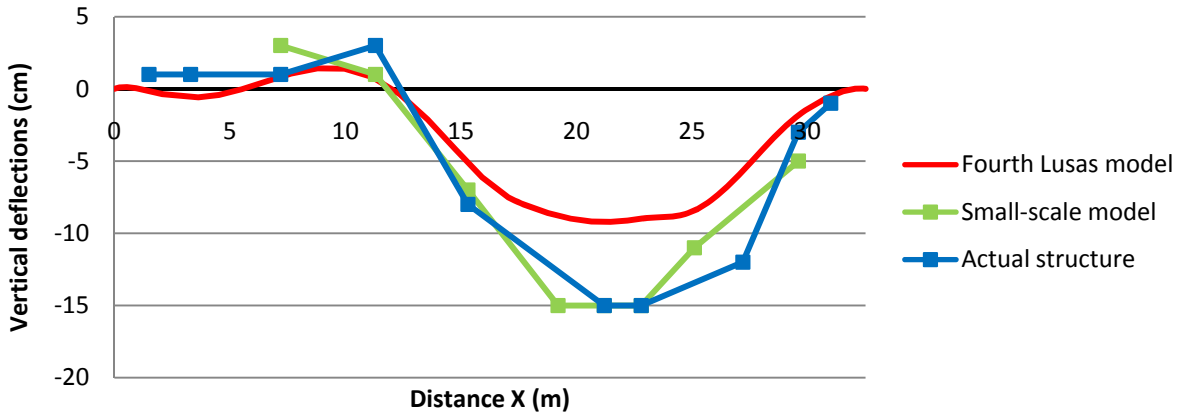

Figure 77: *Vertical deflections along the central undeveloped directrix considering different models*. The results of the fourth Lusas model are coloured in red, the results obtained by Torroja in the actual structure are coloured in blue and the deflections obtained in the small-scale model are coloured in green. The load case four is considered in the fourth Lusas model.

The second analysis of the deflections consisted of the comparison between the fourth Lusas model and the deflections measured in the small-scale model considering different load cases along the central undeveloped directrix. The procedure carried out by Torroja in order to check the structural behaviour of the small-scale model of the Frontón Recoletos consisted of 27 tests realized in different periods (Torroja 1942, p.123-125). In these tests, the vertical and horizontal deflections[42] were measured. In this section, the vertical deflections of three of those tests were compared in order to study two additional load cases considered in the first model:

- Load case 1: Dead weight
- Load case 3: Dead weight with snow load

In order to make easier the comparison and considering possible measurement errors in the small-scale model, the results measured by Torroja are drawn as two lines, which values were obtained increasing and reducing the measured values in 1 centimetre.

The study of the load case one (figure 78) was based on the tests A and B, which showed similar deflections. However, the test B presented some measurement errors. For example, the value obtained at the connection between the smallest cylindrical sector and the wall was -1.5 centimetres instead of the null deflection measured in the test A and supposed initially by the support conditions (Table 1, Appendix B.5). Therefore, in order to avoid the possible measurement errors, the average of both tests was considered. This average deflection was compared with the Lusas results and the following conclusions were obtained: Firstly, the Lusas shape and the maximum values are highly similar to the results measured in the small-

[42] All the details referring to the metering devices used were described in the Report presented to the Spanish Sciences Academy (Torroja 1942 p.121).

scale model above all at the biggest cylindrical sector. For example, the difference of deflections at the coordinate X = 15.3 metres is only 0.3 centimetres. Secondly, the vertical deflections measured by Lusas in the closeness of the connection between the smallest cylindrical sector and the wall are different to the results obtained by the average test. For example, at the point X = 31.5 the difference between both models is 3.7 centimetres (Table 2, Appendix B.5). This problem can be explained if the metering device located in that point was broken or was based on error in the calibration process because the continuity of the deflection shape measured by the average test was broken in that point. In order to check this hypothesis, the average shape along the directrix without considering that anomalous result, produced by the metering device located at the coordinate X = 31.5 metres, was presented (figure 79). This new shape was continuous along all the directrix is more similar to the Lusas results.

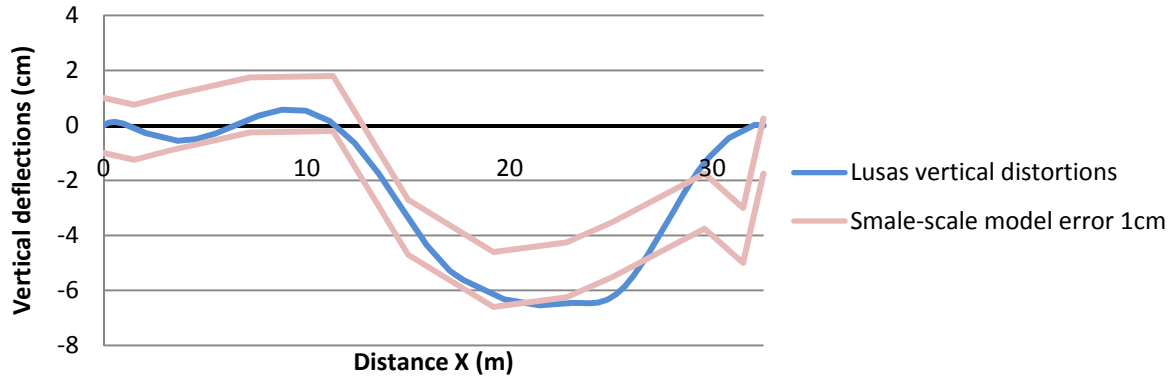

Figure 78: *Vertical deflections along the undeveloped directrix considering different models*. The deflections obtained by the fourth Lusas model are coloured in blue and the values measured in the test realized by Torroja, supposing 1 centimetre of error in the average value, are coloured in pink. The load case one is considered.

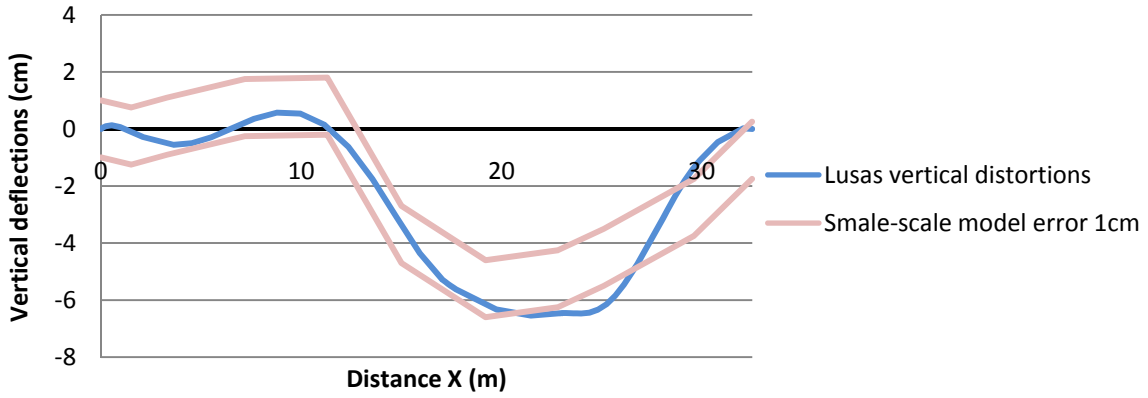

Figure 79: *Vertical deflections along the undeveloped directrix considering different models.* The deflections obtained by the fourth Lusas model are coloured in blue and the values measured in the test[43] realized by Torroja, supposing 1 centimetre of error in the average value, are coloured in pink. The load case one is considered.

[43] Without the peak presented in figure 77 at the coordinate X = 31.5 metres.

The analysis of the load case three (figure 80) was based on the comparison between the test C, where the same load case was considered, and the Lusas results. This analysis showed as a conclusion that the vertical Lusas deflections are similar to the values presented by Torroja above all at the smallest cylindrical sector. For example, the deflection difference at the coordinate X = 29.6 metres is 1.8 centimetres. However, these differences are higher at the biggest lobe. For example, the Lusas deflection at the point X = 7.2 metres is only 11 % of the test value (Table 3, Appendix B.5).

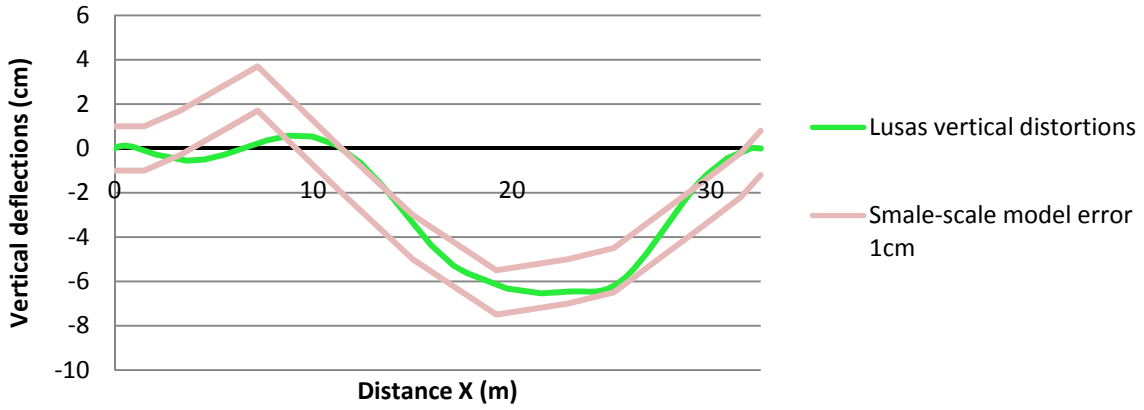

Figure 80: *Vertical deflections along the undeveloped directrix considering different models*. The deflections obtained by the fourth Lusas model are coloured in green and the values measured in the tests realized by Torroja, supposing 1 centimetre of error in the average value, are coloured in pink. The load case three is considered in the fourth Lusas model.

The second element studied was the bending moments, which analysis is divided into two parts: Firstly, the transversal bending moments obtained in the second Lusas model are compared with the fourth Lusas model. After that, the longitudinal bending moments are studied.

The first study of the bending moments was based on the comparison between the transversal bending moments of the second and the fourth Lusas models (figure 81). This comparison was analyzed in order to know how the bending moments varied when the real skylights were considered and was based on the diagrams of transversal bending moments along the central directrix. The conclusion of this comparison showed similar values[44] and shapes in both models as well as the fourth model presented slightly higher values at the connection with the skylights because the discontinuity of the shell increased the stresses. For example, at the connection between the biggest lobe and the skylights the difference is 27 % (Table 18, Appendix B.3). Therefore, the bending moments calculated when the simplified skylights are considered are not on the safety side.

[44] The values at the connections with the skylights were not considered because in that location a beam was placed in order to connect both structures.

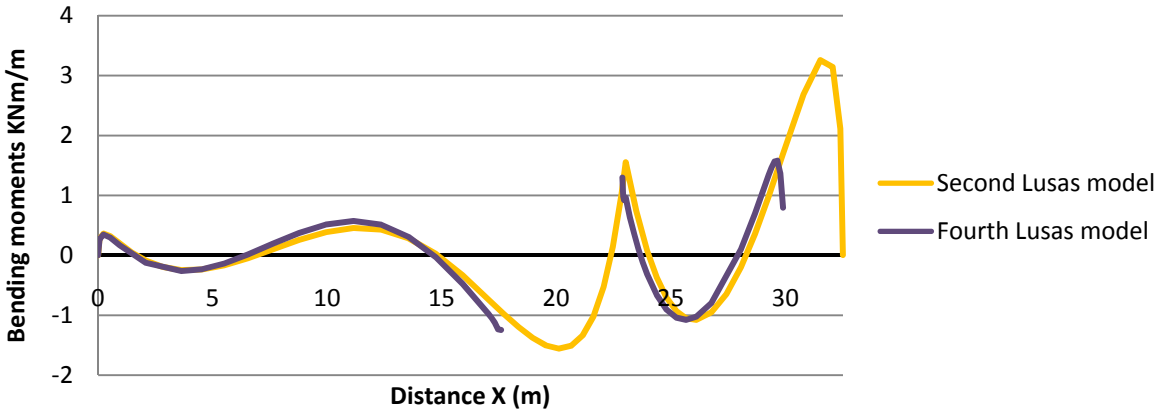

Figure 81: *Transversal bending moments along the central undeveloped directrix considering different models*. The second Lusas model is coloured in orange, and the fourth Lusas model is coloured in purple.

The second study of the bending moments consisted of the study of the longitudinal bending moments. These stresses are practically located at the connection between the skylight beams in the biggest cylindrical sector and the shell. The obtained values are higher than the preceding models. For example, the maximum value in the central directrix represents 37 % of the maximum transversal bending moments obtained in the same Lusas model (Appendix A.7). Therefore, the longitudinal bending moments cannot be considered negligible in those places.

The analysis of the isobars is divided into different parts: Firstly, the overall shape and the maximum values measured along the central directrix are analyzed. After that, the overall shape of the isobar plan diagrams are studied.

The first study of the isobars was based on the comparison of the values along the directrix. These values were compared with the second Lusas results (figure 82 and 83). The main conclusion was that the shape is highly similar in both diagrams. Nevertheless, when the real skylights are considered the maximum values are increased. For example, the peak in the maximum isobars of tension stress measured in the fourth model is 27 % higher regarding the second Lusas model (Appendix B.4).

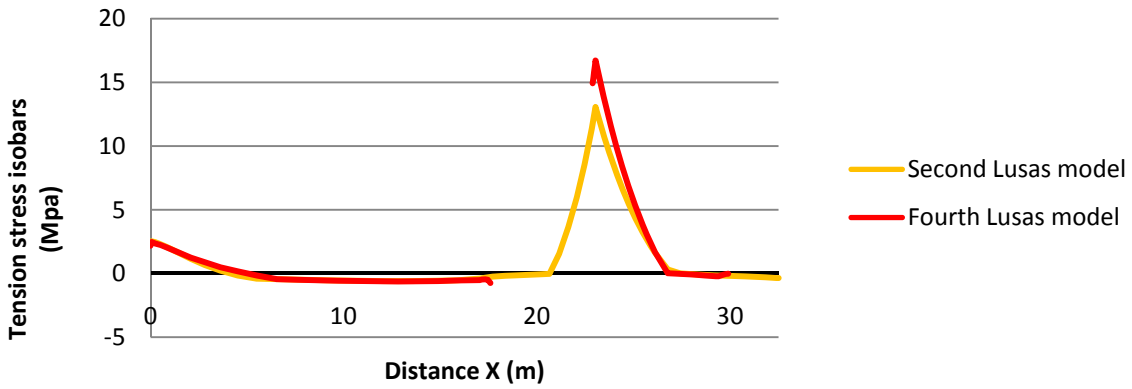

Figure 82: *Tension stress isobars along the central directrix considering different models*. The second Lusas model is coloured orange and the fourth one in red.

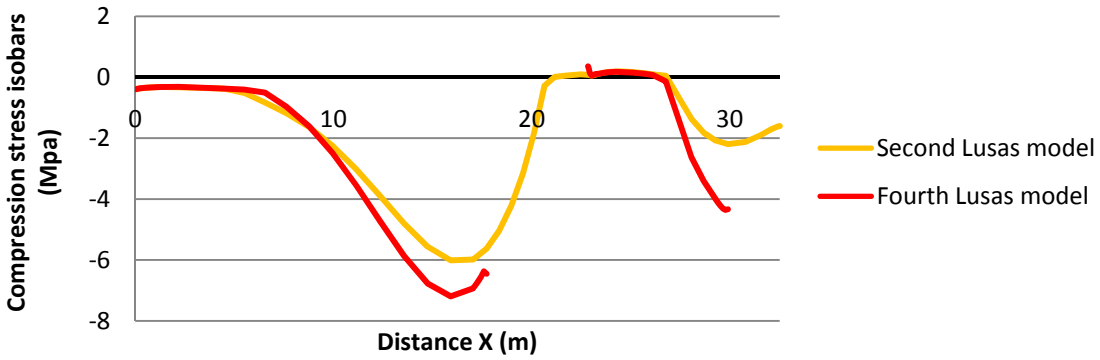

Figure 83: *Compression stress isobars along the central directrix considering different models.* The second Lusas model is coloured orange and the fourth one in red.

Finally, the shape of the compression and tension stress isobars is highly similar to the shape presented in the second model (figures 84 and 85). However, the values are higher because when the real skylights are modelled, the structure is more flexible. For example, the maximum value of the isobars of tension stress in the second Lusas model is 3 MPa lower than the fourth model (figure 84).

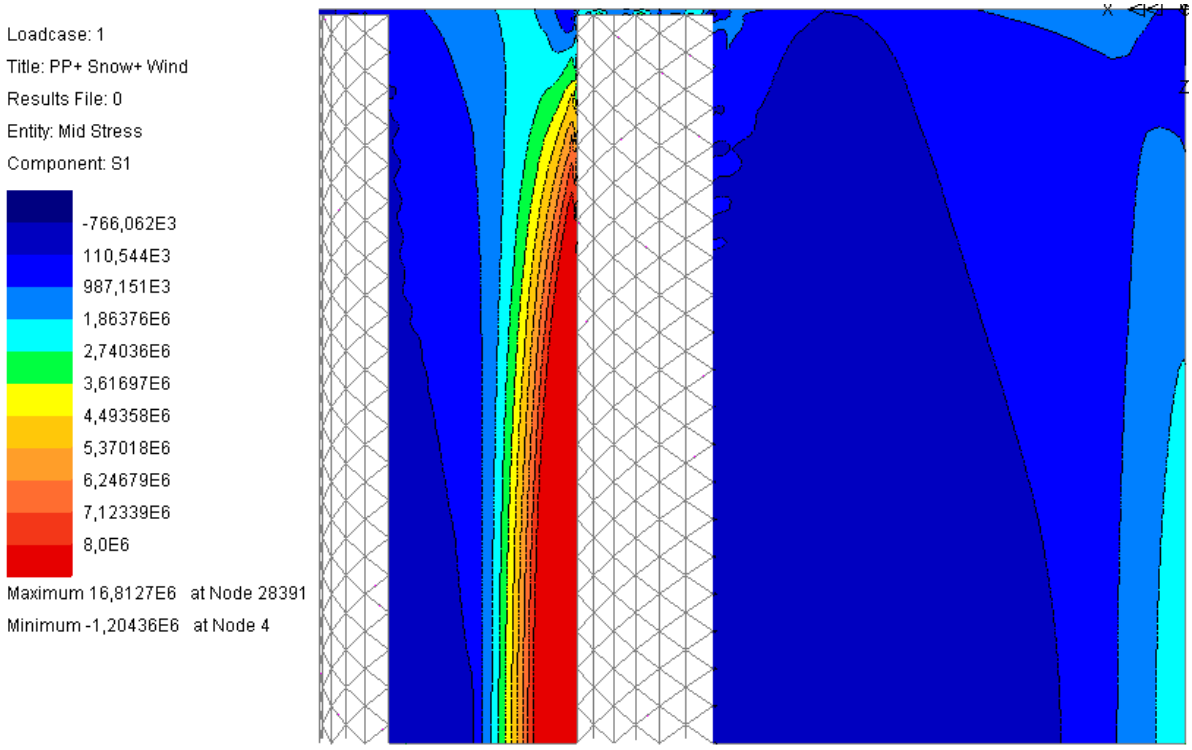

Figure 84: *Plan of the half-undeveloped section of the maximum tension stress isobar for the fourth Lusas model.* The maximum value was 16.8 MPa.

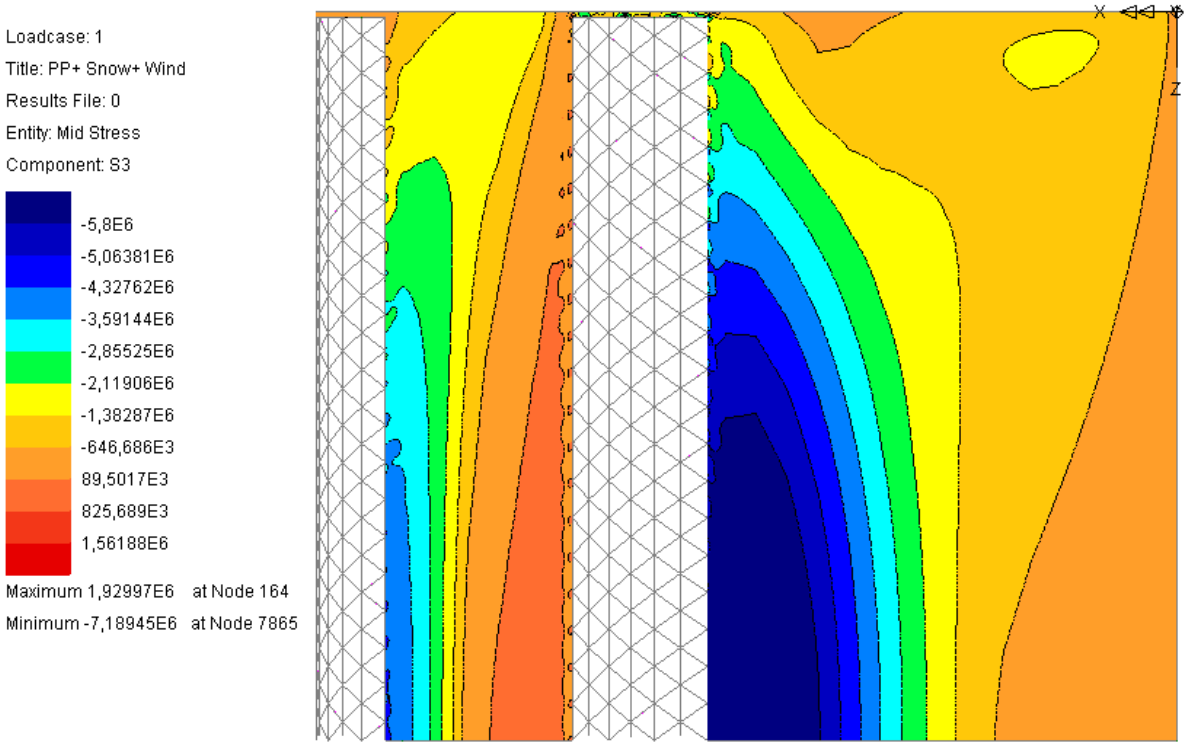

Figure 85: *Plan of the half undeveloped section of the maximum tension stress isobar for the fourth Lusas model.* The maximum value was -7.2 MPa.

3.4.3 Conclusions.

After the analysis of the fourth model, the following conclusions were obtained: Firstly, the general behaviour of the shell is practically independent to the consideration of the skylights because the three-dimensional deflections were highly similar in the first and the fourth Lusas model. This factor checked the Torroja's assumption of considering the skylights as closed shell in order to simplify the theoretical calculations. Secondly, the consideration of the real skylights produces a more flexible structure than the second Lusas model because the continuity of the shell was broken. One example of this phenomenon is the increase of the vertical deflections when the real skylights are introduced in the model. Nevertheless, these deflections are lower than the results obtained by Torroja because continuous supports are considered in the fourth model. Thirdly, the structural behaviour, considering different load cases, is highly similar to the tests carried out by Torroja in the small-scale model. Furthermore, some problems in the measuring device have been detected. Fourthly, the shape of the transversal bending moments along the central directrix is highly similar to the shape of the second Lusas model. However, the fourth model presented slightly higher values at the connection with the skylights because the discontinuity of the shell increased the stresses. This conclusion is also obtained in the analysis of the isobars along the central directrix. Fifthly, the longitudinal bending moments are practically located at the connection between the skylight beams in the biggest cylindrical sector and the shell. The Lusas stresses are higher than the preceding models and cannot be considered negligible in those places. Sixthly, the maximum values of the isobars are higher than the second Lusas model because the flexibility of the structure is higher in the fourth Lusas model.

3.5 Fifth Model: Real Supports.

In the theoretical calculations, the supports were simplified in order to calculate the shell by hand. This simplified supports consisted of a fixed points at the central section of the generators and free deflection along the Z-axis for the rest of edged points. However, the supports that were constructed in the actual structure were more complex. These supports were based on two construction drawings used by Torroja (figures 86 and 87). In these construction drawings is showed how the generators and the directrix had different support conditions: On one hand, the central points of the edged generators were joined to the wall at their centre, and along the rest of their length, they rest on small connecting rods thus permitting the longitudinal expansion of the shell (figure 87). These supports can be easily appreciated in the small-scale model proposed by Torroja (figure 88). On the other hand, the supports at the directrix consisted of six points, which joined the shell with the wall by means of beams and pillars. All the procedure used in order to model the supports in the actual structure is explained in Appendix A.5. The second element incorporated in the real supports that had not been studied in the theoretical calculations was that at the connection between the shell and the wall, different reinforcement beams were constructed. The size of the beam located at the generator connection was 20 per 40 centimetres (Antuña 2003, p.140). This beam produced an eccentric support (figure 30) that was not considered in the model. Nevertheless, the size of the beam located at the directrix connection was not clearly defined. Therefore, on one hand, the size of the edged beam located at the directrix was measured in the constructions drawings and the value considered in the model was 20 centimetres on the other hand, the size in the generator directions was supposed 30 centimetres (Antuña 2003, p.140).

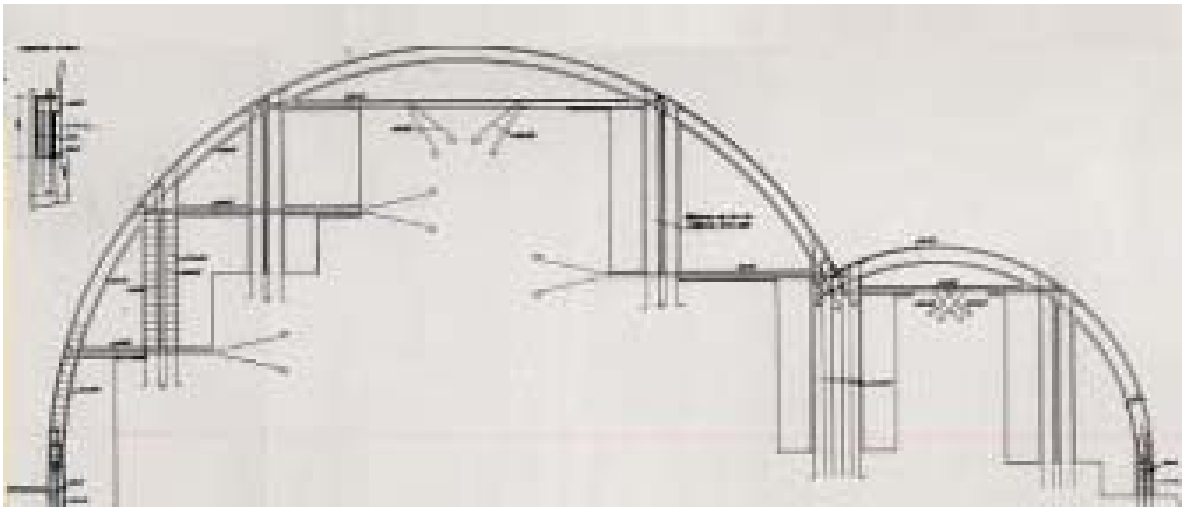

Figure 86: *Construction drawing of the real supports at the directrix*. The supports consisted of six points, which connected the shell with the wall by means of beams and pillars.

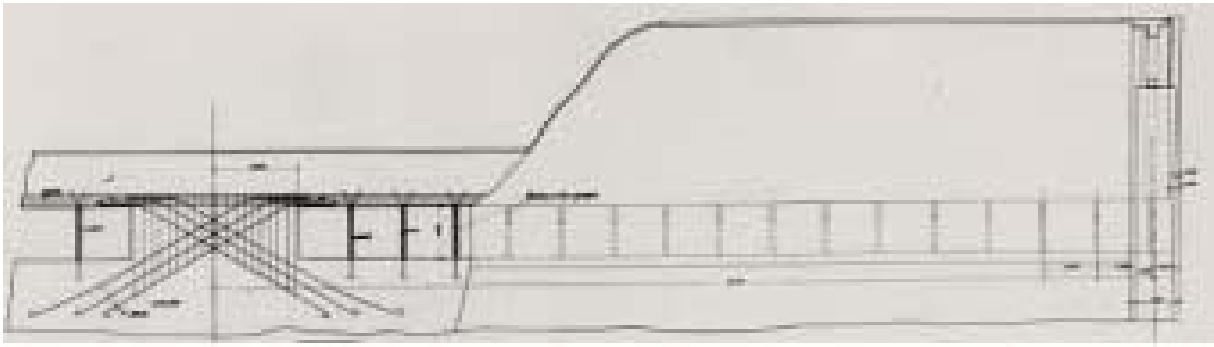

Figure 87: *Construction drawing of the real supports at the generators of half section*. The central section was fixed with anchor bars in two directions. The rest of the generators were connected by small beams separated 1.5 metres.

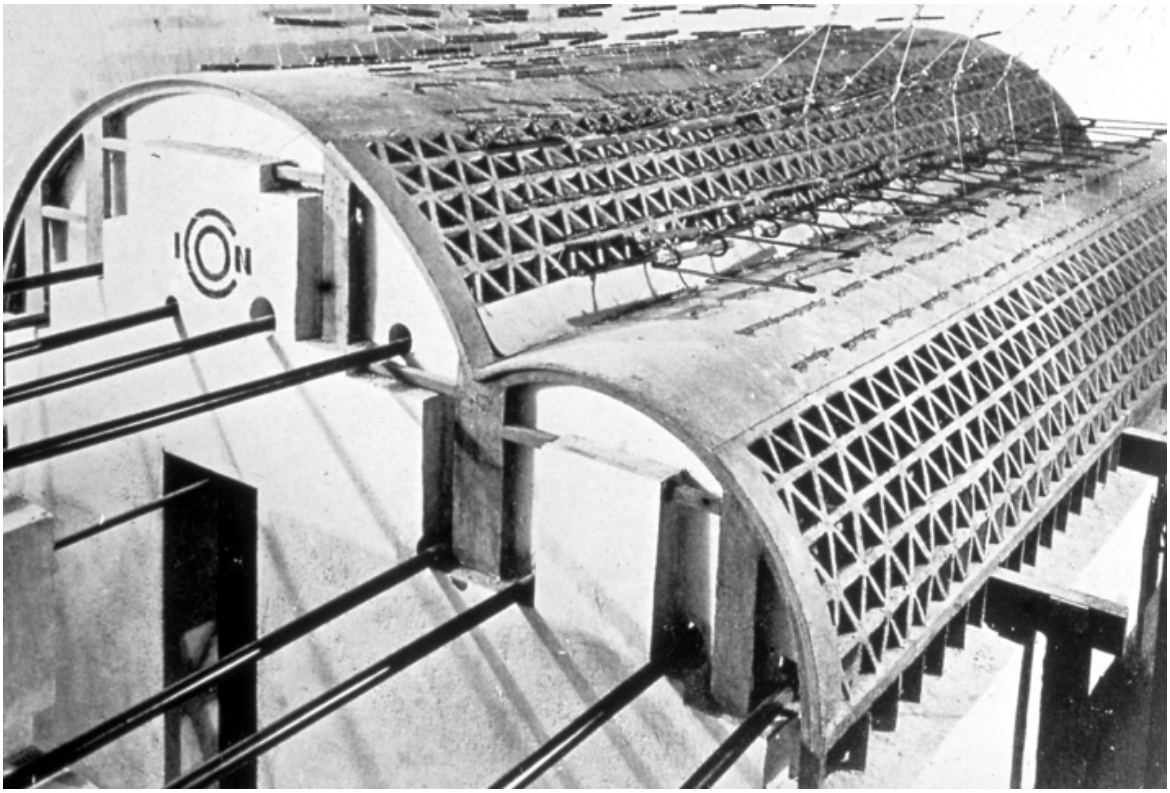

Figure 88: *Picture of the small-scale model tested by Torroja*. The supports can be easily appreciable at the connection between the small cylindrical sector and the wall.

The study of the fifth model is divided into different parts: Firstly, the hypotheses and the objectives are presented. Secondly, the supports used in the constructed structure and the effects in the structural behaviour of the model are studied. Afterwards, the fifth model is analyzed and compared with the preceding models. Finally, the conclusions are showed.

3.5.1 Hypotheses and Objectives.

The fifth model (figure 89) was considered as similar as possible to the real constructed structure. Therefore, the model was based on the Torroja's construction drawings. In these documents, the structure was defined considering the following characteristics: variation of thickness along the shell, skylights defined as lattice frames of equilateral triangles made of reinforced concrete, concentrated supports and edged beams along the shell.

In addition to all the characteristics described in the drawings, in the actual structure a Poisson number different to zero[45] was supposed, instead of the null value used in the preceding models. This assumption was realized in order to consider the transversal contractions and bring the model closer to the actual behaviour of the material used in the structure. However, in order to simplify the model, the concrete was considered to be an elastic, linear and homogeneous material that obeyed Hooke's law with the Elasticity Modulus equal to $30 \cdot 10^9$ N/m^2.

The Lusas model was based on the following characteristics: Firstly, the geometry (figure 89) was divided in two different parts. On one hand, the shell consists of 556 surface elements called QSI4 in order to model the variation of thickness and the connection with the skylights[46]. The mesh used was based on the following considerations: Firstly, the finite elements might be as similar as possible in the cylindrical sectors. Secondly, the number of finite elements have to be balanced between the accuracy and the speed of calculation. Finally, at the most trouble areas, as for example the connection between the shells and the skylight beams, smallest finite elements were supposed in order to reduce errors in those places. On the other hand, the skylights were modelled with 1435 beam elements called BMS3. These beams were divided into five finite elements. Secondly, the supports at the generators were modelled as "Support *A*", which fixed all the translations and allowed the rotations and "Support *B*", which fixed the vertical movements and acted like springs along both the Z-axes, parallel to the generators, and the X-axes, orthogonal to the generators. As was described in the construction drawings (figure 87) the first supports were located at the edged sections of the generators along the five central metres. The Torroja's thought pursued with this supports was creating a stiffer shell avoiding the deflections along the Z-axis in the centre of the structure. In the rest of the generator length, the supports were modelled as a concentrated supports *B* each 1.4 meters[47]. The directrix supports (figure 89) were modelled as concentrated supports *B*. The stiffness of the different springs considered in the model were calculated supposing the simplified model of cantilever beam fixed to the wall. This procedure is explained in Appendix A.5. Finally, the procedure used to define the dead weight as well as the wind and snow loads in the surfaces and skylights was similar to the preceding model and is explained in Appendix A.3.

---

[45] Value proposed by the Professor Costin Pacoste v = 0.2.

[46] At the connection between both elements, beams elements were supposed in order to model correctly the structural behaviour of the actual structure.

[47] The supports in the actual structure were separated 1.5 metres. However, the separation was supposed 1.4 metres in the Lusas model in order to simplify the model.

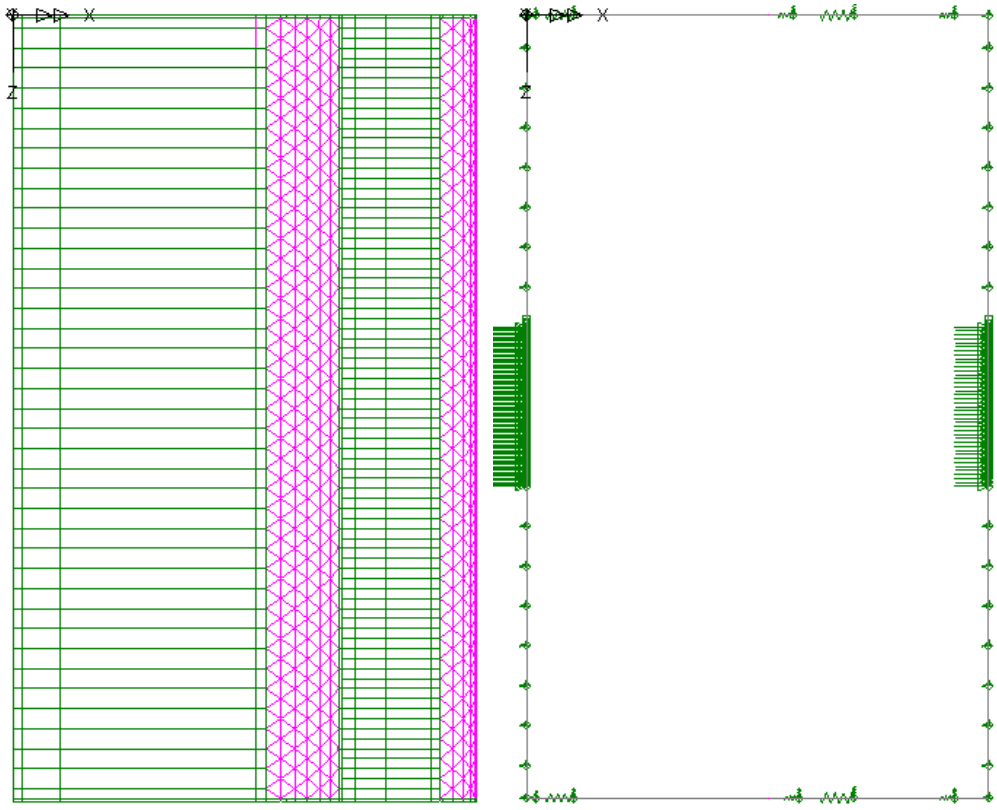

Figure 89: *Fifth Lusas model consisted of surfaces*, which are coloured in green, *and beam elements*, which are coloured in purple and the *supports conditions*: "Supports A" located at the central generator line and "Supports B" located at the rest of the generators and the directrix as concentrated supports.

The objectives pursued by the fifth model were checking the structural behaviour of the constructed structure as well as comparing the obtained values with the preceding models and with the results presented by Torroja. In order to achieve these objectives, a structural analysis was realized.

3.5.2 Study of the Supports.

The objective of the support study was understanding the structural behaviour of the Lusas model when the supports conditions are changed. Therefore, the analysis is divided into two successive[48] steps: Firstly, the real supports are supposed without the assumption of the edged beams. The purpose of this analysis is checking how the stresses are more concentrated when the edged beams are not considered. After this analysis, the reinforcement beams located at the edges are introduced in the model. The objective of this step is checking how the edged beams improve the structural behaviour of the shell. In order to simplify the analysis, only the maximum values of the isobars have been studied.

.

[48] A previous analysis: consideration of the real supports as spring with infinite stiffness was carried out. The conclusions showed by this analysis were similar to the conclusions obtained in the first step.

The analysis of the maximum values of the isobar diagrams showed that when the supports conditions are changed for the real supports without considering the edged beams, the maximum values of the isobars are increased. For example, the maximum compression stress isobars are increased 67 % regarding the maximum values of the fourth Lusas model (Table 27, Appendix B.3). Furthermore, these stresses are located at the points located at the directrix where the shell is connected with the wall instead of at the biggest cylindrical sector (figure 90). These differences can be explained by two factors: Firstly, the real supports generate a more flexible structure. Consequently, the maximum stresses are higher. Secondly, the connection between the shell and the wall consists of concentrated joins at the directrix. Therefore, the stresses are concentrated in those points[49].

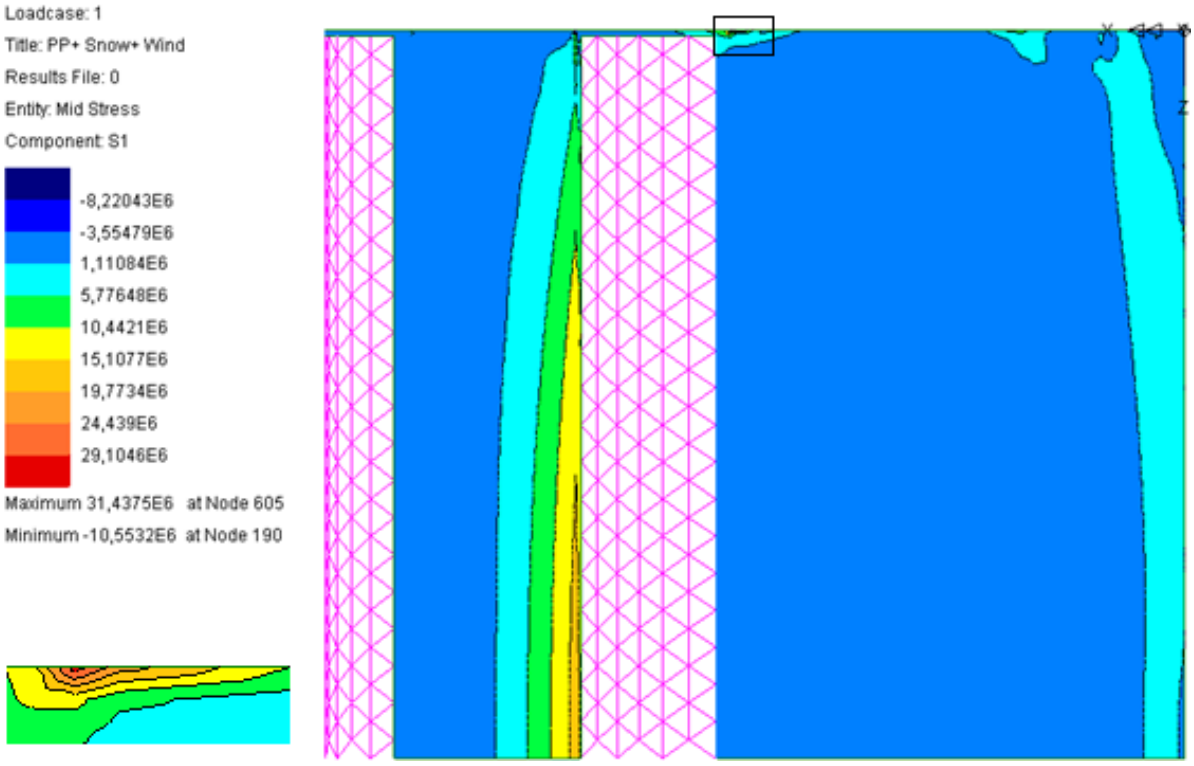

Figure 90: *Plan of half-undeveloped section of the maximum tension stress isobars when the discontinuous supports are considered but not the edged beam*. The zoom located at one connection between the edged directrix and the shell where the maximum values are measured.

The stresses are reduced when the beams along the edges are considered. For example, the value of the maximum compression stress isobars is practically the same measured in the fourth Lusas model (Table 27, Appendix B.3). Furthermore, this maximum value is located at the smallest cylindrical sector instead of at the connection between the directrix and the wall (figure 91). Therefore, the assumption of these edged beams showed the following conclusions: Firstly, the stresses are reduced because the beams along the directrix increase the stiffness of the model. Secondly, the concentration of the maximum stresses along the directrix supports when non continuous supports are considered, was perfectly known by Torroja. Thirdly, the edged beams are incorporated to the model in order to avoid the increase of stresses produced at the concentrated supports.

[49] The stresses were not concentrated at the concentrated supports located at the generator because the stresses were reduced by the shape of the shell.

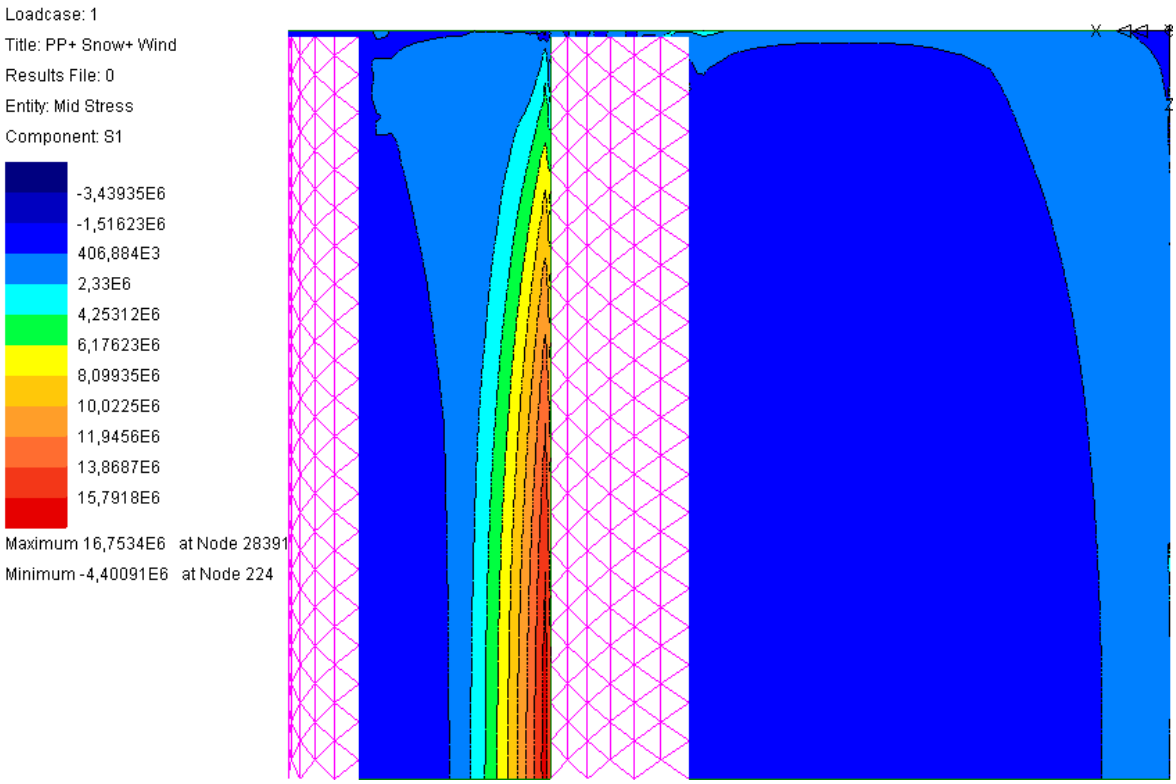

Figure 91: *Plan of half-undeveloped section of the maximum tension stress isobars when the edged beams and the discontinuous supports are considered*. The maximum value is 16.75 MPa.

3.5.3 Analysis.

This analysis was based on the actual structure and therefore the real supports, including the edged beams, were considered. In order to simplify the analysis only the fourth load case four: dead weight, snow and wind loads, was studied.

The first element studied was the deflections. This study is divided into two analyses. The first of these analyses was based on the comparison of the vertical deflections along the central directrix between the fourth and the fifth Lusas model. This study showed that the real supports produce a more flexible structure because higher deflections are obtained. Furthermore, this increase of the deflections produces that the positive deflections measured in the fourth model at the biggest cylindrical sector changed the sign in the fifth model.

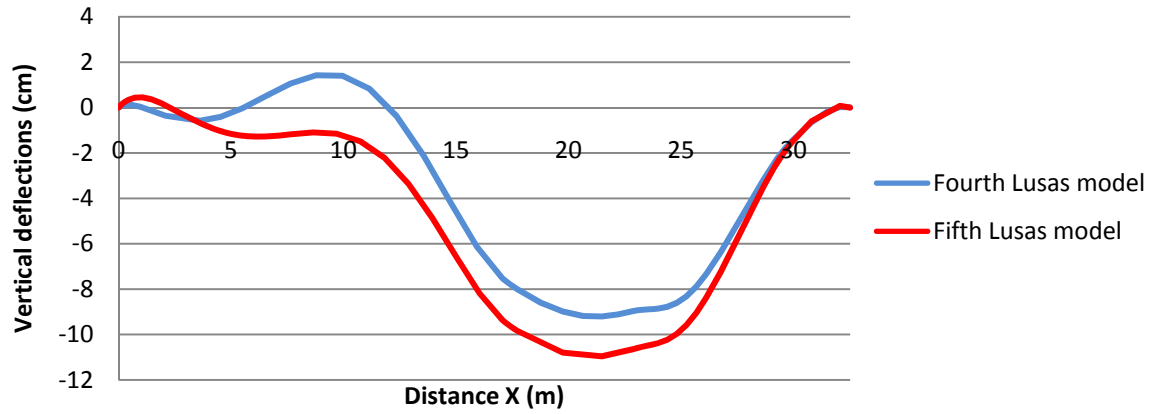

Figure 92: *Vertical deflections along the central undeveloped directrix considering different models*. The fourth Lusas model is coloured in blue and the fifth one in red.

The second analysis of the deflections consisted of the comparison between the fifth Lusas model and the results obtained by Torroja. All these three models were based on the same hypotheses and therefore, the deflections should be more similar than the preceding studied models. However, the first model was more similar to the results measured in the actual structure by Torroja. This factor could be explained because the actual structure was not perfectly modelled in the Lusas model and the variation of different parameters, like the loads conditions, the thickness variation, the supports conditions and the Elasticity Modulus, could explain the observed differences between both models. In Appendix A.8, the variations of these different parameters are studied in order to determine the sensitivity of the model. This study showed as a conclusion that the variation of the loads conditions and the Elasticity Modulus produces large deflections along the central undeveloped directrix and therefore, the combination of both elements could explain the observed difference between both models. The highly similarity between first Lusas model and the deflections measured in the actual structure could be explained by the fact that the considered parameters were adapted by the designer in order to resemble the behaviour of the theoretical model to the behaviour measured in the small-scale structure.

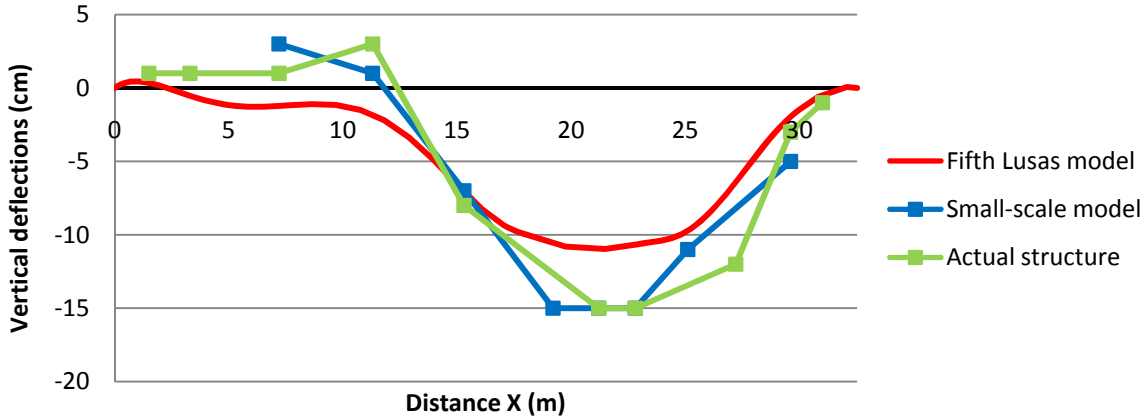

Figure 93: *Vertical deflections along the central undeveloped directrix comparing different models*. The fifth Lusas model is coloured in red, the small-scale Torroja's model in blue, and the real structure in green.

The second element studied were the bending moments. This study was based on two different analyses. First of all the transversal bending moments were studied by means of the comparison between the results obtained by the fourth and the fifth Lusas models (figure 94). This comparison showed similar values and shapes in both models. Nevertheless, the assumption of the real supports increased the bending moments because the structure had less transversal stiffness. This increase of bending moments is located principally at the connection between the directrix and the wall.

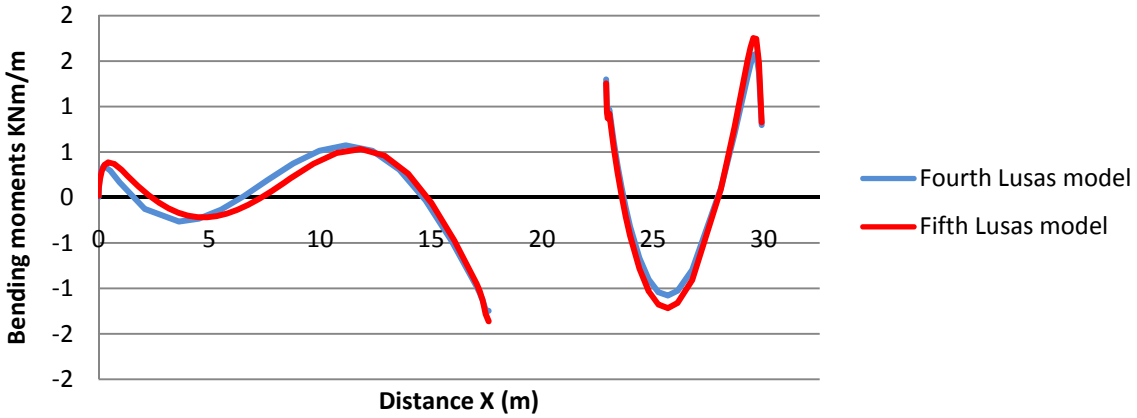

Figure 94: *Transversal bending moments along the central undeveloped directrix considering different models*. The fourth Lusas model is coloured in blue, and the fifth Lusas model is coloured in red.

The second study was based on the longitudinal bending moments. These stresses are increased when the real supports are considered and cannot be considered negligible. The maximum values are located at the connection between the directrix and the wall. The diagrams of longitudinal bending moments are presented in Appendix A.7.

Finally, the last element studied was the isobars. This analysis is divided into two studies. The first study consisted of the comparison of the maximum compression and tension stress isobars along the central undeveloped directrix between the fourth and the fifth Lusas model. (figures 95 and 96). The results of this comparison showed that when the real supports are considered, the maximum values of the tension and compression stress isobars are reduced. However, higher compression stress isobars values are measured at the connection between the skylights and the shells.

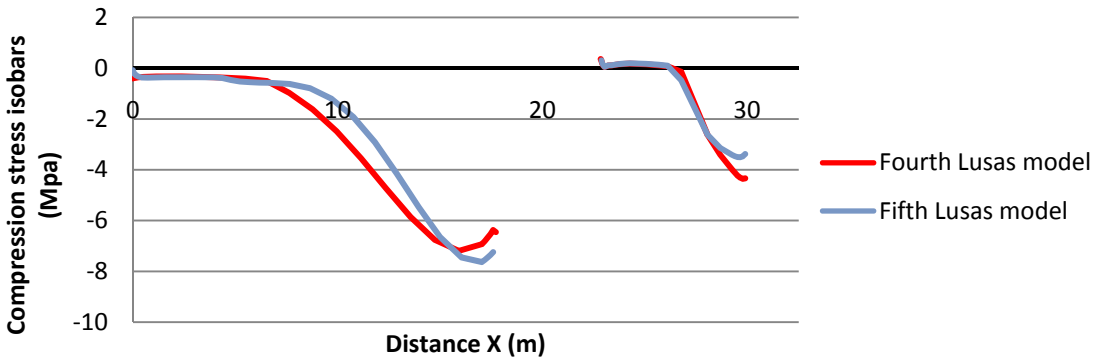

Figure 95: *Compression stress isobars along the central directrix considering different models*. The fourth Lusas model is coloured in blue and the fifth one in red.

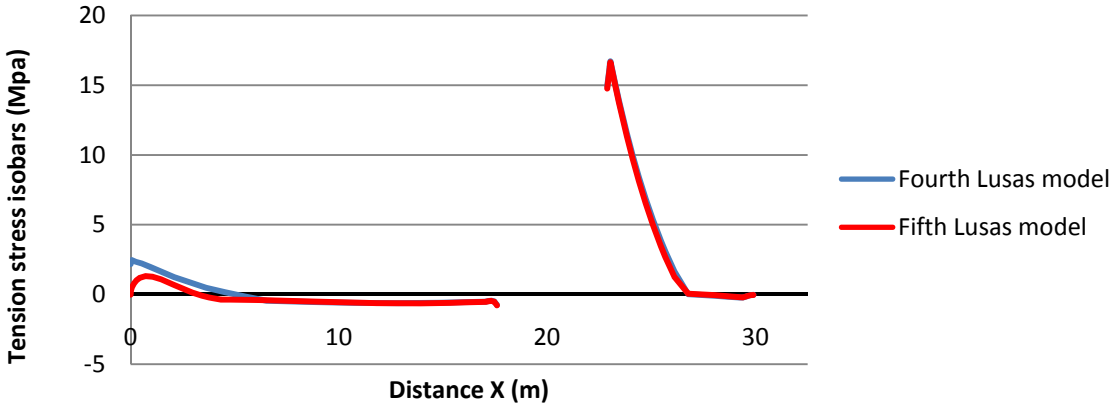

Figure 96: *Tension stress isobars along the central directrix considering different models*. The fourth Lusas model is coloured in blue and the fifth one in red.

The second study of the isobars was based on the analysis of the plans (figure 91 and 97). This analysis showed that the maximum values of the compression stress isobars are located at the connections between the directrix and the wall and the maximum values are increased when the real supports are considered because the structure is more flexible.

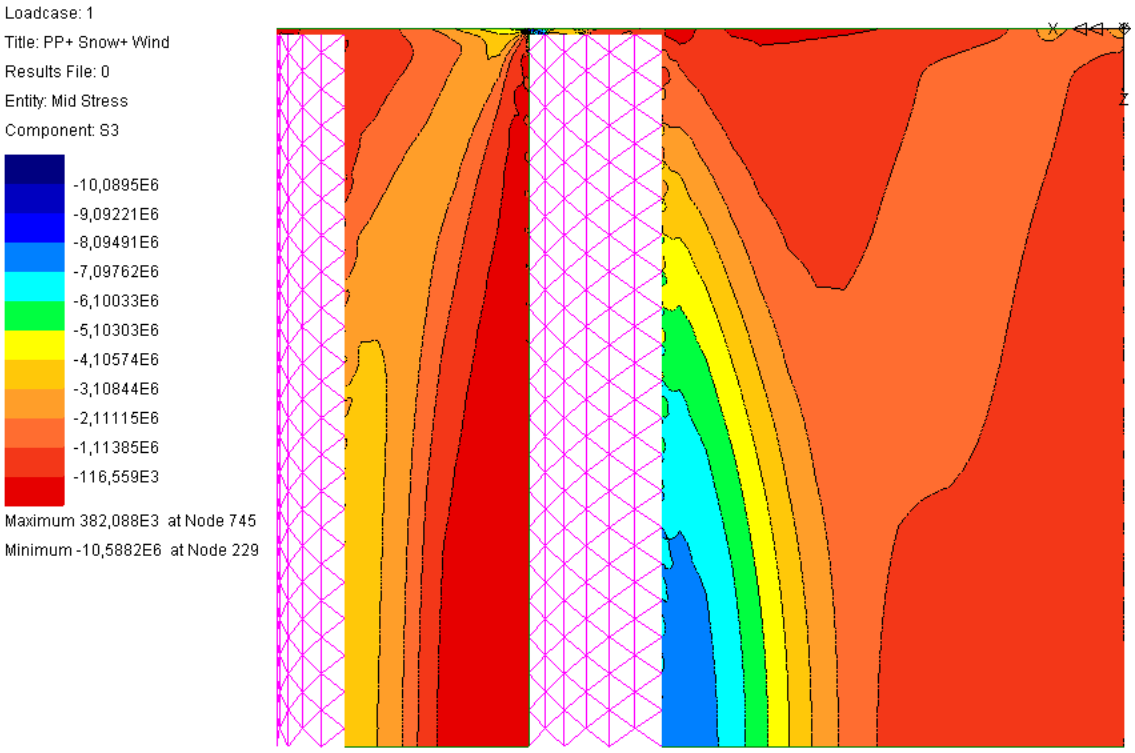

Figure 97: *Tension stress isobars along the plan of half-undeveloped section when the edged beams and the discontinuous supports are considered*. The minimum value is 10.58 MPa.

3.5.4 Conclusions.

After the study of the fifth Lusas model, the following conclusions were obtained: Firstly, when the real supports without the edged beams are introduced in the model, the maximum values of the isobars are increased and concentrated at the directrix points where the shell is connected with the wall. This factor can be explained by two factors: On one hand, the real supports generate a more flexible structure. Consequently, the maximum stresses are higher. On the other hand, the connection between the shell and the wall consists of concentrated joins. Therefore, the stresses are concentrated in those points. Secondly, the values of the isobars are reduced when the beams along the edges are introduced in the model. Furthermore, the maximum value is located at the smallest cylindrical sector instead of at the connection between the directrix and the wall as in the model without the edged beam. Therefore, Torroja incorporated the edged beams to the model in order to avoid the increase of stresses produced at the concentrated supports. Thirdly, the real supports produce a more flexible structure because higher distortions are obtained regarding the fourth Lusas model. Furthermore, this increase of the distortions produces that the positive distortions measured in the fourth model at the biggest cylindrical sector changed the sign in the fifth model. Fourthly, the distortions calculated by the fifth Lusas model are higher than the preceding model because the flexibility of the structure is increased by the concentrated supports. Furthermore, the most similar deflections to the values obtained by Torroja are obtained in the first Lusas model instead of in the fifth one, which is the most similar to the actual structure. This factor can be explained because the theoretical model was adapted with the results obtained in the small-scale model in order to make the structural behaviour of the theoretical model as similar as possible. However, the value of these parameters, for example the loads or the Elasticity Modulus in each point, cannot be measured in the actual structure. Therefore, a study of the parameters that might explain the observed differences between the actual structure and the fifth Lusas model was carried out to identify the sensitivity of the model when these parameters were changed. This study showed that the combination of the value of the Elasticity Modulus and the loads could explain the differences between both models and if the real values of these factors were known, the results of the Lusas model would be closer to the results measured in the actual structure. Fifthly, the transversal bending moments as well as the compression and the tension stress isobars along the central undeveloped directrix are reduced in most points regarding to the fourth model. However, a slight increase of these stresses is observed at the connection between the shell and the skylights. Sixthly, the longitudinal bending moments are located at the connection between the edged directrix and the wall. Seventhly, the maximum values of the compression stress isobars are located at the connection between the directrix and the wall instead of at the smallest cylindrical sector as the preceding models.

3.6 Sixth Model: Reinforcement Ribs.

The initial reinforced shell roofs constructed at the beginning of the twentieth century were based on a cylindrical shape constructed by arches. These arches had a tie beam to resist thrusts and there was therefore only a vertical reaction on the piers. The arches were placed at the bottom side of the shell (Antuña 2006, p.179).

In 1913, Eugene Freyssinet proposed an innovative construction system[50] based on the idea of putting the reinforcement arches in the upper side of the shell improving the aesthetic factor of the building and other characteristics as price.

"This subject, which does not appear on the surface to be very important, has had a great influence in the development of this kind of construction; it considerably simplified their construction and reduced the price. By putting the reinforcement beams on the upper side, the formwork was transformed into a continuous surface, which was made easily and rapidly by workers and could be removed quickly without breaking up the cast. The reinforced beams are constructed after the vault has been constructed, by means of simple formwork"

E.Freyssinet (Antuña 2006, p. 179)

The study of the sixth model is divided into different parts: Firstly, the characteristic of the ribs are studied. Secondly, the hypotheses and objectives of the analysis are explained. Afterwards, the sixth model is analyzed and compared with the preceding models. Finally, the conclusions are showed.

3.6.1 Study of the reinforcement ribs.

During the Civil Spanish war, in the spring of 1937, the Frontón Recoletos received several hits, two of them passing through it. The shock wave from the explosions caused severe deformations in the roof. After that, a design to repair the roof was drawn up. This design consisted of the some reinforced concrete rings, similar to the Freyssinet's arches, located each 5 metres in the upper side of the biggest cylindrical sector along the directrix. These ribs included a tie beam in order to correct the impact deflections, raising the shell when the tension was applied. However, the night of the 15th August of 1939 the roof collapsed (figure) when the repair work was about to begin.

[50] For example, in 1916 eight hangars, formed by a thin vault concrete shell, and reinforced by stiffening beams on the upper side of the vault, were constructed by E. Freysineet (Antuña, 2006, p.179).

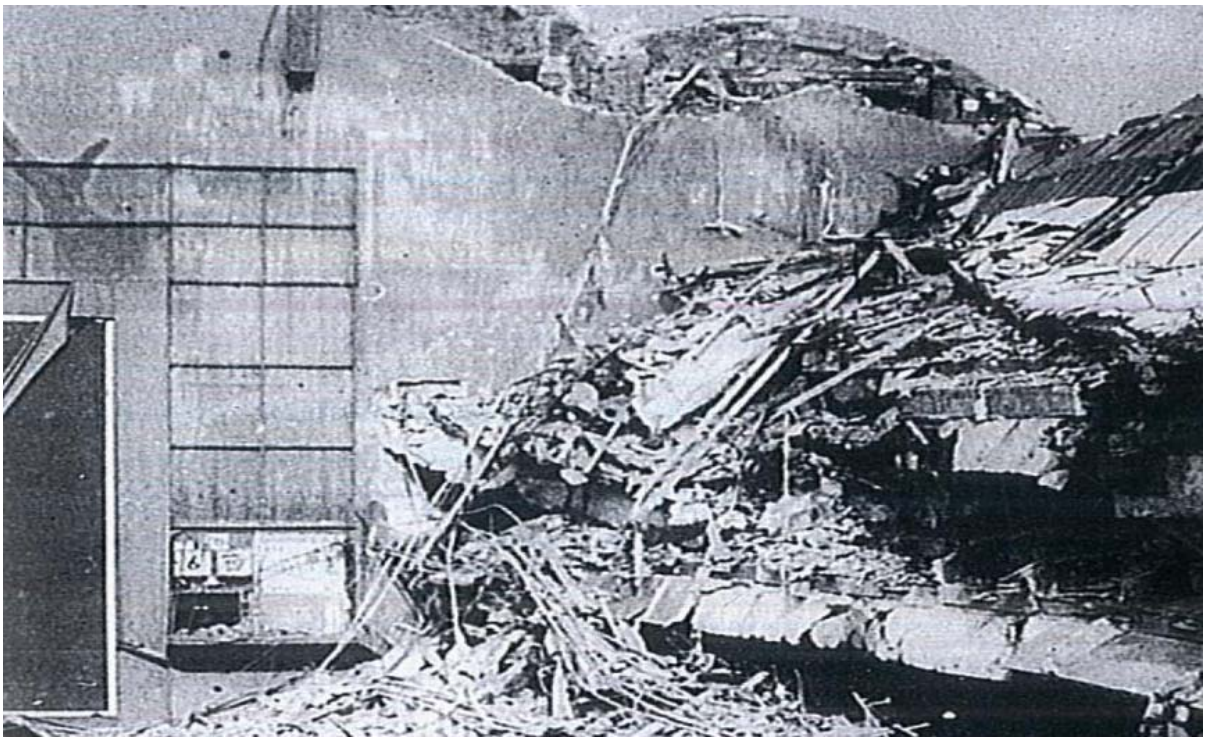

Figure 98: *Collapse of the roof of the Frontón Recoletos.*

The restoration design was drawn up in September of 1939. This design, different to the original structure, consisted of transversal trusses each 5.5 metres. This roof, and all the building, was demolished in 1973. Since then, a residential building is placed at the original location (Antuña 2003, p.148).

Torroja before the Civil Spanish War thought the necessity of the reinforcement ribs in order to increase the transversal stiffness of the shell. "Had I to build it again, I should provide such reinforcement ribs" (Torroja 1962, p.15). However, all the construction drawings and sketches found were thought trying to repair the damaged shell. Therefore, the study was based on these dates instead of the original idea of Torroja.

During the study of the reinforcement ribs, two problems were found. Firstly, the dimensions of the reinforcement rings were not clearly explained in all the consulted bibliography. The only available information was the construction drawings of one reinforcement rib located at the biggest cylindrical sector (figure 99). The dimensions of the ribs, considering that construction drawing, were supposed 45 per 30 centimetres. Secondly, two contradictory reinforcement systems were described: On one hand, the repair sketch proposed by Fernández (figure 102), consisted of five reinforcement ribs, each 13.75 metres, located at both cylindrical sectors (Fernández 2000, p.143). This is a logical system because the area where higher vertical deflections were measured in the actual structure, the smallest cylindrical sector, was reinforced. On the other hand, Antuñez argues that the reinforcement ribs were located each 5 metres following the directrix direction only at the biggest cylindrical sector (Antuña 2003, p.148). This is a logical assumption because the initial work of these reinforcements was raising the damaged shell. Therefore, this system seemed more indicated because the higher number of ribs would have produced fewer concentrated tensions in the shell.

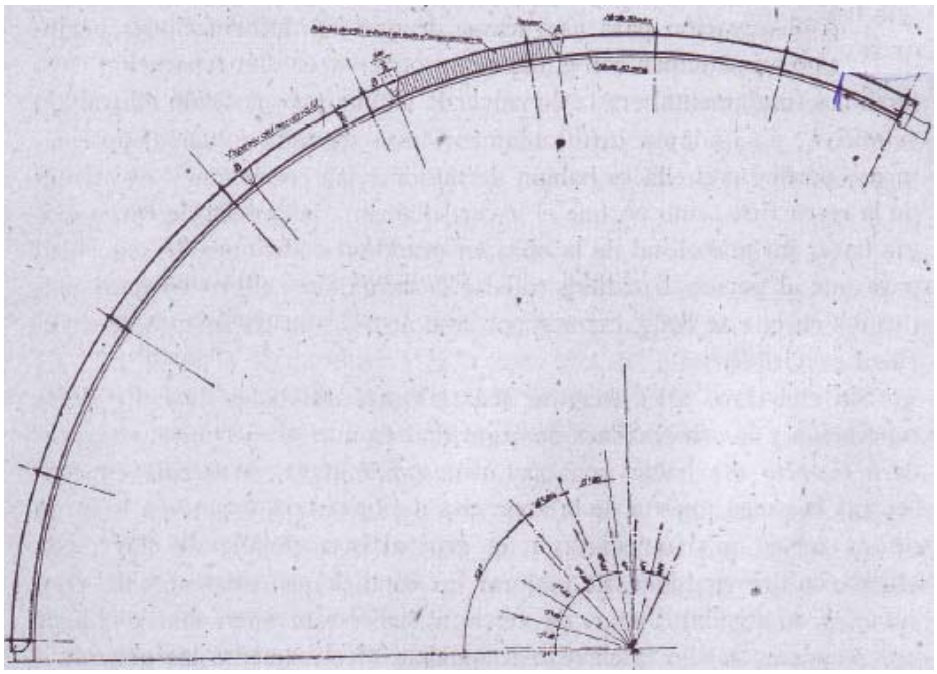

Figure 99: *Construction drawings of the reinforcement rings located at the biggest lobe proposed by Torroja*.

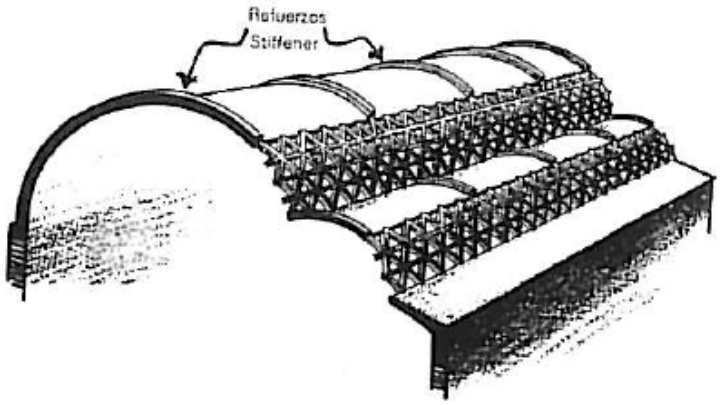

Figure 100: *A sketch showing the proposed solution to repair the roof Frontón Recoletos*

3.6.2 Hypotheses and Objectives.

The sixth model (figure 101) was supposed as similar as possible to the actual structure. Therefore, the model was based on the same characteristics considered in the fifth Lusas model including the consideration of the reinforcement ribs[51].

Three different locations of the ribs were supposed along the study: Firstly, the location explained by Antuña: At the biggest cylinder each 5 metres. Secondly, the location showed in the sketch presented by Fernández (figure 102): At both cylinders each 13.75 metres. Thirdly,

[51] These reinforcement ribs were modelled as beam elements called BMS3. The overall dimensions were 45 per 30 centimetres and the weight was supposed negligible.

the location showed in the sketch proposed by Fernández only in the biggest cylinder. Furthermore, the reinforcement ties were not considered because the geometry was supposed before the bombard and the raising of the shell was not needed.

The main objective of the study was checking if the reinforcement ribs thought by Torroja improved the structural behaviour of the shell. The additional objective was the determination of the most suitable ribs location considering the different proposals realized by different authors.

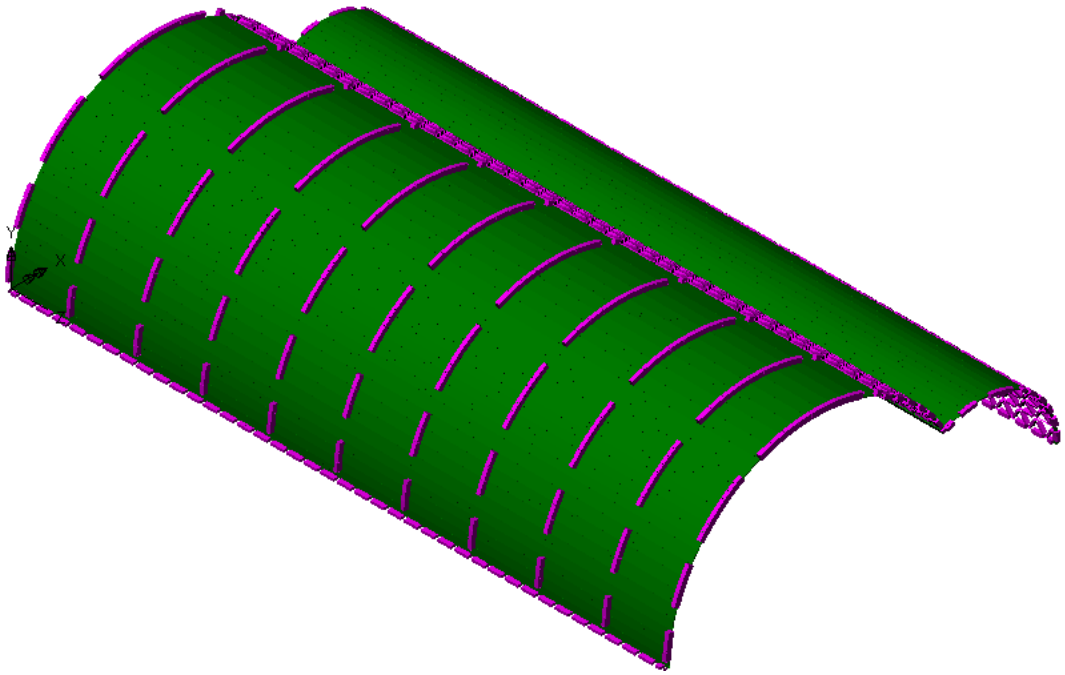

Figure 101: *3-D Lusas model, considering the ribs location supposed by Antuña.*

3.6.3 Study of the Ribs location.

The first analysis was based on the reinforcement ribs at the smallest cylinder. Therefore, two different models, based on the sketch presented by Fernández (figure 100), were compared without considering the reinforcement ties[52]: In the first model, the ribs were supposed only in the biggest cylinder and in the second one in both cylinders. One important conclusion obtained from this analysis was that the structural behaviour is improved when the ribs at the smallest cylinder are considered. For example, the vertical deflections along the central directrix (figure 102) improve overall at the smallest cylindrical sector when the reinforcement ribs are located in both cylinders. Therefore, to be on the safe side, the most adequate disposition of the ribs, in the conception of the structure, is in both cylinders.

[52] The principal objective of the reinforcement ties was raising the damage shell. However, the geometry after the bombards could not be measured because all the measuring devices were removed during the Civil Spanish War, as well as the characteristics of these reinforcements was not clearly explained. Therefore, the reinforcement ties were not considered in the sixth Lusas model.

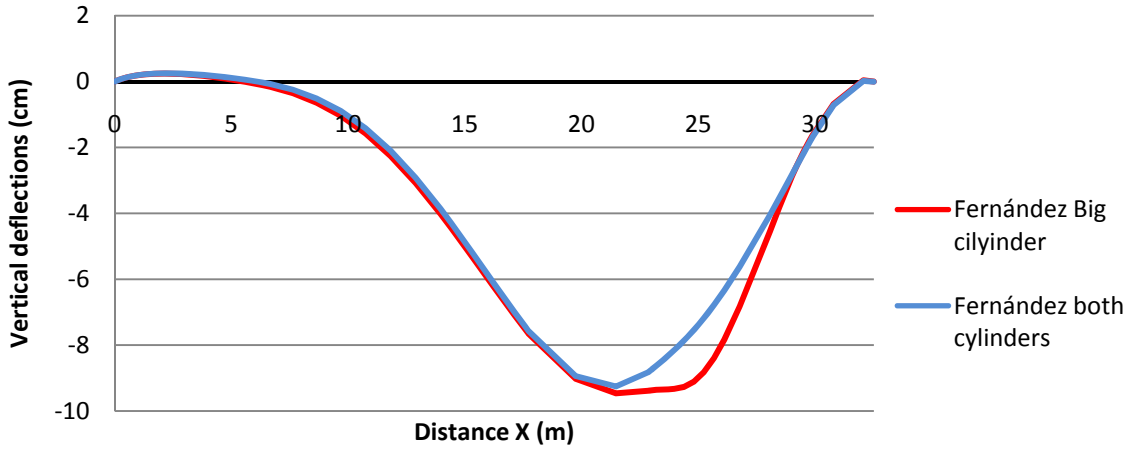

Figure 102: *Vertical deflections along the central directrix considering different reinforcement hypotheses*. The model is based on five reinforcements ribs located only in the biggest cylinder is coloured in red and in the both cylinders in blue.

The second analysis was based on the determination of the optimum number of ribs in the biggest cylinder. If the number of ribs is increased, some undesirable factors appear; Firstly, the prize of the structure is higher because more reinforced concrete is needed. Secondly, the aesthetic value of the building is decreased because the shell is conceived with higher thickness. Thirdly, the shell has more dead loads. In this study, the two compared models were the model proposed by Antuña, which was based on eleven reinforcement ribs, and a modification of the model proposed by Fernández considering only the ribs located at the biggest cylinder, which consisted of only five reinforcement ribs. The comparison between both models was based on the vertical deflections along the central directrix (figure 103) showed that the structural behaviour is improved when more ribs are considered. However, the improvement between both models, 3% at the seagull profile (Table 15, Appendix B.2), cannot be considered good enough because more than the double of ribs were used in the design proposed by Férnandez.

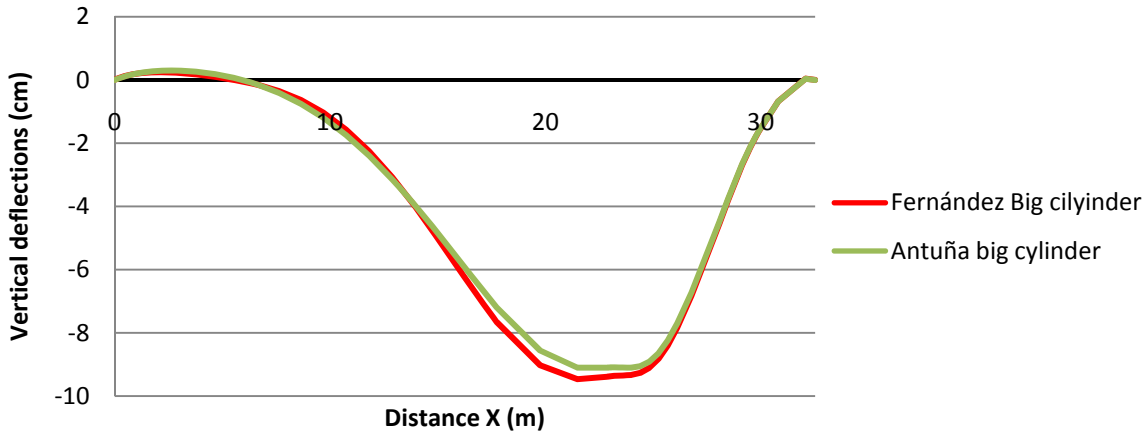

Figure 103: *Vertical deflections along the central directrix considering different reinforcement hypotheses*. The model is based on five reinforcements ribs located in the biggest cylinder, proposed by Fernández, is coloured in red and the model based on eleven reinforcements proposed by Antuña in green.

3.6.4 Analysis.

The objective of this study was checking if the structural behaviour is improved when the reinforcements are considered. In order to simplify the analysis only the model proposed by Antuña[53] is analyzed.

The first element studied was the vertical deflections along the central directrix. This analysis showed that these deflections are reduced (figure 104) when the ribs are considered. Furthermore, the biggest cylindrical sector had a more homogenous behaviour because the deflection shape had only one curvature, producing similar deflections to the simply supported beam improving the structural behaviour of the shell.

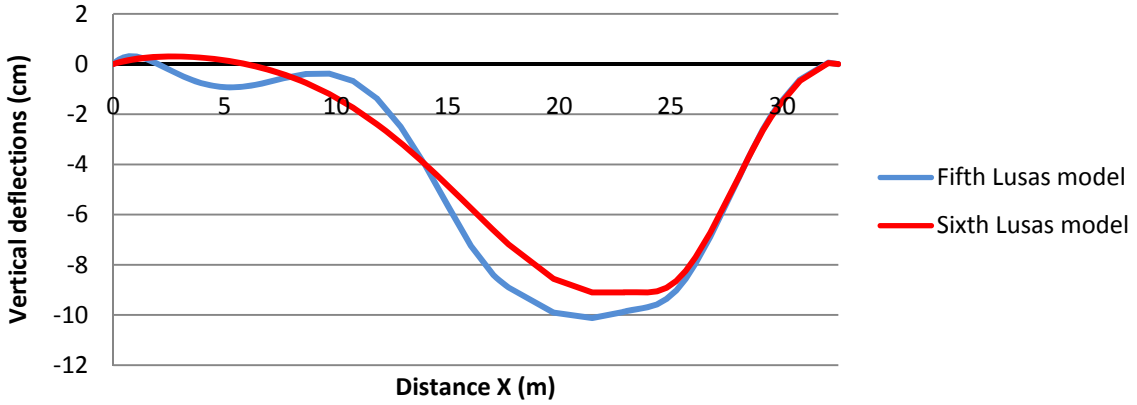

Figure 104: *Vertical deflections along the central directrix considering different models*. The fifth Lusas model is coloured in blue and the sixth one in red.

The other elements studied were the isobars and bending moments by means of the comparison between the fifth and the sixth Lusas model along the central directrix (figures 105, 106 and 107). In these analyses the following conclusions were obtained: Firstly, the assumption of ribs reduces highly the bending moments at the biggest cylindrical sector. Therefore, the ribs could have avoided the fissures located at the biggest cylinder produced by the torsion moment (Torroja 1942, p.147) However, the bending moments at the smallest lobe were slightly worse. Secondly, the maximum tension and compression stress isobars are slightly reduced when the ribs are considered.

[53] Because this model was described also by Torroja in his Report (Torroja 1942, p.159).

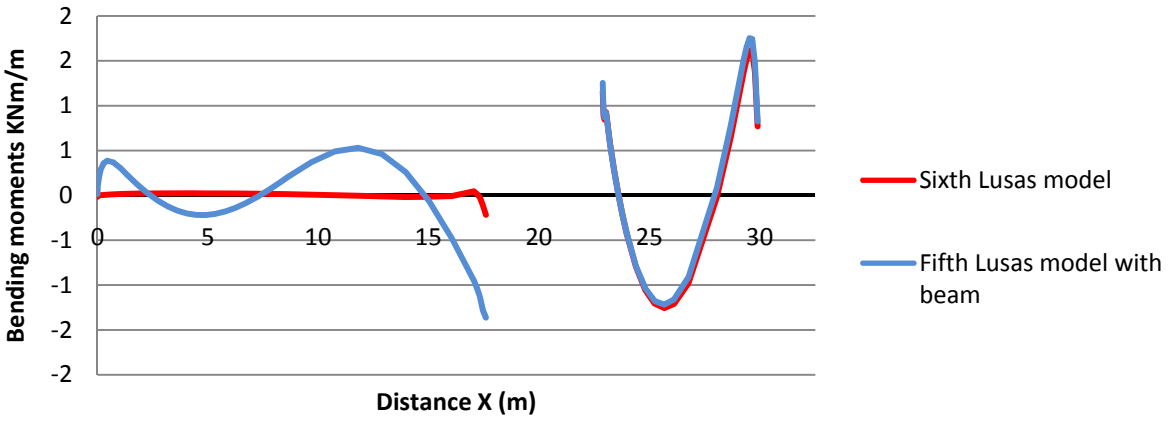

Figure 105: *Transversal bending moments along the central directrix considering different models.* The fifth Lusas model is coloured in blue and the sixth one in red.

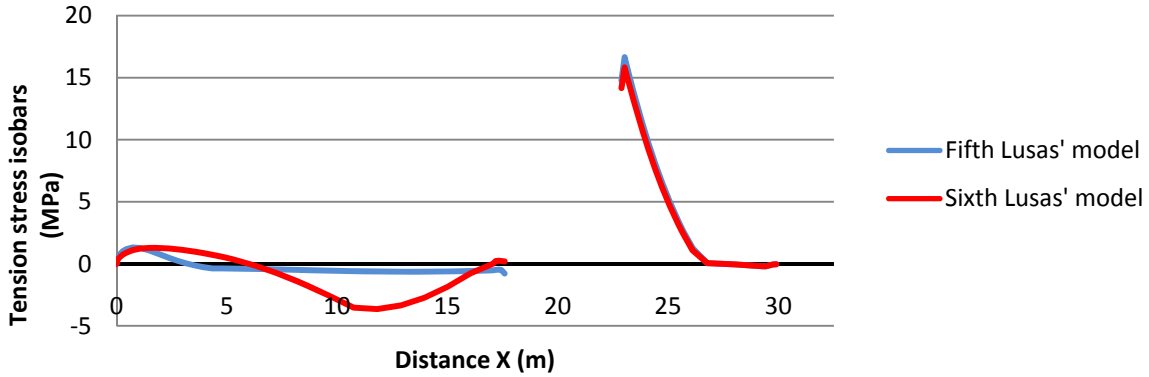

Figure 106: *Tension stress isobars along the central directrix considering different models*. The fifth Lusas model is coloured in blue and the sixth one in red.

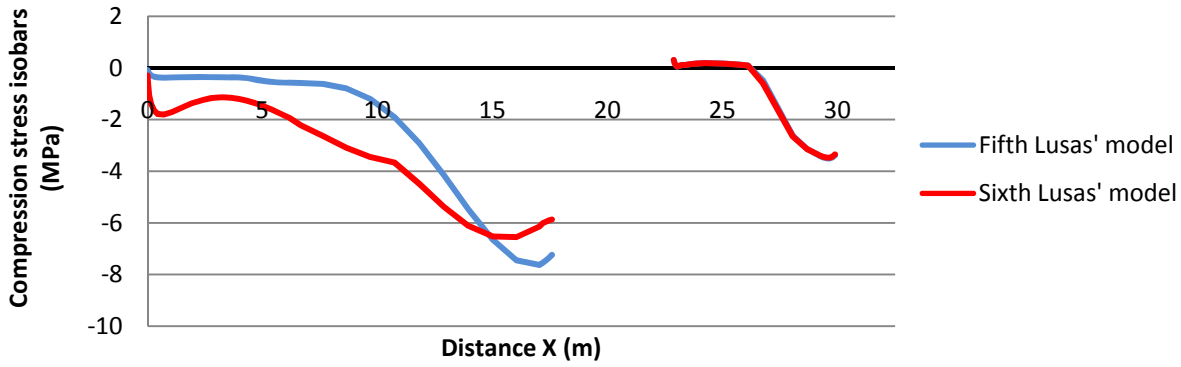

Figure 107: *Compression stress isobars along the central directrix considering different models.* The fifth Lusas model is coloured in blue and the sixth one in red.

All the diagrams of maximum compression and tension stress isobars are presented in Appendix A.10.

3.6.5 Conclusions.

The study of the reinforcement showed some conclusions: Firstly, the ribs thought by Torroja in order to improve the original structure could not be found. Therefore, the location and characteristics were supposed similar to the ribs designed with the purpose of repair the damaged shell after the bombards suffered during the Spanish Civil War. Secondly, the vertical deflections along the central directrix are improved when the reinforcement ribs were located in both cylinders. Therefore, to be on the safe side, the most adequate disposition of the ribs, in the conception of the structure, is located in both cylinders. Thirdly, the structural behaviour is improved when more ribs are considered at the biggest cylindrical sector. Fourthly, when the ribs proposed by Antuña are considered, the vertical deflections along the biggest cylindrical sector have a more homogenous behaviour because the deflection shape have only one curvature, producing a similar shape to the simply supported beam. Fifthly, the assumption of the ribs in the model reduced highly the bending moments at the biggest cylindrical sector. Therefore, the ribs could have avoided the fissures located at the biggest lobe produced by the torsion moments described by Torroja in the actual structure (Torroja 1942, p.147). However, the bending moments at the smallest lobe are slightly worse. Sixthly, the maximum values of the compression and tension stress isobars are slightly reduced in the biggest lobe regarding the preceding model.

3.7 Future research

Some interesting future research necessary to improve the knowledge about the roof of the Frontón Recoletos are proposed.

- Seagull

In all the preceding structures, the connection between the lobes consisted of a longitudinal beam. However, the Frontón Recoletos was designed without that beam because the shell worked as a laminar structure instead of two longitudinal vaults (Torroja 1942, p.15). Therefore, a finite elements model based on substitute the connection between both cylindrical sectors, seagull profile, with a beam could be interesting in order to compare both structural behaviours.

- Wind suctions

The experimental wind suction effects of the cylinder case were used in order to approximate the wind suction law along the directrix in the Frontón Recoletos. However, Torroja proposed the study of the wind suctions in a wind tunnel test (Torroja 1942, p.21) in order to know the accuracy effects of this phenomenon in the particular shape of the Frontón Recoletos structure.

- Temperature dilation

Torroja described the effect of the temperature in the Frontón Recoletos: "… small connecting rods thus permitting the longitudinal expansion of the shell. Transversal expansion presents no problem due to the great transversal flexibility of the shell in this direction" (Torroja 1942, p.11). This phenomenon was also analyzed in the small-scale test (Torroja 1942, p.133). Therefore, a finite elements model based on the temperature dilation in the shell could be studied with the purpose of checking the hypotheses considered by Torroja as well as the results of the small-scale test.

- Supports

At the connection between the biggest cylindrical sector and the wall, the supports were off-centre (figure 30). The purpose of this characteristic was centring the reactive forces in that location (Antuña 2003, p.140). Therefore, that connection could be studied by a finite elements analysis in order to check the effect of the support eccentricity.

- Buckling

A description of the design of the Frontón Recoletos was published by Torroja in 1942, but no mention was made of the study of buckling.

In order to calculate the risk of buckling of a cylindrical surface Antuña applied the Foppl formulas obtaining a safety factor of 0.88 in the Frontón Recoletos. This factor was highly fewer than other contemporary shells. For example, the security factor of the Areneros shells (figure 25) was 5 (Antuña 2003, p.190). Therefore, the analysis of the buckling is really recommended in this structure.

- Ribs ties

After the Civil Spanish War, a design to repair the roof was drawn up. This design consisted of the some reinforced concrete rings defined with the purpose of correcting the bombard deflections, raising the shell. Therefore, a finite elements model based on the ribs ties proposed in the repair works could be studied in order to check the shell raising proposed by Torroja.

- New methods

One of the problems of the thin shells made of concrete was the forming cost. Therefore, innovative forming systems that allow reducing that cost could be studied in the future in order to make this kind of structures more competitive in the future.

- New materials

Studying the structure with current materials as for example, the steel fibre reinforced concrete, which was used in the roof of the L'Oceanográfico in Valencia.

Chapter 4

Conclusions

The Frontón Recoletos is a noteworthy example of the courage showed by Torroja along all his extensive professional experience. This structure was considered a structural challenge due to the innovative characteristics incorporated: the biggest size, the absence of beam at the connection between lobes, the skylights, the support conditions as well as the asymmetrical directrix, which did not allow the application of the theoretical methods existing in the period when the structure was constructed. These methods were based on exact equations modelling the behaviour of the cylindrical shells and were adapted by Torroja in order to calculate the Fronton Recoletos shell. This adaptation and the conception of the structure was thought by Torroja as a way to improve the knowledge about this kind of structures and therefore, all the deflections and stresses were measured during the construction and the first years of the building. Furthermore, this shell is a clear example of the Torroja's thoughts about the structures. Nowadays, the aesthetic sensibility has deeply changed. Many times the shape is designed following only purely aesthetical reasons, without considering the structural or functional requirements; the structural truth is not considered indispensable anymore; and complex and attractive typologies are designed in order to amaze the observer. These aesthetical and architectonics concepts are not better or worse of yesteryear, just completely different to the Torroja's beliefs, which was based on the simplicity and the truth.

Thin concrete shells are not as popular today as they once were, when famous designers such as Torroja or Candela erected structures that became landmark examples of modern architecture. The main reason why large thin concrete shell structures are no longer constructed are the forming cost. This problem could be solved by the development of alternate construction techniques like innovative forming systems. Nevertheless, the cost alone cannot be the only explanation for the decrease in popularity of thin concrete shells. These structures have to be also re-popularized and reintroduced into the minds of designers and builders.

The following conclusions were obtained after the structural analysis of the Frontón Recoletos shell. Firstly, the first Lusas model, which was based on the Torroja's hypotheses during the theoretical calculations, showed clearly the similarity with the experimental deflections measured in the small-scale model and the actual structure. Nevertheless, the transversal bending moments as well as the maximum tension and compression stress isobars were higher than the values obtained by Torroja. This factor was explained by the hypothesis of thickness

variation along the shell supposed in the calculation of the stresses as well as the probable numerical mistakes because the calculations were done by hand. Secondly, Torroja probably adapted the parameters of the theoretical model, like the Elasticity Modulus, in order to obtain a similar behaviour to the measured small-scale structure. For that reason, the vertical deflections obtained by the first model were highly similar to the deflections measured in the actual models. Thirdly, in the second model the transversal bending moments were increased in the places where the thickness was increased, like for example the skylights, because the structure was stiffer in those sections. Fourthly, the wind suction effects improved the structural behaviour of the shell. Therefore, the assumption considered by Torroja of not including these elements in the initial theoretical calculation can be logically assumed. Fifthly, as was supposed by Torroja, the real skylights can logically be simplified as closed shell because the structural behaviour of the second and the fourth Lusas model was highly similar. However, the consideration of skylights increased the deflections and stresses because the structure was more flexible as well as increased the stresses at the connection between the shell and the skylights due to the difference of stiffness between both elements. Sixthly, the real supports decreased the stiffness of the structure and therefore, the deflections and stresses were increased regarding the theoretical supports. Furthermore, the concentration of stresses produced by the concentrated supports was resolved by Torroja by means of beams along the edges in order to distribute the forces. Seventhly, the fifth Lusas model is highly sensible to variations in the loads and the Elasticity Modulus and these factors could not be measured perfectly in the real structure. Therefore, variation of these elements could explain the difference of vertical distortions between the values obtained by Torroja in the actual structure and the fifth Lusas model, which was considered the most similar to the reality. Eighthly, the reinforcement ribs proposed by Torroja improved the structural behaviour of the shell, as the designer supposed, because the stresses and deflections were reduced. Ninthly, considering that originally the structure was calculated by hand, the similarity between the results obtained by Torroja and the Lusas program is surprising high, as for example in the location of the reinforcement bars or in the theoretical vertical deflections. This factor showed that the structural behaviour of the shell was perfectly known by Torroja and the simplifications were logically applied.

All the conclusions obtained in the structural analysis showed the extraordinary talent and courage of Eduardo Torroja, who was able to design, calculate and build perfectly the Frontón Recoletos using his intuition and his structural knowledge in order to adapt the available theories.

Future interesting researches, as for example the study of the temperature dilation or the raising of the shell by means of the ribs proposed by Torroja, can be carried out in order to continue the labour showed by Torroja of improving the knowledge about the thin concrete shell structures.

Bibliography

Antuña, J., 2003. *Las estructuras de edificación de Eduardo Torroja y Miret*, Escuela técnica Superior de Arquitectura Madrid.

Antuña, J., 2006. The Evolution of the Work of Eduardo Torroja, *Second International Congress on Construction History, Queens' College, Cambridge University; 29/03-02/04/2006.*

Billington, D., Hines E. 2004. Anton Tedesko The Introduction of Thin Shell Concrete Roofs in the United States. *Journal of Structural Engineering ASCE, November 2004.*

Billington D., 1979. *Structural Engineering Handbook Mc Graw: Thin shell concrete structures*. Princeton University Cambridge university press.

Calladine, C.R., 1983. *Theory of Shell Structures*. Cambridge, Cambridge university press.

Chilton, J., 2000. *Heinz Isler: The engineer contribution to contemporary architecture.* London Thomas Telford.

Fernandez, J.A., Vera, J.R., 1999. *Eduardo Torroja: Ingeniero*. Madrid, Pronaos.

Fortin, F., 2000. *Sports-The Complete Visual Reference*. Firefly Books.

Guiness, 1990. *Guiness Sports Record Book 1990-1991*. Sterling Publishing C.O.

Medwadowski, S.J., 1998. Concrete thin shell roofs at the turn of the millennium, *Current and Emerging Technologies of Shell and Spatial Structures, Proceedings of the IASS Symposium, April 1997, Edited by J. Abel, R. Astudillo and N.K. Srivastava.*

Meyer, C., Sheer M.H., 2005. Do Concrete Shells Deserve Another Look? Industry professional give mixed opinions. *Concrete International October 2005.*

Teng, J.G. 2001. Steel-concrete composite shells for enclosing large spaces. *Proceedings, International Conference on Steel and Composite Structures, Pusan, Korea, 14–16 June.*

Torroja, E., 1942. Comprobación y comportamiento de un estructura laminar. *Madrid, Memorias de la Real Academia de Ciencias Exactas, Físicas y Naturales de Madrid.*

Torroja, E., 1962a. Informes de la construcción: Revista de información técnica, 1962, año XIV, nº 137, *Madrid, Instituto Eduardo Torroja.*

Torroja, E., 1962b. *Philosophy of structures*. University of California Press Berkeley and Los Angeles.

Torroja, E., 1976. *Razón y ser de los tipos estructurales Artículo de láminas.* 4ª edición, Madrid. Instituto Eduardo Torroja.

Torroja, J.A. 2007, Eduardo Torroja. *I.T nº 79*

Wong, H. T., Teng, J.G.2004. Buckling behavior of model base shells of a Comshell roof system. *Departament of Civil and Structural Engineering, The Hong Kong University, Hong Kong, China. Progress in Structural Engineering, Mechanics and Computations Zingoni. Taylor & Francis Group London*

Figures

Figure 1:

- Tree leaf: http://i67.photobucket.com/albums/h317/labombilla/Gotasdelluvia.jpg last view 15/04/09.
- Igloo: http://www.alaska-in-pictures.com/data/media/9/inupiat-eskimo-igloo_438.jpg last view 3/3/09.

Figure 2:

- Lion Gate:
- http://i.pbase.com/o6/94/689794/1/81199881.ooJIGERc.MyceneaLionGateBW.jpg last view 2/3/09.
- Agrippa Pantheon: http://contenidos.educarex.es/mci/2004/44/@rt.com/Arte_romano/images/Templo_Panteon_Roma_jpg.jpg last view 15/3/09.

Figure 3:

- SidneyOpera: http://en.structurae.de/structures/data/photos.cfm?ID=s0000073 last view 4/4/09.
- L'Oceanogràfic: http://www.fundacioncac.es/cas/artesyciencias/mediateca/download/20049913856o-2178dig_jft.jpg last view 2/3/09.

Figure 4:

- Relaxation park: http://www.via-arquitectura.net/10/110/110-01.jpg last view 2/3/09 and http://www.architecture.com/Images/RIBATrust/Awards/RoyalGoldMedal/2006/Pavillion,Torrevieja-Relaxa_530x421.gif last view 2/3/09.

Figure 5:

- Sagrada Familia: http://www.guideinbarcelona.com/images/barcelona/sagrada-familia-barcelona.jpg last view 2/3/09.
- Antonio Gaudi's reversed model: http://www.gaudidesigner.com/data/file/357.jpg last view 2/3/09.

Figure 6:

- Fedala water tank designed by Torroja :
  http://en.structurae.de/files/photos/2520/shell/image17copy2.jpg last view 2/3/09.

Figure 7:

- Pallazeto dello sport designed by Nervi:
  http://www.galinsky.com/buildings/palazzettodellosport/index.htm last view 2/3/09.

Figure 8:

- Kupolen stadium designed by Sundquist:
  http://upload.wikimedia.org/wikipedia/commons/thumb/7/74/Kupolen,_Borl%C3%A4nge.jpg/180px-Kupolen,_Borl%C3%A4nge.jpg last view 9/5/09.

Figure 9:

- Hangar d'Orly:
  http://www.albaiges.com/ingenieros/15sXX-m1_archivos/image013.jpg last view 4/4/09 and http://www.columbia.edu/cu/gsapp/BT/BSI/ARCH/img0086.jpg last view 4/4/09.
- Church Building:
  http://nisee.berkeley.edu/elibrary/getpkg?id=GoddenE42-44&t=10 last view 4/4/09.

Figure 10:

- Restaurante Los Manantiales designed by Candela:
  http://www.arch.mcgill.ca/prof/sijpkes/abc-structures-2005/concrete/HyparManantiales.jpg last view 4/4/09 and http://farm4.static.flickr.com/3148/2544102546_1ab9ab8a19.jpg?v=0 last view 4/4/09.

Figure 11:

- Trans World Airline designed by Saarinem:
  http://www.bluffton.edu/~sullivanm/saartwa/angle.jpg last view 4/4/09 and http://graphics8.nytimes.com/images/2008/02/22/nyregion/portal600.jpg last view 4/4/09.

Figure 12:

- Table of different thin concrete shells:
  Hines E., Billington, D. Anton Tedesko: The Introduction of Thin Shell Concrete Roofs in the United States. *Journal of Structural Engineering ASCE, November 2004 E. Hines and D. Billington p.1640.*

Figure 13:

- Jena Planetarium:
  http://www.uniroma2.it/didattica/AT21/deposito/8_voltesottilidicementoarmato.pdf last view 12/4/09.
- Hayden Planetarium:
  http://en.structurae.de/photos/index.cfm?JS=17155 last view 12/4/09.

Figure 14:

- First phase of the Bini's System:
  http://www.binisystems.com/shell1-2.html last view 5/3/09.

Figure 15:

- Second phase of the Bini's System:
  http://www.binisystems.com/shell3-4.html last view 5/3/09.

Figure 16:

- Inflating process:
  http://en.structurae.de/structures/data/photos.cfm?ID=s0012106 last view 7/4/09.

Figure 17:

- Modular steel units and cylindrical shape:
  Teng, J.G. 2001. Steel-concrete composite shells for enclosing large spaces. *Proceedings, International Conference on Steel and Composite Structures, Pusan, Korea, 14–16 June p.5.*
- Real structure:
  Comshell web site, http://www.cse.polyu.edu.hk/~cejgt/comshell/comshell.htm last view 7/4/09.

Figure 18:

- African tent:
  http://www.bible-archaeology.info/Tents_nomadic.jpg last view 5/3/09.
- Sami tent:
  http://www.seaice.org.uk/research/graphics/euroclim/Sami_tent_at_Fjellheisen.jpg last view 6/4/09.
- Structure Lomas de Cuernavaca:
  http://www.princeton.edu/main/images/news/2008/10/Chapel-Lomas-de-Cuernavaca-i.jpg last view 5/3/09.

Figure 19:

- Aqueduct Tempul:
- Torroja, J.A. 2007, Eduardo Torroja. *I.T nº 79 p.99.*
- Market Hall:
  http://en.structurae.de/photos/index.cfm?JS=51698 last view 15/04/09 and http://imagespain.com/pics/1269.jpg last view 16/04/09.

Figure 20:

- Inverted model:
  Chilton, J., 2000. *Heinz Isler: The engineer contribution to contemporary architecture.* London Thomas Telford. p.32.
- Station service in Deitingen:
  http://en.structurae.de/structures/data/photos.cfm?id=s0030516 last view 17/04/09.

Figure 21:

- Structural behavior of the vault and long barrel:
  http://www.student.uwa.edu.au/~wongs30/shells__developable_shells.htm last view 15/04/09.

Figure 22:

- 3-D model of the supports:
  Antuña, J., 2003. Las estructuras de edificación de Eduardo Torroja y Miret, *Escuela técnica Superior de Arquitectura Madrid.p.144.*

Figure 23:

- Picture of the inside of the structure of the Frontón Recoletos:
  http://www.urbanity.es/foro/urbanismo-mad/893-de-madrid-al-cielo-album-de-fotos-historicas-87.html last view 15/05/09.

Figure 24:

- Picture of the outside of the structure of the Frontón Recoletos:
  http://www.urbanity.es/foro/urbanismo-mad/893-de-madrid-al-cielo-album-de-fotos-historicas-87.html last view 15/05/09.

Figure 25:

- Cylindrical thin concrete shell:
  Torroja, E., 1942. Comprobación y comportamiento de un estructura laminar. *Madrid, Memorias de la Real Academia de Ciencias Exactas, Físicas y Naturales de Madrid. p.17.*

Figure 26:

- Court of Jai alai:
  http://www.dania-jai-alai.com/page3.htm last view 15/04/09.
- Jai alai player:
  http://www.nytimes-institute.com/miami09/wp-content/uploads/2009/01/jai-alai-2.jpg last view 15/04/09.

Figure 27:

- Different Frontón de Recoletos designs:
  Fernández, J.A., Vera, J.R. 1999. *Eduardo Torroja: Ingeniero*. Madrid, Pronaos, p. 134.

Figure 28:

- Differential element of the shell:
  Torroja, E., 1942. Comprobación y comportamiento de un estructura laminar. *Madrid, Memorias de la Real Academia de Ciencias Exactas, Físicas y Naturales de Madrid. p.30.*
- Reinforced construction drawing:
  Torroja, E., 1942. Comprobación y comportamiento de un estructura laminar. *Madrid, Memorias de la Real Academia de Ciencias Exactas, Físicas y Naturales de Madrid. Figure18.*

Figure 29:

- Comparison sizes between the Frontón and Budapest:
  Figure realized by the Autocad program.

Figure30:

- Joins between the shell and the wall in the Frontón Recoletos:
  Antuña, J., 2003. *Las estructuras de edificación de Eduardo Torroja y Miret*, Escuela técnica Superior de Arquitectura Madrid. Figure 4.67.

Figure 31:

- Wind load law without including the suction effects along the directrix:
  Figure realized by the Lusas program.

Figure 32:

- Wind load law including the suction effects along the directrix:
  Figure realized by the Lusas program.

Figure 33:

- Snow load law along the directrix:
  Figure realized by the Lusas program.

Figure 34:

- Dead weight load law along the directrix:
  Figure realized by the Lusas program.

Figure 35:

- Isobars of maximum compression and tension stress presented by Torroja:
  Torroja, E., 1942. Comprobación y comportamiento de un estructura laminar. *Madrid, Memorias de la Real Academia de Ciencias Exactas, Físicas y Naturales de Madrid. Figures 16 and 17.*

Figure 36:

- Diagram of transversal bending moments along the directrix presented by Torroja:
  Torroja, E., 1942. Comprobación y comportamiento de un estructura laminar. *Madrid, Memorias de la Real Academia de Ciencias Exactas, Físicas y Naturales de Madrid. Figure9.*

Figure 37:

- Deflections along the directrix presented by Torroja for different models:
  Torroja, E., 1962a. Informes de la construcción: Revista de información técnica, 1962, año XIV, nº 137*, Madrid, Instituto Eduardo Torroja, p.4.*

Figure 38:

- Mesh of the first Lusas model and supports and surfaces considered in the model:
  Figure realized by the Lusas program.

Figure 39:

- Maximum values of the tension stress isobars along the central undeveloped directrix:
  Figure obtained with the Excel program using the results obtained by Lusas.

Figure 40:

- Maximum values of the compression stress isobars along the central undeveloped directrix:
  Figure obtained with the Excel program using the results obtained by Lusas.

Figure 41:

- Deflections in the 3-D model calculated by the first Lusas model:
  Figure realized by the Lusas program.

Figure 42:

- Deflections in the 3-D model calculated by the first Lusas model:
  Figure realized by the Lusas program.

Figure 43:

- Absolute vertical deflections in the first Lusas model at the connection between both cylindrical sectors:
  Figure realized by the Lusas program.

Figure 44:

- Absolute Z-deflections in the first Lusas model along the seagull profile:
  Figure realized by the Lusas program.

Figure 45:

- Vertical deflections in the first Lusas model along central directrix for the load case four:
  Figure realized by the Lusas program.

Figure 46:

- Absolute vertical deflections in the first Lusas model along the central undeveloped directrix:
  Figure realized by the Lusas program.

Figure 47:

- Comparison of the deflections measured by different models:
  Figure obtained with the Autocad program cad using the results obtained by Lusas and the Torroja's deflections.

Figure 48:

- Absolute vertical deflections along the central undeveloped directrix considering different models:
  Figure obtained with the Excel program using the results obtained by Lusas and the Torroja's deflections

Figure 49:

- Absolute Lusas Z-deflections in the first Lusas model along the central undeveloped directrix:
  Figure realized by the Lusas program.

Figure 50:

- Transversal Bending moments presented by the first Lusas model along the central undeveloped directrix:
  Figure realized by the Lusas program.

Figure 51:

- Transversal bending moments along the central undeveloped directrix considering different models:
  Figure realized by the Lusas program.

Figure 52:

- Maximum tension stress isobars in the first Lusas model along the plan of the half-undeveloped section:
  Figure realized by the Lusas program.

Figure 53:

- Maximum compression stress isobars in the first Lusas model along the plan of the half-undeveloped section:
  Figure realized by the Lusas program.

Figure 54:

- Variation of thickness along the central directrix:
  Torroja, E., 1962a. Informes de la construcción: Revista de información técnica, 1962, año XIV, nº 137*, Madrid, Instituto Eduardo Torroja p.4.*

Figure 55:

- Variation of thickness in the second Lusas model along the directrix and zoom of the seagull profile:
  Figure realized by the Lusas program.

Figure 56:

- Plan of the surface elements used in the second Lusas model and plan of the mesh used in the second Lusas model:
  Figure realized by the Lusas program.

Figure 57:

- Absolute vertical deflections along the seagull profile obtained by the second Lusas model:
  Figure realized by the Lusas program.

Figure 58:

- Absolute vertical deflections along the central directrix obtained by the second Lusas model:
  Figure realized by the Lusas program.

Figure 59:

- Vertical deflections along the central undeveloped directrix considering different models:
  Figure obtained with the Excel program using the results obtained by Lusas and the Torroja's deflections.

Figure 60:

- Transversal bending moments presented by the second Lusas model along the central undeveloped directrix:
  Figure obtained by the Lusas program.

Figure 61:

- Transversal bending moments along the central undeveloped directrix considering different models:
  Figure obtained with the Excel program using the results obtained by Lusas and the Torroja's deflections.

Figure 62:

- Maximum tension stress isobars along the central undeveloped directrix considering different model:
  Figure obtained with the Excel program using the results obtained by Lusas and the Torroja's deflections.

Figure 63:

- Maximum compression stress isobars along the central undeveloped directrix considering different model:
  Figure obtained with the Excel program using the results obtained by Lusas and the Torroja's deflections.

Figure 64:

- Maximum tension stress isobars in half-undeveloped plan obtained by the second Lusas model:
  Figure obtained by the Lusas program.

Figure 65:

- Maximum compression stress isobars in half-undeveloped plan obtained by the second Lusas model:
  Figure obtained by the Lusas program.

Figure 66:

- Wind suction law considered by Torroja:
  Torroja, E., 1942. Comprobación y comportamiento de un estructura laminar. *Madrid, Memorias de la Real Academia de Ciencias Exactas, Físicas y Naturales de Madrid. Figure 6.*

Figure 67:

- Vertical deflections along the central undeveloped directrix considering different load cases in the third Lusas model:
  Figure obtained with the Excel program using the results obtained by Lusas and the Torroja's deflections.

Figure 68:

- Vertical deflections along the central undeveloped directrix considering different load cases in the third Lusas model:
  Figure obtained with the Excel program using the results obtained by Lusas and the Torroja's deflections.

Figure 69:

- Construction of the skylight beams using wooden frameworks:
  http://www.urbanity.es/foro/urbanismo-mad/893-de-madrid-al-cielo-album-de-fotos-historicas-87.html last view 15/05/09.

Figure 70:

- 3-D view of the fourth Lusas model:
  Figure obtained by the Lusas program.

Figure 71:

- Directrix of the fourth Lusas model and zoom of the skylight in the smallest cylindrical sector:
  Figure obtained by the Lusas program.

Figure 72:

- Fourth Lusas model consisted of surfaces and beams:
  Figure obtained by the Lusas program.

Figure 73:

- Deflections in the 3-D view of the fourth Lusas model:
  Figure obtained by the Lusas program.

Figure 74:

- Deflections in the 3-D view of the fourth Lusas model:
  Figure obtained by the Lusas program.

Figure 75:

- Vertical deflections along the central undeveloped directrix considering different models:
  Figure obtained with the Excel program using the results obtained by Lusas and the Torroja's deflections.

Figure 76:

- Vertical deflections along half seagull profile, from the coordinate Z = 0 metres to Z = 27.5 metres considering different models:
  Figure obtained with the Excel program using the results obtained by Lusas and the Torroja's deflections.

Figure 77:

- Vertical deflections along the central undeveloped directrix considering different models:
  Figure obtained with the Excel program using the results obtained by Lusas and the Torroja's deflections.

Figure 78:

- Vertical deflections along the central undeveloped directrix considering different models:
  Figure obtained with the Excel program using the results obtained by Lusas and the Torroja's deflections.

Figure 79:

- Vertical deflections along the central undeveloped directrix considering different models:
  Figure obtained with the Excel program using the results obtained by Lusas and the Torroja's deflections.

Figure 80:

- Vertical deflections along the central undeveloped directrix considering different models:
  Figure obtained with the Excel program using the results obtained by Lusas and the Torroja's deflections.

Figure 81:

- Bending moments along the central undeveloped directrix considering different models: Figure obtained with the Excel program using the results obtained by Lusas and the Torroja's deflections.

Figure 82:

- Tension stress isobars along the central directrix considering different model:
  Figure obtained with the Excel program using the results obtained by Lusas and the Torroja's deflections.

Figure 83:

- Compression stress isobars along the central directrix considering different model:
  Figure obtained with the Excel program using the results obtained by Lusas and the Torroja's deflections.

Figure 84:

- Plan of the half-undeveloped section of the maximum tension stress isobars for the fourth Lusas model:
  Figure obtained by the Lusas program.

Figure 85:

- Plan of the half-undeveloped section of the maximum compression stress isobars for the fourth Lusas model:
  Figure obtained by the Lusas program.

Figure 86:

- Real supports at the directrix:
  Torroja, E., 1942. Comprobación y comportamiento de un estructura laminar. *Madrid, Memorias de la Real Academia de Ciencias Exactas, Físicas y Naturales de Madrid. Figure 21.*

Figure 87:

- Real supports at the generators:
  Torroja, E., 1942. Comprobación y comportamiento de un estructura laminar. *Madrid, Memorias de la Real Academia de Ciencias Exactas, Físicas y Naturales de Madrid. Figure 21.*

Figure 88:

- Picture of the small-scale model tested by Torroja:
  http://www.urbanity.es/foro/urbanismo-mad/893-de-madrid-al-cielo-album-de-fotos-historicas-87.html last view 15/05/09.

Figure 89:

- Fifth Lusas model consisted of surfaces and the supports conditions:
  Figure obtained by the Lusas program.

Figure 90:

- Plan of half-undeveloped section of the maximum tension stress isobars when the discontinuous supports were considered but not the edged beam:
  Figure obtained by the Lusas program,

Figure 91:

- Plan of half-undeveloped section of the maximum tension stress isobars when the edged beams and the discontinuous supports were considered:
  Figure obtained by the Lusas program,

Figure 92:

- Vertical deflections along the central undeveloped directrix considering different models:
  Figure obtained with the Excel program using the results obtained by Lusas and the Torroja's deflections.

Figure 93:

- Vertical deflections along the central undeveloped directrix considering different models:
  Figure obtained with the Excel program using the results obtained by Lusas and the Torroja's deflections.

Figure 94:

- Bending moments along the central undeveloped directrix considering different models:
  Figure obtained with the Excel program using the results obtained by Lusas and the Torroja's deflections.

Figure 95:

- Tension stress isobars along the central directrix considering different models:
  Figure obtained with the Excel program using the results obtained by Lusas and the Torroja's deflections.

Figure 96:

- Compression stress isobars along the central directrix considering different models:
  Figure obtained with the Excel program using the results obtained by Lusas and the Torroja's deflections.

Figure 97:

- Plan of half-undeveloped section of the maximum compression stress isobars when the edged beams and the discontinuous supports were considered:
  Figure obtained with the Lusas program.

Figure 98:

- Collapse of the Frontón Recoletos roof:
  http://www.urbanity.es/foro/urbanismo-mad/893-de-madrid-al-cielo-album-de-fotos-historicas-87.html last view 15/05/09.

Figure 99:

- Construction drawings used by Torroja of the reinforcement rings located at the biggest lobe:
  Torroja, E., 1942. Comprobación y comportamiento de un estructura laminar. *Madrid, Memorias de la Real Academia de Ciencias Exactas, Físicas y Naturales de Madrid. Figure 159.*

Figure 100:

- A sketch showing the proposed solution to repair the Frontón Recoletos roof:
  Fernandez, J.A., Vera, J.R., 1999. *Eduardo Torroja: Ingeniero.* Madrid, Pronaos. p.143.

Figure 101:

- 3-D Lusas model, considering the ribs location supposed by Antuña:
  Figure obtained by the Lusas program.

Figure 102:

- Vertical deflections along the central directrix considering different reinforcement hypotheses:
  Figure obtained with the Excel program using the results obtained by Lusas and the Torroja's deflections.

Figure 103:

- *V*ertical deflections along the central directrix considering different reinforcement hypotheses:
  Figure obtained with the Excel program using the results obtained by Lusas and the Torroja's deflections.

Figure 104:

- Vertical deflections along the central directrix considering different models:
  Figure obtained with the Excel program using the results obtained by Lusas and the Torroja's deflections.

Figure 105:

- Transversal bending moments along the central directrix considering different models:
  Figure obtained with the Excel program using the results obtained by Lusas and the Torroja's deflections.

Figure 106:

- Tension stress isobars along the central directrix considering different models:
  Figure obtained with the Excel program using the results obtained by Lusas and the Torroja's deflections.

Figure 107:

- Compression stress isobars along the central directrix considering different models:
  Figure obtained with the Excel program using the results obtained by Lusas and the Torroja's deflections.

Appendix A

Lusas calculations

Lusas is a finite element analysis programme, also called FEAP, where the finite elements are applied to the analysis of static or dynamic physical objects and systems. The object of the programme is representing by a geometrically similar simplified model the structure. Equations of equilibrium, derived from applicable physical considerations, are applied to each element, and a system of simultaneous equations is constructed. Finally, solving this system is obtained the outputs, which show the structural behaviour of the structure.

The FEAP is used to analyze objects and systems that are of sufficient complexity that analysis with simpler closed-form analytical methods will not yield results of adequate accuracy, and permits the solution of problems, which could not otherwise be solved.

There are some FEA programmes adequate to solve the Frontón Recoletos, as for example Abaqus or Ansys. However, the chosen program was Lusas.

- *Units*

The units used in the programme are the same defined in the International System: Newton to forces, Metres to lengths, Seconds to times, and Calvin to temperatures.

- *Version of Lusas*

The calculations have been done using the programme Lusas 14.1.

A.1 Lusas Elements

Two different Lusas elements were used in the different Lusas models: QSI4 in the surfaces and BMS3 in the beams. Both elements are described in this chapter.

The first element QSI4 is used in thin shells in 3D and taking into account both membrane and flexural deformations. As required by thin plate theory, transverse shearing deformations are excluded. This element has six freedoms, three deformations and three rotations in each node (figure A).

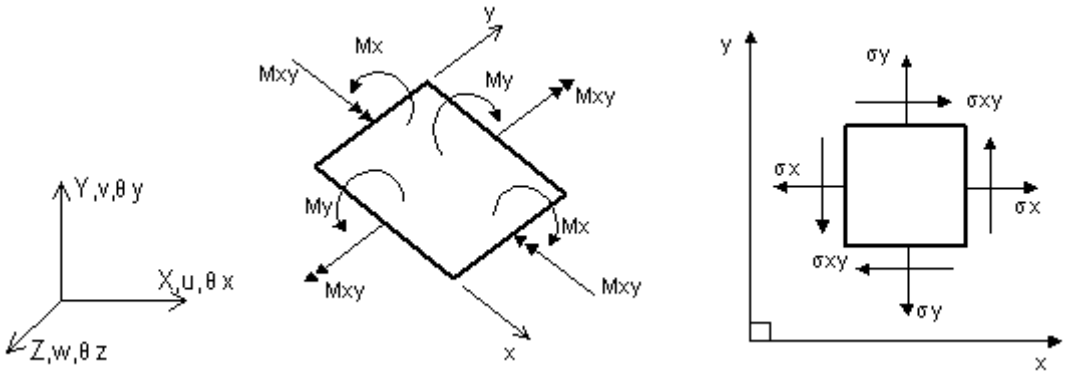

Figure A: *Freedoms of the QSI4 element: three deformations (u, v, w) and three rotations (fix, fiy and fiz), Lusas outputs for the element QSI4.* These figures were obtained from Lusas manual.

The output of the Lusas program (figure A) for the element QSI4 are:

- Stress resultant: Nx, Ny, Nxy, Mx, My, Mxy: forces, moments/unit width in local directions.
- Stress (default): σx, σy, σxy, σmax, σmin, β, σe: in local direction
- Strain: εx, εy, γxy, ψx, ψy, ψxy: membrane, flexural strains in local directions.

For the comparison with the diagrams obtained by Torroja (figure A) the maximum and minimum values of the axial forces, called N, distributed along the thickness of the shell were used.

The second element BMS3 is defined as a straight beam element in 3D for which shear deformations are included and the geometric properties are constant along the length. This element, like the surface elements, has six freedoms, three deformations and three rotations in each node.

The output of the Lusas program (figure B) for the element QMS3 are:

- Force (default): Fx, Fy, Fz, Mx, My, Mz: in local directions.
- Element output is with respect to the beam centre line.

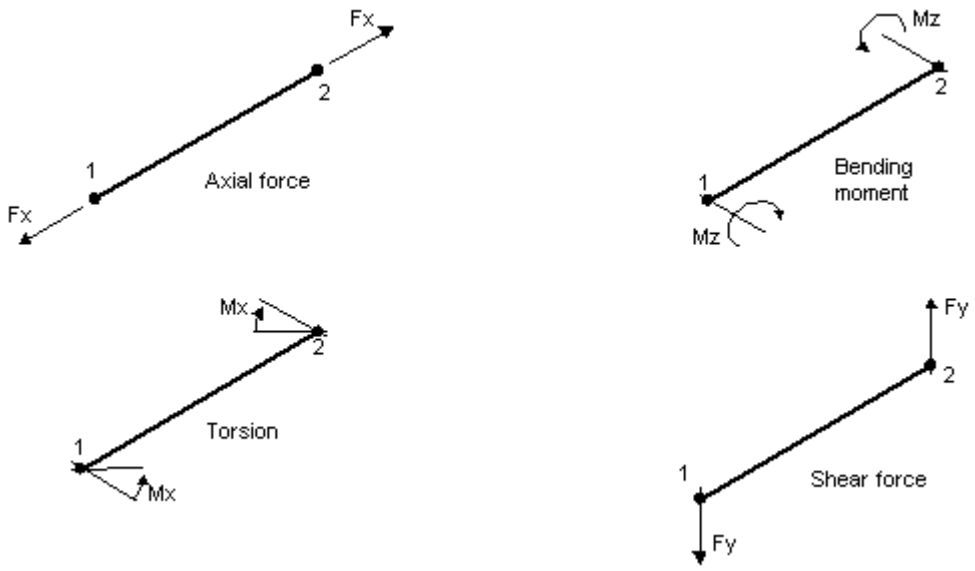

Figure B: *Lusas outputs for the element QMS.* This figure was obtained from Lusas manual.

A.2 Lusas Outputs.

The Lusas outputs used along the thesis were the following: Firstly, the Isobar lines, which were obtained using the “Contour Results” option, “Stress (middle)-Thin shell”, component “S1” for the maximum, tension stress isobars and “S3” for the maximum compression stress isobars. The display was homogenized for all the isobars with the next characteristic: in the “Contour Display” option are checked the boxes “Filled”, “Lines” and “Smoothed” and in the “Contour Range” option are defined 11 intervals with maximum values 8 MPa, in the case of tensions and -5.8 MPa for compressions. These values, corresponding to the maximum stresses obtained by Torroja in the numerical calculations, were measured in the isobars. Secondly, deflection diagram at the central directrix was calculated using the option: “Deformed mesh”. Thirdly, the deformations at the central directrix were obtained using the “Graph through 2D” option, “Displacement”, Component “DY” or “DZ”. Fourthly, the bending moments along the central directrix were calculated using the “Graph through 2D” option, “Stress thin shell”, Component “Mx” for the transversal bending moments and “My” for the longitudinal bending moments. Lastly, the video was obtained by the option “Animation wizard” along the central directrix considering a sinoidal variation of the loads.

A.3 Loads

The snow and wind load laws along the directrix were defined by Torroja in cylindrical coordinates depending on the angle "φ" (formula 3, 9). However, in order to introduce these variations in the Lusas program, two cardinal coordinate systems were defined. These systems were located at the centres of the both cylindrical sectors. In order to obtain the laws in the new coordinate system: Firstly, the relations between both systems[54] were obtained using trigonometry (formula A and B). After that, the values in the laws presented by Torroja were changed (formula C, D and E).

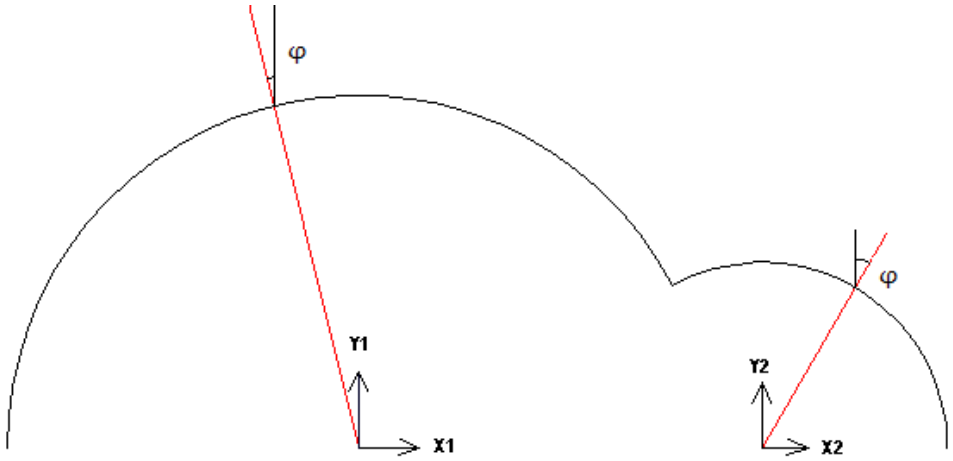

Figure B: *Local cardinal coordinate system located at the centres of the lobes*[55]. This picture was obtained using Autocad program.

$$sin\,\varphi = \frac{y_i}{\sqrt{x_i^2 + y_i^2}} \qquad [A]$$

$$cos\,\varphi = \frac{Abs(x_i)}{\sqrt{x_i^2 + y_i^2}} \qquad [B]$$

$$Snow = 637{,}47 \cdot \frac{y_i}{\sqrt{x_i^2 + y_i^2}} \qquad [C]$$

$$Wind = 980{,}66 \cdot \frac{Abs(x_i)}{\sqrt{x_i^2 + y_i^2}} \qquad [D]$$

[54] To obtaining the relation between both coordinate system was used the absolute value in Cos(φ) because as was explained in the section 2.3 of this thesis, Torroja supposed compressions in both sides of the shell.

[55] y_i and x_i= Local cardinal coordinates in each of the cardinal coordinate systems.

$$\text{Wind Suction} = 0{,}4 \cdot \frac{Abs(x_i)}{\sqrt{x_i^2 + y_i^2}} - 3 \cdot \frac{y_i}{\sqrt{x_i^2 + y_i^2}} \qquad [E]$$

The wind load is orthogonal to the surface in each point. Therefore, the Lusas loading option "local distributed loads" along Z direction was used in shells and skylights beams. This distribution is defined per unit area. However, in order to define the wind law in the skylights beams, the original wind distribution was changed because each beam had to resist the wind effect at the windows located in both sides of the beam, which means that the beams had a virtual wide, called 2*c* (figure B). In order to obtain the parameter *"c"* (formulas F, G and H), the area of the triangular windows was distributed in three virtual beams, which were formed by the beam length per the virtual wide (figure B). As each beam is joined by two windows, the virtual beams wide will be 2*c* = 0.4 metres. Therefore, the wind load along the beams per unit length is the 40 % of the wind load for shells per unit area.

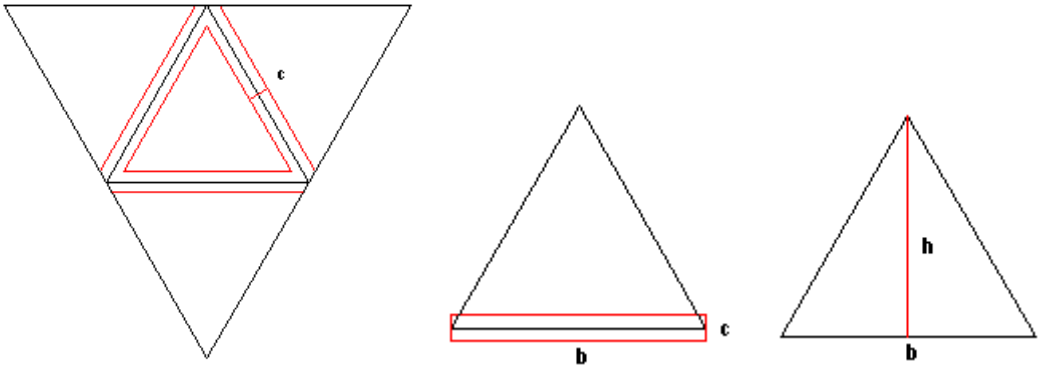

Figure B: *Beam elements and triangular windows.*

$$Triangle\ Area = 3\ Virtual\ beam\ Area \qquad [F]$$

$$\frac{b \cdot \sqrt{b^2 + \frac{b^2}{2}}}{2} = 3 \cdot b \cdot c \qquad [G]$$

$$c = \frac{\sqrt{b^2 + \frac{b^2}{2}}}{2} = 0{,}2\ m \qquad [H]$$

The snow load is always vertical, therefore, the Lusas loading option "global distributed" along Y direction was used. This load is distributed differently for shells and skylights beams: for the first is per unit area and for the second one per unit length.

A.4 Definition of the thickness.

The variation of the thickness was defined by means of the utility called "Surface function variation" which consists of a single function in terms of the parametric coordinates of the surface "u", direction along the local x axis, and "v", direction along the local y axis.

A.5 Definition of the Real supports.

The real supports at the generators (figure 87) consisted of a fixed section located at the centre and parallel beams at the rest of the generator each 1.5 meters. These beams fixed the vertical movements and acted like springs in the Z direction, parallel to the generators, as well as in the X direction, orthogonal to the generators.

As the beam acted like a spring in two directions, different coefficient *K* of stiffness was obtained for each direction. The supports were simplified supposing a cantilever beam fixed in the wall (figure E). For this simple structure the stiffness *K* can be obtained knowing the deformation when concentrated force is applied at the edge (formula I, K and L). The Modulus of Inertia *I*, (formula J) was calculated knowing the dimensions of the rectangular section, *A* per *B*, and is different for each direction.

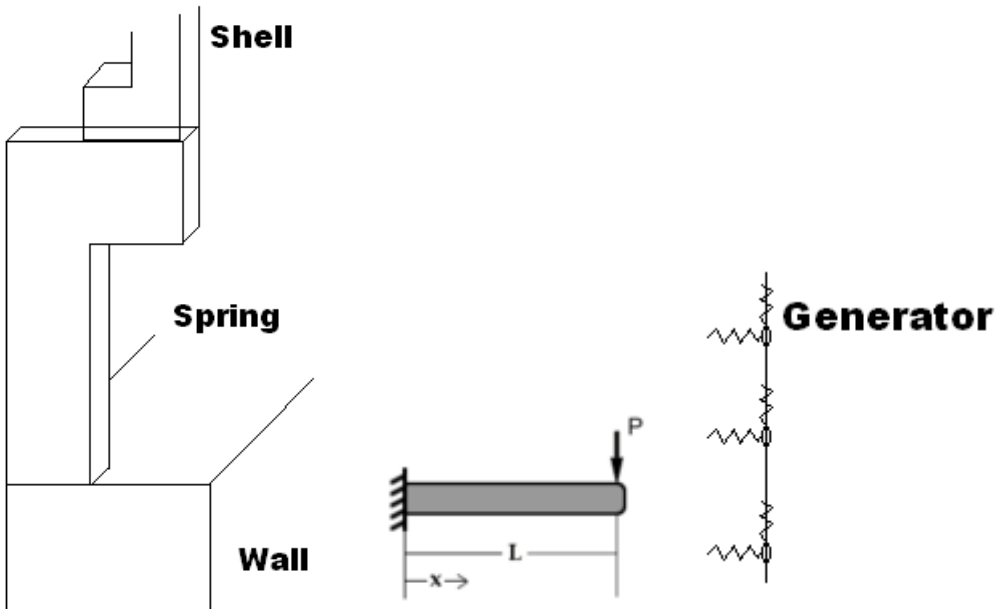

Figure E: *Springs model*, *cantilever beam*: the symbol P corresponds to the concentrated load applied at the edge of the beam as well as the symbol L is defined as the longitude of the beam and *model of spring at the generators.*

$$K \cdot \delta = P \qquad [I]$$

$$\delta = \frac{P \cdot L^3}{3 \cdot E \cdot I} \qquad [J]$$

$$I = \frac{A \cdot B^3}{12} \qquad [K]$$

$$K = \frac{P}{\delta} = \frac{3 \cdot E \cdot I}{L^3} \qquad [L]$$

In the next tables, all the measured dates and the final coefficient *K* used in each concentrated support are summarized. The same spring is considered for all the supports located at the edged generators. However, different springs are considered in each point of the connection between the shell and the wall at the directrix. This connection was based on six points, which were listed from left to right in figure 86. Each of these points has different number of stiffer beams and pillar and therefore, the final spring stiffness is supposed as the sum of all those elements.

	Direction of the spring	H (m)	A (m)	B (m)
Generators	X	1.8	0.5	0.1
Generators	Z	1.8	0.1	0.5

Table 1: *Characteristics measured in figure 87 in order to obtain the stiffness of the spring in the generators.* The spring generators consisted only of one pillar. All the characteristics are presented in metres.

	Direction of the spring	H (m)	A (m)	B (m)
Directrix support 1	X	1.5	0.3	0.3
Directrix support 1	Z	1.5	0.3	0.3

Table 2: *Characteristics measured in figure 86 in order to obtain the stiffness of the spring in the first support between the directrix and the wall.* The spring in this point consisted of one pillar.

	Direction of the spring	H (m)	A (m)	B (m)
Directrix support 2	X	2.0	0.3	0.3
Directrix support 2	X	2.0	0.6	0.3
Directrix support 2	Z	2.0	0.3	0.3
Directrix support 2	Z	2.0	0.3	0.6

Table 3: *Characteristics measured in figure 86 in order to obtain the stiffness of the spring in the second support between the directrix and the wall.* The spring in this point consisted of one pillar and one beam.

	Direction of the spring	H (m)	A (m)	B (m)
Directrix support 3	X	3.0	0.6	0.3
Directrix support 3	X	2.0	0.3	0.3
Directrix support 3	Z	3.0	0.3	0.6
Directrix support 3	Z	2.0	0.3	0.3

Table 4: *Characteristics measured in figure 86 in order to obtain the stiffness of the spring in the third support between the directrix and the wall.* The spring in this point consisted of one pillar and one beam.

	Direction of the spring	H (m)	A (m)	B (m)
Directrix support 4	X	3.0	0.6	0.3
Directrix support 4	X	1.5	0.3	0.3
Directrix support 4	Z	3.0	0.3	0.6
Directrix support 4	Z	1.5	0.3	0.3

Table 5: *Characteristics measured in figure 86 in order to obtain the stiffness of the spring in the fourth support between the directrix and the wall.* The spring in this point consisted of one pillar and one beam.

	Direction of the spring	H (m)	A (m)	B (m)
Directrix support 5	X	3.0	0.9	0.3
Directrix support 5	X	1.5	0.3	0.3
Directrix support 5	X	3.0	0.3	0.3
Directrix support 5	Z	3.0	0.3	0.9
Directrix support 5	Z	1.5	0.3	0.3
Directrix support 5	Z	3.0	0.3	0.3

Table 6: *Characteristics measured in figure 86 in order to obtain the stiffness of the spring in the fifth support between the directrix and the wall.* The spring in this point consisted of one pillar and two beams.

	Direction of the spring	H (m)	A (m)	B (m)
Directrix support 6	X	3.0	0.3	0.3
Directrix support 6	X	1.5	0.6	0.3
Directrix support 6	Z	3.0	0.3	0.3
Directrix support 6	Z	1.5	0.3	0.6

Table 7: *Characteristics measured in figure 86 in order to obtain the stiffness of the spring in the sixth support between the directrix and the wall.* The spring in this point consisted of one pillar and one beam.

In next table are listed the values of the different K_i coefficient in the spring X and Z expressed in MN/m.

	Kx (MN/m)	Kz (N/m)
Generator	8.0	0.3
Directrix Support 1	9.0	9.0
Directrix Support 2	34.2	11.4
Directrix Support 3	12.8	6.0
Directrix Support 4	18.0	11.5
Directrix Support 5	40.5	13.5
Directrix Support 6	18.0	11.3

A.6 Load Combination Study.

In this section are showed the maximum tension stress and compression stress isobar diagrams calculated by Lusas considering four different load cases:

- Load case 1: Dead weight
- Load case 2: Dead weight with wind, without suction, load.
- Load case 3: Dead weight with snow load.
- Load case 4: Dead load with snow and wind, without suction, loads.

All these diagrams are coloured in red for tension stress and in blue for compression stress where the maximum isobars obtained by Torroja were exceeded.

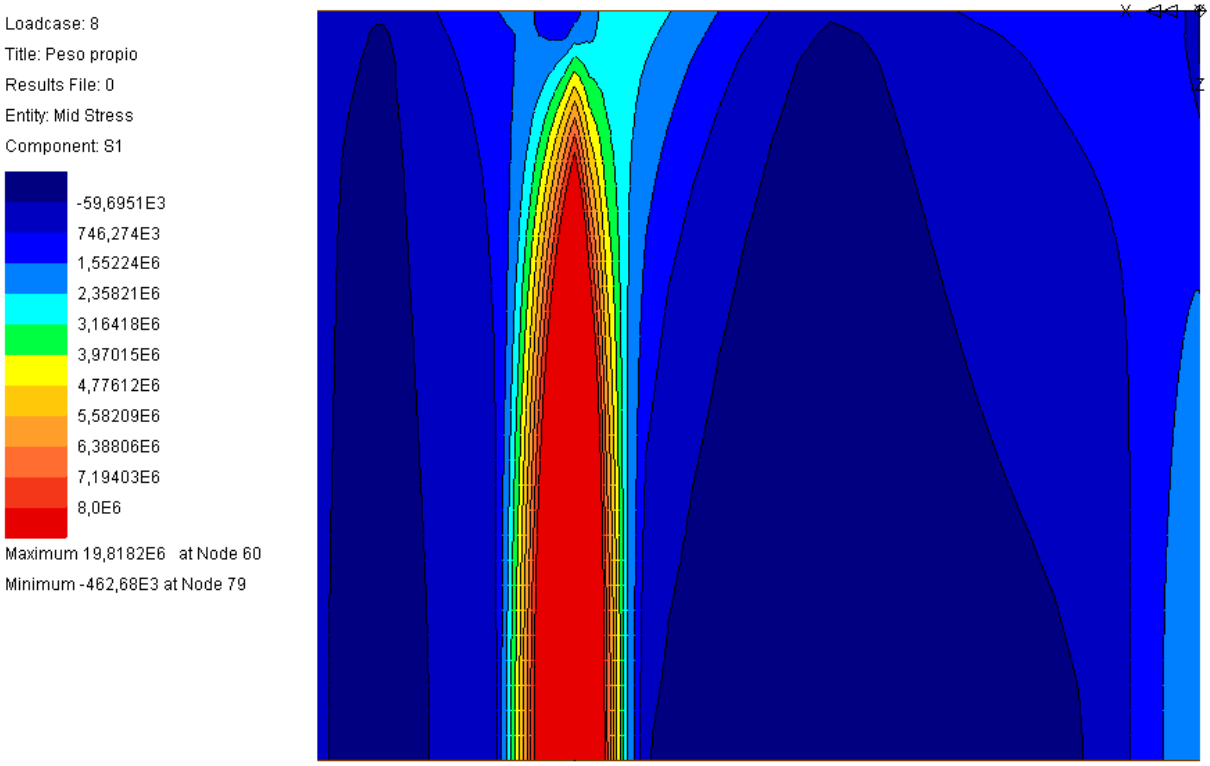

Figure F: *Maximum tension stress isobars considering the load case one*. The maximum value is 19.8 MPa that means 1.5 times the maximum value measured by Torroja.

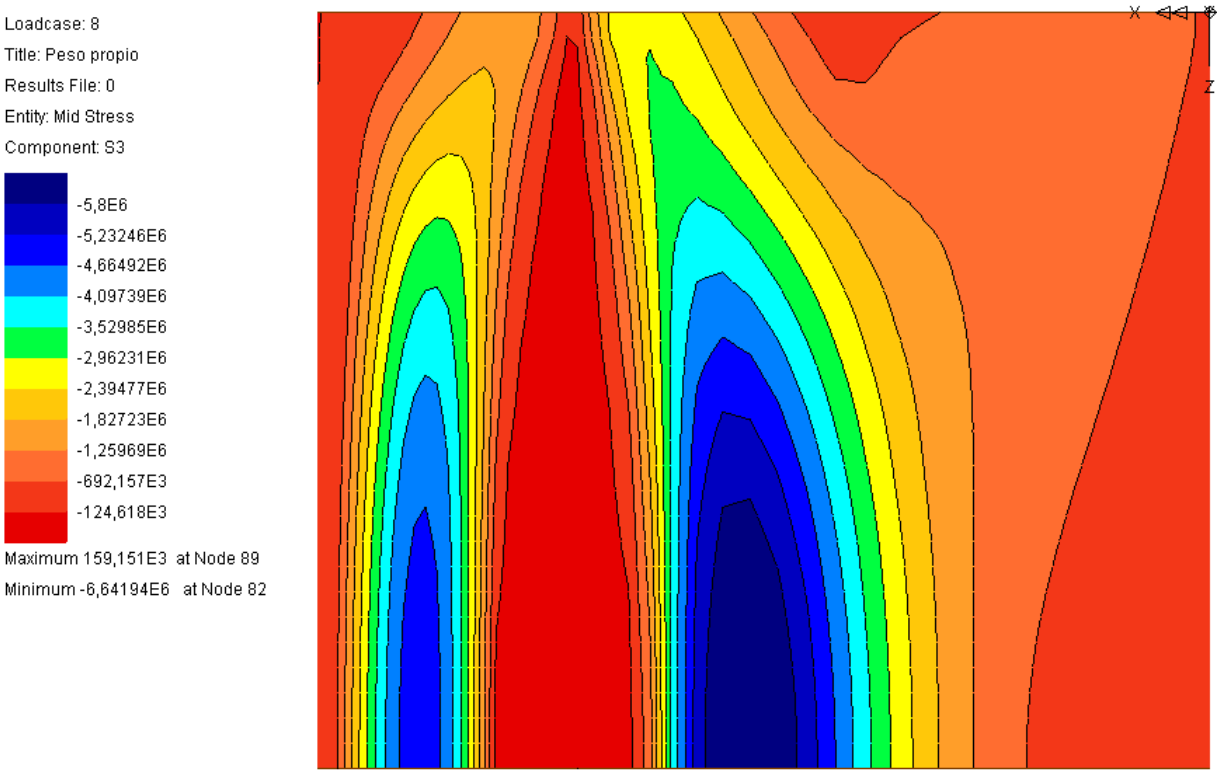

Figure G: *Maximum compression stress isobars considering the load case one*. The maximum value is -6.64 MPa that means 15 % higher than the values measured by Torroja.

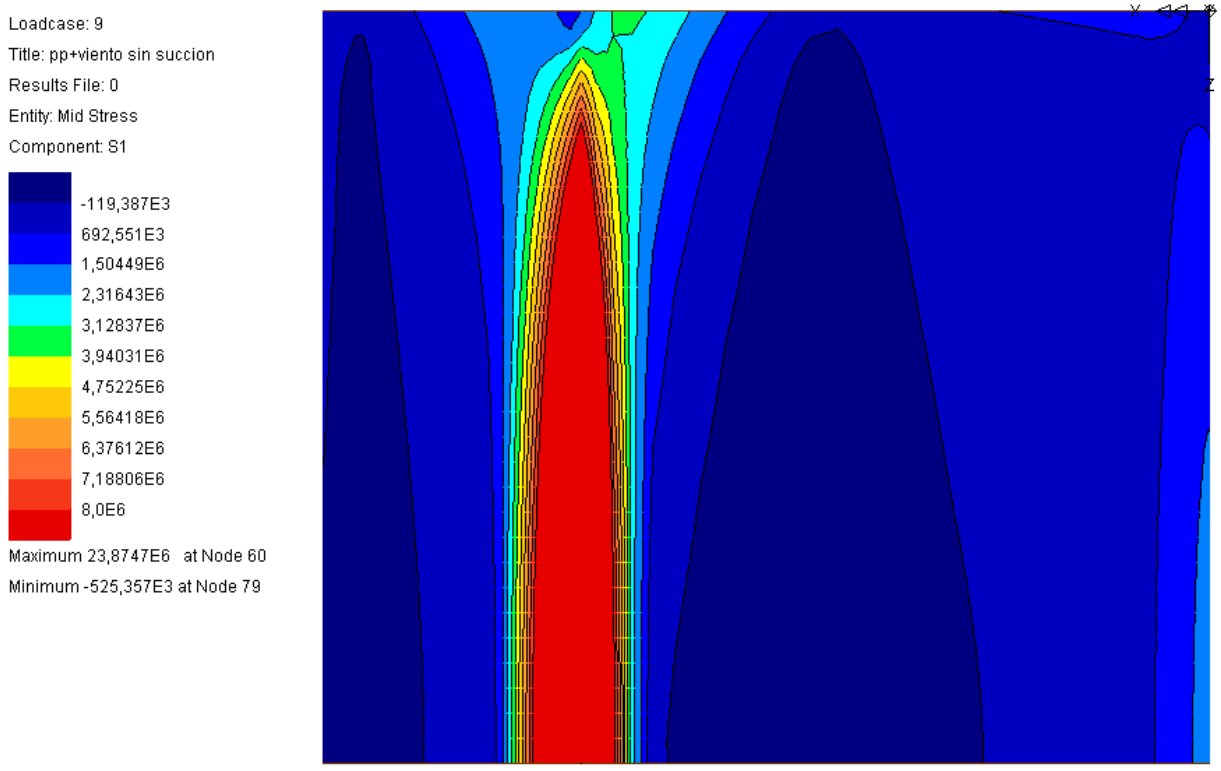

Figure H: *Maximum tension stress isobars considering the load case two*. The maximum value is 23.87 MPa that means around 2 times the values measured by Torroja.

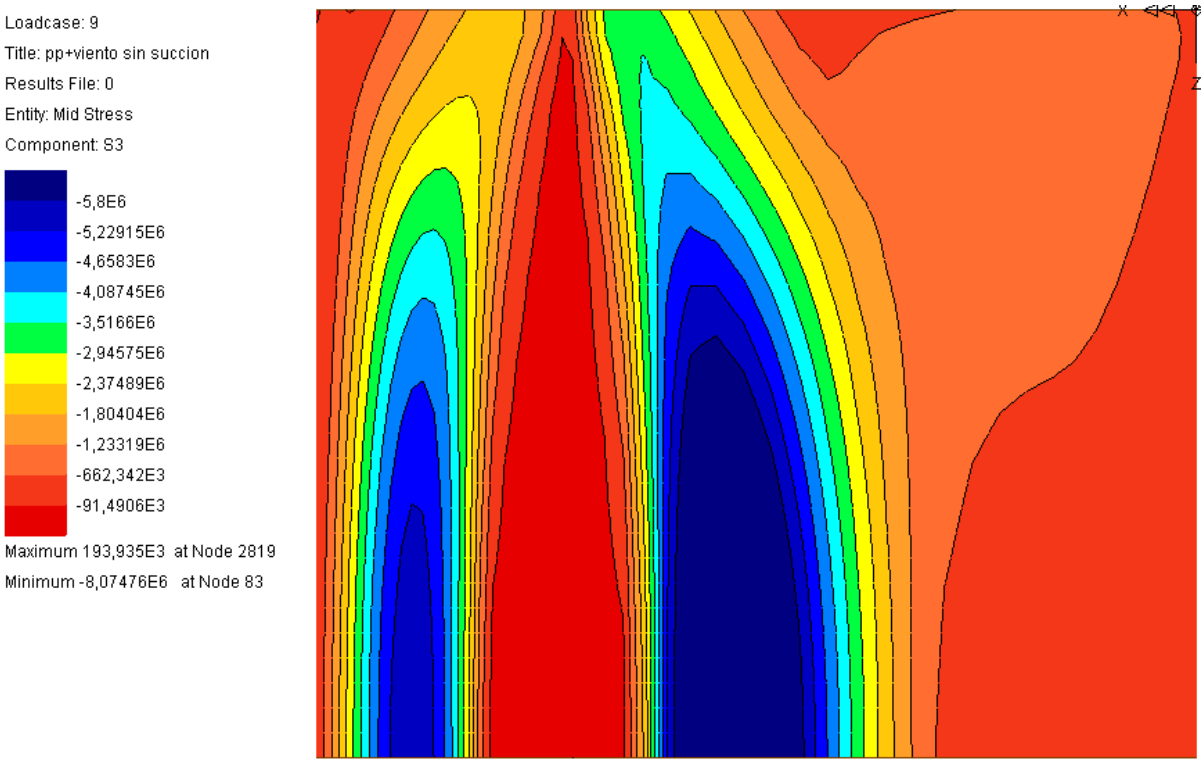

Figure I: *Maximum compression stress isobars considering the load case two*. The maximum value is -8.1 MPa that means 40 % higher than the values measured by Torroja.

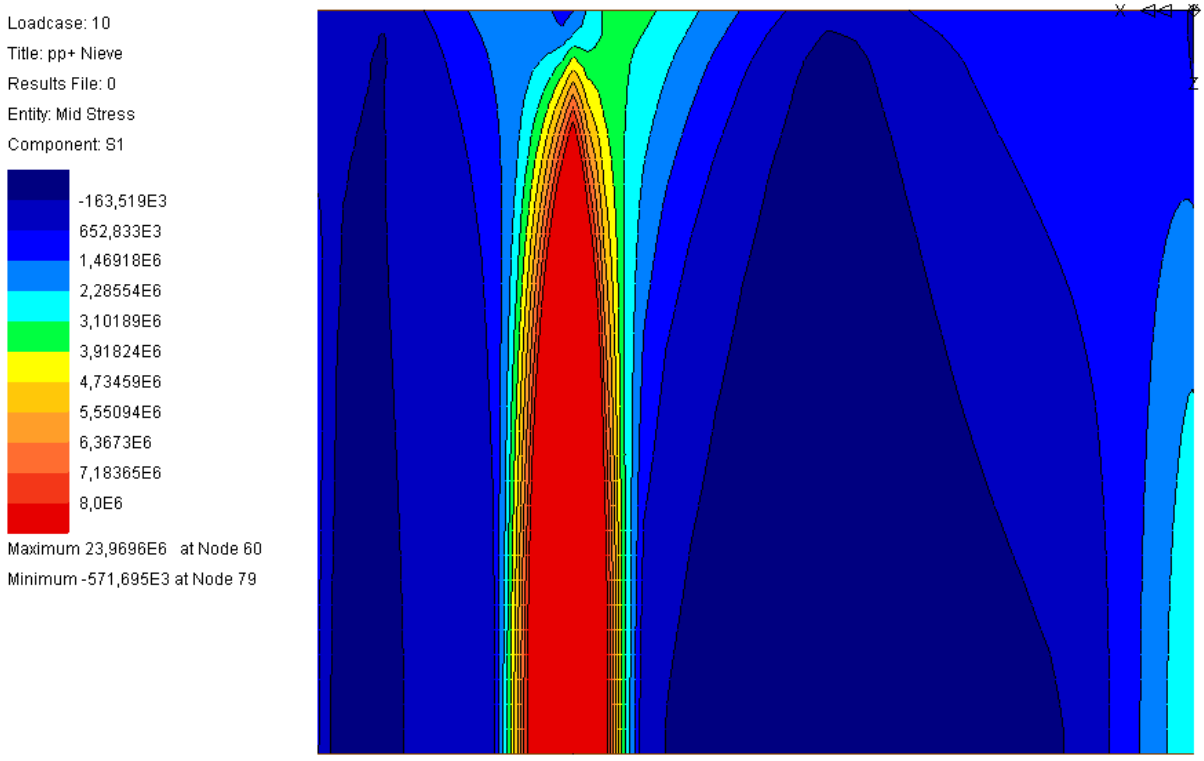

Figure J: *Maximum tension stress isobars considering the load case three.* The maximum value is 23.97 MPa that means around 2 times the values measured by Torroja.

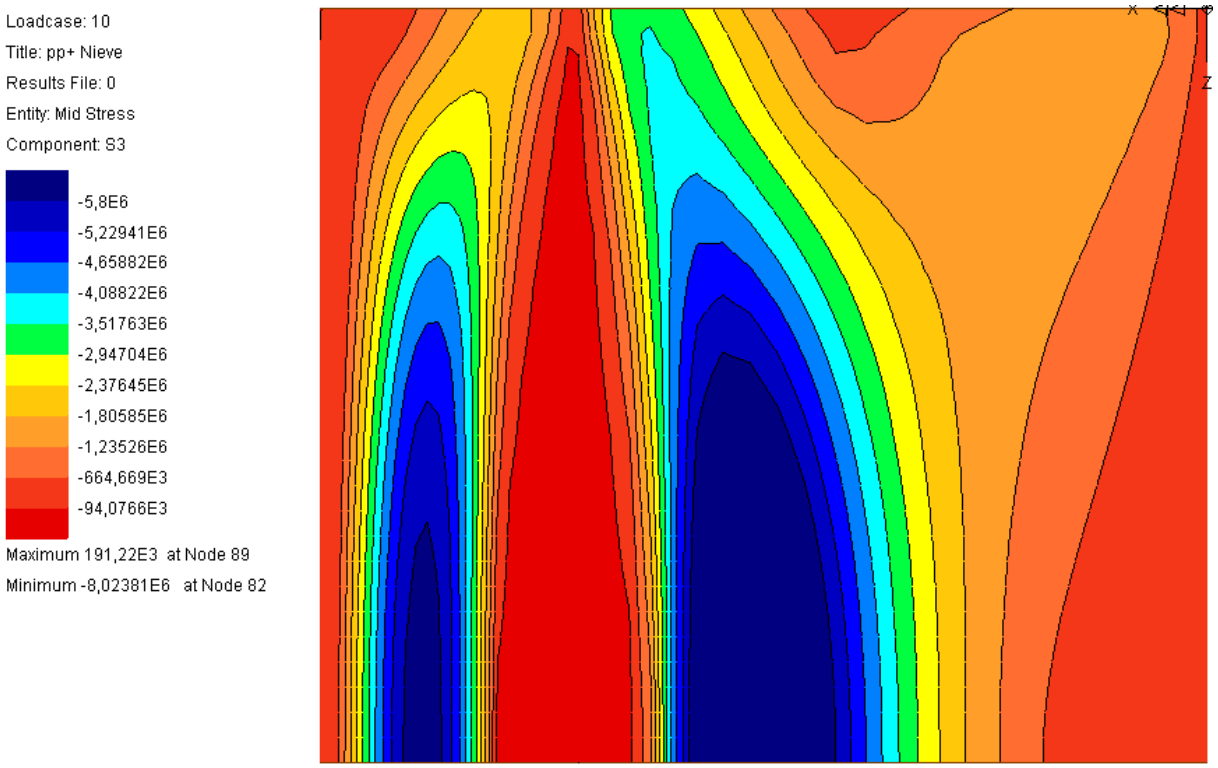

Figure K: *Maximum tension stress isobars considering the three*. The maximum value is -8.02 MPa that means 38 % higher than the values measured by Torroja.

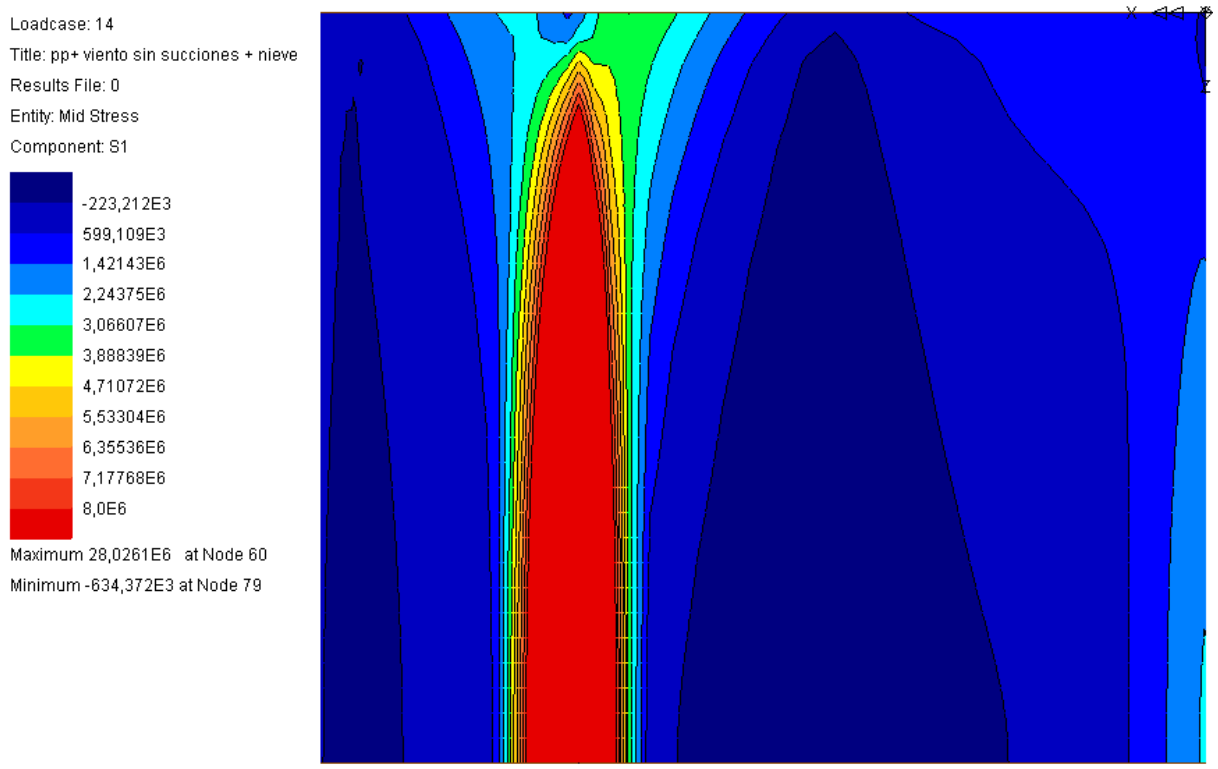

Figure L: *Maximum tension stress isobars considering the load case four*. The maximum value is 28.03 MPa that means 2.5 times the values measuered by Torroja.

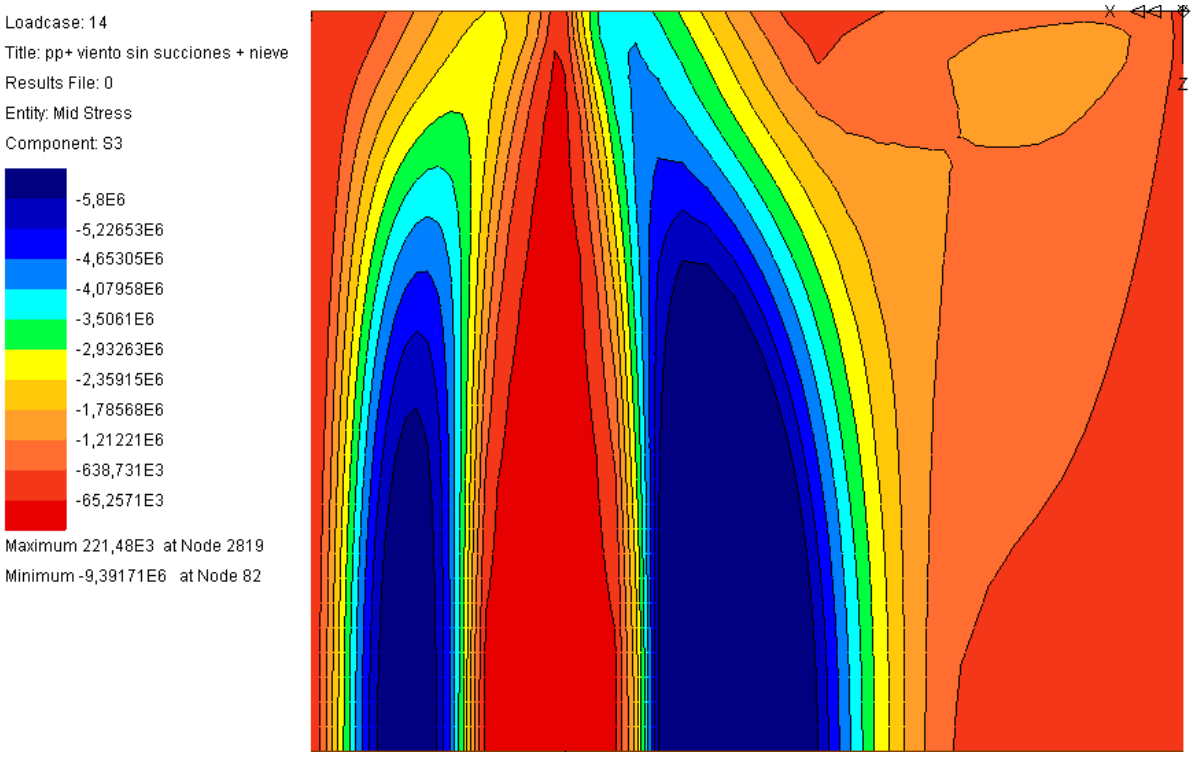

Figure M: *Maximum tension stress isobars considering the load case four*. The maximum value is -9.39 MPa that means 62 % higher than the values measured by Torroja.

A.7 Bending moments

All the bending moment diagrams consist on half-undeveloped section of the plan. In horizontal the directrix is located: On the left is located the biggest lobe and on the right is located the smallest cylindrical sector.

In order to compare easily the values measured by Torroja: the points of the transversal bending moment diagrams calculated by Lusas where the maximum values obtained by Torroja[56] were exceeded are coloured in blue and red.

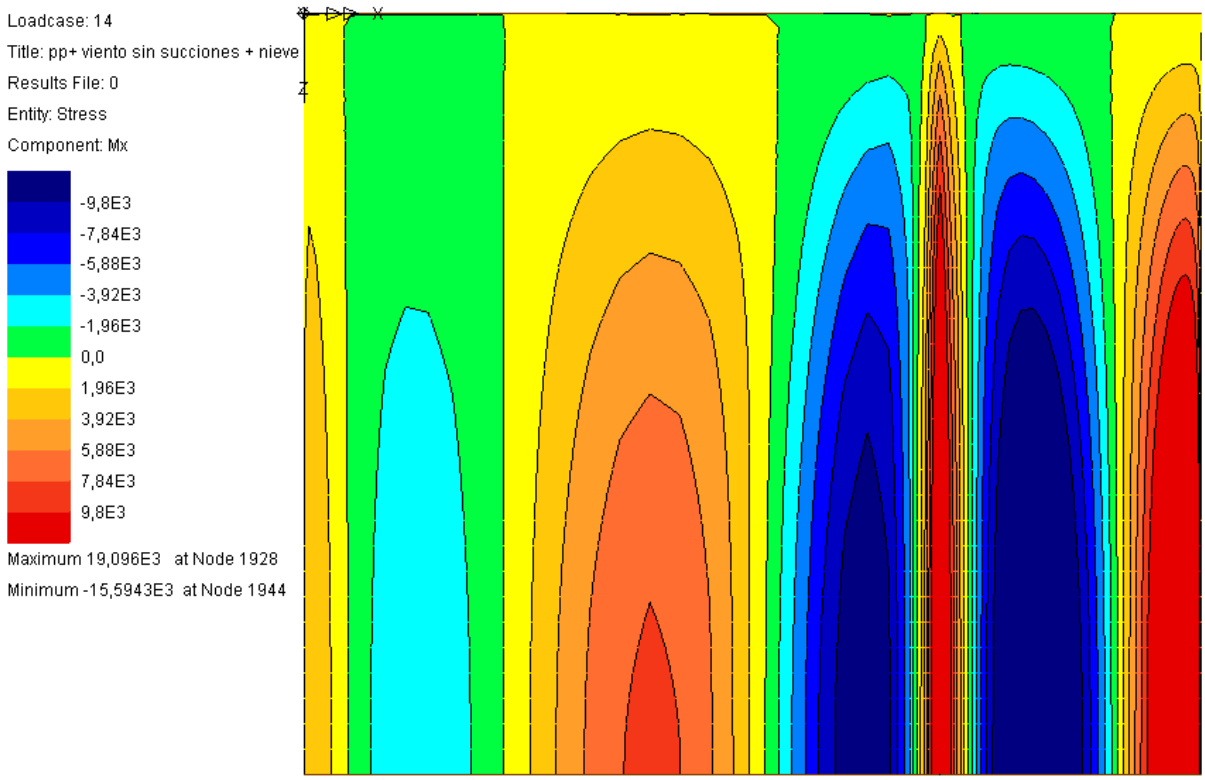

Figure N: *Transversal bending moments calculated by the first Lusas model*. The maximum value[57], 1948 kg·m/m, is located at the smallest cylindrical sector as well as the minimum value at the connection between both lobes and in the smallest cylinder.

[56] Around 1000 kg·m/m introduced in the programme as 9.8 kN·m/m.

[57] The maximum value was 19.09 kN·m/m, which corresponds with 1948 kN·m/m after changing the force units.

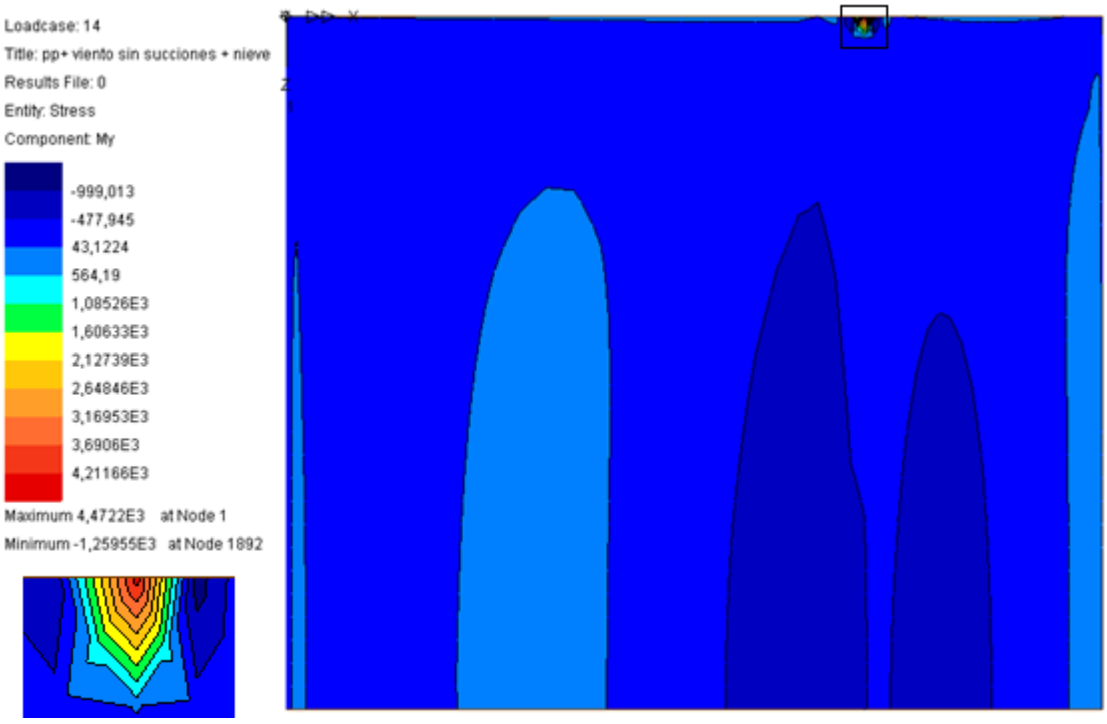

Figure P: *Longitudinal bending moments calculated by the first Lusas model*. The maximum values, around 456 kg·m/m, are located at the connection between the seagull and the wall. However, compared with the values measured in the transversal bending moments, around 4 times higher, these stresses can be neglected.

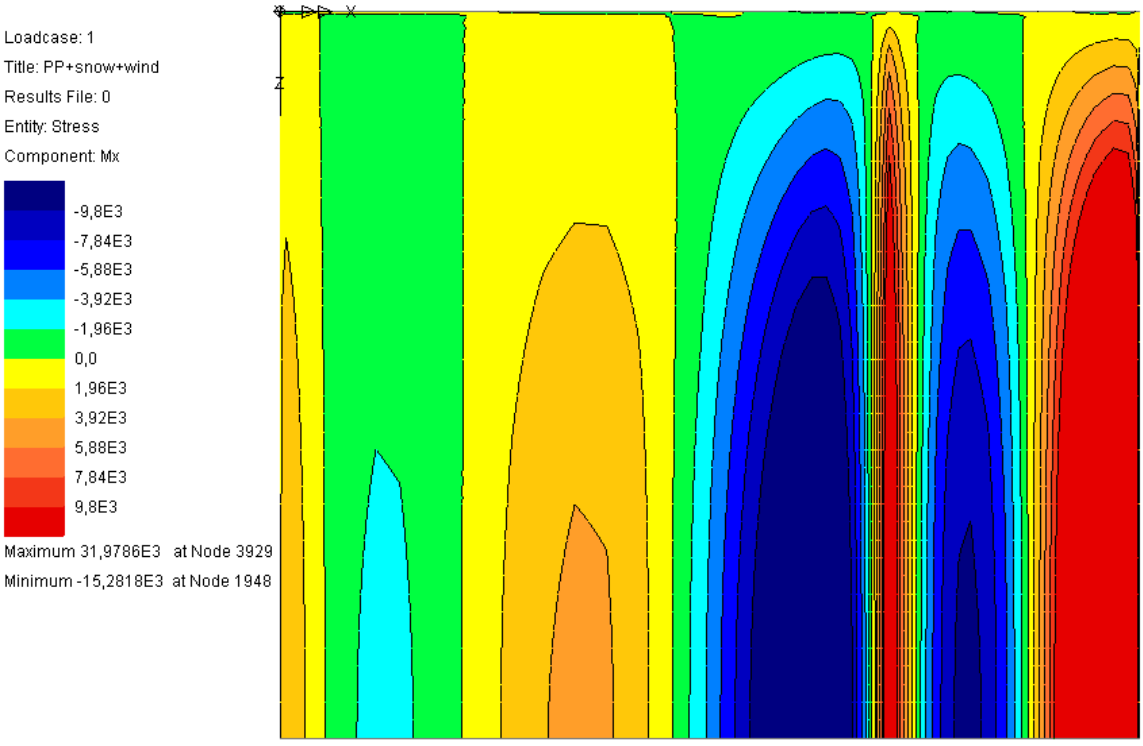

Figure Q: *Transversal bending moments calculated by the second Lusas model*. The maximum value measured in the diagram, around 3259 kg·m/m, is more than three times the maximum value obtained by Torroja.

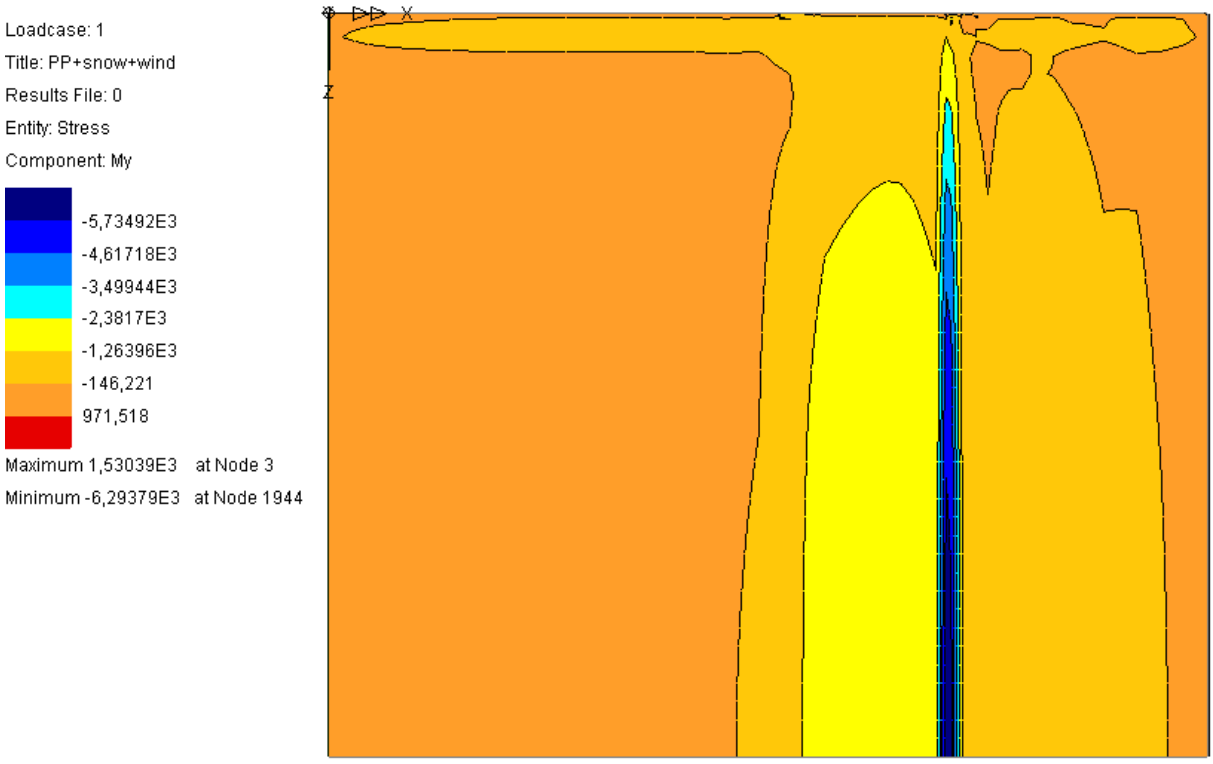

Figure R: *Longitudinal bending moments calculated by the second Lusas model*. The maximum value, around 636 kg·m/m is located at the connection between both cylindrical sectors. However, this value compared with the maximum values of the transversal bending moments, around 5 times higher, can be neglected.

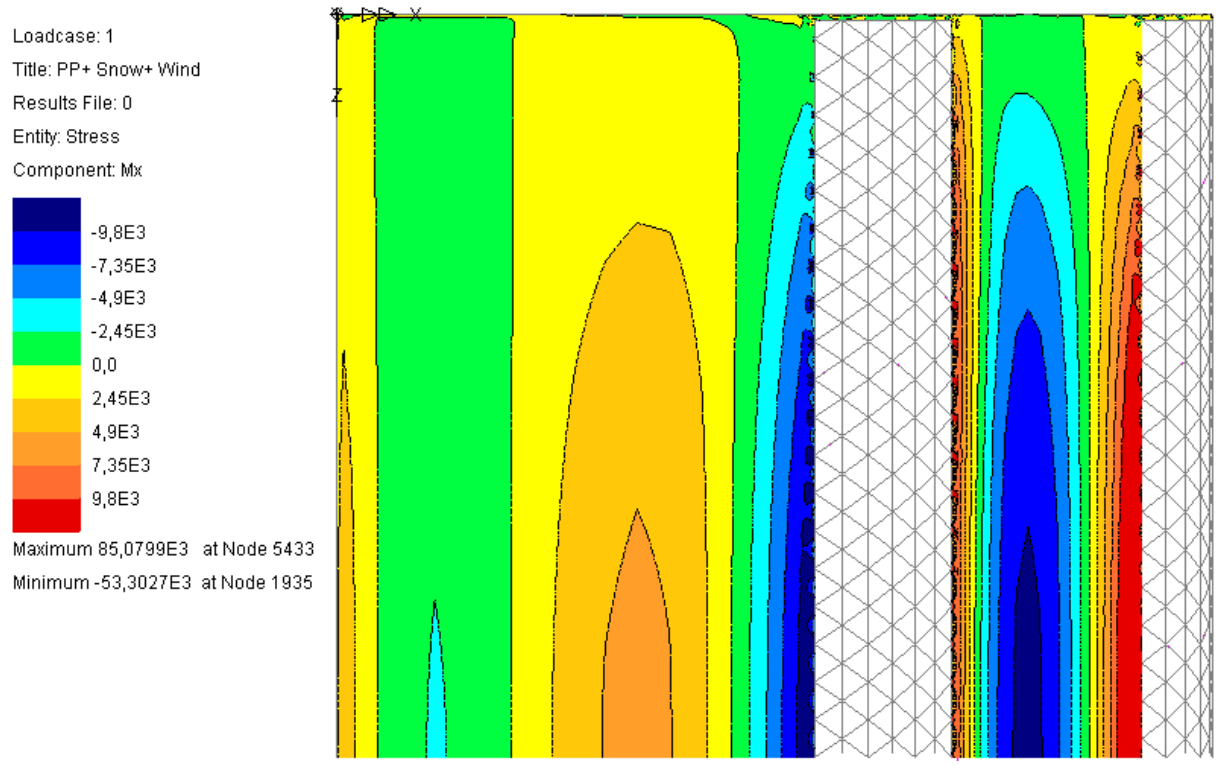

Figure S: *Transversal bending moments calculated by the fourth Lusas model*. The maximum value, around 850 kg·m/m is located at the connection between the skylights and the shells.

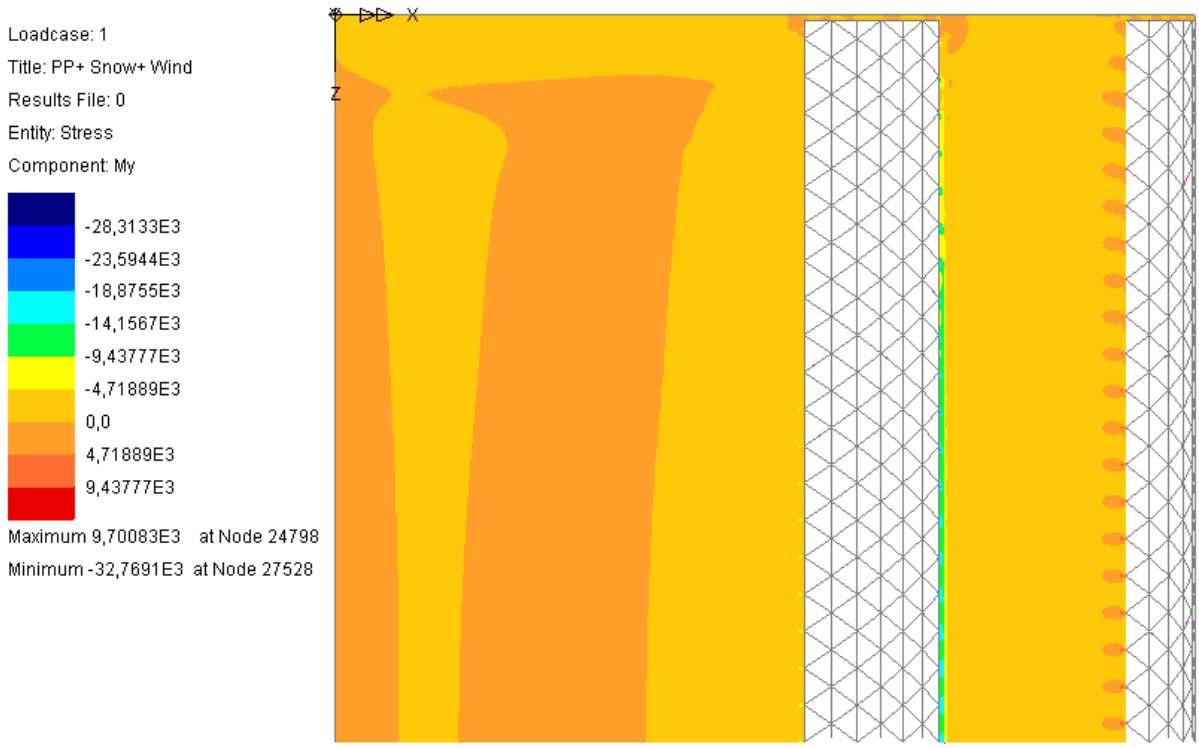

Figure T: *Longitudinal bending moments calculated by the fourth Lusas model*. The maximum value, around 330 kg·m/m is located at the connection between the skylights and the shell.

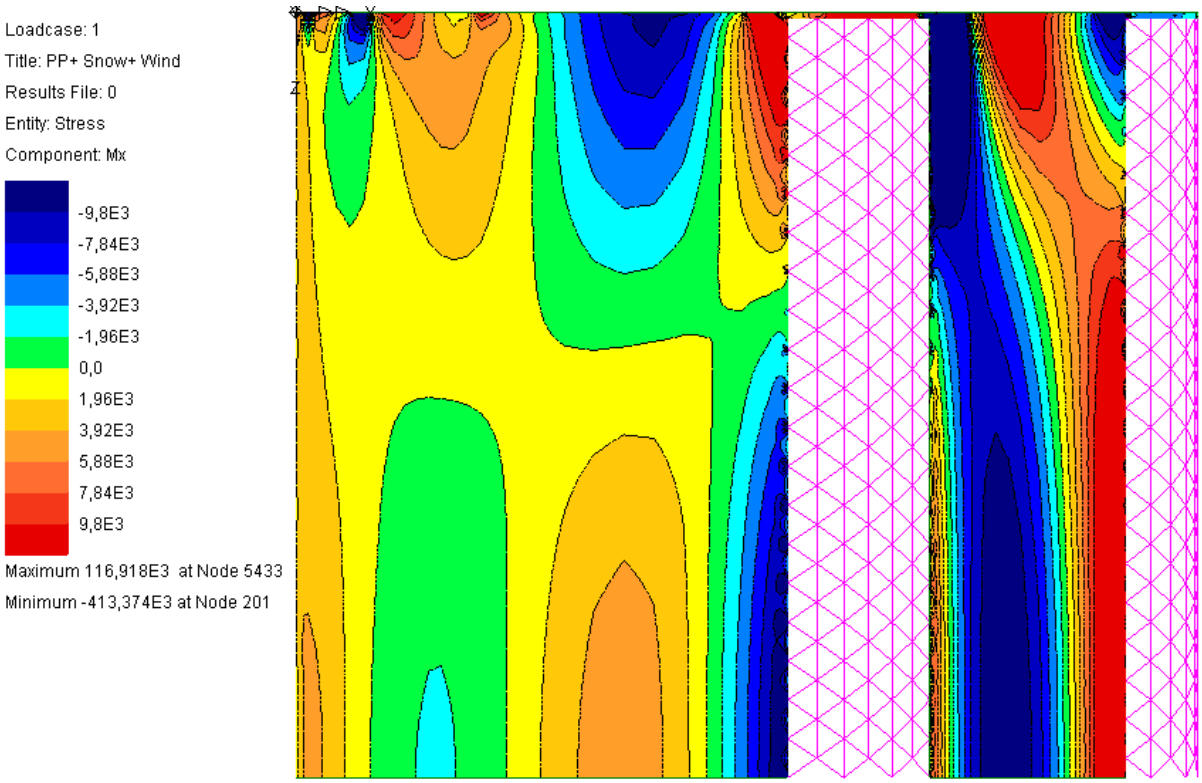

Figure U: *Transversal bending moments calculated by the second Lusas model*. The maximum value, around 1170 kg·m/m is located at the connection between the shell and the wall.

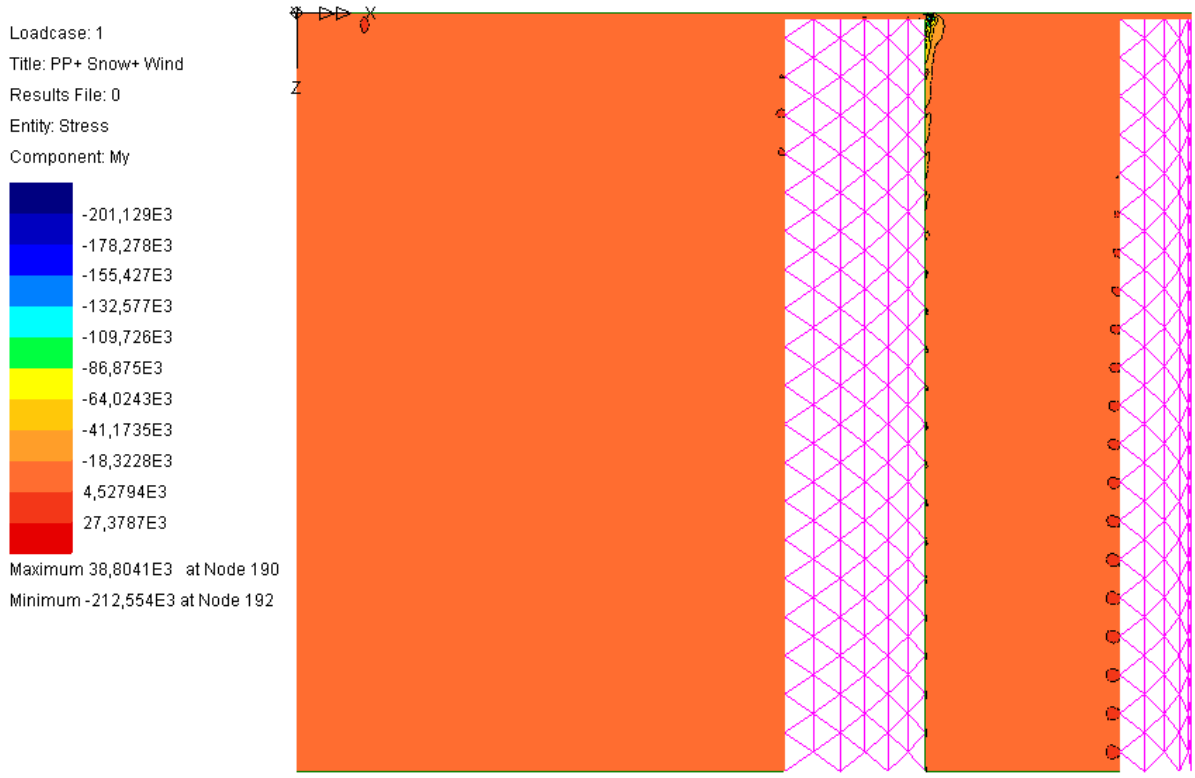

Figure V: *Longitudinal bending moments calculated by the second Lusas model*. The maximum value, around 2120 kg·m/m is located at the connection between directrix and the wall.

A.8 Study of the wind suction effects.

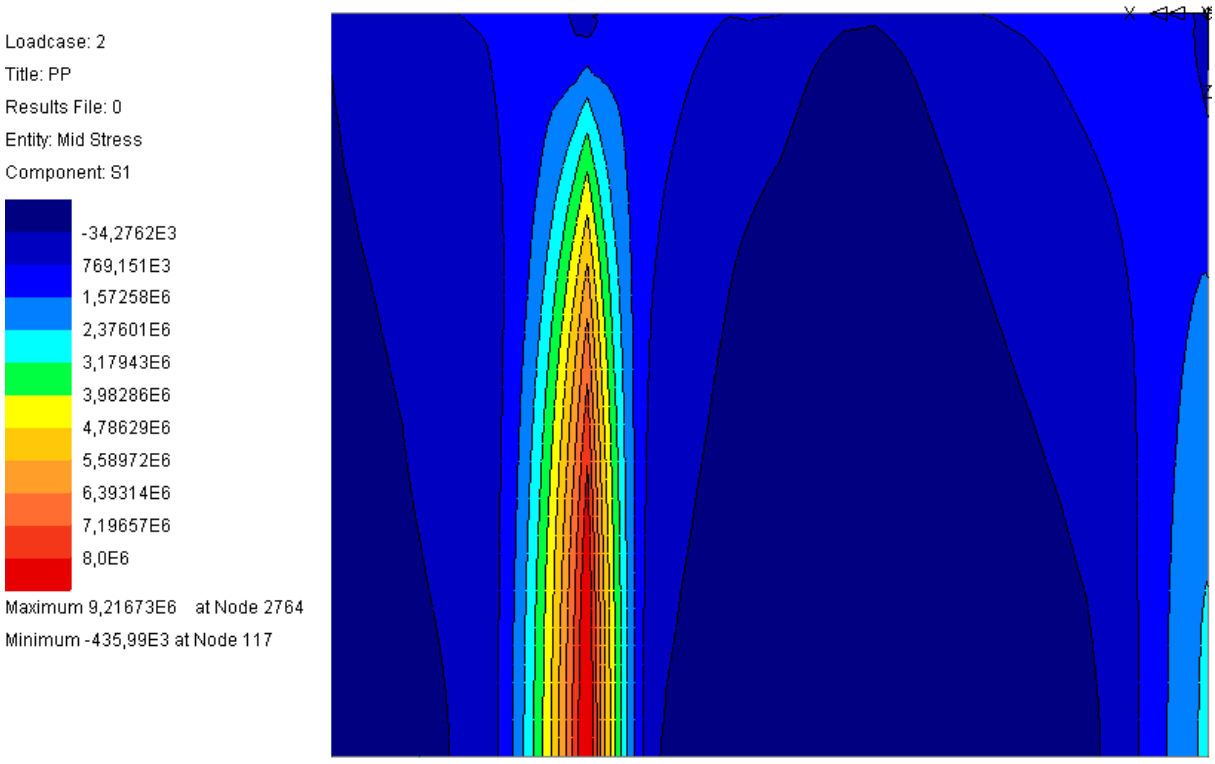

Figure W*: Maximum tension stress isobars calculated by the third Lusas model, considering the first load case: dead weight.*

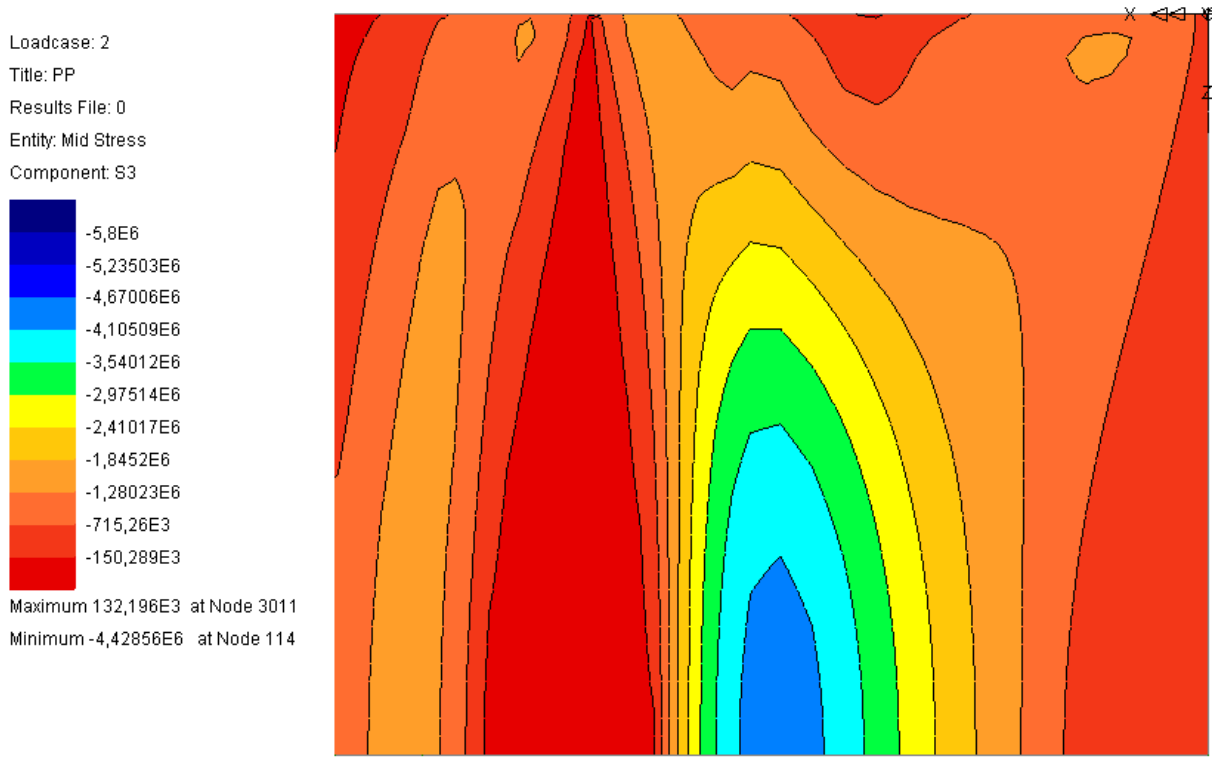

Figure X*: Maximum compression stress isobars calculated by the third Lusas model, considering the first load case: dead weight.*

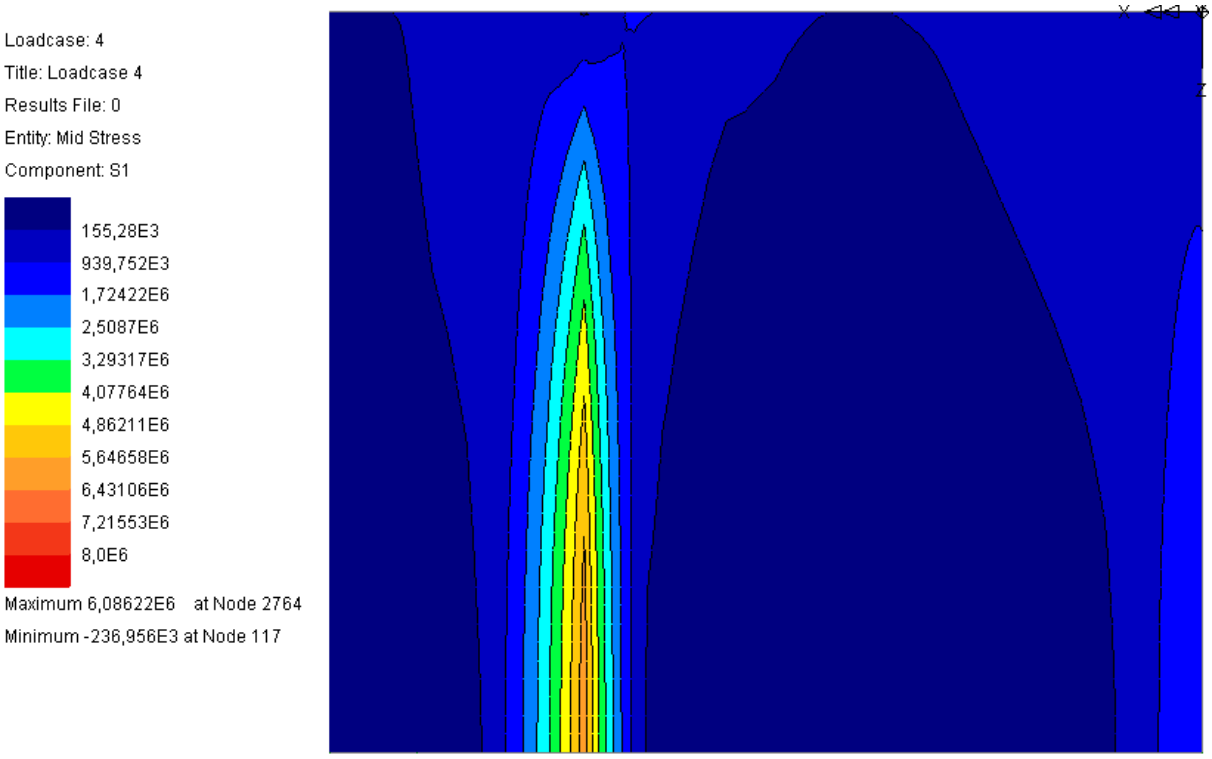

Figure Y*: Maximum tension stress isobars calculated by the third Lusas model, considering the second load case: dead weight and wind including suction effects.*

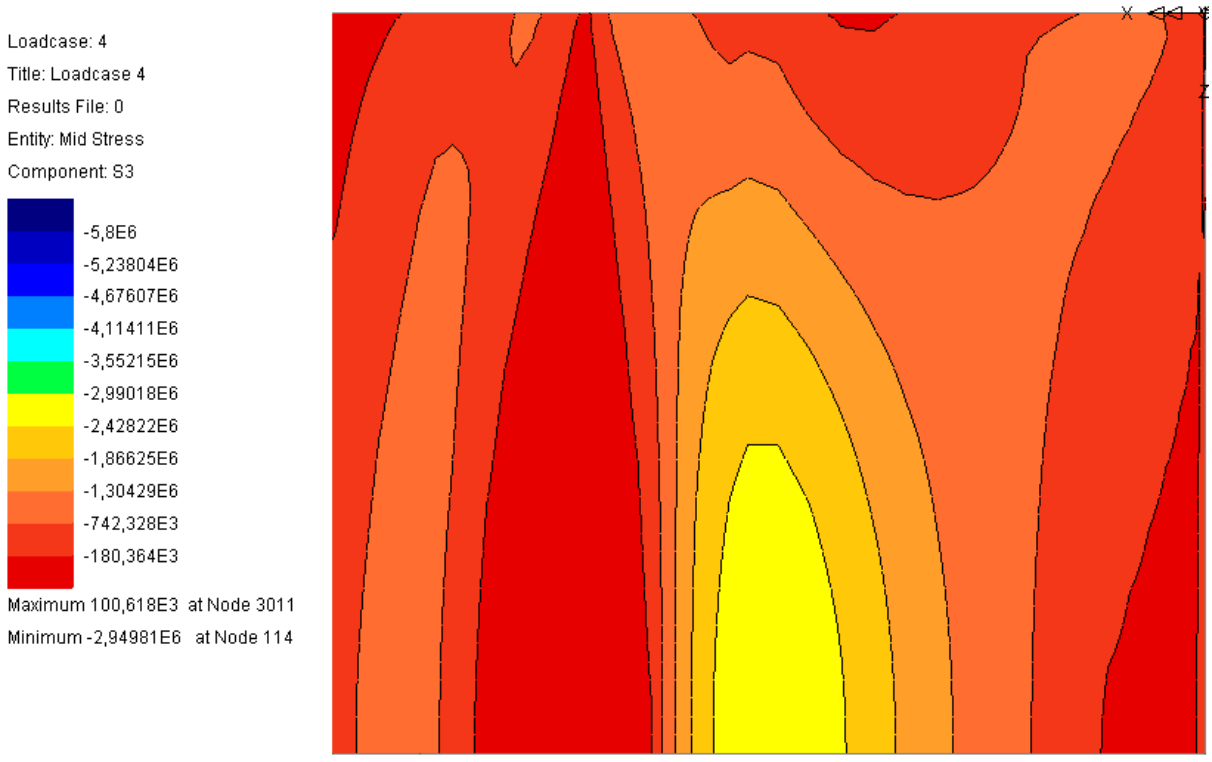

Figure Z*: Maximum compression stress isobars calculated by the third Lusas model, considering the second load case: dead weight and wind including suction effects.*

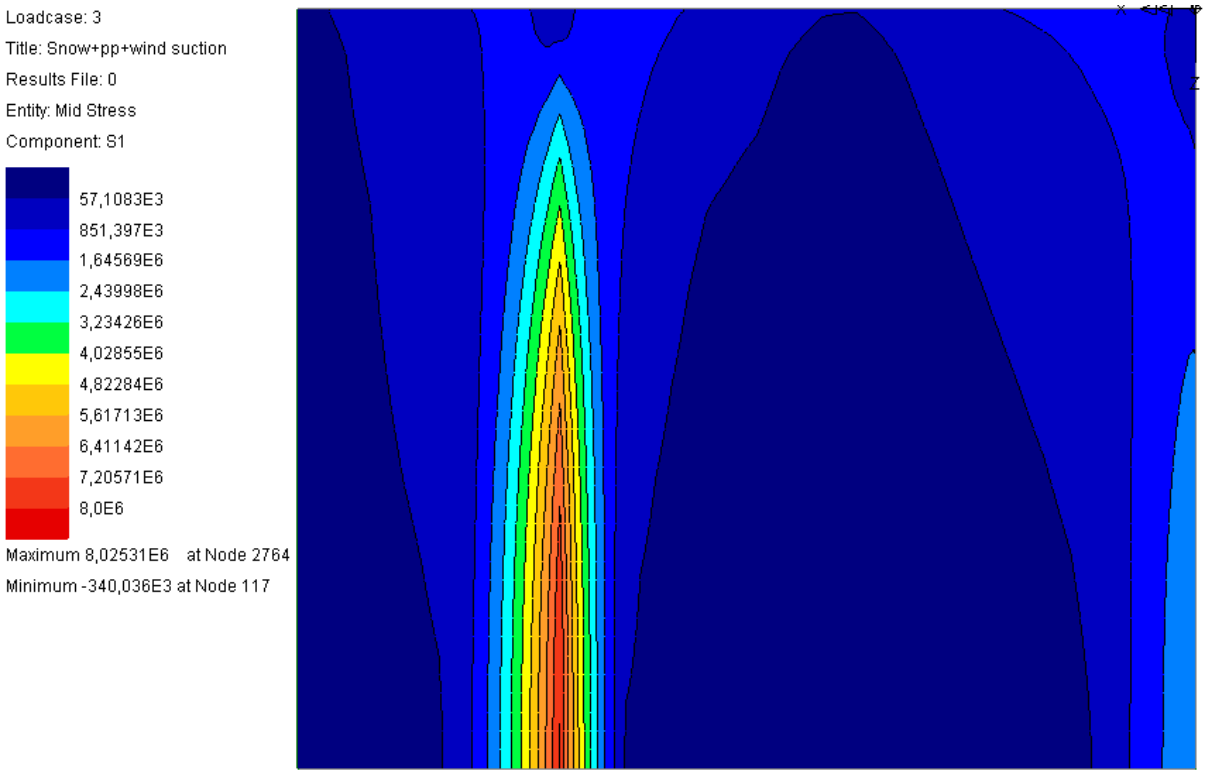

Figure A1*: Maximum tension stress isobars calculated by the third Lusas model, considering the fourth load case: dead weight, snow and wind including suction effects.*

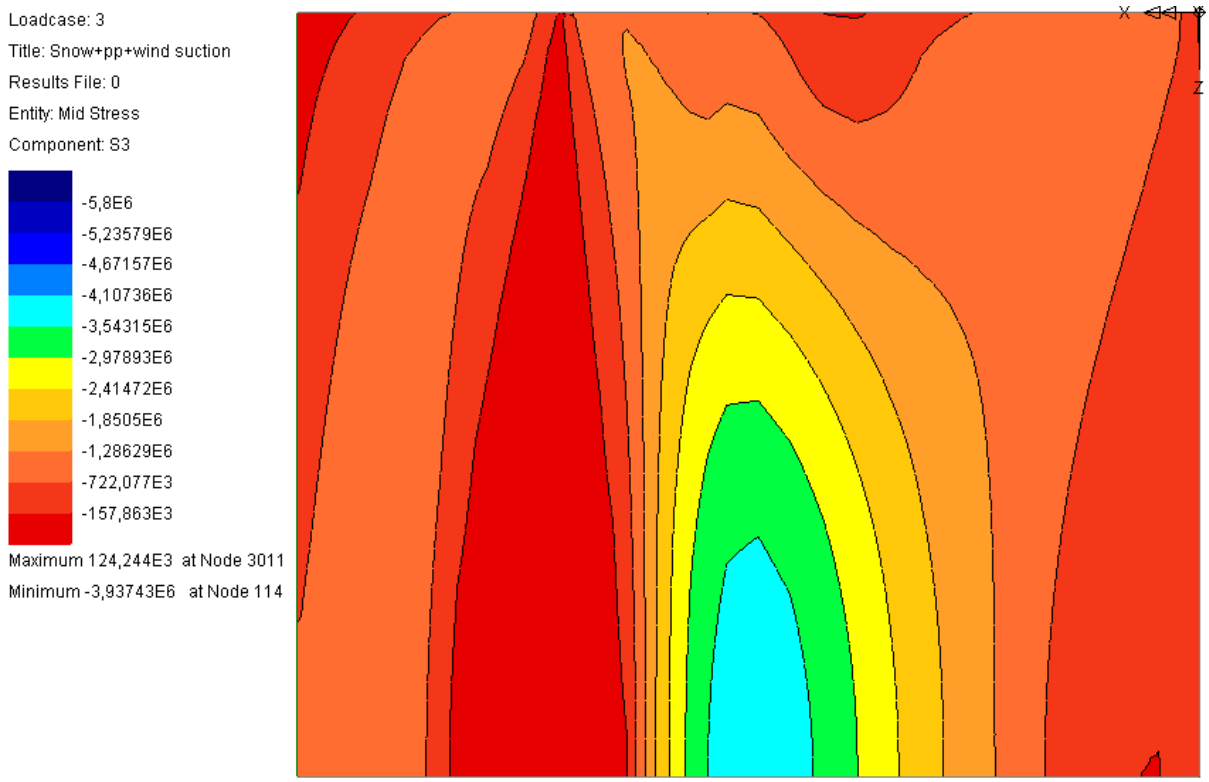

Figure B1*: Maximum compression stress isobars calculated by the third Lusas model, considering the fourth load case: dead weight, snow and wind including suction effects.*

In this Appendix the bending moments considering different load cases are presented. After that, the comparison of the compression and tension stress isobars are showed.

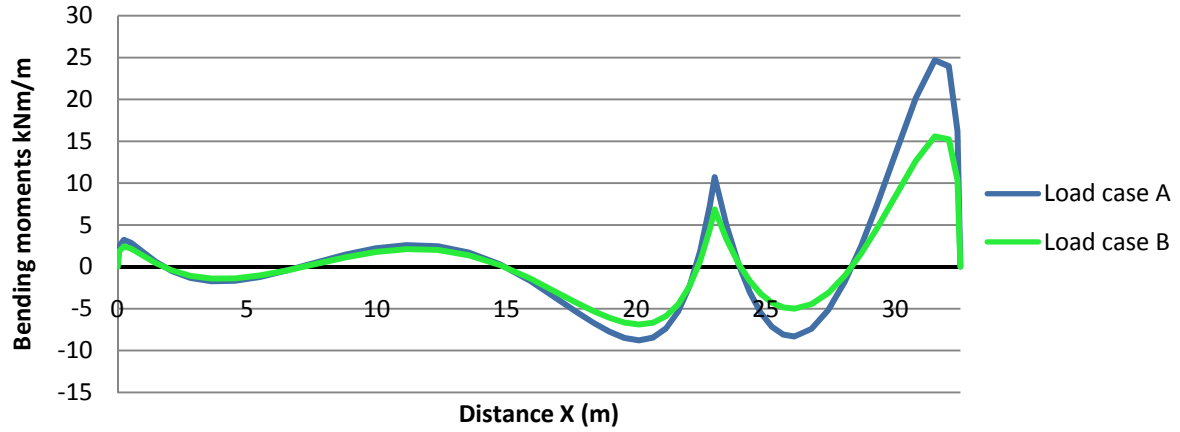

Figure C1: *Bending moments along the central undeveloped directrix considering the load case A, which is coloured in blue, and the load case B, which is coloured in green.*

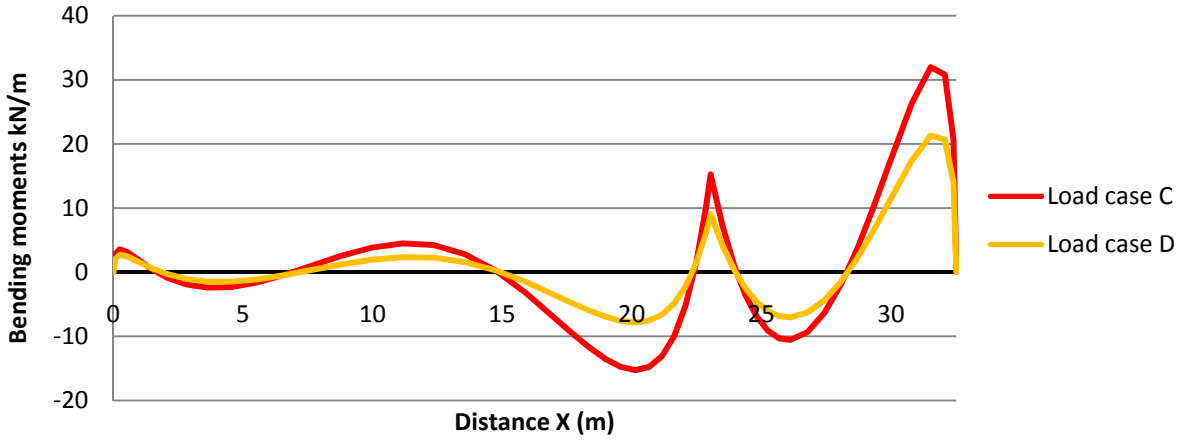

Figure D1: *Bending moments along the central undeveloped directrix considering the load case C, which is coloured in red, and the load case D, which is coloured in orange.*

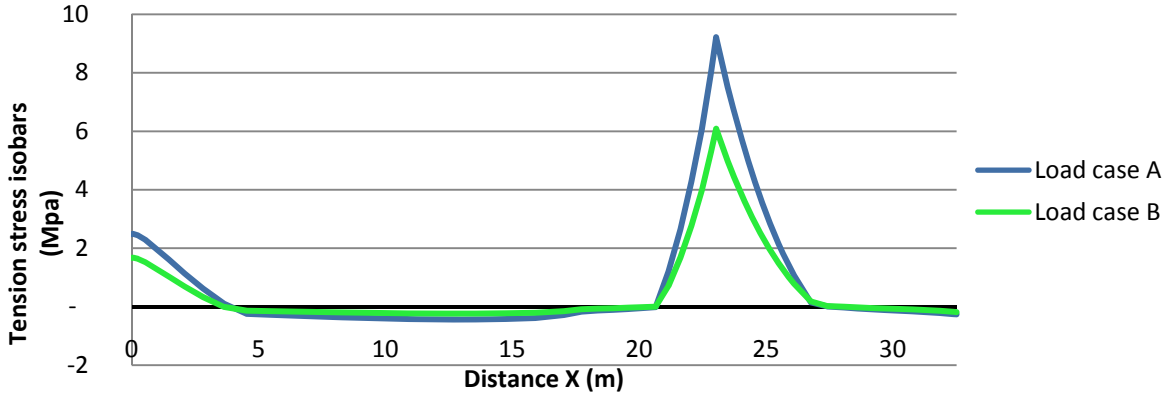

Figure E1: *Maximum values of the tension stress isobars along the central undeveloped directrix considering the load case A, which is coloured in blue, and the load case B, which is coloured in green.*

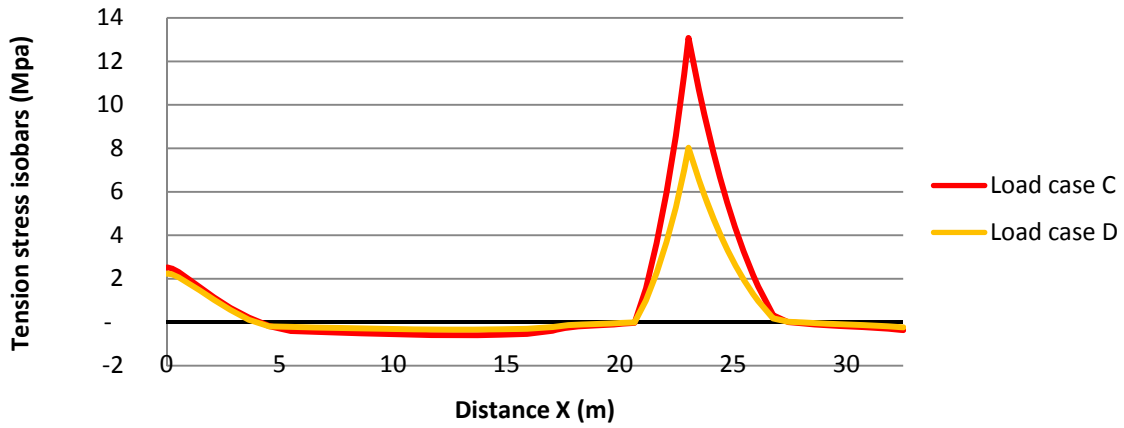

Figure E1: *Maximum values of the tension stress isobars along the central undeveloped directrix considering the load case C, which is coloured in red, and the load case D, which is coloured in orange.*

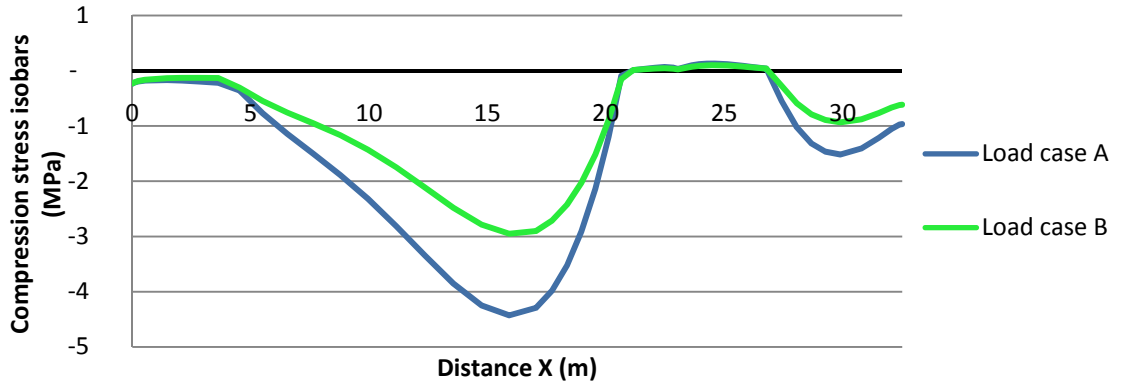

Figure F1: *Maximum values of the compression stress isobars along the central undeveloped directrix considering the load case A, which is coloured in blue, and the load case B, which is coloured in green.*

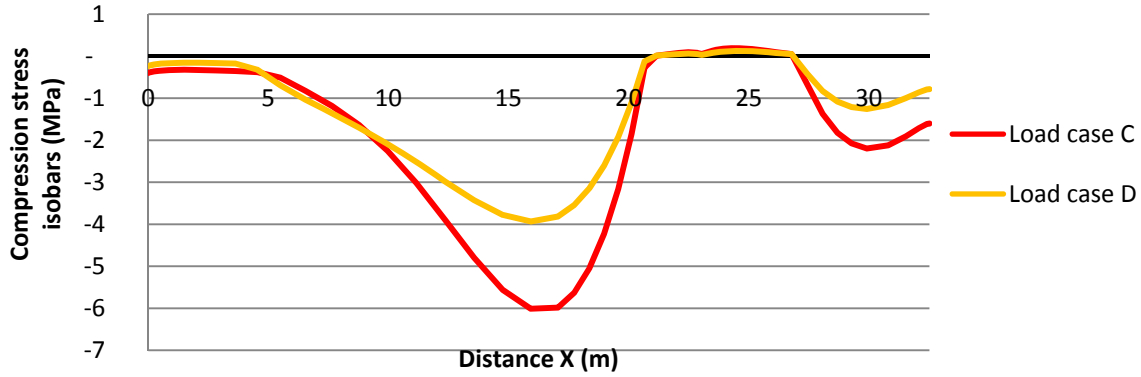

Figure G1: *Maximum values of the compression stress isobars along the central undeveloped directrix considering the load case C, which is coloured in red, and the load case D, which is coloured in orange.*

A.9 Study of variation of parameters.

In this Appendix the variations of different parameters, which could explain the differences observed between the vertical deflections measured by Torroja in the actual structure and the fifth Lusas model, are studied. These parameters are the following:

- Different stiffness of the concentrated supports located at the generators: In the fifth Lusas model, non-axial deflections were considered in determining the conditions of supports and therefore, vertical springs were not modelled. Furthermore, the pillars located at the generators were supposed fixed to the wall and the increase of elasticity produced by the buckling of the wall was not considered[58]. After the analysis of the figure H1, the obtained conclusion is that the variation of supports has practically no influence in the vertical distortions along the central undeveloped directrix.

Figure H1: *Vertical distortions along the central undeveloped directrix considering different supports conditions.* The basic fifth Lusas model is coloured in red, the model considering the axial deflections, called K_y, is coloured in blue and the model based on the reduction of the stiffness of the wall, is coloured in purple.

[58] The effect of buckling of the wall was supposed a 10 % reducing the stiffness of the springs that connect the pillars on the wall with the roof.

- Different loads conditions: The loads in the real structure could not be measured. Furthermore, the wind behaviour could not be studied in the wind tunnel test and therefore, the similarity between the theoretical and actual loads could not be verified. Different hypothesis of increase of loads are analyzed. After the analysis of figure Y, the conclusion is that increase of loads, especially of dead weight, can cause large variations in the vertical deflections along the central undeveloped directrix.

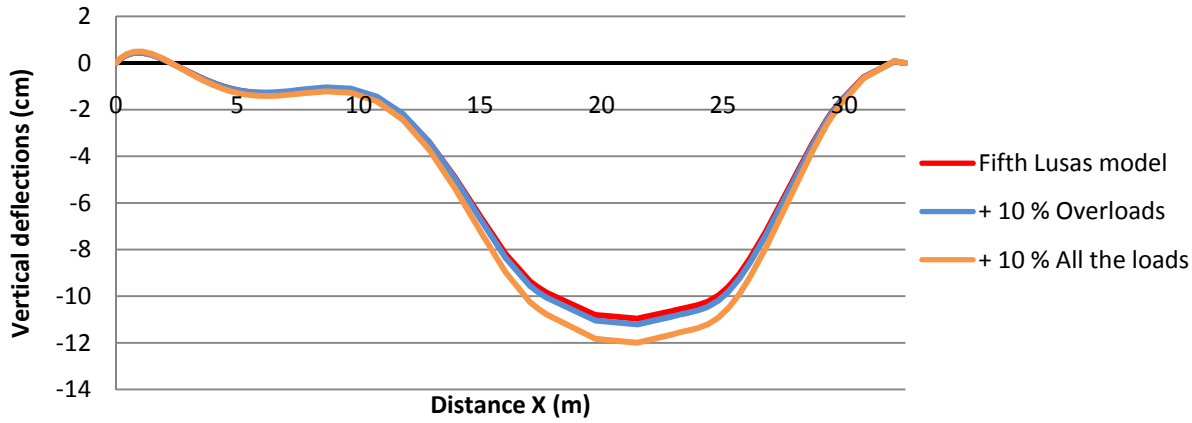

Figure I1: *Vertical distortions along the central undeveloped directrix considering different loads.* The basic fifth Lusas model is coloured in red, the model considering 10 % more of overloads is coloured in blue and the model considering 10 % more in all the loads, is coloured in orange.

- Different thickness along the shell: The real thickness of the constructed structure could be different to the thickness considered in the construction drawings. In figure J1, different reductions of thickness are considered and compared with the fifth Lusas model showing that reductions of one or two millimetres thickness practically have no influence on the vertical distortions along the central undeveloped directrix.

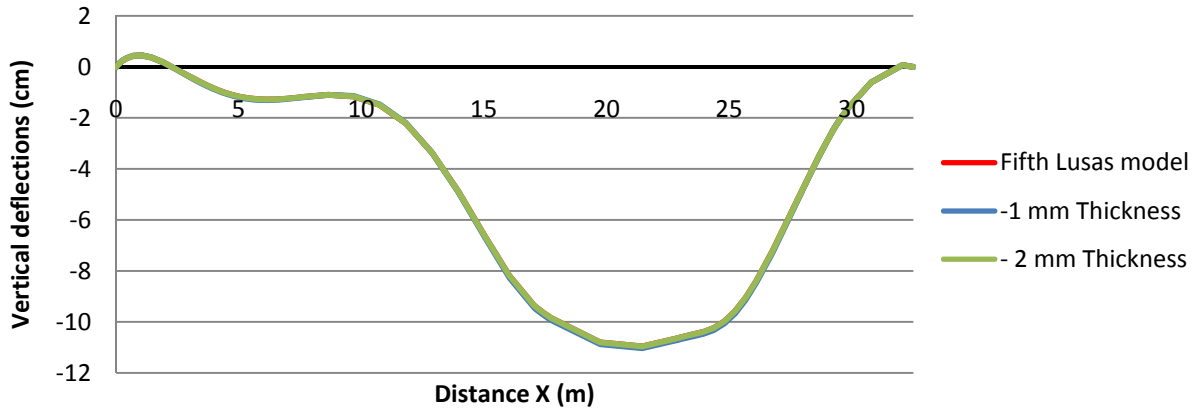

Figure J1: *Vertical distortions along the central undeveloped directrix considering different thickness.* The basic fifth Lusas model is coloured in red, the model considering one millimetre of thickness reduction is coloured in blue and the model considering two millimetres thickness reduction, is coloured in green.

- The variation of Elasticity Modulus: This element depends of the material characteristics. For example, Torroja considered in the small-scale model a coefficient between 250000 and 350000 kg/cm^2 (Torroja 1942, p.117). In figure K1, the variation of the Elasticity Modulus was considered obtaining as a conclusion that the variation of this factor produces highly variation of vertical deflections along the central undeveloped directrix.

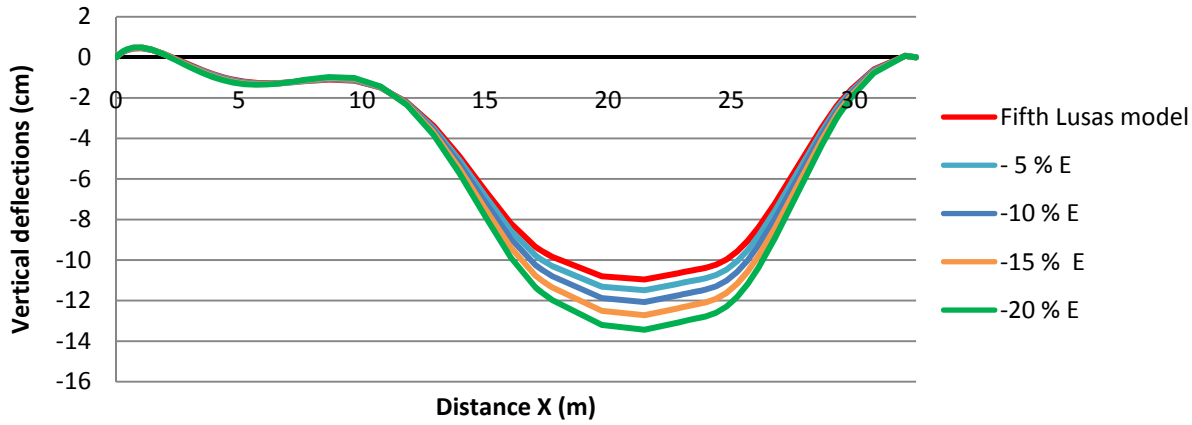

Figure K1: *Vertical distortions along the central undeveloped directrix considering different Elasticity Modulus.* The basic fifth Lusas model is coloured in red, the model considering 5 % of Elasticity Modulus reduction is coloured in light blue, the model considering 10 % of Elasticity Modulus reduction is coloured in dark blue, the model considering 15 % of Elasticity Modulus reduction is coloured in orange and the model considering 20 % of Elasticity Modulus reduction is coloured in green.

A.10 Study of ribs.

The behaviour of the shell is studied considering different ribs hypotheses: The first and the second models were based on the Fernández's Sketch (figure 100), and therefore only five reinforcement ribs are proposed. The difference between both models is that the second one included the ribs in both lobes. The third model is based on reinforcements at the biggest cylindrical sector each five metres (Antuña 2003, p.148).

In this appendix, the comparison of the three models is based on the diagrams of maximum tension stress and compression stress isobars.

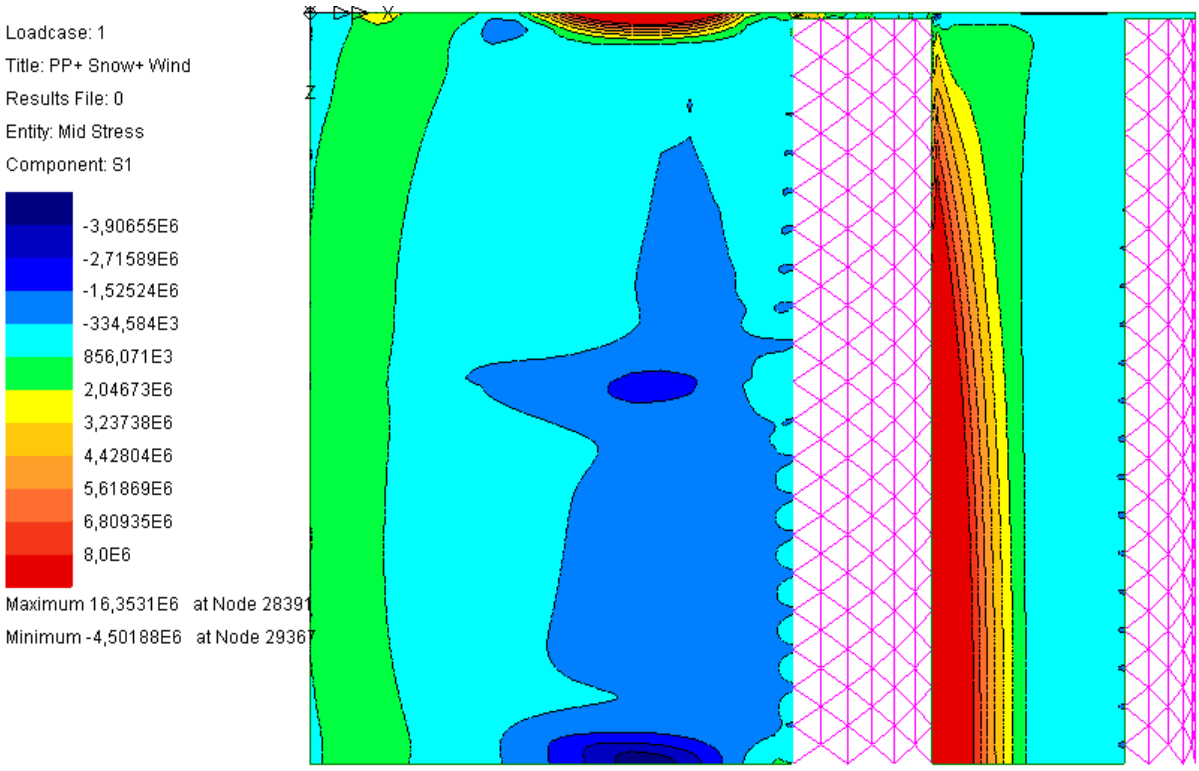

Figure L1*: Maximum tension stress isobars calculated by the sixth Lusas model, considering five ribs in the biggest cylindrical lobe.*

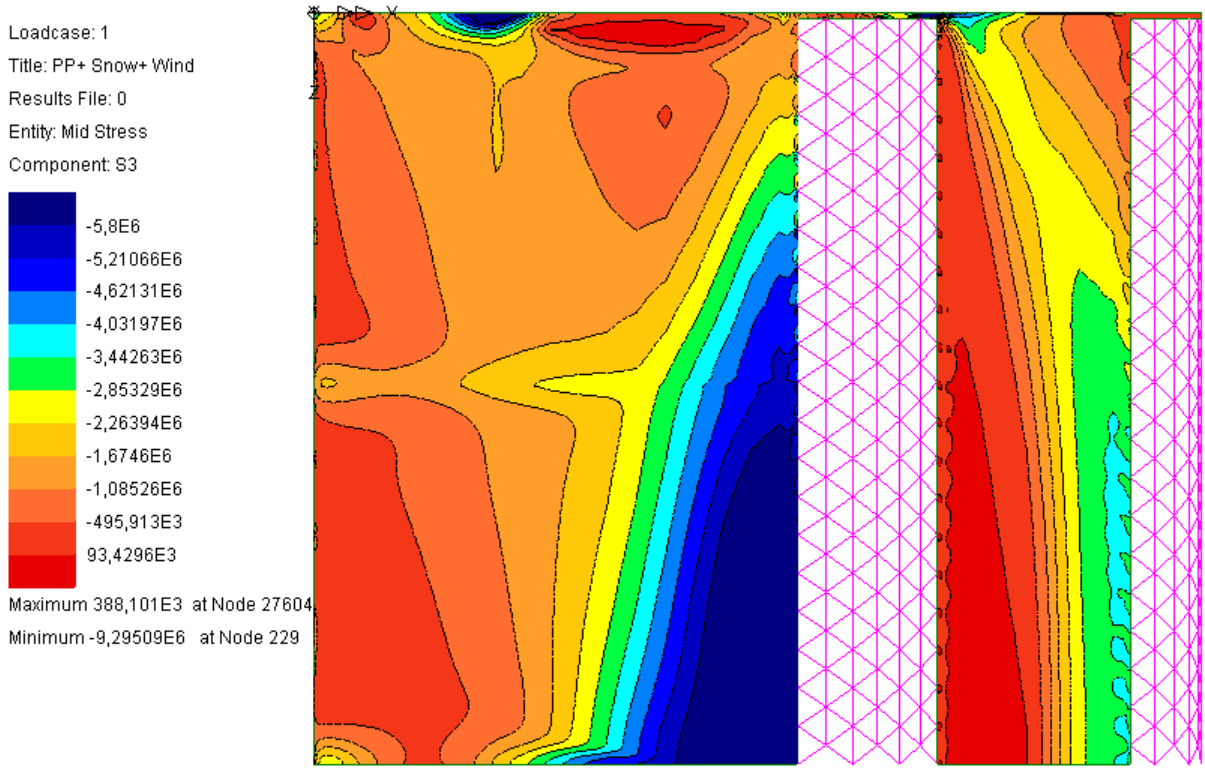

Figure M1*: Maximum tension stress isobars calculated by the sixth Lusas model, considering five ribs in the biggest cylindrical lobe.*

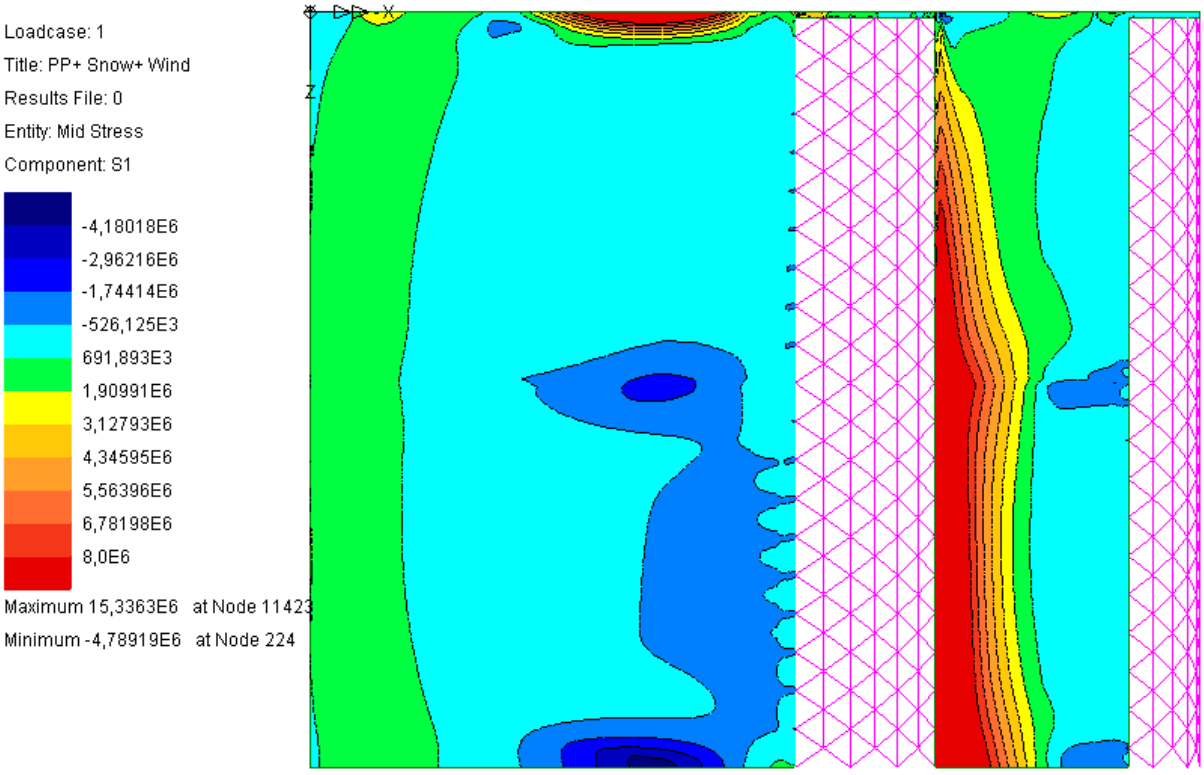

Figure N1*: Maximum tension stress isobars calculated by the sixth Lusas model, considering five ribs in both cylindrical sectors.*

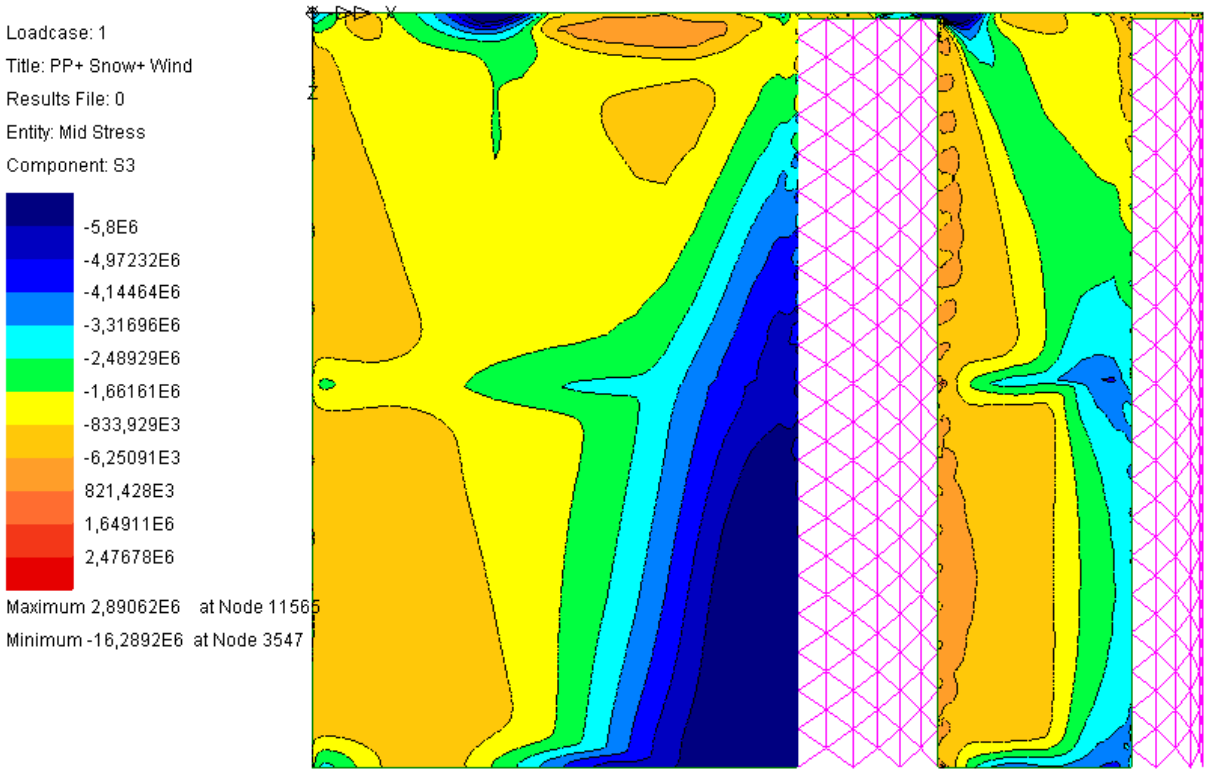

Figure O1*: Maximum compression stress isobars calculated by the sixth Lusas model, considering five ribs in both cylindrical sectors.*

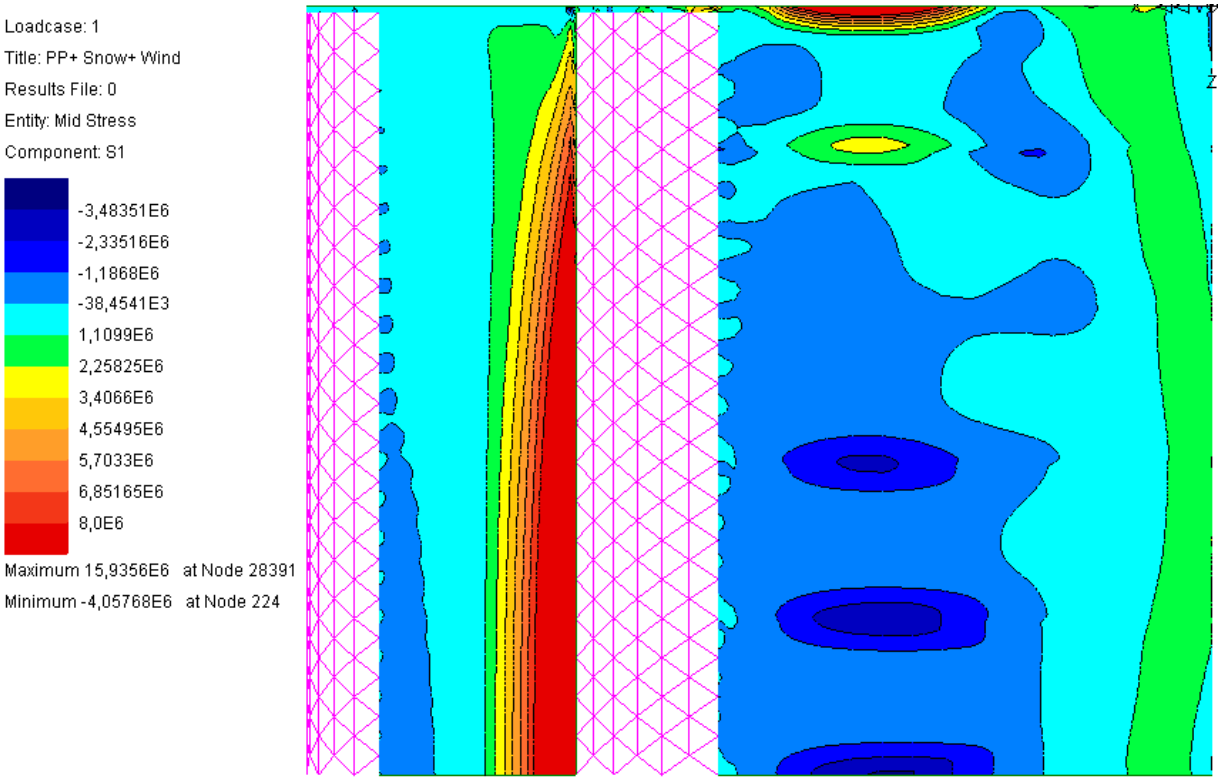

Figure P1*: Maximum tension stress isobars calculated by the sixth Lusas model, considering the ribs proposed by Antuña in the biggest cylindrical sector.*

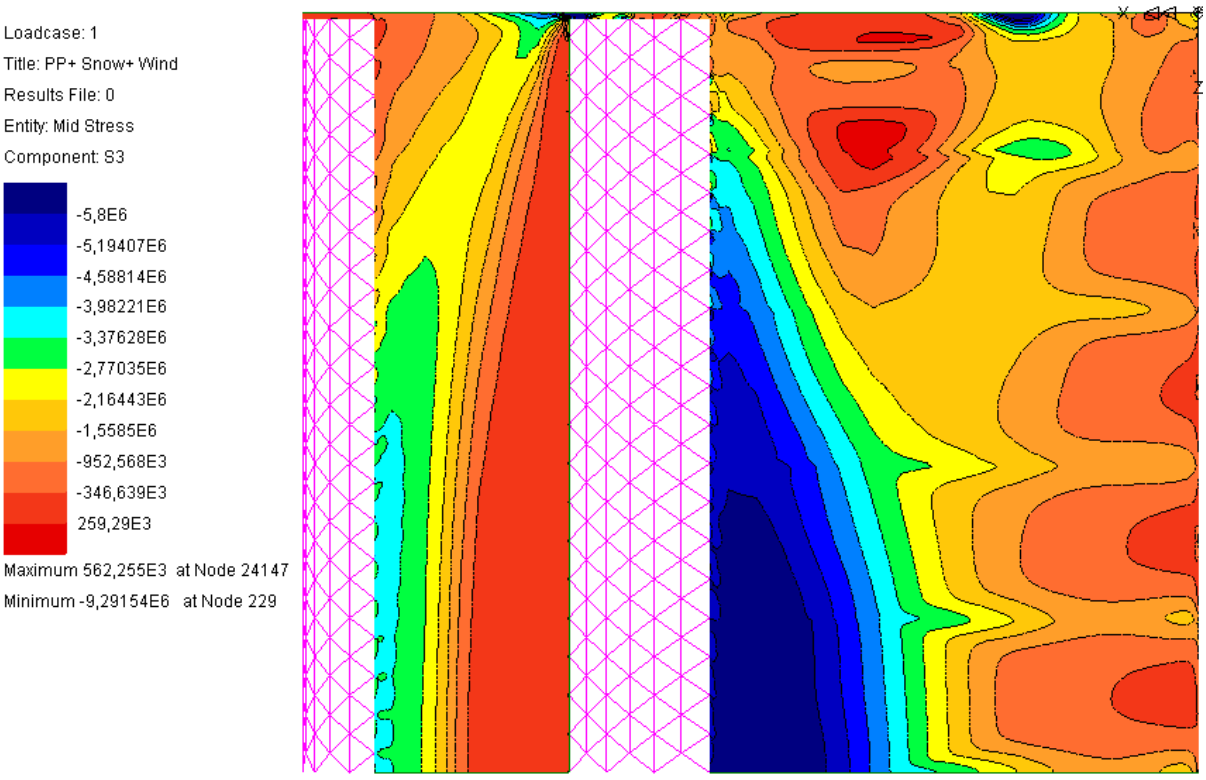

Figure Q1*: Maximum compression stress isobars calculated by the sixth Lusas model, considering the ribs proposed by Antuña in the biggest cylindrical sector.*

Appendix B

Tables and outputs

B.1Table of similar structures

Name	*w(m)*	*L(m)*	*h(cm)*	*Ratio*
Roma ATAG	13.9	20.8	8	265:1
Jena	11.9	23.2	8	290:1
Rostow	12	21	5	420:1
Areneros	8	22	5	440:1
Hamburgo	9.2	24.4	5.5	445:1
Roma STA	15	25	8	315:1
Villaverde	17.5	25	5	500:1
Frankfurt Merk	14.1	36.9	7	525:1
Braila, Romania	10.5	30	5	600:1
Budapest	11.6	40	6	665:1
Recoletos	32.5	55	8	690:1
Dywidag-Halle	11	35	5	700:1

Table 1: *Overall dimensions of the similar structures to the Frontón Recoletos drawn in figure 25.*

B.2Tables of deflections

In this Appendix are listed the deflections measured in different Lusas models.

X (m)	First Lusas model (cm)	Actual structure (cm)	Δ (Cm)	% Regarding Reality
1.5	-0.2	1	1.2	20%
3.3	-0.8	1	1.8	80%
7.2	1.2	1	0.2	120%
11.3	2.7	3	0.3	90%
15.3	-3.8	-8	4.2	48%
19.2	-14.6			
21.2	-15.1	-15	0.1	101%
22.5	-13.9	-15	1.1	93%
25.1	-14.7			
27.2	-12.8	-12	0.8	107%
29.6	-5.5	-3	2.5	183%
31	-0.9	-1	0.1	90%

Table 2: *Vertical deflections measured in centimetres in the first Lusas model and the actual structure.* All the deflections were measured in the same X-axis coordinates. The column "Δ (cm)" represents the difference between the results obtained by Lusas and the actual structure. In the last column, the percentage regarding the value measured by Torroja is presented. The symbol[59] "+" means positive deflections, which represents the raising of the shell. The deflections of the actual structure were measured in the figure 37 using the proposed rule.

[59] These symbols are used in all the tables of this Appendix.

X (m)	First Lusas model (cm)	Small-scale (cm)	Δ (Cm)	% Regarding small-scale model
1.5	-0.2			
3.3	-0.8			
7.2	1.2	3	-1.8	40%
11.3	2.7	1	1.7	270%
15.3	-3.8	-7	3.2	54%
19.2	-14.6	-15	0.4	97%
21.2	-15.1	-15	-0.1	101%
22.5	-13.9	-15	1.1	93%
25.1	-14,7	-11	-3.7	134%
27.2	-12.8			
29.6	-5.5	-5	-0.5	110%
31	-0.9			

Table 3: *Vertical deflections measured in centimetres in the first Lusas model and small-scale model.* All the deflections were measured in the same X-axis coordinates. The column "Δ (cm)" represents the difference between the results obtained by Lusas and the small-scale model. The deflections of the small-scale model were measured in figure 37 using the proposed rule.

X (m)	Second Lusas model (cm)	Actual structure (cm)	Δ (Cm)	% Regarding Reality
1.5	-0.1	1	1.1	10%
3.3	-0.8	1	1.8	80%
7.2	0.4	1	0.6	40%
11.3	0.7	3	2.3	23%
15.3	-4.2	-8	3.8	53%
19.2	-6.4			
21.2	-6.8	-15	8.2	45%
22.5	-6.7	-15	8.3	45%
25.1	-6.5			
27.2	-4.5	-12	7.5	38%
29.6	-1.3	-3	1.7	43%
31	-0.5	-1	0.5	50%

Table 4: *Vertical deflections measured in centimetres in the second Lusas model and the actual structure*. The characteristics are the same expressed in table 2.

X (m)	Second Lusas model (cm)	Small-scale (cm)	Δ (Cm)	% Regarding small-scale model
1.5	-0.1			
3.3	-0.8			
7.2	0.4	3	2.6	13%
11.3	0.7	1	0.3	70%
15.3	-4.2	-7	2.8	60%
19.2	-6.4	-15	8.6	43%
21.2	-6.8	-15	8.2	45%
22.5	-6.7	-15	8.3	45%
25.1	-6.5	-11	4.5	59%
27.2	-4.5			
29.6	-1.3	-5	3.7	26%
31	-0.5			

Table 5: *Vertical deflections measured in centimetres in the second Lusas model and the small-scale model*. The characteristics are the same expressed in table 3.

X (m)	Fourth Lusas model (cm)	Actual structure (cm)	Δ (Cm)	% Regarding Torroja
1.5	-0.4	1	1.4	40%
3.3	-0.5	1	1.5	50%
7.2	0.8	1	0.2	80%
11.3	0.8	3		
15.3	-5.1	-8	2.9	64%
19.2	-8.7			
21.2	-9.2	-15	5.8	61%
22.5	-9.0	-15	6.0	60%
25.1	-8.4			
27.2	-5.7	-12	6.3	48%
29.6	-1.7	-3	1.2	59%
31	-0.6	-1	0.3	65%

Table 6: *Vertical deflections measured in centimetres in the fourth Lusas model and the actual structure.* The characteristics are the same expressed in table 2.

X (m)	Fourth Lusas model (cm)	Small-scale (cm)	Δ (Cm)	% Regarding Small-scale
1.5	-0.4			
3.3	-0.5			
7.2	0.8	3	-1.8	27%
11.3	0.8	1	1.7	80%
15.3	-5.1	-7	3.2	73%
19.2	-8.7	-15	0.4	58%
21.2	-9.2	-15	-0.1	61%
22.5	-9.0	-15	1.1	60%
25.1	-8,4	-11	-3.7	76%
27.2	-5.7			
29.6	-1.7	-5	-0.5	35%
31	-0.6			

Table 7: *Vertical deflections measured in centimetres in the fourth Lusas model and the small-scale model*. The characteristics are the same expressed in table 3.

	Vertical deflection (cm)	Δ (Cm)	% Regarding load case A	X (m)
Load case A	0.2			10.00
Load case B	0.31	0.11	65%	10.00

Table 8: *Vertical deflections measured in centimetres in the third Lusas model considering different load cases*. The column "Δ (cm)" represents the difference between the both load cases. In the last column, the percentage regarding the deflection measured in the load case A is presented. All the deflections were measured in the coordinate X = 10 metres.

	Vertical deflection (cm)	Δ (Cm)	% Regarding load case A	X (m)
Load case A	-4.60			23.00
Load case B	-3.11	1.49	67%	23.00

Table 9: *Vertical deflections measured in centimetres in the third Lusas model considering different load cases*. The characteristics are the same expressed in table 8, however, the vertical deflection was measured in the point X = 23 metres also called seagull profile.

	Vertical deflection (cm)	Δ (Cm)	% Regarding load case C	X (m)
Load case C	1.00			10.00
Load case D	0.16	0.86	16%	10.00

Table 10: *Vertical deflections measured in centimetres in the third Lusas model considering different load cases*. The characteristics are the same expressed in table 8.

	Vertical deflection (cm)	Δ (Cm)	% Regarding load case C	X (m)
Load case C	-6.61			23.00
Load case D	-4.04	2.56	61%	23.00

Table 11: *Vertical deflections measured in centimetres in the third Lusas model considering different load cases*. The characteristics are the same expressed in table 10, however, the point where the vertical deflections were measured is X = 23 metres.

	Z Deflection (cm)	X (m)
Fourth model	9.02	21.41

Table 12: *Z- deflections measured in centimetres in the fourth Lusas model in the coordinate X = 21.41 metres.*

	Vertical deflection (cm)	Δ (Cm)	% Regarding second model	X (m)
Second model	-6.61			23.00
Fourth model	-8.84	2.33	135%	23.00

Table 13: *Vertical deflections measured in centimetres in the second and the fourth Lusas model*. The column "Δ (cm)" represents the difference between both models. In the last column, the percentage regarding the second model is presented. The vertical deflections were measured in the coordinate X = 23 metres.

	Vertical deflection (cm)	Δ (Cm)	% Regarding second model	Z (m)
Second model	-6.61			27.50
Fourth model	-9.09	2.43	137%	27.50

Table 14: *Vertical deflections measured in centimetres in the second and the fourth Lusas model*. The characteristic are the same expressed in table 13, however, the point where the vertical deflections are measured was located in the middle of the seagull profile, Z = 27.5 metres.

	Vertical deflection (cm)	Δ (Cm)	% Regarding Antuña	Z (m)
Antuña Big cylinder	-9.09			23.00
Fernández Big cylinder	-9.37	0.28	103%	23.00

Table 15: *Vertical deflections measured in centimetres in the sixth Lusas model considering different ribs hypotheses*. The rest of characteristic are the same expressed in table 13.

B.3Table of transversal bending moments.

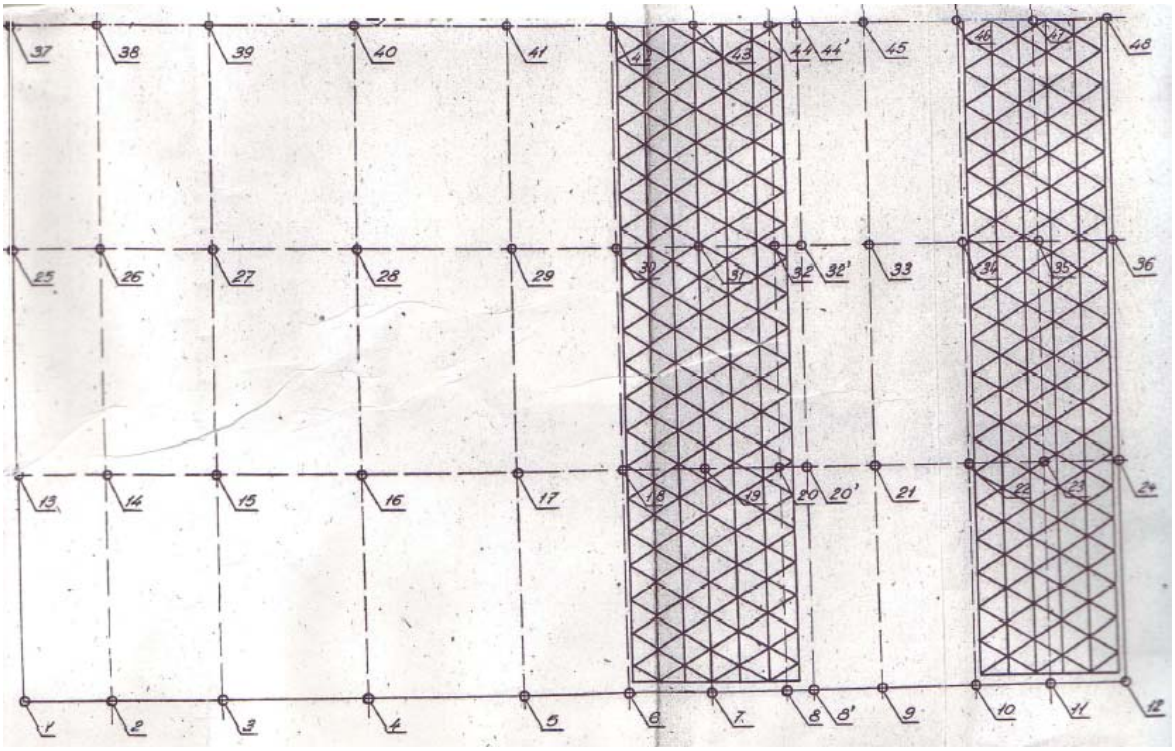

Figure M1: *Points measured by Torroja:* Reference of this picture: Torroja, E., 1942. Comprobación y comportamiento de un estructura laminar. *Madrid, Memorias de la Real Academia de Ciencias Exactas, Físicas y Naturales de Madrid, figure 20.*

Point	X (m)	First Lusas model (Nm/m)	Torroja (Nm/m)	Δ (Nm/m)	% Regarding Torroja
37	0	0	0	0	
38	1.5	-25	-350	325	7%
39	3.3	-306	-140	166	219%
40	7.2	5	110	105	5%
41	11.3	765	375	390	204%
42	15.3	418	150	268	279%
43	19.2	-992	-500	492	198%
44	22.8	1223	620	603	197%
44´	23.8	357	70	287	510%
45	25.1	-1121	-1030	91	109%
46	29.6	153	500	347	31%
47	31.5	1784	1020	764	175%
48	32.51	0	0	0	

Table 16: *Transversal bending moments measured in* Nm/m *in the first Lusas model and in the Torroja's model*[60]. The points are presented in figure A. The column "Δ (cm)" represents the difference between both models. In the last column, the percentages regarding the values obtained by Torroja are presented.

Point	X (m)	Second model (Nm/m)	Torroja (Nm/m)	Δ (Nm/m)	% Regarding Torroja
37	0	0	0	0	
38	1.5	-44	-350	306	13%
39	3.3	-244	-140	104	174%
40	7.2	41	110	69	37%
41	11.3	454	375	79	121%
42	15.3	143	150	7	95%
43	19.2	-1427	-500	927	285%
44	22.8	902	620	282	145%
44´	23.8	309	70	239	441%
45	25.1	-856	-1030	174	83%
46	29.6	1357	500	857	271%
47	31.5	3242	1020	2222	318%
48	32.51	0	0	0	

Table 17: *Transversal bending moments measured in* Nm/m *in the second Lusas model and in the Torroja's model.* The characteristic are the same presented in table 16.

[60] The bending moments presented by Torroja can be consulted in his report (Torroja 1942, p.97-98).

	Bending moment (kNm/m)	Δ (kNm/m)	% Regarding second model	X (m)
Second model	-0.96			17.50
Fourth model	-1,22	0.26	127%	17.50

Table 18: *Transversal bending moments measured in* kNm/m *in the second and the fourth Lusas model at the point X = 17.5 metres*. The characteristics are the same presented in table 16.

B.4Table of isobars.

	Tension stress sobars (MPa)	% Regarding Torroja	X (m)
Torroja	8.00		21.59
Load Case 1	19.80	248%	20.11
Load Case 2	23.87	298%	20.11
Load Case 3	23.96	300%	20.11
Load Case 4	28.06	351%	20.11

Table 19: *Peak of the maximum tension stress isobars represented in figure 39 considering the first Lusas model and measured in* MPa. These peaks are reached in different X coordinates. Furthermore, the percentages regarding the maximum value obtained by Torroja are presented.

	Compression stress isobars (MPa)	% Regarding Torroja	X (m)
Torroja	-5.80		24.80
Load Case 1	-6.64	114%	13.55
Load Case 2	-8.10	140%	13.55
Load Case 3	-8.02	138%	13.55
Load Case 4	-9.39	162%	13.55

Table 20: *Peak of the maximum compression stress isobars represented in figure 40 considering the first Lusas model and measured in* MPa. The characteristics are the same expressed in table 19.

	Tension stress isobars (MPa)	% Regarding Torroja	X (m)
Torroja	3.00		32.50
Load Case 4	-0.14	5%	32.50

Table 21: *Maximum tension stress isobars in the first Lusas model at the point X = 32.5 metres and the percentage regarding the value measured in the Torroja's model.*

	Tension stress isobars (MPa)	% Regarding Torroja	X (m)
Torroja	8.00		21.59
First Lusas model	13.01	163%	20.11
Second Lusas model	28.06	351%	23.03

Table 22: *Maximum tension stress isobars in different models, including the percentage regarding the maximum value measured in the Torroja's model.*

	Compression stress isobars (MPa)	% Regarding Torroja	X (m)
Torroja	-5.80		24.80
First Lusas model	-9.39	162%	13.55
Second Lusas model	-6.01	104%	15.91

Table 23: *Maximum compression stress isobars in different models including the percentage regarding the maximum value measured in the Torroja's model.*

	Tension stress isobars (MPa)	% Regarding Torroja	X (m)
Torroja	-5.80		24.80
First Lusas model	-9.39	162%	24.80
Second Lusas model	-0.63	11%	24.80

Table 24: *Maximum tension stress isobars in different models at the point X = 24.8 metres including the percentage regarding the maximum value measured in the Torroja's model.*

	Tension stress Isobars (MPa)	% Regarding Torroja
Torroja	-8	
First Lusas model	-9.39	162%
Second Lusas model	-6.01	104%

Table 25: *Maximum tension stress isobars and percentage regarding the results obtained by Torroja.*

	Tension stress isobars (MPa)	% Regarding Torroja
Torroja	8	
First Lusas model	28.01	350%
Second Lusas model	13.08	162%

Table 26: *Maximum compression stress isobars and percentage regarding the results obtained by Torroja.*

	Tension stress isobars (MPa)	% Regarding fourth Lusas model
Fourth Lusas model	16.81	
Without edged beam	31.43	167%
With edged beam	16.63	99%

Table 27: *Maximum tension stress isobars considering different edged beam hypotheses and percentage regarding the maximum value of the fourth Lusas model.*

B.5 Small-scale model deflections.

Point	X (m)	Test A (cm)	Test B (cm)	Test Average (cm)
1	0	0	0	0
2	1.5	0	-0.5	-0.25
3	3.3	0	0.2	0.1
4	7.2	0.8	0.7	0.75
5	11.3	0.8	0.8	0.8
6	15.3	-4.2	-3.2	-3.7
7	19.2	-6	-5.2	-5.6
8	22.8	-5.5	-5	-5.25
9	25.1	-5	-4	-4.5
10	29.6	-3	-2.5	-2.75
11	31.5	-4	-4	-4
12	32.5	-1.5	0	-0.75

Table 1: *Vertical deflections measured in the test A and B carried out by Torroja in the small-scale model and the average of both tests.* For these tests, the load combination is the dead weight. The points are presented in figure 78. The symbols of the deflections are the same expressed in table 2 (Torroja 1942, p.126).

Point	X (m)	Average (cm)	Fourth Lusas model (cm)	Δ (Cm)	% Regarding Average
1	0	0	0	0	
2	1.5	-0.25	-0.1	0.15	40%
3	3.3	0.1	-0.5	0.6	500%
4	7.2	0.75	0.2	0.55	27%
5	11.3	0.8	0	0.8	
6	15.3	-3.7	-3.4	0.3	92%
7	19.2	-5.6	-6	0.4	107%
8	22.8	-5.25	-6.4	1.15	122%
9	25.1	-4.5	-6.2	1.7	138%
10	29.6	-2.75	-1.4	1.35	51%
11	31.5	-4	-0.3	3.7	8%
12	32.5	-0.75	0	0.75	

Table 2: *Comparison between the average vertical deflections, measured in the test A and B, and the vertical deflections obtained by the Fourth Lusas model*. The column "Δ (cm)" represents the difference between both models. In last column, the percentage regarding the Average value is presented. The points are listed in figure 80.

Point	X (m)	Test D (cm)	Fourth Lusas model (cm)	Δ (Cm)	% Regarding D
1	0	0	0	0	
2	1.5	0	0	0	
3	3.3	0.7	-0.5	1.2	71%
4	7.2	2.7	0.3	2.4	11%
5	11.3	-0.9	-0.1	0.8	11%
6	15.3	-4	-4.7	0.7	118%
7	19.2	-6.5	-7,8	1.3	120%
8	22.8	-6	-8.3	2.3	138%
9	25.1	-5.5	-8	2.5	145%
10	29.6	-2.5	-1.7	1.8	68%
11	31.5	-1.2	-0.2	1	17%
12	32.5	0	0	0	0

Table 3: *Comparison between the vertical deflections measured in the test D carried out by Torroja in the small-scale model and the vertical deflections obtained in the fourth Lusas model.* The characteristics are the same expressed in figure M1. The values of the test D are obtained from the Torroja's report (Torroja 1942, p.126).

Appendix C

Pictures

In this appendix the different pictures taken in the "Archivo Torroja" by the professor Ignacio Payá Zaforteza are presented.

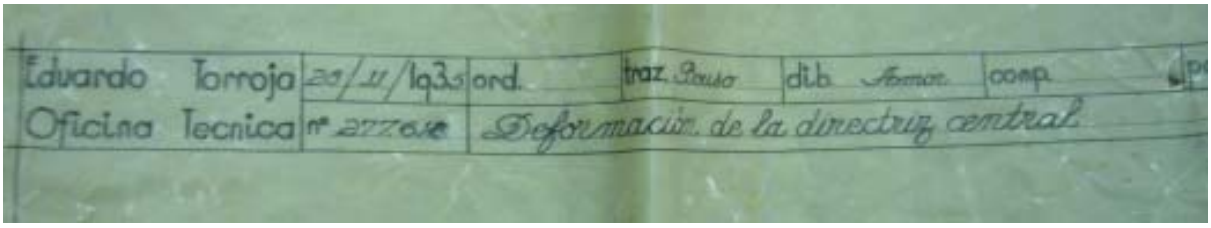

Figure P1: *Construction drawing where the location of the deflections, along the central directrix, are explained.*

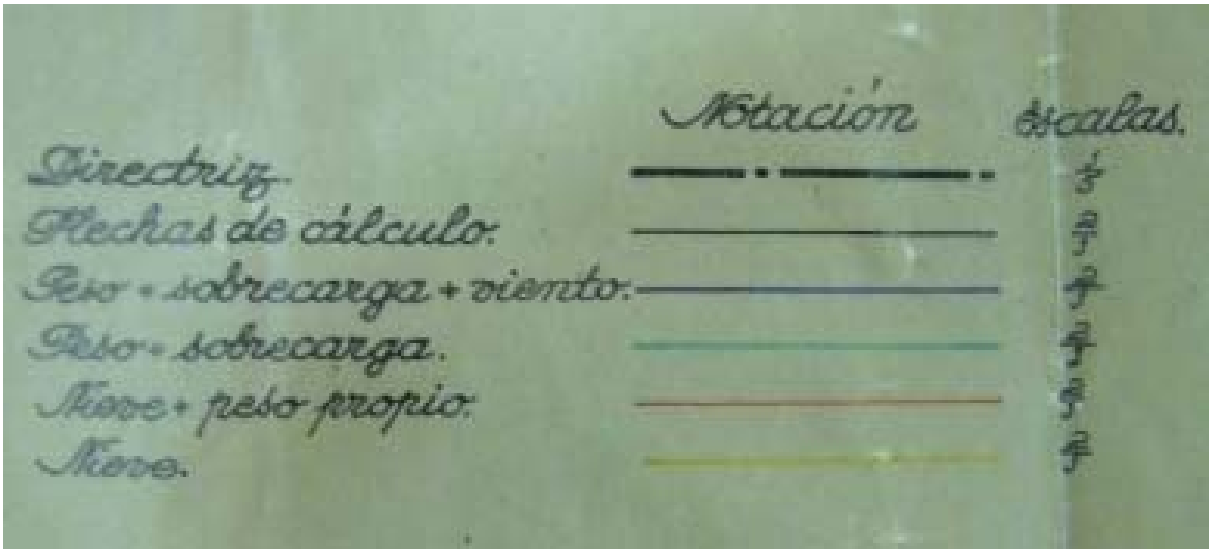

Figure Q1: *Load cases considered by Torroja in the deformations*: Load case 1: dead weight, Load case 2: dead weigh with snow, Load case 3: dead weigh with wind and Load case 4: dead weigh with snow and wind.

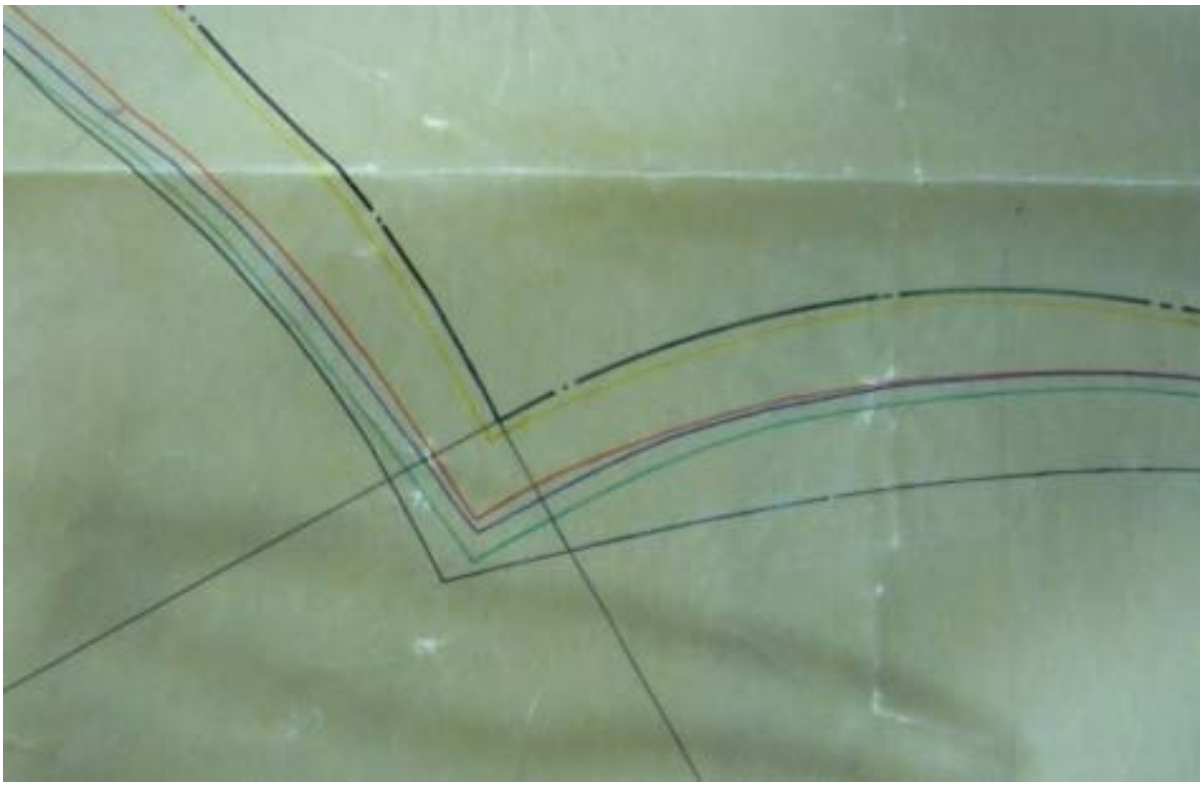

Figure R1: *Detail of the orthogonality in the seagull profile when different load cases are applied.*

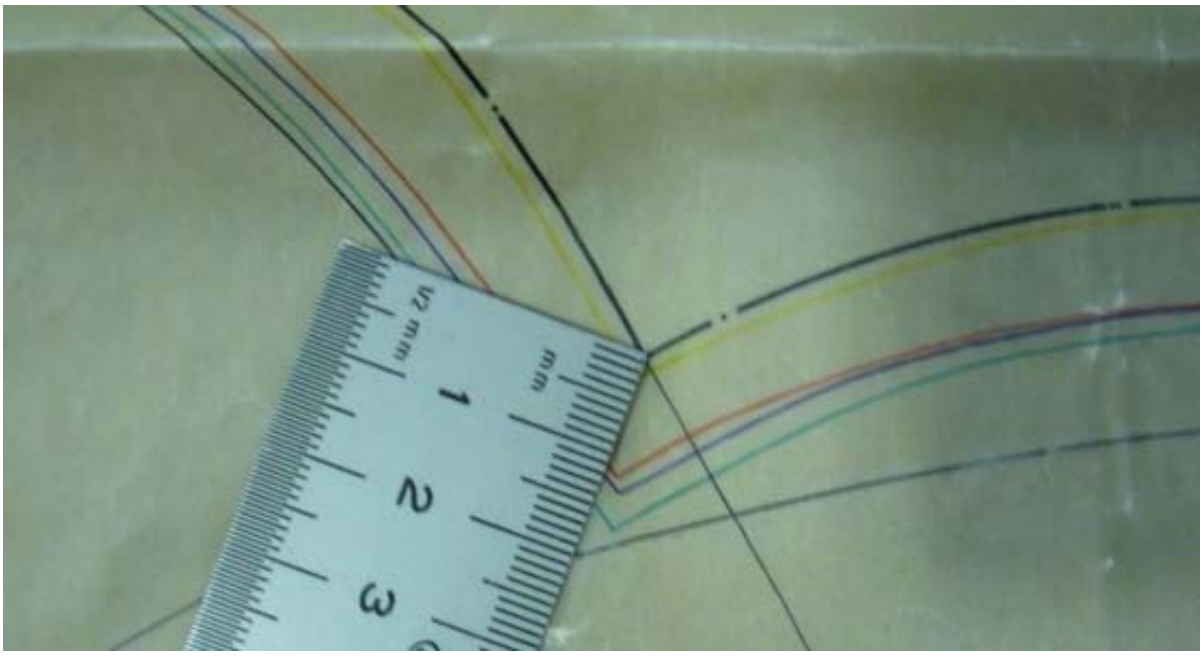

Figure T1: *Detail of the deformation at the connection between both lobes compared with the measure of the real rule.*

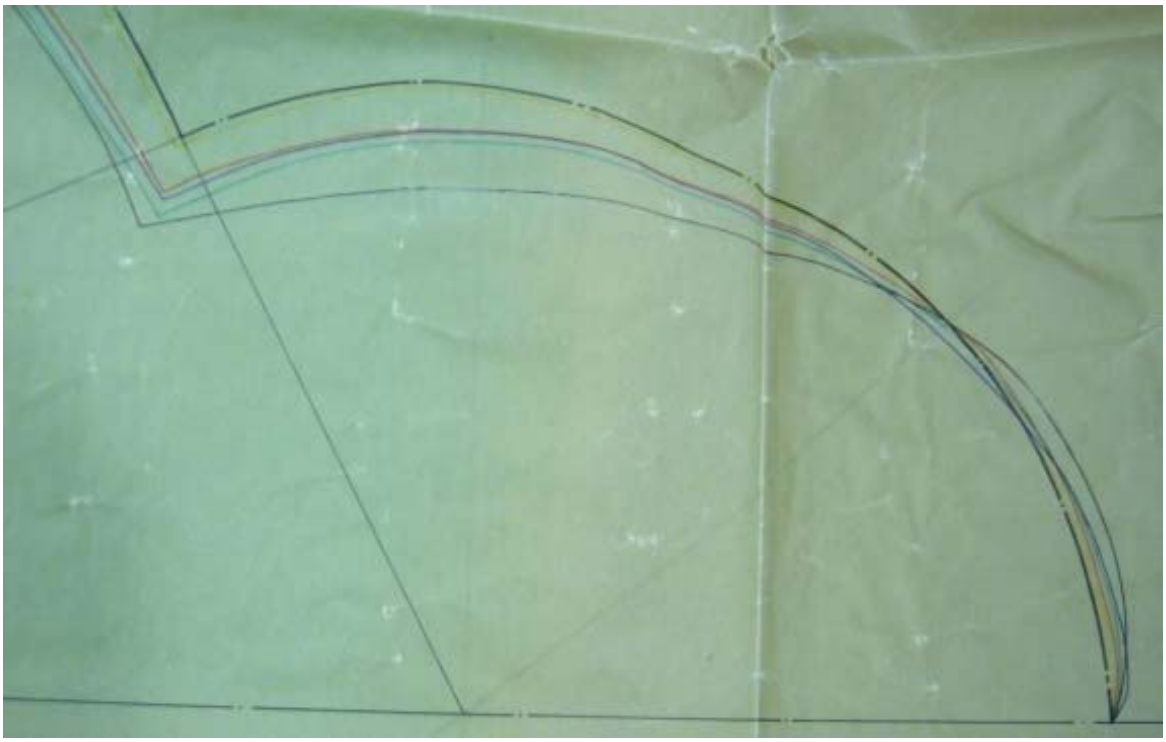

Figure U1: *Detail of the deformations at the smallest cylindrical sector.*

Appendix D

Torroja's reflections

The following Torroja's reflections were compiled by Juan Antonio Fernández Ordoñez in his book "Eduardo Torroja: Ingeniero" (Fernández 2000, p.147).

"The following will be considered a deception, and therefore fit to be proscribed: if the appearance of a construction induces us to think that the phenomena, functional and resistant, are completely different from the real ones concealed in an interior structure"

"The expression of a resistant phenomenon, intrinsic and apparently impossible, is always anti-aesthetic"

"Joining together the tensile phenomenon with the aesthetic effect"

"The structure should be beautiful in itself, without needing additions or frills"

"In the purest joy of aesthetic emotion, simplicity is a virtue"

"If use is to be made of an ornamental theme, make it clearly independent and highlight it by contrast with the austere simplicity, without pretentions that are alien to its task"

"Use the landscape as a pedestal or an accompaniment. Construction in a landscape should rhyme with it. The building, with its dynamism and proportions, imposes itself on the landscape and dominates it"

"Making builds with an object in mind that he is not always successful in reaching"

E. Torroja

TRITA-BKN. Master Thesis xxx,
Structural Design and Bridges YEAR
ISSN 1103-4297
ISRN KTH/BKN/EX-xxx-SE

www.kth.se